ANALYSIS AND DESIGN OF ADSORPTIVE PROCESSES FOR AIR QUALITY CONTROL

by

Krista M. Knight

A thesis submitted in partial fulfillment of the
requirements for the degree of

DOCTOR OF PHILOSOPHY
(Mechanical Engineering)

at the

UNIVERSITY OF WISCONSIN-MADISON

1992

Abstract

Volatile organic compounds (VOCs) are a common type of indoor air pollutant, with individual concentrations typically in the parts per billion (ppb) range. The usual method for removing VOCs from indoor air is by adsorption on fixed-bed activated carbon filters. These filters have a finite useful lifetime and must be periodically replaced; for some organics, the lifetime is short. By using a rotary configuration, a charcoal filter can be continually regenerated, extending its useful life and possibly allowing removal of a wider range of VOCs. In this thesis, the potential of such a configuration is explored through analysis of a rotary regenerative activated carbon wheel with infinite transfer coefficients.

Acknowledgements

I'd like to thank the University of Wisconsin-Madison Graduate School and the U.S. Department of Energy for funding this research. I'd also like to thank Prof. Sandy Klein and Prof. John Mitchell for being my advisors.

My teammates in the UW Women's Ice Hockey Club have contributed in many ways to my life, adding an entirely new and different dimension: where else would I have ever learned about banana facials? I'd like to thank my parents for supporting me in whatever I've chosen to do, and for keeping me up to date with what's going on with the rest of the family. Most of all, I'd like to thank my husband, Bill. I love you. Hopefully now our life will be somewhat more organized. I'm looking forward to free weekends: skiing, canoeing, or whatever. This is a time of transition for us; who knows where we'll be a year from now or what each of us will be doing. But I'm sure we'll be having fun.

Table of Contents

List of Figures

List of Tables

Nomenclature

A	1) surface area of the adsorbent; m^2, or 2) adsorption potential defined by Equation 2.4.11
c_{air}	specific heat of the air; J/(kgmol air·K)
c_m	specific heat of the matrix; J/(kg matrix·K)
(cfm)	volumetric flowrate of the air, ft^3/min
f	the fraction of outdoor air
h	enthalpy of the gas phase; J/(kgmol clean air)
H	enthalpy of the solid phase; J/(kg clean matrix)
Δh_s	differential isosteric heat of adsorption; J/(kgmol i)
Δh_{fg}	heat of vaporization; J/kgmol
k	Langmuir isotherm constant for a gas phase concentration expressed as a mole ratio; (kgmol air/kgmol i)
k'	Langmuir isotherm constant for a gas phase concentration expressed as a partial pressure; (kgmol i+air)/(kgmol i·atm)
K_0	isotherm slope at the reference temperature; (kgmol air)/(kg mtx·atm)
K	linear isotherm slope for a gas phase concentration expressed as a mole ratio; (kgmol air)/(kg mtx)

K'	linear isotherm slope for a gas phase concentration expressed as a partial pressure; (kgmol air)/(kg mtx·atm)
L	length of the matrix in the flow direction; m
m_m	mass of clean adsorbent; kg clean adsorbent
$\dot{m}_r$	mass flow rate of the air supplied to the zone; kg/s
n	number of moles
$\dot{n}_{air}$	molar flowrate of clean air; kgmol/s
p	partial pressure; atm
P	total pressure; atm
$\dot{P}$	pollutant generation rate; kgmol/s
q	amount adsorbed; (kgmol i)/(kg mtx)
q_{diff}	differential heat of adsorption (Equation 2.3.10); J/kgmol or kcal/gmol
Q	total volumetric flowrate of air; (m^3 air)/s
Q_{int}	integral heat of adsorption (Equation 2.3.9); J/kgmol or kcal/gmol
r	wheel radius; m
R	ideal gas constant; J/(kgmol·K)
(rpm)	wheel rotation speed; rev/min
s	shock speed

S	entropy
T	temperature; °C or K
T_0	reference temperature for isotherm slope; in this paper, T_0=25°C
T_{ref}	reference temperature for enthalpy calculations; °C or K
U	internal energy
v	specific volume of the gas phase; m^3/kgmol
v_{air}	air velocity; m/s
V	volume; m^3
W	amount of contaminant adsorbed per mass of adsorbent; (kgmol i)/(kg mtx)
W_0	Langmuir isotherm constant; (kgmol i)/(kg mtx)
x	dimensionless axial distance
y_i	contaminant mole fraction; (mol i)/(mol i+air)
z	axial distance; m
$1/\Gamma$	normalized period duration; (kgmol air)/(kg matrix)
λ	eigenvalue or wavespeed
ϕ	the spreading pressure
ϕ_j	angle of the wheel taken up by period j, in radians,
$\tilde{\rho}_{air}$	density of the air; kgmol/m^3

$\hat{\rho}_c$	bulk density of the granular activated carbon; kg/m^3
σ	c_m/c_{air}, the specific heat ratio; (kgmol air)/(kg matrix)
θ	time; s
θ_1	duration of the process period; s
θ_B	breakthrough time; s
μ	chemical potential
τ	normalized time; (kgmol air)/(kg matrix)
ω	gas phase contaminant concentration (mole ratio); (kgmol i)/(kgmol air)

Subscripts:

11	process side inlet
12	process side outlet
21	regeneration side inlet
22	regeneration side outlet
int	intermediate state
g	gas phase
L	left side of the waves
m	matrix
o	outdoor

P	process side
R	1) regeneration side, or
	2) right side of the waves
s	solid phase
z	zone

Chapter 1

Introduction

1.1 Project motivation

In response to increasing energy costs and concern over conservation of energy, many buildings, including homes, schools, and office buildings, have been tightened to prevent energy losses through infiltration. At the same time, outdoor ventilation rates have been decreased. While these measures have been successful in reducing energy requirements, problems with the quality of indoor air have resulted in some cases. "Sick Building Syndrome" is the term used when people complain of minor health problems such as fatigue, dryness, mucous membrane irritation, and headaches.

The increasing value placed on energy has also resulted in the investigation of alternative air conditioning systems, such as desiccant air conditioning systems. A typical system is illustrated in Figure 1.1. A desiccant, such as silica gel or lithium chloride, is used to adsorb water vapor from the air to meet the latent load. Although this process increases the air temperature, by over-drying the air, evaporative cooling can be used to bring the air to the supply state. Even if conventional air conditioning methods are used in the desiccant system to cool the desiccant-dried air to the supply state, there may be an energy savings over a strictly conventional system. In order to meet the latent load, the traditional vapor-compression cycles must over-cool the air to remove the moisture and then reheat the air to the supply state. No cooling below the supply temperature is required for the desiccant system.

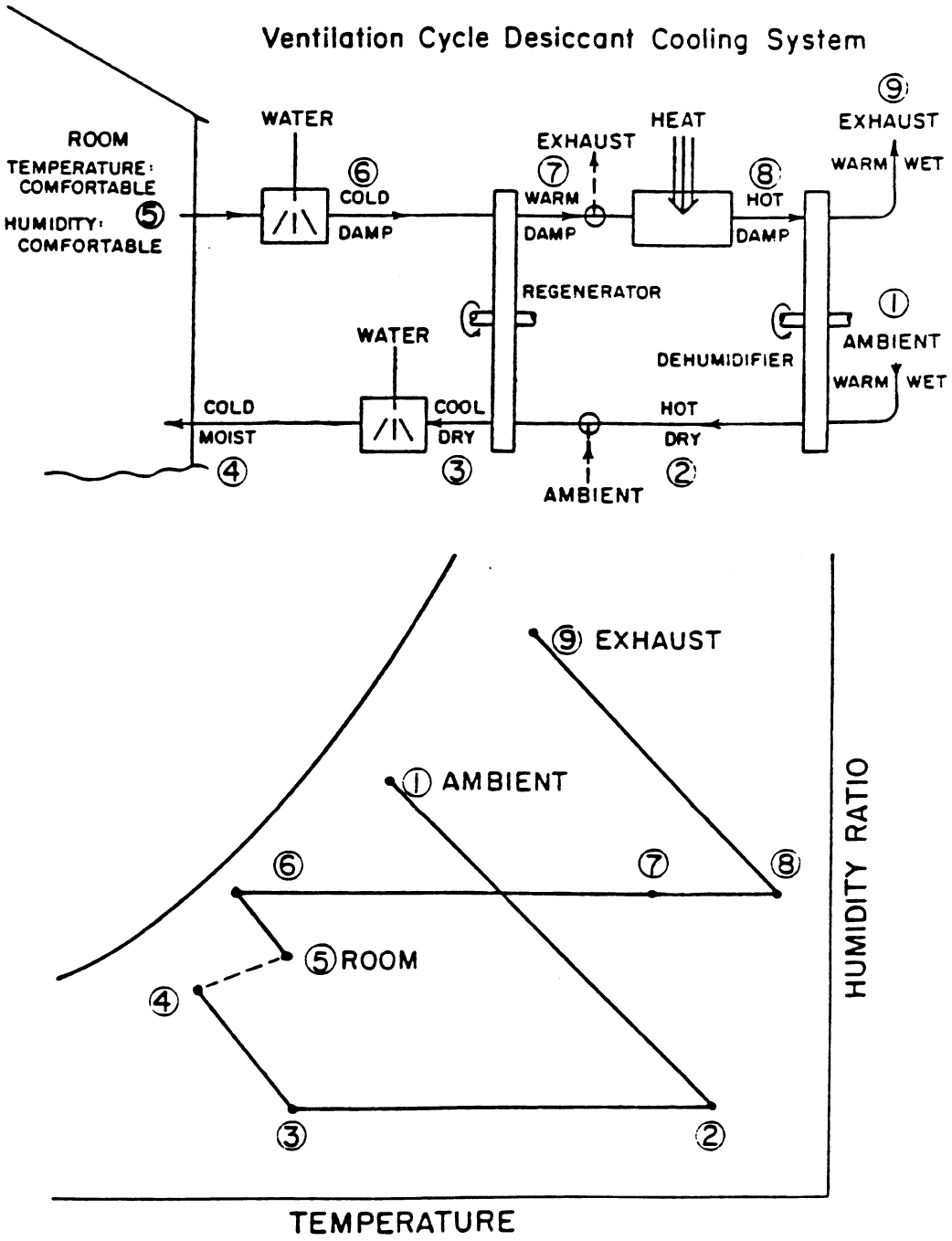

Figure 1.1 Schematic and psychrometric diagram of a ventilation cycle desiccant cooling system (from reference [1]).

Eventually the desiccant must be regenerated, i.e., the adsorbed water vapor must be driven off. Often this is accomplished by blowing a hot air stream through the desiccant; solar energy is a possible source for the heat. For the system in Figure 1.1, the desiccant material is impregnated on a wheel which rotates through the process (adsorption) and regeneration (desorption) air streams in a cyclic steady-state operation. This is called a rotary regenerative configuration, and allows continual in-place regeneration of the desiccant.

The National Renewable Energy Laboratory (NREL), formerly the Solar Energy Research Institute (SERI), has been investigating the long-term effect of contaminants on the air conditioning potential of desiccant systems, specifically with regards to reduction of the water vapor adsorption capacity of the desiccant material. Alternatively, it may be possible to utilize the capability of the desiccant to adsorb various contaminant vapors to improve the indoor air quality, thus combining the desiccant air conditioning and pollutant removal capabilities into one unit. This idea was the motivation for this study.

1.2 Indoor air quality

Studies have shown that the numbers and concentrations of contaminants found in indoor air are much larger than in outdoor air [2-5]. Pollutants found in indoor air are emitted from sources within buildings, such as people, building materials, carpets, copying machines, etc., and are also transported from the outdoors by the ventilation system. Typical indoor pollutants include particulates, bioaerosols, radon, various inorganic vapors, e.g., CO, NO, NO_2, NH_3, and volatile organic compounds (VOCs), e.g., formaldehyde. The number of volatile organic compounds (VOCs) alone is often greater

than 100, although the concentrations, which are often in the low ppb range, are several orders of magnitude less than industrial safety limits [3,4,6,7]. Yet complaints about indoor air quality occur.

While the irritating effect of each contaminant alone is usually negligible, complex interactions between pollutants, temperature, and humidity can result in irritating sensory stimuli. The method of these interactions is not well understood, such that prediction of indoor air problems from air sample analysis is difficult at best [3,8]. Often the only way to "measure" indoor air quality is by using people. In the standard ASHRAE 62-1989 [9], acceptable indoor air quality is defined as follows:

> **acceptable indoor air quality:** air in which there are no known contaminants at harmful concentrations as determined by cognizant authorities and with which a substantial majority (80% or more) of the people exposed do not express dissatisfaction.

Because most people spend a majority of their time (about 90%) indoors [10], exposure to indoor pollutants exceeds that from outdoor pollutants.

There are essentially three approaches to improving indoor air quality. The first is pollution prevention, accomplished by removing the sources of the indoor pollutants, e.g., by using different building materials. There are several limitations to this method. It may be impractical to eliminate some pollutant sources such as copying machines. Also, some indoor pollutants are actually outdoor pollutants which are transported from the outdoors and trapped inside.

Second, the pollutants can be diluted by ventilation with outdoor air. This is by far the most common approach, however energy is required to heat or cool the outdoor air. In response to the rising concerns over indoor air quality, in the latest version of the standard ASHRAE 62-1989 [9], Ventilation for Acceptable Indoor Air Quality, minimum

required flowrates have been raised from 5 to 15 cfm/person, with many applications requiring higher flowrates. If the outdoor air does not meet outdoor air quality standards, it must be cleaned before entering the occupied space.

The third approach consists of removal of the pollutants from the indoor air by various types of air cleaning devices. These devices offer the prospect of saving energy by reducing outdoor ventilation rates. ASHRAE 62-1989 allows for this possibility in the Air Quality Procedure, which states that the minimum required flowrates may be disregarded if contaminant concentrations are reduced below acceptable limits by some other means, although the limits are not well defined. Typical equipment used for air cleaning includes particulate filters, electrostatic precipitators, and for organic vapors, activated carbon adsorption filters.

Because desiccant air conditioning systems make use of the adsorption process, and because adsorption is used in air quality control primarily for removing VOCs from air, this study has focused on the removal of VOCs from indoor air, and in particular, using activated carbon for an adsorbent. The reason for using activated carbon as an adsorbent is discussed in Chapter 2. The following section describes more about VOCs in indoor air.

1.3 Volatile organic compounds (VOCs)

The most commonly found groups of VOCs in indoor air are the aliphatic hydrocarbons (reference [11] mentions specifically those with 6 to 17 carbon atoms), followed by the aromatic hydrocarbons, chlorinated hydrocarbons and other

miscellaneous hydrocarbons, e.g., ketones and aldehydes [2,3,11,12]. Molhave [11] cites toluene and the three xylenes as the most frequently found compounds. Berglund et al. [13] put together a list of over 300 VOCs that have been identified in indoor air.

Often many of the individual VOCs are not identified. Typically 100-150 individual VOCs will be present in an air sample [2,5,8,11,12,14]. Several authors have stated that about 20-30 of the VOCs are found in nearly all air samples [5,11]. Some references which contain at least partial lists of indoor air VOCs include [2-6,10,14-17].

The concentrations of the individual VOCs in indoor air are typically in the ppb range [2,5,6,10,12,15,17-19], which, as previously mentioned is several orders of magnitude less than industrial safety limits [3,4,6,7]. As an example, some measured toluene concentrations (in offices and schools) reported in the literature are listed in Table 1.1. Most of the values were reported in units of $\mu g/m^3$; the third column of the table lists the concentration in units of parts per billion (ppb) at a temperature of 20°C. The range is 1 to 20 ppb

Table 1.1 Literature reported values of the concentration of toluene in indoor air.

Reference	Toluene concentration in $\mu g/m^3$	Toluene concentration in ppb at 20°C.
[15]	6.9-9.7	1.8-2.5
[6]	33.1-91.0	8.6-23.8
[16]	4.7-17.0; 17.0-27.0; 8.6-21.0; 17-62	1.2-4.4; 4.4-7.0; 2.2-5.5; 4.4-16.2
[4]	0.39-0.50; 9.43-12.34	0.10-0.13; 2.46-3.22
[2]	approximately 20	approx. 5.2
[17]		1.8±1.7, 8.2±1.5, 1.5±1.2

Molhave [11] has postulated that the total combined effect of many VOCs is irritating for total VOC concentrations greater than 2 mg/m^3, whereas for VOC concentrations between 0.16 and 2 mg/m^3, irritation may result with the addition of other factors, e.g., low humidity, and below 0.16 mg/m^3, there should be no irritation resulting from the VOCs. However, in a study by Fanger et al. [20], many people were dissatisfied with the indoor air at VOC concentrations lower than 0.16 mg/m^3, although the dissatisfaction could be due to pollutants other than the VOCs present in the indoor air. Table 1.2 lists some reported values of total VOC concentrations.

Table 1.2 Literature reported values of the total concentration of VOCs in indoor air.

Reference	Total VOC concentration in mg/m^3.
[18]	0.237±0.182; 0.401±0.653; 1.090±0.728
[6]	1.9; 2.3; 5.2; 11.0
[20]	0.01 to 0.43

Some VOCs are found in both indoor and outdoor air, while other VOCs have primarily indoor sources. For example, benzene, toluene, *o*-, *m*-, and *p*-xylene are usually found in outdoor air, in addition to having indoor sources [12]. Some of the aliphatic hydrocarbons, on the other hand, have in some studies been found only in indoor air [12]. The number of VOCs in indoor air is greater than in outdoor air: Berglund et al. [5] reported 1.4 times as many organics indoors as outdoors and Johansson [2] found 160 VOCs indoors versus only 50 outdoors (3.2 times more indoors).

Usually the individual indoor VOC concentrations are greater than the outdoor concentrations [2,3], and the relative concentration of each individual pollutant is often

different. In [19], indoor concentrations as high as 4.5 times outdoors were reported, and in [4], indoor concentrations as high as 11 times outdoors were reported, although most indoor organic concentrations were between 1 and 3 times the outdoor concentrations. However, outdoor concentrations in some places, e.g., on a sidewalk, may be higher than indoor concentrations [15]. Several references [6,19] have noted a diurnal variation in the VOC concentrations, including lower levels over weekends, indicating that at least some of the VOC pollutant sources are related to humans and their activities.

As an example of an indoor air quality study, consider the work of Grot, Hodgson, Daisey, and Persily [6], who studied the indoor air quality of a new federal office building located in Portland, OR. Measurements were made on four days: August 4, 1987, October 14, 1987, January 13, 1988, and October 28, 1988. The ventilation rates on the four days were 0.5, 1.36, 0.24, and 1.99 air changes per hour, respectively. Shown in Figure 1.2 are the four concentration values for 25 VOCs they identified. Figure 1.3 is a distribution of the 25 VOCs by molecular weight. As noted in [6], the measured VOC concentrations are 1/1000 of OSHA levels, much lower than the ASHRAE 62-1989 suggestion of 1/10 OSHA levels. Total VOCs, depending on the ventilation rate, ranged from over 1 mg/m^3 to over 5 mg/m^3.

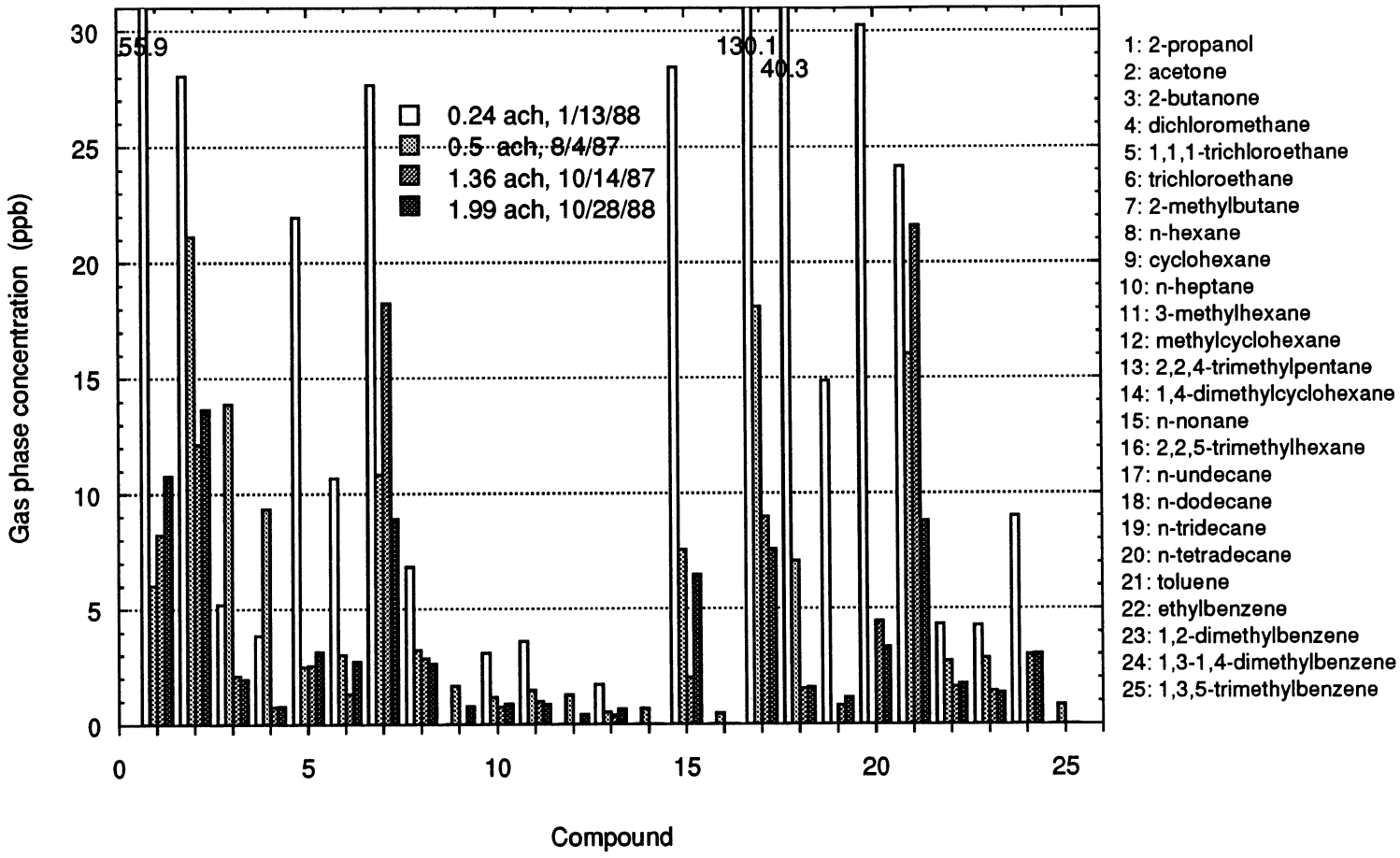

Figure 1.2 VOC concentrations measured by Grot et al. [6] on four different days with ventilation rates of 0.24, 0.5, 1.36, and 1.99 air changes per hour.

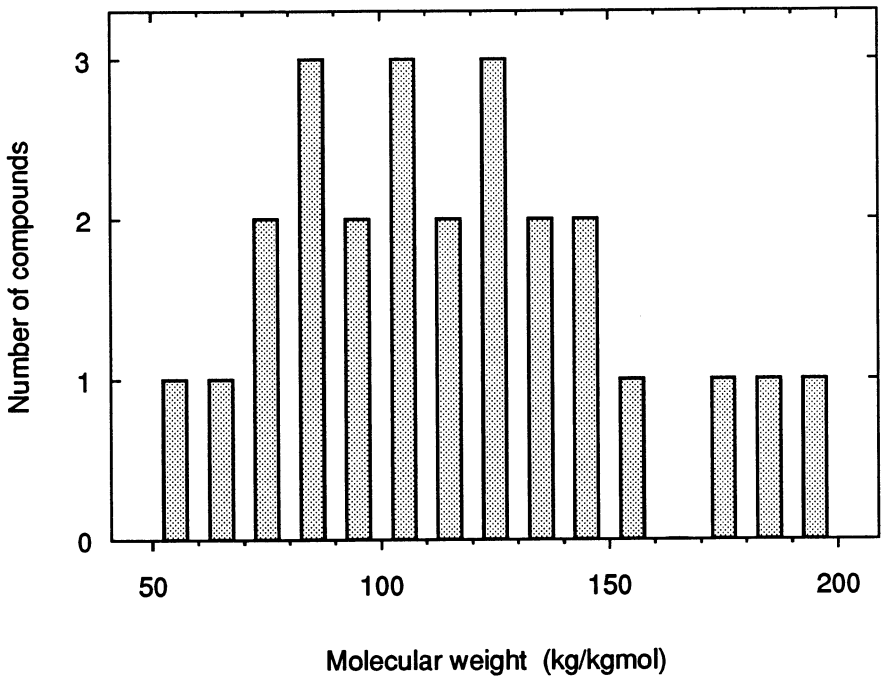

Figure 1.3 Distribution of the molecular weights of 25 VOCs identified by Grot et al. [6].

In response to a survey, 20% of the people rated the air quality as poor and 30% complained of stuffiness. Eye irritation, headaches, and sleepiness were also problems for some occupants. The building was equipped with a VAV system and ventilation rates were normally about 1.0 to 1.2 air changes per hour. Grot et al. [6] point out that this corresponds to a greater ventilation rate than required by ASHRAE 62-1989, which would be about 0.8-0.9 air changes per hour. Thus even though the building design meets the ASHRAE standard, according to ASHRAE's own definition of acceptable indoor air quality, the building has an indoor air quality problem.

1.4 Design considerations

The goal of this project was to consider the design of an adsorption filter for removing VOCs from indoor air. In particular, the rotary regenerative configuration for an adsorption filter is examined. Some of the design considerations are as follows:

1. There are multiple VOCs to be removed, and the identities of the individual VOCs are not always known.
2. The concentration levels of the VOCs are in the low ppb range.
3. Each VOC must be reduced to some acceptable concentration, which at present is unknown.
4. The filter operation may be affected by the air conditioning/heating requirements and vice versa.

In considering the practical application of this technology, it is necessary to reduce all problem causing pollutants to acceptable concentrations. The exact cause of most indoor air quality problems is unknown - the specific problem pollutants are unknown and the problem concentration levels are unknown. Thus, at present, various types of filters offer only an improvement in indoor air quality rather than a total solution to the problem. One of the big advantages of filters is the possibility of reducing indoor concentrations below outdoor concentrations.

1.5 Thesis outline

This chapter describes the original idea behind the project and briefly outlines the indoor air quality problem. The project goals and design considerations are presented, along with a brief description of the contents of each chapter.

Chapter 2 contains a description of adsorption and how it is quantified, including the adsorption of mixtures. Some information about activated carbon and why it is used for VOC adsorption is also included. References for isotherm data of VOCs on activated carbon are given, in particular for the low concentration range.

Chapter 3 covers relevant background information for carbon filter modeling and design. The chapter begins with a brief description of carbon filters as they exist today, including how they are sized. Maximum possible lifetime calculations are presented. The last part of the chapter reviews related applications, e.g., respirator cartridges.

Chapter 4 presents the model equations, including assumptions and nomenclature. A low concentration assumption and the resulting simplified equations are also presented. References which either developed or used different models for adsorption processes are also listed.

Chapter 5 explains the method used to solve the equilibrium equations, both with and without the low concentration assumption. The validity of the low concentration assumption is examined. The low concentration linear isotherm solution is presented in terms of the process and regeneration periods, and expressions for the regions of complete regeneration and complete processing are presented.

In Chapter 6, the effect of different variables and parameters on the intermediate concentration, the process period average outlet concentration, and the steady-state zone concentration is presented and discussed. Chapter 7 contains the conclusions and recommendations for future study.

Chapter 2

Adsorption

2.1 Introduction

Smísek and Cerny [21] define **adsorption** as the increase in concentration of a substance at the interface between two phases. More commonly, adsorption is defined as molecules of a gas or liquid adhering to the surface of a solid. Adsorption can be thought of as a phase change similar to condensation, although adsorption can occur above the critical temperature. The advantage of adsorption is that a significant amount of vapor phase mixture separation can occur at pressures below the saturation vapor pressure. It is unknown whether the adsorbed phase exists as a liquid or a gas phase.

The solid is called the **adsorbent** and the gas or liquid, both in the adsorbed phase and the non-adsorbed phase is called the **adsorbate**. The reverse process, in which the adsorbed molecules leave the surface, is called **desorption**. Adsorption is a surface phenomenon, distinguishing it from absorption which involves actual penetration of the gas or liquid within the crystal lattice. Some common applications which use adsorption include odor control, solvent recovery, separation processes, chromatography, dehumidification, and purification.

There are two types of adsorption, which are differentiated by the nature of the intermolecular forces responsible for adsorption: **physical adsorption** and **chemisorption**. Physical adsorption occurs when weak intermolecular attractive forces (van der Waals forces) cause the adsorption, and is a reversible process. For non-polar adsorbates and adsorbents, the adsorption forces are the dispersion forces, i.e., the forces

due to temporary dipoles resulting from fluctuations in the electron clouds. The larger the molecule size, the farther the electrons are from the nucleus and the more free the electrons are to move, resulting in stronger intermolecular forces. Molecular size generally increases with molecular weight, so that molecules with larger molecular weights are expected to adsorb more strongly. With polar adsorbates or adsorbents, there will also be force contributions from the dipole forces which are stronger than the dispersion forces. The adsorption forces are the same forces responsible for non-ideal gas behavior and condensation, but rather than acting between gas molecules, the forces are between the gas molecules of the adsorbate and the molecules of the solid adsorbent.

Chemisorption involves an exchange or sharing of electrons between the adsorbate molecules and the adsorbent molecules, resulting in stronger adsorption forces than found in physical adsorption. As such, chemisorption is generally irreversible.

Similar to condensation, adsorption is an exothermic process. For physical adsorption, the heat of adsorption is larger than the heat of vaporization; typical values of the heat of adsorption are between 2 and 20 kcal/gmol. For chemisorption, the heat of adsorption is usually larger.

Further discussion about adsorption will be limited to physical adsorption of gases on a solid. Therefore, the term adsorption implies physical adsorption and any reference to a fluid phase refers to the gas or vapor phase. The solid phase consists of both the solid adsorbent and the adsorbed vapor.

The equilibrium amount of a gas adsorbed, e.g., the moles of adsorbate adsorbed per mass of adsorbent, depends on several things, including the gas phase concentration, the temperature, and the identity of both the adsorbate and the adsorbent. Increasing the concentration increases the amount adsorbed; decreasing the temperature also increases

the amount adsorbed. At a given temperature, a graph showing the amount of gas adsorbed plotted versus the gas phase concentration is called an adsorption isotherm. A graph of the gas phase concentration as a function of temperature for a constant amount adsorbed is called an adsorption isostere.

When the gas in contact with the adsorbent is a mixture, more than one of the components of the mixture may adsorb. There is a competitive effect between the different components. Based on experimental work [22], the amount of each gaseous component adsorbed from a mixture will be less than would be adsorbed if the gas phase consisted only of that component. Components which are more strongly adsorbed singly are also those which will be preferentially adsorbed from the mixture [22].

2.2 Activated carbon

Although gases adsorb on any solid, certain solids have characteristics which enhance adsorption. Some common adsorbents include activated carbon, silica gel, molecular sieves, zeolites, polymers, and activated alumina. For a more complete list and descriptions, see, for example, Treybal [23], Ruthven [24], or Suzuki [25]. Because adsorption is a surface phemonenon, the amount of surface area available for adsorption significantly affects the amount of adsorbate which is adsorbed. Solids commonly classified as adsorbents are extremely porous, and correspondingly have large surface areas. Typical surface areas of activated carbon, for example, are on the order of 1000 m^2/g. Dubinin [26] classified pores by size into micropores (equivalent radii < 6-7 Å), supermicropores (6-7 Å < radii < 15-16 Å), transitional pores (18-19 Å < radii < 1000-2000 Å), and macropores (radii > 1000-2000 Å). Although these terms are commonly used, the definitions are not universal; for example, in the ASTM Standard D

2652 [27], micropores are defined as pores with radii < 40 Å, transitional pores as 40 Å < radii < 5000 Å, and macropores as radii > 5000 Å. For activated carbon, about 95% of the total surface area is in pores with radii less than 18-20 Å [21].

In addition to the total surface area, the pore size distribution also affects the adsorption characteristics of that solid. A wide pore size distribution allows many different gases (of different sizes) to be adsorbed; a narrow pore size distribution limits the gases which may be adsorbed, e.g., an adsorbent with only small pores will not adsorb larger gas molecules. For example, activated carbon usually has a wide pore size distribution while molecular sieves usually have a very narrow pore size distribution. Typical graphs of the pore size distribution for various adsorbents are shown in Ruthven [24] and Suzuki [25].

Surface polarity also affects the amount of gas adsorbed. Polar adsorbents adsorb polar adsorbates (e.g., water) more strongly than non-polar adsorbates; this is due to the presence of dipole forces in addition to dispersion forces. Polar adsorbents are sometimes referred to as hydrophilic. Non-polar adsorbents, referred to as hydrophobic, are much less sensitive to the adsorbate polarity.

The goal of a filter in removing VOCs from indoor air is to remove many different organics simultaneously. These different organics are of different sizes and different polarities, so that a non-polar adsorbent with a wide pore size distribution is desirable. Activated carbon is the only adsorbent which satsifies both criteria, and as such is the adsorbent currently used in such filters. Although some information about other adsorbents is presented in this work, e.g., values of the heat of adsorption on molecular sieves, activated carbon is the only adsorbent considered for the VOC filter in this work.

Activated carbon (also called activated charcoal) can be made from a variety of sources, such as wood, coal, fruit pits, fruit shells (e.g., coconut shells or walnut shells) and various synthetic polymers. A two-stage process is necessary to create the highly porous activated carbon: carbonization and activation. The final product and its properties are dependent on both the starting material and the processing procedure (time, temperatures, method, etc.). The following is a summary of the description in *Active Carbon* [21] of the manufacturing process:

Carbonization. The carbonization part of the process involves pyrolysis of the starting material, typically at temperatures of 400-600°C. The non-carbon elements present are removed as gases, leaving an irregular arrangement of elementary graphitic crystallites. The spaces between the crystallites are at least partially filled with amorphous carbon as a result of the deposition and decomposition of tarry substances. The carbon at this point is not "active"; the specific surface area is only on the order of several m^2/g.

Activation. The second part of the process is activation, in which an activation agent (steam, CO_2, etc.) reacts with the carbon. Initially, "burn-off" occurs, in which the amorphous carbon is burnt out and the pores between the crystallites are opened up. Later, some of the carbon of the crystallites is burned. Continued heating will eventually lead to destruction of micropores, while increasing the number of transitional pores and macropores. Activation with steam is typically at 750 to 950°C; activation with CO_2 is typically at 850-1100°C.

The two-step process just described is called physical activation. An alternative method of producing activated carbon is chemical activation, in which a substance which restricts the formation of tar (e.g., zinc chloride) is added to the starting material before carbonization. A separate activation step is then unnecessary.

There are several types of activated carbon: granular, powdered, and fibers. The manufacturing process begins with crushing of the initial substance (e.g., wood charcoal). There are then two possible paths. One option is that it can be sized, carbonized, and activated to form granular activated carbon, and, if desired, then dry ground to produce powdered activated carbon. The alternative is to form pressed activated carbon. After the initial crushing, the carbon is ground. It is then mixed with wood tar and kneaded to a uniform plastic mass. Extrusion of the mass into strings of 1-8 mm diameter which are cut to lengths of 3-15 mm result in carbon pellets of uniform size and shape. The pellets are then aged and "pre-dried" before undergoing the carbonization and activation process. The result is a more uniformly shaped granular activated carbon.

Activated carbon fibers can be produced through several means [25]. Synthetic fibers may be carefully carbonized and activated to produce activated carbon fibers. Alternatively, the plastic mass obtained in making pressed activated carbon may be spun to produce fibers, which are then activated.

Another "type" of activated carbon is activated carbon impregnated media. This is not actually a different type of activated carbon, but rather powdered activated carbon that is thermally bonded to a substrate, e.g., non-woven polyester or fiberglass [28].

There is only a finite amount of space available for adsorption on a sample of activated carbon, and eventually the activated carbon will saturated, unable to adsorb anything more. The carbon can then be regenerated. Regeneration is a desorption

process, accomplished by any combination of the following: clean air, high temperatures, low pressures, or steam to drive off the adsorbate. If the pores of the activated carbon become permanently clogged, resulting in a decrease in the adsorption capacity even after regeneration, the carbon can be reactivated. Reactivation means that the carbon goes through the activation process again; there is a loss of carbon in the process and the pore structure may be changed.

Because of the different starting materials used, and variation in the process procedure, there are many different activated carbons. Some may have an extensive micropore structure; others may have more larger pores. Calgon Carbon Corporation, for example, makes 29 types of activated carbon in 150 different grades [29]. For adsorption of VOCs from air, a highly microporous carbon is desirable.

There are several systems of rating activated carbons, including the iodine number, the carbon tetrachloride activity, and the molasses number. The carbon tetrachloride activity test [30] consists of passing a CCl_4-air mixture (total flow is 1670 ± 15 ml/min, CCl_4 concentration is 250 ± 10 mg/l) through a carbon bed of known weight. The temperature is maintained at 25°C. After every 10 minutes, the bed is weighed; when the change in weight is small enough, the carbon tetrahloride activity is equal to 100 times the increase in weight of the bed (from the initial desorbed bed) divided by the weight of the carbon.

In addition to classifying carbon by its adsorptive properties, granular activated carbon is also classified by size, according to the U.S. Sieve Series [31]. Table 2.1 lists the opening size associated with the U.S. Sieve Series. Smaller numbers indicate larger

granule sizes. Typically a carbon will be classified by a lower and upper bound, e.g., 8 x 12, which indicates granule sizes ranging from 2.82 mm^2 (1.68 x 1.68 mm) to 5.66 mm^2 (2.38 x 2.38 mm).

Table 2.1. U.S. Sieve Series [31]

U.S. Sieve #	Opening	
	in	mm
4	0.187	4.76
6	0.132	3.36
8	0.094	2.38
12	0.066	1.68
20	0.033	0.84
30	0.023	0.59
40	0.017	0.42
50	0.012	0.30

The actual solid density of activated carbon is typically 2.0-2.1 g/cm^3. A more useful property is the apparent or bulk density, defined as the mass of carbon per volume of the particles, i.e., the volume includes both the pore volume and the inter-particle volume. Typical activated carbon bulk densities are 0.4-0.5 g/cm^3 [31].

Activated carbon, or at least variations on it, have been around for a long time. As early as 1600 B.C., wood chars were used in Egypt for medicinal purposes [25]. In Japan, a well from the 13th century A.D. was found with a charcoal filter in the bottom [25]. After noting that water was stored in charred barrels on long sea voyages, a Russian chemist in 1785 discovered the deodorization and decolorization properties of activated carbon [21]. During World War I (1917-1918), activated carbon was used in gas masks; in the U.S., a campaign with the slogan "Eat-More-Coconut" was mounted to get coconut

shells to make the carbon from. Fruit pits and other nut shells were also collected [32]. One of the main uses of activated carbon after the war was in refining (decolorizing) sugar [21,25].

Today, in addition to the commercial building VOC removal application, activated carbon has many uses. Tabletop filters sold to clean air in homes contain thin activated carbon filters. Many range hood filters are activated carbon. Activated carbon is used for water purification, including fish tank filters. Activated carbon still has medicinal uses. It is used in shoe insoles to eliminate odors. It is also used in solvent recovery applications. On the research front, activated carbon has been used to increase hydrogen storage capacilities and allow storage at more practical temperatures [*Solar Energy*, August 1991, p. 27]. Activated carbon is also in the news as a "power source" in electric car batteries. Advantages over lead-acid batteries include being less expensive and having an output density (W/kg) 20 times greater [*Autoweek*, April 30, 1990, p. 5].

2.3 Thermodynamics

This section briefly reviews the thermodynamics of adsorption. General references on which this section is based include [33], [34], and [35]. By studying the thermodynamics of adsorption, a method for estimating the heat of adsorption can be obtained. The heat of adsorption is needed to calculate temperature changes due to adsorption within an adsorbent bed. In addition, thermodynamics has been used to develop a method for estimating multiple species adsorption [36].

Consider a single adsorbing species. Assume that the adsorbent is thermodynamically inert, i.e., the adsorbent surface area is unchanged by changes in

temperature and pressure, and adsorbed molecules do not affect the adsorbent's thermodynamic properties. The internal energy of the gas phase (U_g) and the adsorbed phase (U_s) can be expressed as functions of thermodynamic variables:

$$U_g = U_g(S_g, V_g, n_g) \tag{2.3.1}$$

$$U_s = U_s(S_s, V_s, A, n_s) \tag{2.3.2}$$

and

$$dU_g = T dS_g - P dV_g + \mu_g dn_g \tag{2.3.3}$$

$$dU_s = T dS_s - P dV_s + \phi dA + \mu_s dn_s \tag{2.3.4}$$

where the subscripts g and s stand for the gas and adsorbed phase, respectively. The ϕdA term in Equation 2.3.4 is a two-dimensional work term, where A is the adsorbent surface area and ϕ is a two-dimensional pressure called the spreading or surface pressure. Often the three-dimensional work term for the adsorbed phase, $P dV_s$, is negligible [34].

An equation analogous to the Clausius-Clapeyron equation for vapor-liquid equilibrium can be derived for vapor-adsorbate equilibrium. Through the equality of the chemical potentials of the adsorbed and gas phases at equilibrium, the following equation can be derived:

$$\left(\frac{\partial P}{\partial T}\right)_{A,n_s} = \frac{h_g - \tilde{H}_s}{T(v_g - \tilde{V}_s)} \tag{2.3.5}$$

where

$$h_g = \frac{H_g}{n_g} \tag{2.3.6}$$

$$\tilde{H}_s = \left(\frac{\partial H}{\partial n_s}\right)_{P,T,A} \tag{2.3.7}$$

The quanities v_g and $\tilde{V}_s$ are defined similarly. Assuming an ideal gas and that $\tilde{V}_s \ll v_g$:

$$\left(\frac{\partial \ln P}{\partial (1/T)}\right)_{A,n_s} = -\frac{\Delta h_s}{R} = -\frac{h_g - \tilde{H}_s}{R} \tag{2.3.8}$$

The quantity Δh_s is called the isosteric heat of adsorption. Frequently the symbol q_{st} or q_{iso} or q_s is used in the literature. Equation 2.3.8 can be used to calculate values of Δh_s from isotherm data at multiple temperatures. The calculation process, however, is by no means exact. Because isotherm data are required at a constant amount adsorbed, interpolation between measured isotherm data points is usually necessary, and the value of Δh_s is therefore dependent to some extent on the interpolation method.

The linearity of plots of $\ln p$ versus $1/T$ (van't Hoff plots), for a constant amount adsorbed, indicate that Δh_s is essentially independent of temperature [33] ($\Delta h_s/R$ is the slope). Δh_s has been observed, however, to be a function of the amount adsorbed, decreasing with increased coverage. Examples of the variation of Δh_s with amount adsorbed appear in [37], [38] and [39]. Often the isosteric heat of adsorption at zero coverage will be reported, obtained by extrapolating the van't Hoff plot to a value of $1/T = 0$.

Other different heats of adsorption can be obtained depending on which thermodynamic variables are held constant. At least four different heats of adsorption are defined in [33]. The integral heat of adsorption is as follows:

$$Q_{\text{int}} = n_s(U_g - U_s) \tag{2.3.9}$$

and the "differential" heat of adsorption (although many of the other heats, including Δh_s, are also differential quantities) is defined as:

$$q_{diff} = \left(\frac{\partial U_g}{\partial n_s}\right)_{V_g,T} - \left(\frac{\partial U_s}{\partial n_s}\right)_{V_s,A,T} \tag{2.3.10}$$

The differential heat of adsorption defined by Equation 2.3.10 corresponds to the heat of adsorption which would be measured calorimetrically. Assuming an ideal gas, it is related to the isosteric heat of adsorption by [33]:

$$\Delta h_s = q_{diff} + RT \tag{2.3.11}$$

The magnitude of the RT term is small ($RT \sim$ 0.6 kcal/gmol) in comparison with the other terms, such that $\Delta h_s \approx q_{diff}$.

Table 2.2 lists some values of the heat of adsorption reported in the literature. It is not a complete list, but is intended to illustrate typical values. Values range from approximately 4 to 22 kcal/gmol. The units of kcal/gmol are commonly used in reporting heats of adsorption values. Deitz has indexed papers with information about the heat of adsorption for the years 1900-1942 [32] and 1943-1953 [40].

The isosteric heat of adsorption has been observed by some authors to be roughly a linear function of the carbon number, e.g., [41]; others have indicated that it is a linear function of molecular weight, e.g., [42]. The heat of adsorption is larger than the heat of vaporization, although it decreases to the heat of vaporization as the amount adsorbed increases.

The spreading pressure, ϕ, often comes up in thermodynamic analyses of adsorption. In particular, it is used in Myers and Prausnitz's ideal adsorbed solution

Table 2.2 Literature reported values of the heat of adsorption.

	Carbons			Molecular Sieves		
	Δh (kcal/gmol)	type	Ref.	Δh (kcal/gmol)	type	Ref.
CH_4 methane	4.71	*	[43]	4.9		[44]
	3.9; 4.8		[44]	5.7	0	[41]
	5.32; 5.10		[45]	5.1	0	[50]
	5.2	0	[46]			
C_2H_2 acetylene	7.0		[44]			
	7.0	0	[46]			
C_2H_4 ethylene	5.6; 7.1		[44]	8.4		[44]
	7.3	0	[46]	8.5	0	[41]
C_2H_6 ethane	5.2; 7.5		[44]	9.4; 6.63		[44]
	7.4	0	[46]	9.0	0	[41]
C_3H_6 propylene	10.2		[44]	11.2		[44]
	9.8	0	[46]	11.4	0	[41]
C_3H_8 propane	10.3		[44]	8.5		[44]
	10	0	[46]	11.7	0	[41]
iC_4H_{10} i-butane	12.5	0	[46]	13.0; 8.71		[44]
	11.0		[44]			
nC_4H_{10} n-butane	13	0	[46]	13.9	0	[41]
	10.6-14.2		[47]			
C_3H_6O acetone	13.3-14.9		[39]			
C_6H_6 benzene	10.4	?	[48]	21.8	0	[41]
	13.5-16.2		[38]			
C_7H_8 toluene	15.1-17		[47]			
chlorinated hydrocarbons	8.3-13.4		[49]			
	9-16	*	[49]			

Note about the type: All heats are isosteric unless indicated otherwise in the type column. ? indicates unknown type of heat of adsorption; * indicates the integral heat of adsorption; 0 indicates the isosteric heat of adsorption at zero coverage.

theory, which can be used to predict the adsorption of mixtures [36]. From the condition that $d\mu_s = d\mu_g$ at equilibrium, an expression for the spreading pressure at constant temperature can be derived:

$$A\,d\phi = n_s(v_g - v_s)\,dP \qquad (T = \text{const.}) \tag{2.3.12}$$

Assuming an ideal gas and that $v_s \ll v_g$:

$$d\phi = \frac{n_s}{A} RT\,d\ln P \qquad (T = \text{const.}) \tag{2.3.13}$$

integrating yields:

$$\phi = \frac{RT}{A}\int_0^P n_s(P,T)\,d\ln P \qquad (T = \text{const.}) \tag{2.3.14}$$

Since the area is often unknown, and rarely is the absolute value of the spreading pressure required, the following "reduced" spreading pressure is often used instead:

$$\Phi = T\int_0^P n_s(P,T)\,d\ln P \qquad (T = \text{const.}) \tag{2.3.15}$$

For a non-ideal gas, fugacity can be substituted in place of pressure in the above equations.

2.4 Equilibria

Adsorption phase equilibria are often presented in the form of adsorption isotherms. The isotherm relates the vapor phase concentration of the adsorbing species to the adsorbed phase concentration at a given temperature. Vapor phase concentrations are expressed in a variety of units, including partial pressure, volume fraction, and moles per

unit volume. Sorbed phase concentrations are most often expressed as moles or volume of adsorbate per unit mass of adsorbent. There are six common shapes of isotherms, as classified by the International Union of Pure and Applied Chemistry, shown in Figure 2.1. The x-axis is the gas phase concentration, expressed as the ratio of the partial pressure to the saturation pressure. The y-axis is the amount adsorbed, which increases as the gas phase concentration increases.

There are numerous correlations used to describe adsorption isotherms. Some are based on theory, some are purely empirical. Table 2.3 lists some examples of different isotherm correlations. q is the moles adsorbed per unit mass; p is the vapor phase pressure of the adsorbing species, which in the presence of a carrier gas is the partial pressure of the adsorbing species; V is the volume adsorbed per unit mass. A as used in the isotherm expressions in Table 2.3 is not the area (as in Equation 2.3.2), but rather the adsorption "potential", defined in Equation 2.4.11. At very low concentrations, statistical theory predicts that the isotherm is linear with a finite non-zero slope. Not all of the isotherm correlations listed in Table 2.3 are linear with a finite non-zero slope in the limit of zero concentration; the third column of the table indicates the limiting isotherm slope for each correlation. For some of the correlations a theoretical temperature dependence for the parameters exists.

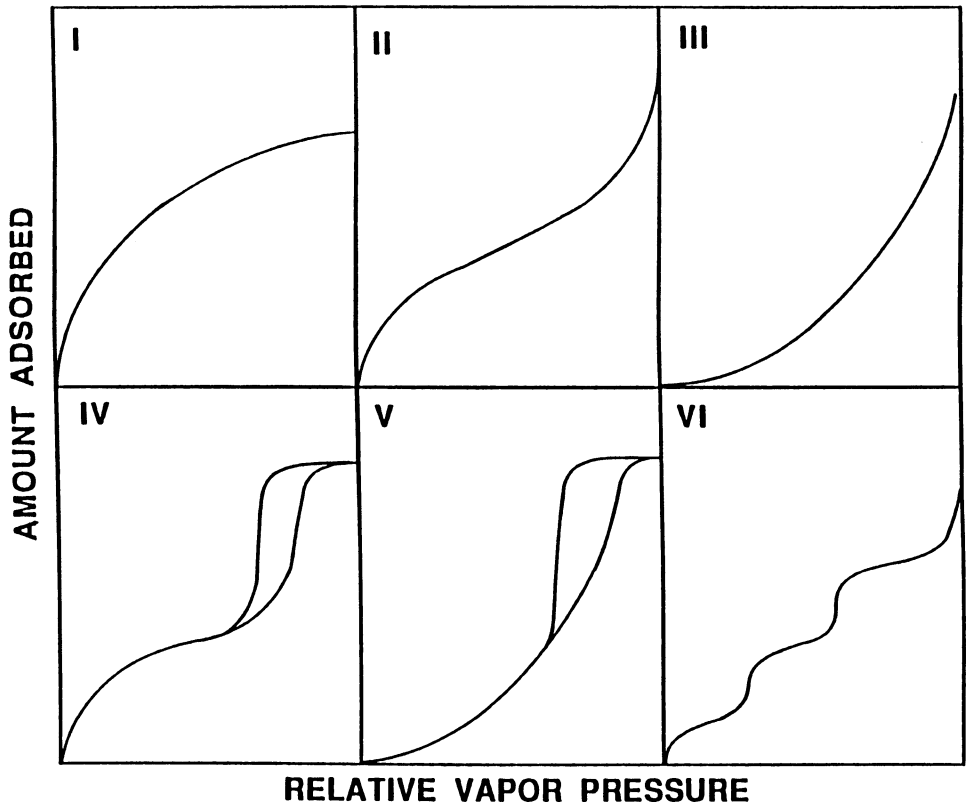

Figure 2.1 The six different isotherm types as classified by the International Union of Pure and Applied Chemistry, from ref. [51]

Table 2.3 Examples of isotherm correlations

	Equation	$\lim_{\omega \to 0}\left(\frac{\partial W}{\partial \omega}\right)$	Ref.
Linear	$q = Kp$	K	[52]
Freundlich	$q = k_F p^{(1/n_F)}$	∞	[24]
Langmuir	$\frac{q}{q_0} = \frac{kp}{1+kp}$	$q_0 k$	[24]
BET	$\frac{q}{q_0} = \frac{k_B(p/p_s)}{(1-p/p_s)(1-p/p_s+k_B p/p_s)}$	$\frac{q_0 k_B}{p_s}$	[53]
Radke & Prausnitz	$q = \left[\frac{1}{Kp} + \frac{1}{k_F p^{(1/n_F)}}\right]^{-1}$	∞	[54]
Toth	$\frac{q}{q_0} = \left[\frac{1}{(Kp)^t} + 1\right]^{-1/t}$	∞	[55]
Chakravarti-Dhar	$\frac{q}{q_0} = \frac{(k_m p)^{1/n}}{1+(k_m p)^{1/n}}$	∞	[56]
Dubinin-Radushkevich	$V = V_0 \exp(-kA^2)$	0	[26]
Dubinin-Astakhov	$V = V_0 \exp\left[-\left(\frac{A}{E}\right)^n\right]$	0	[26]

The references listed are either the original references for the isotherm or a later summary reference or book. Many of these correlations can be found and are well explained in books on adsorption, e.g., [21], [25], [24].

This work will focus on only two isotherm correlations: the linear and the Langmuir. Due to the very low concentrations of VOCs in indoor air, it is reasonable to expect that the adsorption would be in the linear region. The Langmuir isotherm will also be used to examine the consequences if the isotherm is not linear at the concentrations of

interest. The Langmuir isotherm was chosen over other isotherm correlations for several reasons: it is mathematically simple, it is one of the more commonly used isotherm correlations, and it has a finite slope at low concentrations.

2.4.1 Linear isotherm

At very low pressures, interactions between adsorbed molecules can be assumed to be negligible, so that equilibrium is described by a linear Henry's Law type equation [52]:

$$N = ap, \qquad p \to 0 \tag{2.4.1}$$

where N is the number of molecules adsorbed, a is a temperature dependent constant, and p is the equilibrium gas pressure. In terms of the variables used in the filter modeling, Equation 2.4.1 can be written as:

$$W = q = K'p = K'Py \approx K'P\omega = K\omega \tag{2.4.2}$$

where it has been assumed that the mole fraction, y, is equal to the mole ratio, ω. Recall that $\omega = y/(1-y)$, so that for low concentrations, the assumption that $\omega = y$ is excellent. Because the isotherm constant K depends on the total pressure, the pressure must always be stated for the K value to have any meaning. Throughout this work, a total pressure of 1 atm is always used, so that the values of K' and K are identical. The units, however, are different: K' is in units of [kgmol/(kg·atm)] and K is in units of [kgmol/kg].

The temperature dependence of the isotherm constant, K, can be derived from Equation 2.3.8 (the Clausius-Clapeyron type equation for vapor-adsorbate equilibrium) where the heat of adsorption, Δh_s, has been assumed independent of temperature:

$$K = K'P = K_0 P \exp\left[\frac{\Delta h_s}{R}\left(\frac{1}{T} - \frac{1}{T_0}\right)\right] \tag{2.4.3}$$

T_0 and K_0 are a reference temperature and the isotherm slope at the reference temperature. Note that the reference isotherm slope, K_0, is in units of K', i.e., [kgmol/kg atm] whereas K is in units of [kgmol/kg]. This means that the value of K_0 is independent of the total pressure.

In the literature, it is common to find the expression for the linear isotherm slope as

$$K' = K_0 \exp\left[\frac{\Delta h_s}{RT}\right] \tag{2.4.4}$$

where in this case, K_0 is the isotherm slope in the limit of $1/T \rightarrow 0$.

Since the linear isotherm constant, K, is not a function of gas or adsorbed phase concentration, Equation 2.4.3 implies that within the linear regime, the isosteric heat of adsorption is independent of concentration. This independence is not observed in practice.

2.4.2 Langmuir isotherm

The Langmuir isotherm, which is based on kinetic theory and derived by assuming that the rate of adsorption and desorption are equal, is a Type I isotherm (Figure 2.1). In terms of the partial pressure the Langmuir isotherm is as follows:

$$q = \frac{q_0 k' p}{1 + k' p} \tag{2.4.5}$$

Rewriting it in terms of the variables W and ω, where as for the linear isotherm, the constant k is equal to $k'P$:

$$W = \frac{W_0 k \omega}{1 + k\omega} \tag{2.4.6}$$

In the limit as ω becomes small,

$$W = W_0 k \omega \tag{2.4.7}$$

and the slope at low concentrations is finite, equal to $W_0 k$. The quantity W_0 is the monolayer capacity and is independent of temperature. From the kinetic derivation, the quantity k theoretically is of the following form [57]:

$$k = k'P = P k_0 T^{1/2} \exp\left[\frac{\Delta h_s}{RT}\right] \tag{2.4.8}$$

Instead of using the above equation for the temperature dependence of k, in this work the temperature dependence of k will be taken as identical to that of the linear isotherm constant (Equation 2.4.3), so that the linear and Langmuir forms agree at low concentrations. This is a reasonable approximation, since the precise form of the nonlinear isotherm is not that important - the nonlinear isotherm is used simply to examine the effect of the nonlinearity. Equation 2.4.6 can be rewritten in terms of the linear isotherm constant, $K = W_0 k$, to get:

$$W = \frac{W_0 K \omega}{W_0 + K\omega} \tag{2.4.9}$$

where

$$K = K_0 P \exp\left[\frac{\Delta h_s}{R}\left(\frac{1}{T} - \frac{1}{T_0}\right)\right] \tag{2.4.10}$$

2.4.3 Potential Theory

A different theory of adsorption was first introduced by Polanyi, called the potential theory of adsorption. Dubinin [26,58,59] has done a lot of work to further advance this theory. Because the original principles on which the potential theory was based have no physical meaning for adsorption in micropores, Dubinin has proposed renaming it the theory of volume filling of micropores. Whereas kinetic theory is based on the assumption that adsorption is a 2-D layer by layer surface area filling process, Dubinin maintains that adsorption is a 3-D volume filling process, and in fact, that the concept of surface area is invalid and irrelevant for adsorption on microporous adsorbents [26]. Evidence to support the volume based theory exists in the measured fractal dimensions of adsorbents. The fractal dimension of a surface is "a quantitative, size-independent measure of the surface irregularity" [60]. For non-porous adsorbents, the fractal dimension is around 2 [61,62], indicating an area-based filling process, whereas for microporous adsorbents, the fractal dimension is closer to 3 [61,62], indicating a volume-based filling process; see Table 2.4.

The so-called adsorption potential, A, which is not actually a potential but rather the differential molar work of adsorption [26], is equal to:

Table 2.4 Fractal dimensions of some microporous adsorbents.		
Adsorbent	Fractal dimension	Reference
highly microporous activated carbon	3.03 ± 0.25	[61]
granular activated carbon: Tsurumi HC-8	2.71 ± 0.14	[62]
granular activated carbon: Fujisawa B-CG	2.80 ± 0.16	[62]
silica gel	2.94 ± 0.04	[63]
activated alumina: Alcoa grade F-20	2.79 ± 0.03	[62]

$$A = RT \ln\left(\frac{p_s}{p}\right) \tag{2.4.11}$$

A is the change in the Gibbs free energy for adsorption based on a standard reference state of saturated vapor at the system temperature, T. For non-ideal gas behavior, fugacities can be substituted into Equation 2.4.11 in place of the pressures. The fundamental postulate of the potential theory states that the adsorption potential is independent of temperature for a given volume filling, i.e.,

$$\left(\frac{\partial A}{\partial T}\right)_V = 0 \tag{2.4.12}$$

where V is the volume of adsorbate per unit mass of adsorbent. By assuming a constant density, the number of moles adsorbed, W, can be substituted for V. Agreement with Equation 2.4.12 is very good for experimental isotherm data measured on microporous

adsorbents; see, for example, [26,47,58]. A plot of the amount adsorbed versus the adsorption potential is called a characteristic curve. If Equation 2.4.12 is satisfied, isotherm data points from different temperatures fall on a single curve.

Dubinin and Astakhov [26] proposed an isotherm form based on the similarity of the shape of the characteristic curve to the Weibull distribution:

$$\theta = \frac{V}{V_0} = \exp\left[-\left(\frac{A}{E}\right)^n\right] \tag{2.4.13}$$

where E and n are constants for an isotherm; n is a small positive integer. If n depends only on the adsorbent (and not the adsorbate), then at a given adsorbate filling, the characteristic curves of different adsorbates can be related by a constant, β, called the similarity or affinity coefficient:

$$\frac{A_2}{A_1} = \frac{E_2}{E_1} = \beta \tag{2.4.14}$$

Notice that β is a constant since E does not depend on θ. β can be approximated as the ratio of the parachors (a quantity related to the surface tension and the molar volume [64]) of the adsorbates [26]; it has also been suggested that the ratio of the molar volumes be used to estimate β [58]. Table 2.5, taken from [21], lists some experimentally obtained β values for an activated carbon with benzene as the reference vapor. Many authors have attempted correlating isotherm data for different adsorbates in this manner [65-71]. Different predictors are used to estimate β; in particular, there are many variations on ways to calculate the molar volume. Often at least curves from similar families collapse, e.g., all of the paraffins on one curve.

Table 2.5. Selected values of the affinity coefficient for adsorption on an activated carbon with benzene as the reference vapor.			
Benzene	1.00	n-Hexane	1.35
Cyclohexane	1.04	n-Heptane	1.59
Toluene	1.25	Acetone	0.88
Propane	0.78	Dichloromethane	0.66
n-Butane	0.90	Tetrachloromethane	1.05
n-Pentane	0.78	Tetrafluoroethylene	0.59
Taken from [21]; references for the β value given in [21].			

There are other isotherm equations based on the potential theory which are commonly used. The Dubinin-Radushkevich equation is essentially the same as Equation 2.4.13, except with n=2:

$$V = V_o \exp\left[-B\frac{T^2}{\beta^2}\ln^2\left(\frac{p_s}{p}\right)\right] = V_o \exp\left[-\frac{\kappa_s}{\beta^2}A^2\right] \tag{2.4.15}$$

Experimental values of β, κ_s, and V_0 obtained for 13 different hydrocarbons on 7 different activated carbons are presented in [72]. They also attempted to predict V_0 from adsorbent properties. κ_s was observed to be approximately constant for different carbons.

The Dubinin-Polstyanov equation consists of two terms and is based on two peaks in the pore size distribution:

$$V = V_{o1} \exp\left[-\left(\frac{A}{E_1}\right)^2\right] + V_{o2} \exp\left[-\left(\frac{A}{E_2}\right)^2\right] \tag{2.4.16}$$

Stoeckli [73] has proposed that for heterogeneous micropores, the following form is appropriate:

$$V(y) = \int_0^\infty f(B)\exp\left[-By\right] dB \tag{2.4.17}$$

$$y = \left(\frac{T}{\beta}\right)^2 \ln^2\left(\frac{p_s}{p}\right)$$

where $f(B)$ is the distribution of the micropore volume.

All of the isotherm equations for the potential theory are expressed as the volume adsorbed per unit mass of adsorbent. By assuming a constant density, W can be substituted for V in the above equations.

The potential theory can also be used to predict the concentration dependence of the isosteric heat of adsorption [21,26]:

$$\Delta h_s = \Delta h_{vap} + A + \alpha R T^2 \left(\frac{\partial \ln p/p_s}{\partial \ln V}\right)_T \tag{2.4.18}$$

where α is the thermal coefficient of volume expansion:

$$\alpha = \frac{1}{v}\left(\frac{\partial v}{\partial T}\right)_{\ln(p/p_s)} \tag{2.4.19}$$

v is the molar volume of the adsorbate.

Often the potential theory based isotherm equations fit the data better than other isotherm equations (Langmuir, Fruendlich, BET), particularly over a large range of data [68,74,75]. Because there is also some ability to predict adsorption of other species, and because theoretically only two isotherm points are needed to predict the complete form of the isotherm at all temperatures, the potential theory is a more complete theory.

One of the drawbacks of the potential theory of adsorption, however, is its incompatibility with Henry's Law at low concentrations. The isotherm slope in the limit of zero concentration is zero (although many other isotherms have similar problems, e.g., see Table 2.3). In addition, based on theory and the second law of thermodynamics, the temperature invariance of the adsorption potential is only valid for fillings greater than 15 to 20 percent [26]. This makes the potential theory inapplicable for work with very low concentrations.

However, the isotherm equations, such as the Dubinin-Astakhov equation, can be "patched" to a linear isotherm by assuming that the isotherm is linear at concentrations below the point where $(\partial V/\partial p) = V/p$ [25,26]. For example, for the Dubinin-Astakhov equation, the isotherm is assumed linear at pressures less than:

$$p_{lin} = p_s \exp\left[-\left[\frac{1}{n}\left(\frac{E}{RT}\right)^n\right]^{\frac{1}{n-1}}\right] \tag{2.4.20}$$

and the Henry's Law constant is then as follows:

$$K' = \frac{W_0}{p_s}\exp\left[\frac{n-1}{n}\left\{\frac{1}{n}\left(\frac{E}{RT}\right)^n\right\}^{\frac{1}{n-1}}\right] \tag{2.4.21}$$

2.5 Mixtures

For the application of VOC removal from indoor air, it will be necessary to consider the adsorption of multiple gases simultaneously. The equilibrium for one species may be affected by the presence of other adsorbing species. Isotherm expressions for multicomponent equilibria exist [21,24], but require data for all adsorbing combinations to determine the parameters. An alternative technique, developed by Myers and

Prausnitz [36], called the Ideal Adsorbed Solution Theory, provides a thermodynamic basis for obtaining the mixture isotherm from the pure component isotherms. By equating the chemical potentials of each species, similar to solution theory for vapor-liquid equilibria, the following expression is obtained:

$$P y_i \nu_i = f_i^o(\Phi)\gamma_i x_i \tag{2.5.1}$$

where

P	=	total pressure
y_i	=	vapor phase mole fraction of species i
ν_i	=	fugacity coefficient of species i
$f_i^o(\Phi)$	=	the equilibrium gas phase fugacity of pure i at the standard state, which is the temperature and reduced spreading pressure (Φ) of the mixture
γ_i	=	activity coefficient of species i in the adsorbed phase
x_i	=	adsorbed phase mole fraction of species i

The reduced spreading pressure is given by Equation 2.3.15.

Assuming ideal gas behavior for the vapor phase ($f_i^o = p_i^o$, $\nu_i = 1$), for an ideal adsorbed solution ($\gamma_i = 1$), Equation 2.5.1 simplifies to the equivalent of Raoult's Law:

$$P y_i = p_i = p_i^o(\Phi)x_i \tag{2.5.2}$$

The concentrations involved in VOC removal from indoor air are sufficiently low that ideal solution behavior will be assumed.

Writing Equations 2.5.1 and 2.3.15 for each of the N adsorbing components, along with the requirement that the reduced spreading pressure of each species in their standard state is equal to the reduced spreading pressure of the mixture:

$$\Phi_1^o = \Phi_2^o = \ldots = \Phi_i^o = \ldots = \Phi_N^o \tag{2.5.3}$$

and that the mole fractions sum to one:

$$\sum_{i=1}^{N} x_i = 1 \tag{2.5.4}$$

$$\sum_{i=1}^{N} y_i = 1 \tag{2.5.5}$$

results in (3N+1) equations and (4N+1) unknowns. By specifying N of the unknowns, e.g., P, $y_1, y_2, \ldots, y_i, \ldots, y_N$ the other unknowns may be determined.

Myers and Prausnitz demonstrated a number of examples for which the results of their theory were quite good [36]. In [74], it is demonstrated that it is important to have pure component isotherm correlations which fit the data well. In addition, because the spreading pressure involves integration from the point of zero concentration, the behavior of the different isotherm correlations in the low pressure region is also important. Recall that in Section 2.4 (Table 2.3) it was shown that many of the isotherm correlations do not exhibit the expected finite linear behavior at low concentrations. Even though $(\partial q/\partial p)_{p\to 0} = 0$ for the Dubinin-Radushkevich equation, it gave the best results. The results were even better than the Langmuir equation, which has a finite slope at p=0, primarily because the Dubinin-Radushkevich equation fit the pure component isotherm data significantly better than the Langmuir equation. Use of the Freundlich equation resulted in significant errors, due in part to the fact that $(\partial q/\partial p)_{p\to 0} = \infty$ [74].

If a linear isotherm is assumed, corresponding to Henry's Law type behavior, then the ideal adsorbed solution theory leads to the result that each component is adsorbed as if the others were not there, i.e., there are no interference effects. This is consistent with the theoretical basis of the linear isotherm [52].

Costa et al. [76] used real adsorbed solution theory, i.e., they did not assume that the activity coefficients were equal to one, to predict the adsorption equilibrium for binary and ternary mixtures of methane, ethane, ethylene, and propylene on activated carbon. Other similar theories, for example which take into account the energetic non-uniformity of the pores, have been developed [77-79].

2.6 Isotherm data of VOCs

As documented in Chapter 1, the VOC concentrations in indoor air are very low, typically in the ppb range. Isotherm data at these low concentrations are virtually non-existent, which makes the design of filters for this application difficult. In all, only six sources of low concentration isotherm data for hydrocarbons on activated carbons were found, and even these low concentration data are at higher concentrations than encountered in indoor air. In Figures 2.2 through 2.7, much of the isotherm data from these six references are replotted. Note that the scales for each graph are different. In Figure 2.8, the data from all six sources are plotted together for comparison. The symbols correspond to those used in the individual graphs.

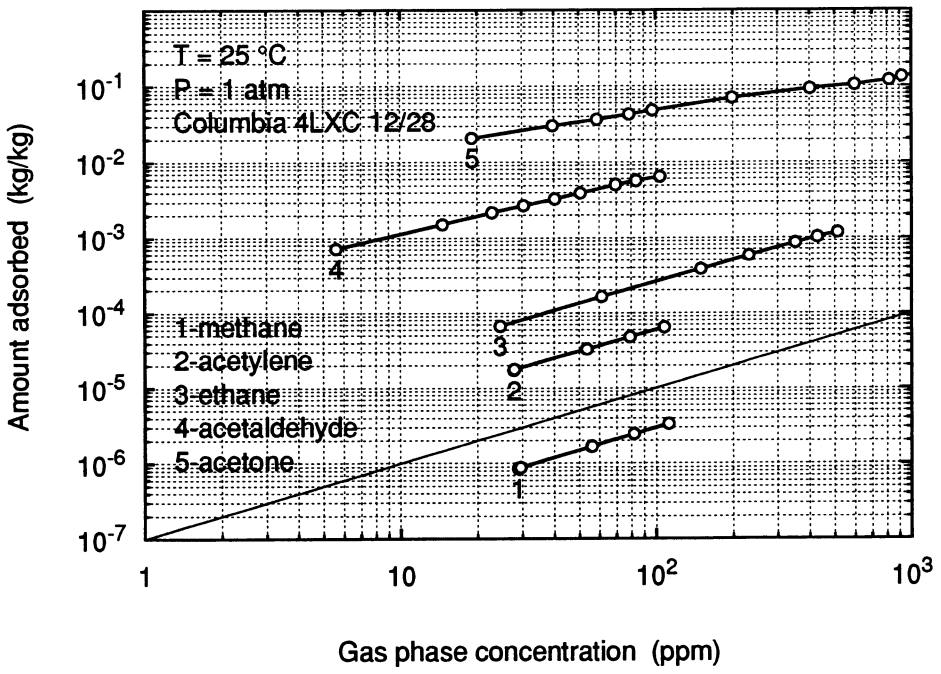

Figure 2.2 Isotherm data replotted from Forsythe [80].

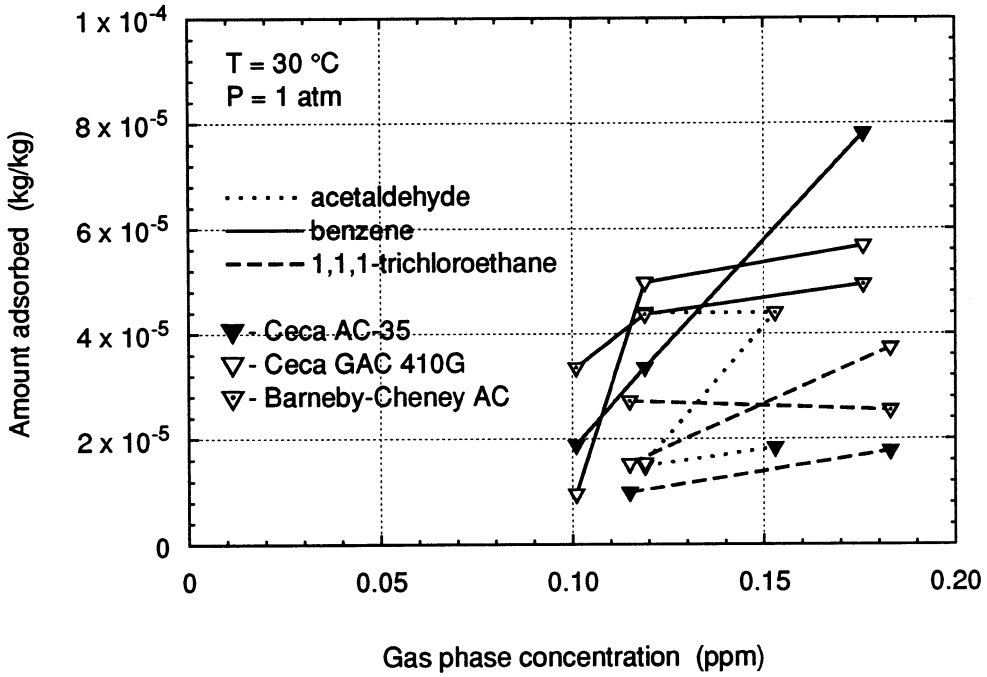

Figure 2.3 Isotherm data replotted from Ramanathan et al. [81].

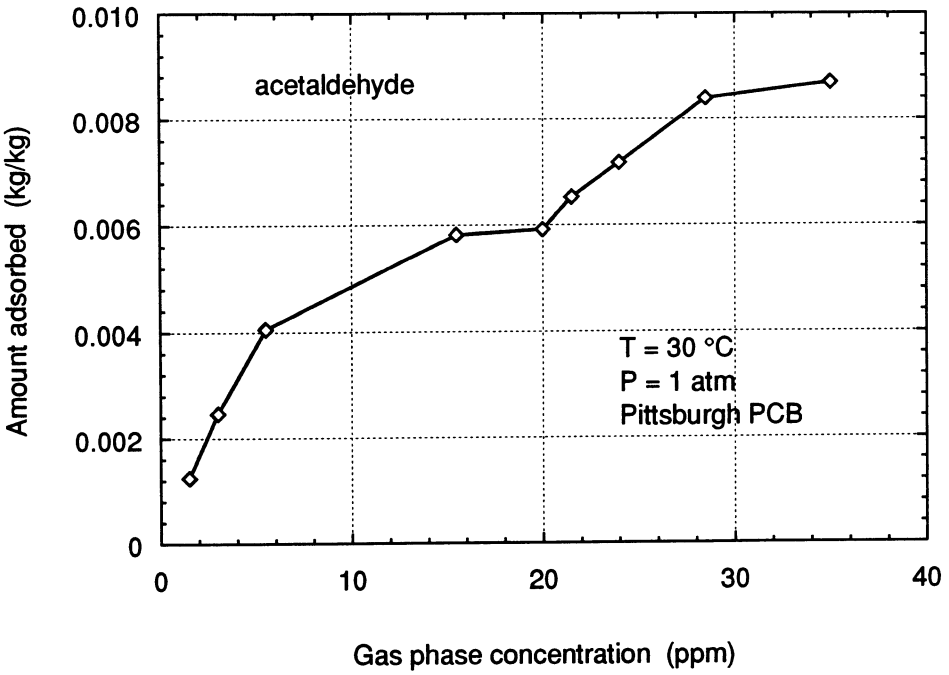

Figure 2.4 Isotherm data replotted from Kyle and Eckhoff [82].

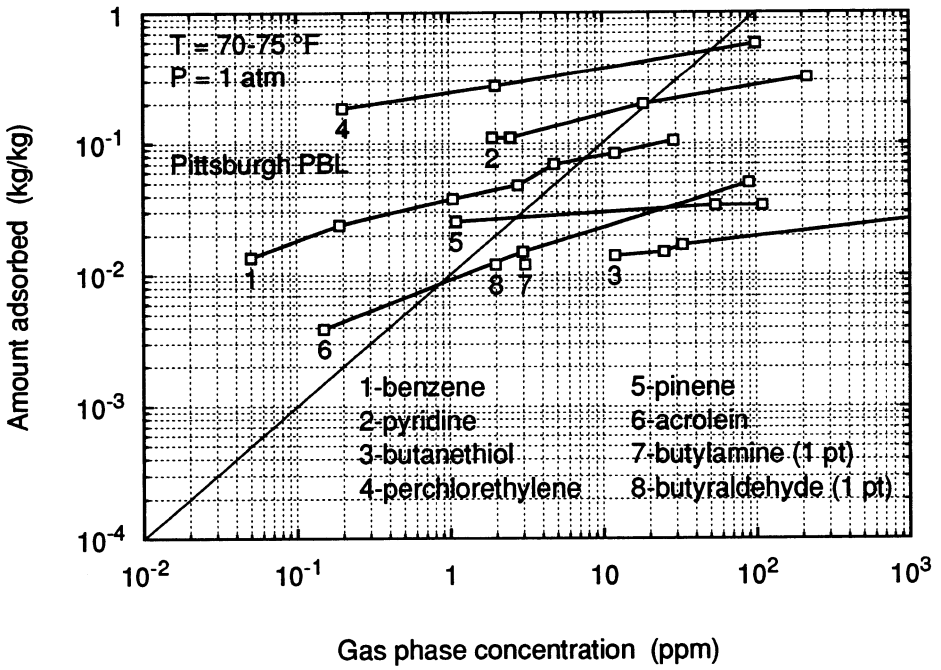

Figure 2.5 Isotherm data replotted from Clapham et al. [83].

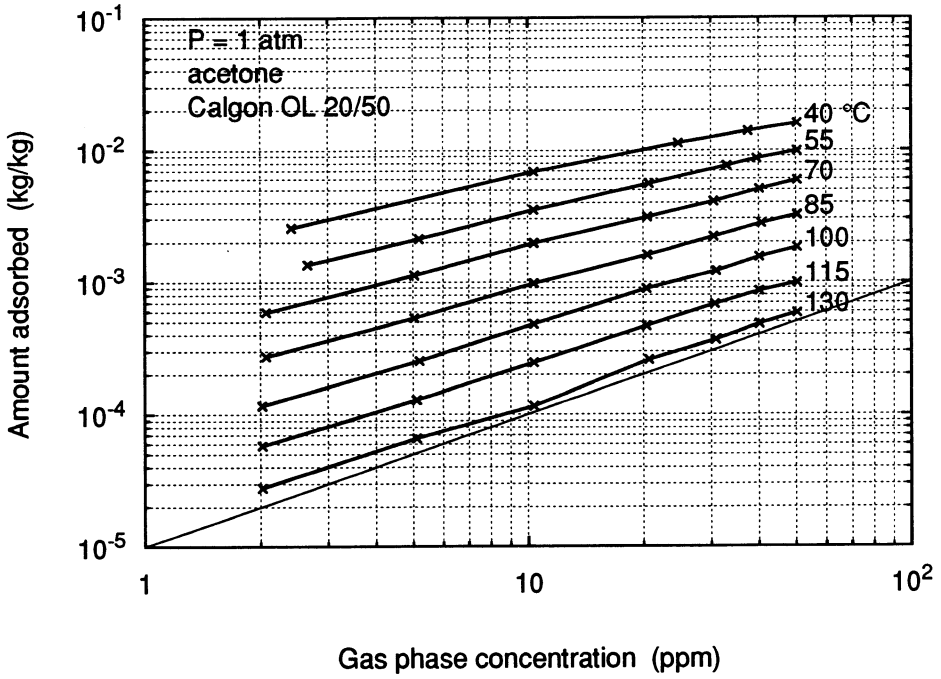

Figure 2.6 Isotherm data replotted from Schaefer [39].

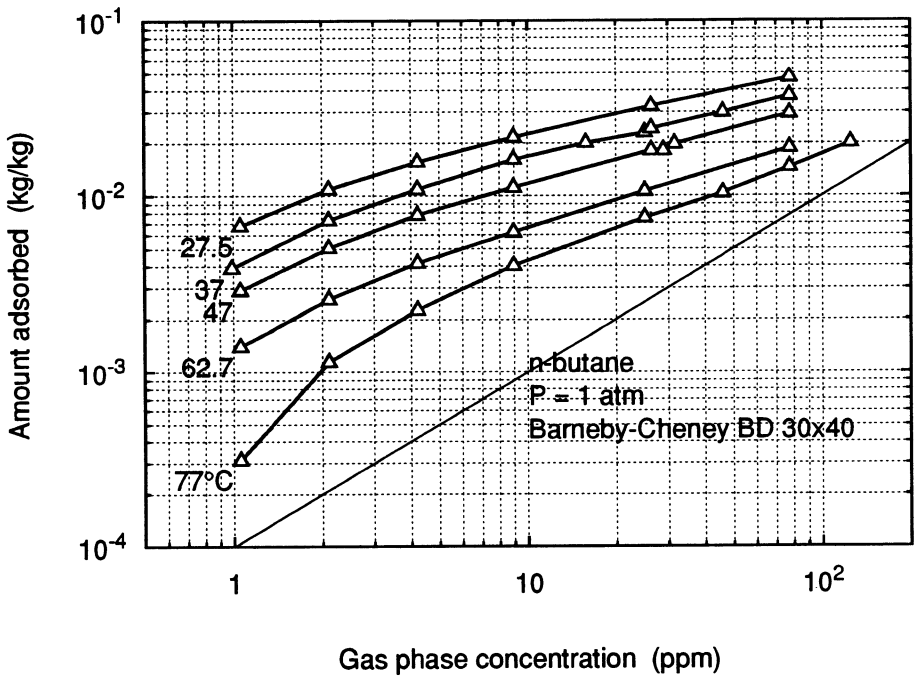

Figure 2.7(a) Isotherm data replotted from Robell et al. [47].

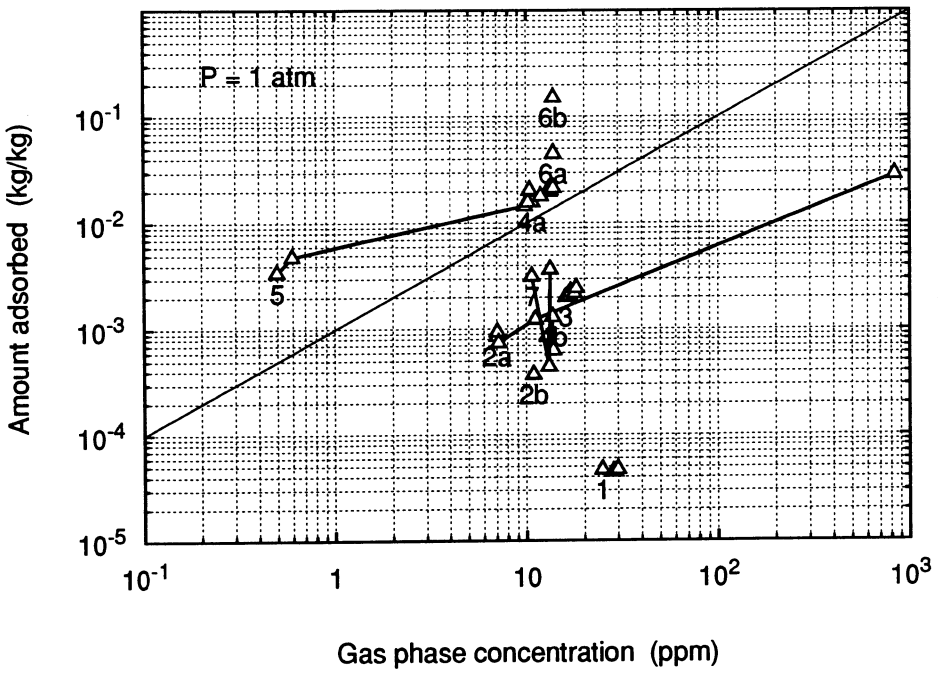

		Mesh size	Temperature, °C	# of data points
1	C_2H_4	16 x 20	24	5
2	C_3H_6	30 x 40	a=25-27, b=46	5,1
3	C_3H_8	30 x 40	25	6
4	n-C_4H_{10}	8 x 12	a=25, b=105-107	6,2
5	n-C_4H_{10}	30 x 40	24-27	6
6	C_7H_8	8 x 12	a=107, b=67	1,1
7	CH_3CCl_3	30 x 40	101-102	3

Figure 2.7(b) Isotherm data replotted from Robell et al. [47].

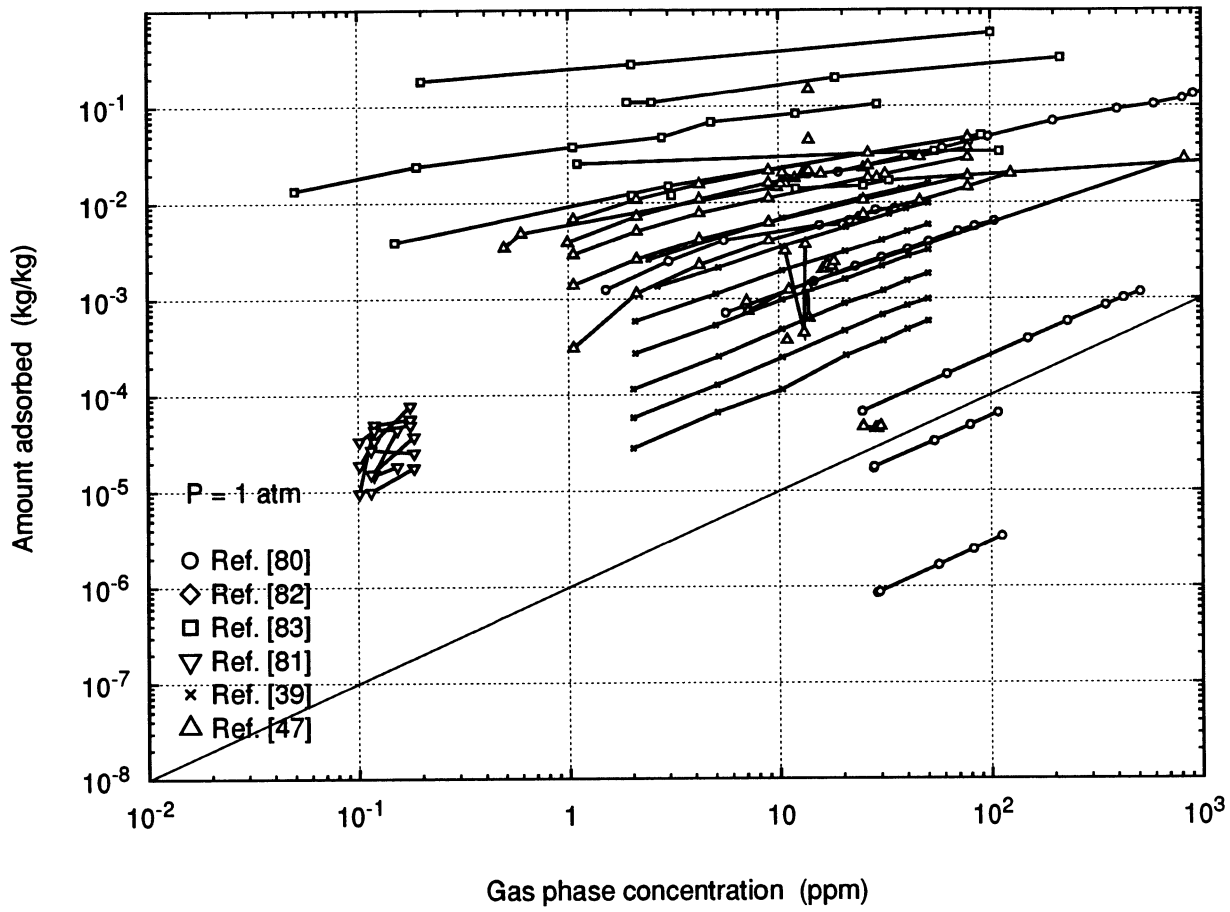

Figure 2.8 Isotherm data from the five low concentration references, i.e., the data from Figures 2.2-2.7 all plotted on one graph.

If the isotherm is linear, then on a log-log plot, the isotherm is a straight line with a slope equal to one. In each of the log plots, a line of slope one has been drawn to help indicate how linear or nonlinear each data set is. Although many of the isotherms appear to be nonlinear, the concentrations are considerably higher than the low ppb concentrations found in indoor air.

The range of the low concentration data is somewhat disturbing. For example, for a benzene concentration of 100 ppb at 25°C, the amount adsorbed ranges from 1.24×10^{-7} kgmol/kg carbon [81] to 2.44×10^{-4} kgmol/kg carbon [83]. Table 2.6 compares the different carbons used by the two groups of authors. The difference in the measured values is three orders of magnitude, and while some of the difference might be attributable to the different carbons, it seems unlikely that the different carbons could account entirely for the difference.

Table 2.6. Comparison of benzene data and carbons from [81] and [83].

	Ramanathan et al., 1988, T=30°C, [81]			Clapham et al., 1970, T=21-24°C, [83]
Amount adsorbed at approx. 100 ppb (kgmol/kg)	1.24×10^{-7}	2.42×10^{-7}	4.30×10^{-7}	2.44×10^{-4}
Carbon name	CECA GAC 410G	CECA AC-35	Barneby Cheney AC	Pittsburgh BPL
CCl_4 activity	60	65	60	62.7
Surface area (m^2/g)	1050-1150	1150	1050-1150	1000-1200
Base material	Coal	Pinewood charcoal	Coconut shell	Bituminous coal

At higher concentrations, there is much more isotherm data available for hydrocarbons on activated carbon. Table 2.7 lists some of the isotherm data. Hines et al. [84] have compiled a database of isotherm data on various adsorbents. Their list is based

on a search of eighteen databases (e.g., Chemical Abstracts); much of the older data are not included in this list. Deitz put together an extensive bibliography of all kinds of adsorption information, including isotherm data for the years 1910-1942 [32] and 1943-1953 [40]. Some of the most commonly cited data includes that of Lewis et al. [22,68], Ray and Box [85], and Szepesy and Illes [86,87].

Table 2.7. Isotherm data on various activated carbons.

Compound	References
CH_4	45, 46, 65-67, 68, 74, 76, 80, 85-91
C_2H_2	46, 68, 80, 85, 86, 90, 92
C_2H_4	46, 47, 68, 76, 85-90, 92-94
C_2H_6	46, 68, 74, 76, 80, 85-91, 93
C_3H_6	46, 47, 68, 76, 85-90, 94, 95
C_3H_8	46, 47, 65, 68, 85-88, 90, 91, 94, 95
i-C_4H_{10}	46, 68, 91
n-C_4H_{10}	46, 47, 65, 85, 91
i-C_5H_{12}	91
n-C_5H_{12}	65, 91
C_6H_6	48, 72, 77, 81, 83, 90, 96, 97
C_7H_8	47, 72, 77, 98
acetaldehyde	80-82, 99
acetone	39, 72, 77, 80, 90, 99
cyclohexane	48, 90, 97
others	47, 65, 68, 72, 77, 81, 83, 90, 93, 97-99, 100

Some references which contain isotherm data for VOCs on silica gel include [22, 42, 67, 68, 91, 92, 94, 95, 101-104]. Some references which contain isotherm data for VOCs on molecular sieves and zeolites include [37, 50, 75, 90, 93, 105-107].

Isotherm data on the adsorption of binary and ternary mixtures also exists, although almost all of the data are at higher concentrations than of interest for VOC removal from indoor air. Figure 2.9 illustrates isotherm data for n-butane on an activated carbon with various amounts of toluene pre-adsorbed on the carbon. Isotherms at 27°C and 67°C are plotted for 0, 5, 10, and 50 ml STP toluene/g carbon pre-adsorbed (0, 0.021, 0.041, and 0.206 kg toluene/kg carbon, respectively). It is evident that the pre-adsorbed toluene has a significant effect on the amount of n-butane adsorbed. References for higher concentration data include [22, 74, 76, 89, 91, 92, 94, 95, 108] for activated carbon, [22, 42, 91, 92, 94, 95, 101] for silica gel, and [50] for molecular sieves.

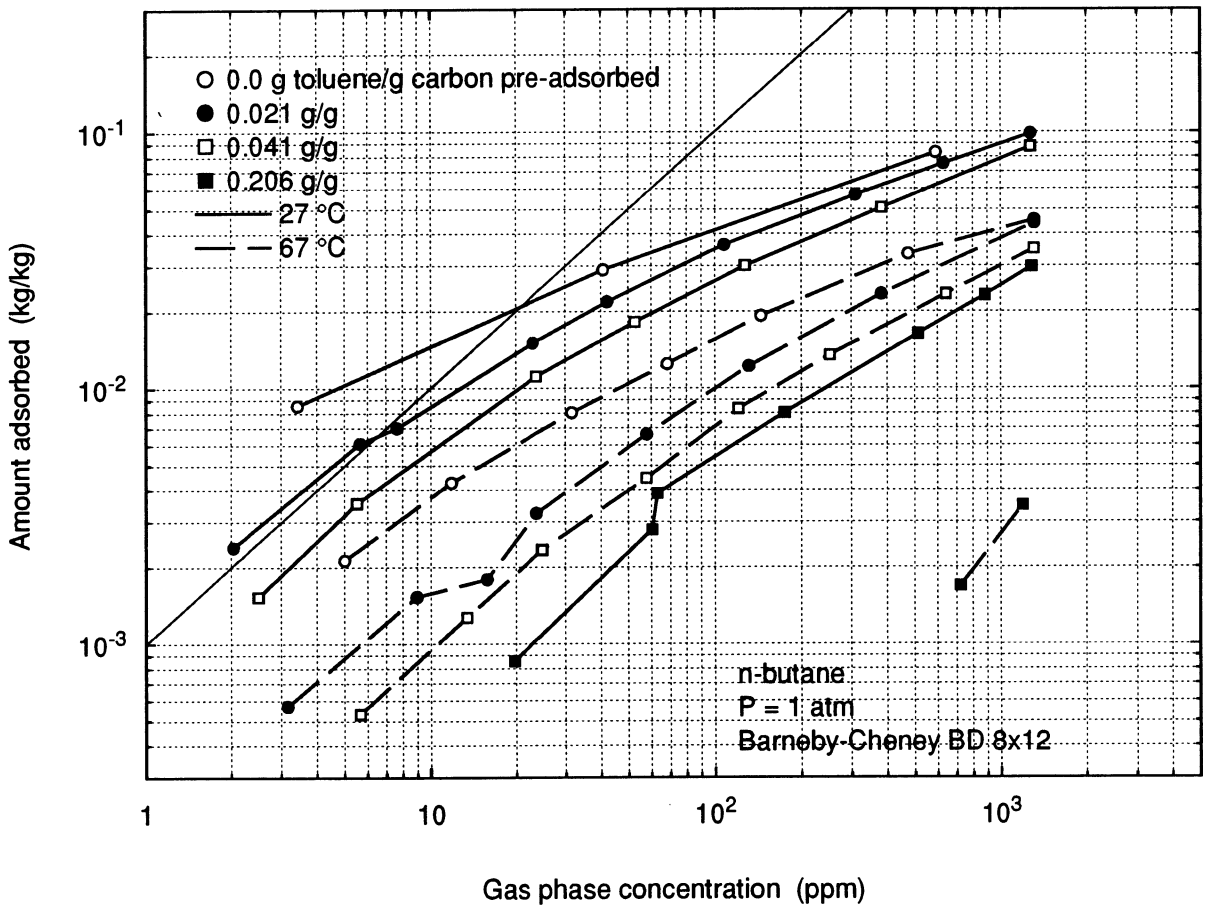

Figure 2.9 Isotherm data illustrating the effect of pre-adsorbed toluene on the adsorption of n-butane. The data is replotted from Robell et al. [47].

As previously mentioned, Lewis et al. [22] found that the more strongly adsorbed pure components are those which are preferentially adsorbed in mixtures. In addition, the amount adsorbed when part of mixture was observed to be less than adsorbed when the component was pure. Based on isotherm measurements of methane, acetylene, ethane, propylene, propane, i-butane, and n-butane on two different activated carbons and silica gel, Lewis et al. [68] found that the amount adsorbed generally increased with increasing molecular weight and increasing critical temperature, although the correlation was not absolute. For silica gel, unsaturation of the hydrocarbon molecule also played a role; the degree of saturation may also have some affect for adsorption on activated carbon. The amount adsorbed for different classes of VOCs on activated carbon has also been observed to roughly correlate with normal boiling point [109].

2.7 Adsorption of water vapor and VOCs

Of particular interest for the application of VOC removal from indoor air is the effect of water vapor on the adsorption of organic compounds. As a general rule of thumb, it has been stated that water has no effect on organic adsorption on activated carbon at relative humidities less than 50% [110]. Whereas the pure component organic isotherms are almost all Type 1 isotherms, the water vapor isotherm on activated carbon is usually Type 5 [77, 98]. The point at which the hysteresis begins is around 50% relative humidity. In Figure 2.10, isotherm data from [98] has been replotted.

Ripperger and Germerdonk [98] reported that for simultaneous adsorption of toluene and water vapor on activated carbon, the difference in the toluene adsorption with water vapor at relative humidities of 0 and 55% was small. At a relative humidity of 90%, the amount of toluene adsorbed was significantly reduced. The same behavior was

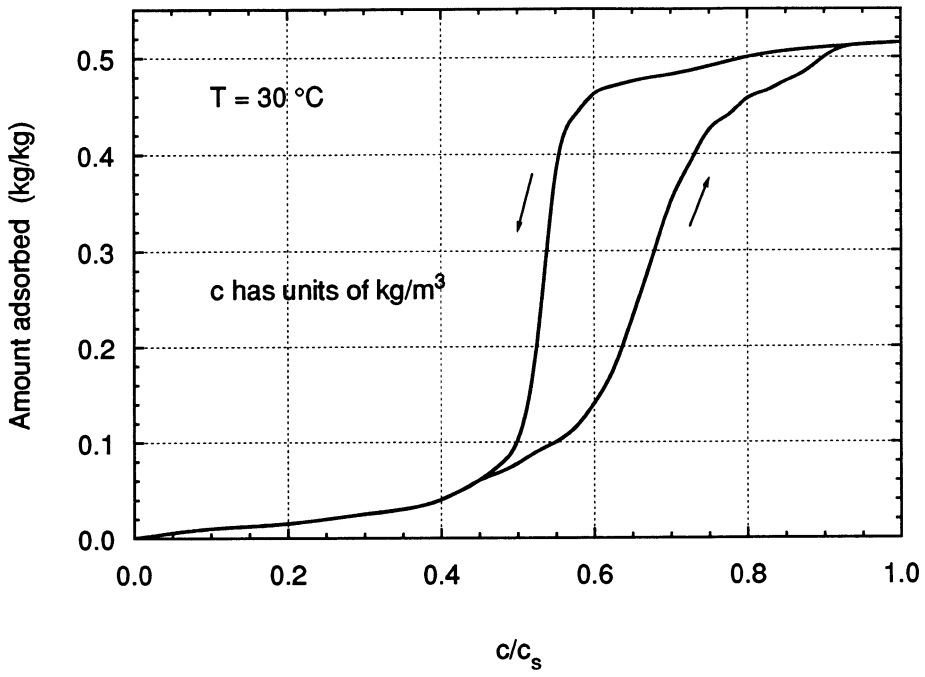

Figure 2.10. Adsorption isotherm of water vapor on an activated carbon, replotted from Ripperger and Germerdonk [98].

observed for the adsorption of butan-1-ol and water vapor. They also found that if water vapor were initially adsorbed on the carbon, it decreased the amount of toluene adsorbed, but had no effect on the amount of butan-1-ol adsorbed. This difference was attributed to the fact that butan-1-ol is highly water soluble.

Werner [111] measured adsorption data for trichloroethylene and water vapor on activated carbon at trichloroethylene concentrations of roughly 50, 100, 170, and 225 ppm and relative humidities of 5, 25, 50, 65, and 85%. Werner's data, reproduced in Figure 2.11, indicates that relative humidities less than 50% did lessen the amount of trichloroethylene adsorbed, although the effect was stronger as the relative humidity increased. Werner found that the effect of relative humidity on the amount adsorbed was greater at the lower trichloroethylene concentrations. This phenomonon was also

observed by Nelson et al. [112]. Robell et al. [47] measured some VOC adsorption data at several relative humidities. Breakthrough curves illustrating the effect of relative humidity are presented in [112] and [113].

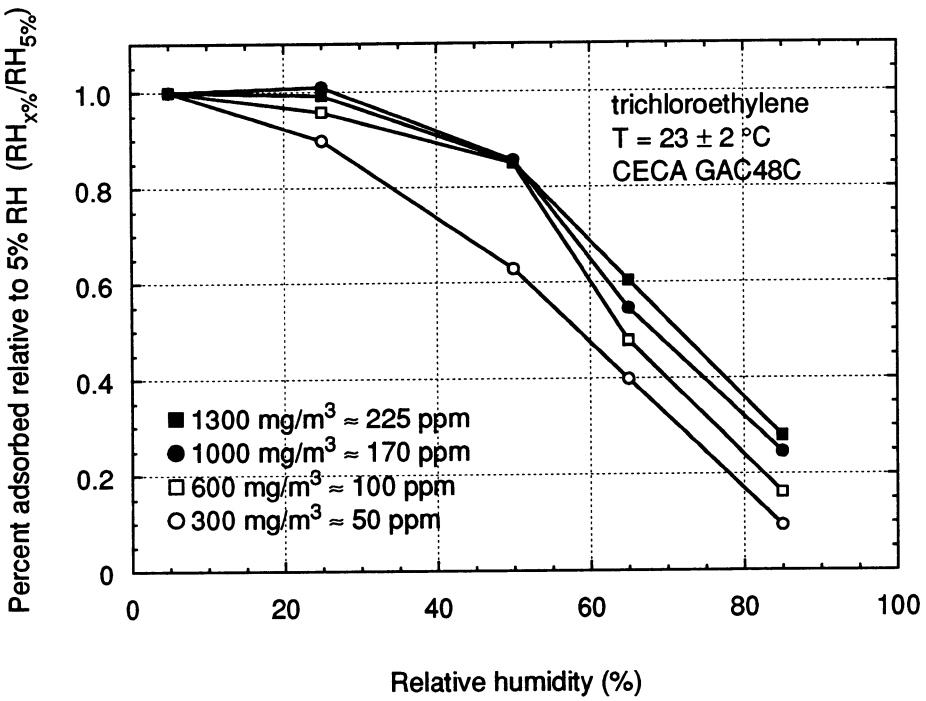

Figure 2.11. Effect of relative humidity on the amount of trichloroethylene (TCE) adsorbed on activated carbon at different TCE concentration levels (from [111]).

The standard theories of multicomponent adsorption may not apply for adsorption with water vapor. It is believed that capillary condensation of the water vapor occurs within the pores at high relative humidities, and more complex methods are required to account for this phenomenon [77, 98].

2.8 Isotherm data for carbon filter design

Clearly, to design a carbon adsorption filter for removing VOCs from indoor air, isotherm data for all of the different VOCs on the particular carbon of choice would be required. For several reasons, this is a completely unrealistic expectation. First of all, the identity of all of the VOCs is usually not known, nor even how many different VOCs are present. Secondly, the isotherm data at the very low concentration encountered in indoor air does not exist. Even the higher concentration isotherm data does not come close to including all of the compounds found in indoor air. Third, the interaction effects of the many VOCs at the low concentrations are unknown.

As a first approximation, because the concentrations are so low, it is reasonable to assume a linear isotherm for the individual VOCs. As a consequence of this assumption, any interference effects between competing adsorbates is negligible. Thus the multicomponent adsorption problem has been reduced to many single component adsorption problems.

As for the lack of very low concentration isotherm data, one might consider using the higher concentration isotherm data to estimate the initial slopes, e.g., by using Equation 2.4.21. However, the fitted correlations are not based on any data in the low concentration range, and as a result, the accuracy of these correlation in predicting the low concentration slopes is questionable. For example, Figure 2.12 illustrates the values of the isotherm slope at 25°C as estimated from Equation 2.4.21 with parameters taken from [72] for twelve different organics on Tsurumi HC-8 coconut shell carbon. The mole fraction (at 1 atm total pressure) below which the isotherm should be linear according to Equation 2.4.20, y_{lin}, is also shown.

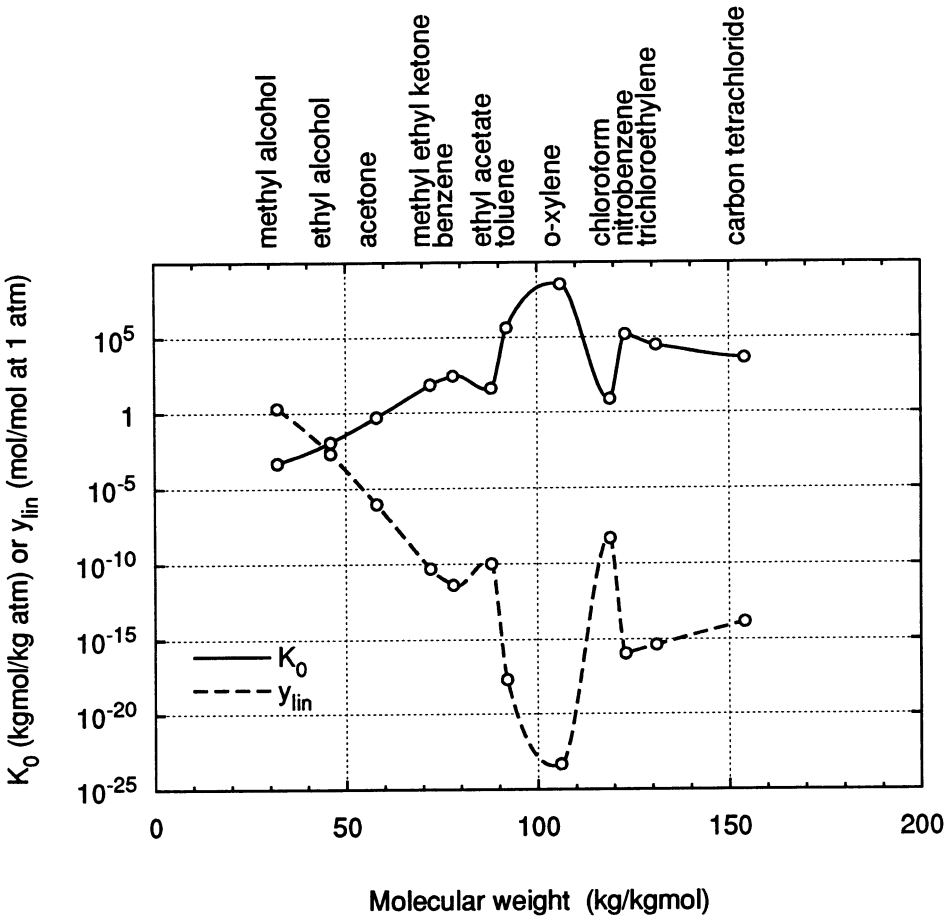

Figure 2.12. Limiting isotherm slopes estimated from Equation 2.4.21, using the parameter values given in [72]. Also shows the mole fraction at 1 atm total pressure below which the isotherm should be linear according to Equation 2.4.20.

For the filter design in this work, a range of isotherm slopes will be considered. Some of the graphs presented later on will have K_0 as an x-axis; each K_0 value would correspond to a different VOC. To get an idea of the range of K_0 values to consider, the initial slopes of the five organics studied by Forsythe [80] were estimated. Because only a rough estimate was necessary, the initial slopes were estimated by assuming that the isotherm was linear from the lowest concentration data point through the point (0,0). Table 2.8 lists these estimates.

Table 2.8. Estimates of limiting isotherm slopes from the isotherm data of Forsythe [80].

Compound	K_0 [kgmol/(kg·atm)]
methane	1.87×10^{-3}
acetylene	2.39×10^{-2}
ethane	9.06×10^{-2}
acetaldehyde	2.91
acetone	1.88×10^{1}

Notice the wide variety in the range of isotherm slopes. Because there is a general trend of increasing K_0 with increasing molecular weight, organics with even higher slopes would be expected in indoor air (see, for example, Figure 1.3). The range of isotherm slopes as predicted by the method used in Figure 2.12 is even larger, although the accuracy of these estimates is highly suspect. Figure 2.13 illustrates the K_0 values of Table 2.8 plotted versus molecular weight, normal boiling point, and critical temperature.

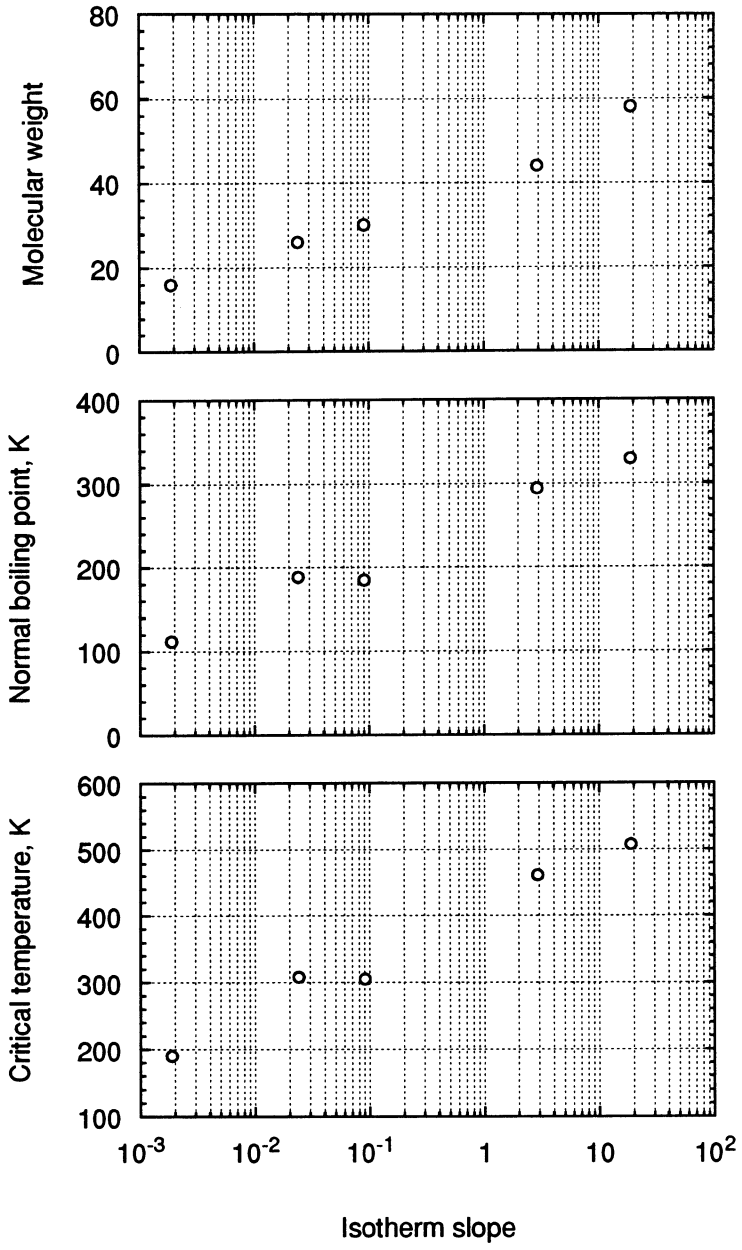

Figure 2.13. Limiting isotherm slopes (estimated from [80]) correlated with molecular weight, normal boiling point, and critical temperature.

Chapter 3

Background Information

In this chapter, the current state of the art in activated carbon filters is examined. A simple estimate of the useful lifetime of fixed-bed carbon filters is presented. A review of related applications of activated carbon and some other adsorbents is also included.

3.1 Activated carbon filters

Activated carbon filters used in HVAC systems for VOC control typically consist of an arrangement of thin (25-30 mm [114]) fixed bed filters filled with granular activated carbon. Textbooks also illustrate a cylindrical canister configuration for carbon filters [21, 49, 114]. Typical carbon mesh sizes used for air filtration are in the 6 to 14 range [114]. In general, smaller carbon granules result in better adsorptive qualities, improving both the transport rate and the equilibrium. However, as the granule size decreases the pressure drop through the filter increases.

As an example, Cambridge Filter Corporation [115] sells three different activated carbon filters for air quality control. Potential applications for these filters, as listed in their brochure, are reproduced in Table 3.1. Two of the filters (Purecel® Model 45FT and Side-Carb® Model STM/STS) consist of removable carbon trays inserted in a metal box-like frame, shown in Figure 3.1(a). The third type of filter, Purecel® Model FB, consists of a single corrugated type carbon bed, shown in Figure 3.1(b). International Air Filter [116] sells a filter similar to the Purecel® Model 45FT. The size of the filters

ranges from the Purecel® Model 45FT45, roughly 1 ft x 2 ft x 2 ft and 150 lbs (0.3 m x 0.6 m x 0.6 m, 68 kg) [115] to the Purecel® Model ST-M-60-120, approximately 6 ft x 12 ft x 2.5 ft and 3472 lbs (1.9 m x 3.6 m x 0.8 m, 1575 kg) [117].

Table 3.1 Potential applications for the Purecel and Side-Carb activated carbon filters sold by Cambridge Filter Corporation, as listed in their brochure [115].

- Tightly sealed buildings with little fresh air makeup - "Sick Building Syndrome"
- Work areas where off-gassing is prevalent
- Airports (jet fuel exhaust emissions)
- Work areas affected by high air pollution levels
- Work areas with large numbers of personnel
- Office buildings with air intakes low to ground level
- Any areas where odor control is essential

Initial filter selection is based solely on air flowrates, with no consideration of contaminant concentration levels. The Purecel® 45FT45 is rated for 1000 cfm (1700 m^3/hr), up to 500 fpm velocity (2.54 m/s) [115], while the ST-M-60-120 is rated for 36000 cfm (61200 m^3/hr) and up to 500 fpm velocity (2.54 m/s) [117]. Based on a carbon weight of approximately 10 lb/tray (4.54 kg/tray) [118], Cambridge uses roughly 60 lb carbon/1000 cfm (16 kg/1000 m^3/hr) in their filters. International Air Filter advertises 45 lb carbon/1000 cfm (12 kg/1000 m^3/hr) [116]. Kasmark [119] states that many installed carbon filter systems were designed with 45 lb/1000 cfm (12 kg/1000 m^3/hr).

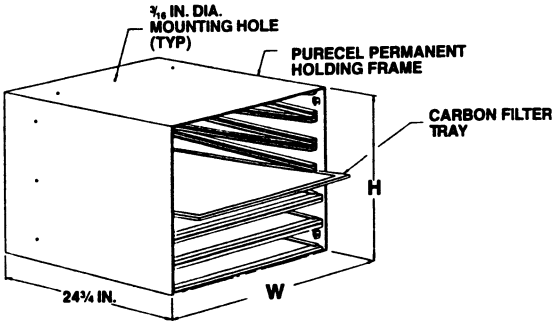

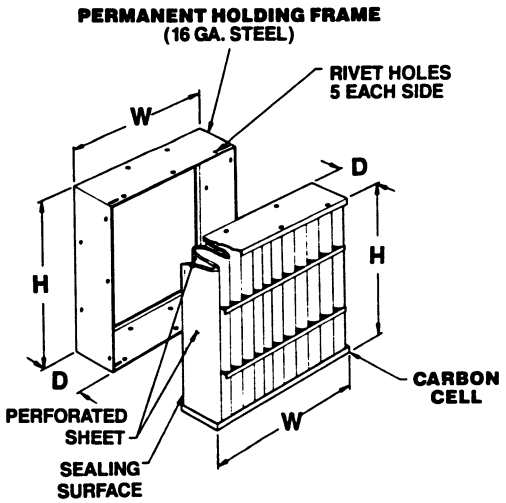

Figure 3.1 Typical activated carbon filters for VOC control, from [115].

To determine which vapors are suitable for removal by a carbon filter, the Barnebey-Cheney Company developed a list of common odors and rated them with a number from 1 to 4 indicating the relative adsorption capacity. The ratings, taken from [120], are as follows:

4. High capacity for all materials in this category, which includes most odor-causing substances. One pound takes up about 20% to 50% of its own weight (average about 33 1/3%).

3. Satisfactory capacity for items in this category, taking up about 10% to 25% of its weight (average 16.7%).

2. Includes substances not highly adsorbed but which might be taken up sufficiently for good service under particular conditions.

1. Adsorption capacity is low for these materials. Activated carbon is unsuitable for removing these except under most unusual circumstances.

The numbers are "based on removal of the substance from dilute concentrations encountered in air recovery and purification applications, assuming air temperature of 100°F or less" [120]. The list has been reproduced in Figure 3.2. This list is widely available, for example, it was included with literature distributed by Cambridge Filter Corporation [120] and Lewcott Corporation [28].

The list includes many VOCs, for example, Acetone(3), Benzene(4), Formaldehyde(2), Toluene(4), and Xylene(4). Both Trichloroethylene(4) and Carbon Tetrachloride(4) are listed. For someone unsure of the exact nature of the air quality problem, the list also includes Odors(4), Vapors(4), Fumes(3), Chemicals(3), Noxious Gases(3), Household Smells(4), Stuffiness(4), and Irritants(4). Odors are further categorized, with the list including Mixed Odors(4), Odorants(4), Reodorants(4), Stale Odors(4), Persistent Odors(4), and Lingering Odors(4). Some of the more specific odors include Combustion Odors(3), Cooking Odors(4), Pet Odors(4), Animal Odors(3),

Cancer Odor(4), Fish Odors(4), Film Processing Odors(3), Embalming Odors(4), and Theatrical Makeup Odors(4). Some of the other potential air contaminants listed include Spilled Beverages(4), Sauerkraut(4), Gangrene(4), Burned Flesh(4), and Aged Manuscripts(4).

Boiling point is also used to determine the suitability of activated carbon for adsorbing a particular vapor. Cambridge Filter Corporation suggests that a boiling point of 0°F can be used as a cutoff to determine whether or not a vapor will be adsorbed: the farther above 0°F the boiling point is, the more strongly it will be adsorbed, while the lower the boiling point is below 0°F, the less strongly it will be adsorbed [120]. Godish lists similar criteria based on boiling point and critical temperature [114].

Another quantity used to categorize the adsorptive capacity of activated carbon for different vapors is the retentivity. Retentivity is defined as the percent (by weight) of a vapor which remains adsorbed in the presence of air free of that vapor. The vapor is originally adsorbed by passing an air stream saturated with the vapor through the adsorbent. Table 3.2 lists some typical retentivity values [49, 121]. Theoretically, physical adsorption should be reversible, i.e., when the air concentration is zero, the vapor will desorb from the carbon. In general, the mass transfer process for desorption is much slower than for adsorption, even at higher temperatures. As an example, a graph in [122] showing experimental results from a carbon bed breakthrough test shows a step change from 0 to 340 ppm toluene. The influent concentration was maintained at 340 ppm for 450 mintues, at which time it was dropped to 0 ppm, starting a desorption process. 1000 minutes into the desorption, the effluent concentration was still at 10 ppm.

2	Acetaldehyde	4	Chloro Nitropropane	4	Fertilizer	3	Methyl Chloride	4	Propyl Acetate
4	Acetic Acid	4	Chloropicrin	3	Film Processing Odors	4	Methyl Chloroform	4	Propyl Alcohol
4	Acetic Anhydride	4	Cigarette Smoke	4	Fish Odors	3	Methyl Ether	4	Propyl Chloride
3	Acetone	4	Citrus and Other Fruits	4	Floral Scents	4	Methyl Ethyl Ketone	4	Propyl Ether
1	Acetylene	4	Cleaning Compunds	3	Fluorotrichloromethane	3	Methyl Formate	4	Propyl Mercaptan
3	Acids	3	Coal Smoke	4	Food Aromas	4	Methyl Isobutyl Ketone	2	Propylene
3	Acrolein	3	Combustion Odors	2	Formaldehyde	4	Methyl Mercaptan	2	Propyne
3	Acryaldehyde	4	Cooking Odors	3	Formic Acid	3	Methylal	3	Putrefying Substances
4	Acrylic Acid	3	Corrosive Gases	3	Freon	4	Methylcyclohexane		
4	Acrylonitrile	4	Creosote	2	Fuel Gases	4	Methylcyclohexanol	4	Putrescine
4	Adhesives	4	Cresol	3	Fumes	4	Methylcyclohexanone	4	Pyridine
4	Aged Manuscripts	4	Crotonaldehyde	4	Gangrene	4	Methylene Chloride	2	Radiation Products
4	Air Wick	4	Cyclohexane	4	Garlic	3	Mildew	4	Rancid Oils
4	Alcohol	4	Cyclohexanol	4	Gasoline	4	Mixed Odors	4	Resins
4	Alcoholic Beverages	4	Cyclohexanone	4	Heptane	3	Mold	4	Reodorants
2	Amines	4	Cyclohexene	4	Heptylene	4	Monochlorobenzene	4	Ripening Fruits
2	Ammonia	4	Dead Animals	3	Hexane	3	Monofluorotrichloromethan	4	Rubber
4	Amyl Acetate	4	Decane	3	Hexylene	4	Moth Balls	4	Sauerkraut
4	Amyl Alcohol	4	Decaying Substances	3	Hexyne	4	Naphtha (Coal tar)	4	Sewer Odors
4	Amyl Ether	4	Decomposition Odors	4	Hospital Odors	4	Naphtha (Petroleum)	4	Skatole
3	Animal Odors	4	Deodorants	4	Household Smells	4	Naphthalene	3	Slaughtering Odors
3	Anesthetics	4	Detergents	1	Hydrogen	4	Nicotine	4	Smog
4	Aniline	4	Dibromoethane	2	Hydrogen Bromide	3	Nitric Acid	4	Smoke
4	Antiseptics	4	Dichlorobenzene	2	Hydrogen Chloride	4	Nitro Benzene	4	Soaps
4	Asphalt Fumes	3	Dichlorodifluoromethane	3	Hydrogen Cyanide	4	Nitroethane	3	Solvents
3	Automobile Exhaust	4	Dichloroethane	2	Hydrogen Fluoride	2	Nitrogen Dioxide	4	Sour Milk
3	Bacteria	4	Dichloroethylene	3	Hydrogen Iodide	4	Nitroglycerine	4	Spilled Beverages
4	Bathroom Smells	4	Dichloroethyl Ether	2	Hydrogen Selenide	4	Nitromethane	4	Spoiled Food Stuffs
4	Benzene	3	Dichloromonofluoromethane	3	Hydrogen Sulfide	4	Nitropropane	4	Stale Odors
3	Bleaching Solutions	4	Dichloro-Nitroethane	4	Incense	4	Nitrotoluene	4	Stoddard Solvent
4	Body Odors	4	Dichloropropane	4	Indole	4	Nonane	4	Stuffiness
4	Bromine	3	Dichlorotetrafluoroethane	3	Inorganic Chemicals	3	Noxious Gases	4	Styrene Monomer
4	Burned Flesh	3	Diesel Fumes	3	Incomplete Combustion	4	Octylene	3	Sulfur Compounds
4	Burned Food	3	Diethyl Amine	3	Industrial Wastes	4	Octane	2	Sulfur Dioxide
4	Burning Fat	4	Diethyl Ketone	4	Iodine	4	Odors	3	Sulfur Trioxide
3	Butadiene	4	Dimethylaniline	4	Iodoform	4	Odorants	4	Sulfuric Acid
2	Butane	4	Dimethylsulfate	4	Irritants	4	Onions	4	Tar
4	Butanone	4	Dioxane	4	Isophorene	4	Organic Chemicals	3	Tarnishing Gases
4	Butyl Acetate	4	Dipropyl Ketone	3	Isoprene	4	Ozone	4	Tetrachloroethane
4	Butyl Alcohol	4	Disinfectants	4	Isopropyl Acetate	4	Packing House Odors	4	Tetrachloroethylene
4	Butyl Cellosolve	4	Embalming Odors	4	Isopropyl Alcohol	4	Paint & Redecorating Odor	3	Tetrahydrofuran
4	Butyl Chloride	1	Ethane	4	Isopropyl Ether	4	Palmitic Acid	4	Theatrical Makeup Odors
4	Butyl Ether	3	Ether	4	Kerosene	4	Paper Deteriorations		
2	Butylene	4	Ethyl Acetate	4	Kitchen Odors	4	Paradichlorbenzene	4	Tobacco Smoke
2	Butyne	4	Ethyl Acrylate	4	Lactic Acid	4	Paste and Glue	4	Toilet Odors
3	Butyraldehyde	4	Ethyl Alcohol	4	Lingering Odors	3	Pentane	4	Toluene
4	Butyric Acid	3	Ethyl Amine	4	Liquid Fuels	4	Pentanone	4	Toluidine
4	Camphor	4	Ethyl Benzene	4	Liquor Odors	3	Pentylene	4	Trichloroethylene
4	Cancer Odor	3	Ethyl Bromide	4	Lubricating Oils & Greases	3	Pentyne	4	Turpentine
4	Caprylic Acid	3	Ethyl Chloride	4	Lysol	4	Perchloroethylene	4	Urea
4	Carbolic Acid	3	Ethyl Ether	4	Masking Agents	4	Perfumes, Cosmetics	4	Uric Acid
3	Carbon Bisulfide	3	Ethyl Formate	4	Medicinal Odors	4	Perspiration	4	Valeric Acid
1	Carbon Dioxide	4	Ethyl Mercaptan	4	Melons	4	Persistent Odors	4	Valeric Aldehyde
1	Carbon Monoxide	4	Ethyl Silicate	4	Menthol	4	Pet Odors	4	Vapors
4	Carbon Tetrachlorid	1	Ethylene	4	Mercaptans	4	Phenol	4	Varnish Fumes
4	Cellosolve	4	Ethylene Chlorhydrin	4	Mesityl Oxide	3	Phosgene	4	Vinegar
4	Cellosolve Acetate	4	Ethylene Dichloride	1	Methane	4	Pitch	3	Vinyl Chloride
4	Charred Materials	3	Ethylene Oxide	3	Methyl Acetate	4	Plastics	3	Viruses
4	Cheese	4	Essential Oils	4	Methyl Acrylate	3	Poison Gases	3	Volatile Materials
3	Chemicals	4	Eucalyptole	3	Methyl Alcohol	4	Popcorn and Candy	4	Waste Products
3	Chlorine	3	Exhaust Fumes	3	Methyl Bromide	4	Poultry Odors	4	Waterproofing Compounds
4	Chlorobenzene	3	Fabric Finishes	4	Methyl Butyl Ketone	2	Propane		
4	Chlorobutadiene	4	Fecal Odors	4	Methyl Cellosolve	3	Propionaldehyde	3	Wood Alcohol
4	Chloroform	4	Female Odors	4	Methyl Cellosolve Acetate	4	Propionic Acid	4	Xylene

Figure 3.2 Activated carbon capacity index for odors, from [120].

	Retentivity, %		Retentivity, %
Acetaldehyde	7	Hydrogen Sulfide	3
Acetic Acid	30	Indole	25
Acetone	15	Iodine	40
Acetylene	2	Iodoform	30
Acryaldehyde	15	Isopropyl Acetate	23
Acrylic Acid	negligible	Isopropyl Alcohol	26
Ammonia	20	Isopropyl Chloride	20
Amyl Acetate	34	Isopropyl Ether	18
Amyl Alcohol	35	Menthol	20
Benzene	24	Methyl Acetate	16
Body Odors	high	Methyl Alcohol	10
Bromine	40 (dry)	Methyl Chloride	5
Butane	8	Methylene Chloride	25
Butyl Acetate	28	Methyl Ether	10
Butyl Alcohol	30	Methyl Ethyl Ketone	25
Butyl Chloride	25	Methyl Isobutyl Ketone	30
Butyl Ether	20	Methyl Mercaptan	20
Butylene	8	Naphthalene	30
Butyne	8	Nicotine	25
Butyraldehyde	21	Nitric Acid	20
Butyric Acid	35	Nitro Benzene	20
Camphor	20	Nitrogen Dioxide	10
Caprylic Acid	35	Nonane	25
Carbon Disulfide	15	Octane	25
Carbon Tetrachloride	45	Ozone	decomposes
Chlorine	15 (dry)	Packing House Odors	good
Chloroform	40	Palmitic Acid	35
Cooking Odors	high	Pentane	12
Cresol	30	Pentylene	12
Crotonaldehyde	30	Phenol	30
Decane	25	Propane	5
Diethyl Ketone	30	Propionic Acid	30
Ethyl Acetate	19	Propylene	5
Ethyl Alcohol	21	Propyl Mercaptan	25
Ethyl Chloride	12	Propyne	5
Ethylene	3	Putrescine	25
Ethyl Ether	15	Pyridine	25
Ethyl Mercaptan	23	Sewer Odors	high
Essential Oils	high	Skatole	25
Eucalyptole	20	Sulfur Dioxide (dry)	10
Food Odors	high	Sulfur Trioxide	15
Formaldehyde	negligible	Sulfuric Acid	30
Formic Acid	7	Toilet Odors	high
Heptane	23	Toluene	29
Hexane	16	Turpentine	32
Hydrogen Bromide	12	Valeric Acid	35
Hydrogen Chloride	12	Water	none
Hydrogen Fluoride	10	Xylene	34
Hydrogen Iodide	15		

Table 3.2 Retentivity of vapors by activated carbon, from [49]. The retentivity is the weight percent retained in a dry air stream at 20°C and 1 atm.

Fixed-bed activated carbon adsorption filters have a finite useful lifetime, yet the guidelines for determining filter replacement schedules are often crude. Godish [114] references a source which recommends replacing filters once a year. Cambridge Filter Corporation recommends three techniques for evaluating the lifetime of their filters [120]. The first, the "Sniff Test", consists of simply recording the times at which odors become noticeable and eventually developing a replacement schedule.

The second method, called the "Mason Jar Test", requires the customer to periodically remove a sample of carbon from the beds and place it in a Mason Jar. The same amount of fresh carbon is placed in a similar Mason Jar. Teaspoons of trichlorethylene are added to each jar until a sweet odor is detected. The ratio of the number of teaspoons added to the carbon sample (taken from the filter) to the number of teaspoons added to the fresh carbon indicates the remaining relative life of the bed. Both the Mason Jar Test and the Sniff Test are suggested as approximate methods only [120].

The third method, "Laboratory Testing", consists of removing a sample of carbon from the bed and sending it to a laboratory. The testing procedure is detailed in U.S. Government Specification MIL-C-17605B and involves measuring the carbon tetrachloride activity of the carbon (similar to ASTM D3467-88).

A drawback of these techniques is that all three are post-installation. No verification of these methods was found, and in fact, both the carbon tetrachloride activity standard, ASTM D3467-88, and Kovach [123] indicate that CCl_4 activity is not a reliable indicator of adsorber performance for other adsorbates. Trichloroethylene ($CHCl:CCl_2$) has a molecular weight of 64 and carbon tetrachloride (CCl_4) has a molecular weight of 153.82. Both have a rating of 4 on the odor list of Figure 3.2. By comparison with the distribution of VOC molecular weights from Grot et al. [6], shown

in Figure 1.3(a), it can be seen that trichloroethylene is a relatively light compound whereas carbon tetrachloride is a relatively heavy compound. This suggests that trichloroethylene would be adsorbed less strongly than most indoor air VOCs, while carbon tetrachloride would be adsorbed more strongly than most indoor air VOCs.

Only one study involving actual testing of an in-duct type carbon filter was found. Hammerton [124] tested both granular carbon fixed-bed filters and impregnated activated carbon fixed-bed filters (e.g., [28]) in a transient, closed-loop system. The air was initially charged with a contaminant concentration equal to twice the 8 hour OSHA permissible level. No contaminant was added to the air once the test had begun, and thus these tests do not represent actual filter operating conditions. Results for methyl ethyl ketone were presented in [124]. As an example of a test, an initial concentration of 400 ppm methyl ethyl ketone was reduced to less than 50 ppm after one minute of operation and approximately 10 ppm after five minutes.

Other aspects of the filter operation were also included in [124]. The initial adsorption rate was observed to be indendent of concentration, but varied for different contaminants. An investigation of desorption revealed that desorption was slow for both the granular and impregnated carbon, and regeneration of the impregnated carbon was not economically feasible due to temperature limitations imposed by the binders and the support frame.

3.2 Maximum lifetime estimate

A simple estimate of the maximum lifetime of a fixed-bed adsorption filter can be obtained by assuming that the entire filter is saturated before breakthrough occurs, that there is no interference from other adsorbing contaminants, and that the filter remains at a

constant temperature. These assumptions will lead to an overestimate of the actual filter lifetime. The amount of contaminant adsorbed on the filter (assuming the entire filter is saturated) divided by the contaminant flowrate gives an estimate of the maximum time until breakthrough:

$$\theta_B = \frac{m_m W}{\omega \tilde{\rho}_{air} Q} \tag{3.2.1}$$

As an example, consider Cambridge Filter Corporation's Model 45FT45, which consists of 6 removable carbon trays, at approximately 10 lbs (4.5 kg) each, for a total of 60 lbs (27.2 kg) of carbon in the unit. The filter is rated for 1000 cfm (1700 m^3/hr). For the adsorption of benzene at 100 ppb, the reported equilibrium amount adsorbed ranges from roughly 9.69 kg/kg = 1.24×10^{-7} kgmol/kg (Figure 2.3) [81] to approximately 1.91 kg/kg = 2.44×10^{-4} kgmol/kg carbon (Figure 2.5) [83]. At a temperature of 25°C and a flowrate of 1000 cfm (1700 m^3/hr), the maximum lifetime, using the two different isotherm values, is 29 minutes or 40 days, respectively. Although 100 ppb may be higher than actual inlet concentrations encountered in indoor air quality situations, within the range where the isotherm is linear, the lifetime estimate is independent of inlet concentration, i.e.

$$\theta_B = \frac{m_m K}{\tilde{\rho}_{air} Q} \tag{3.2.2}$$

Figure 3.3 illustrates the maximum lifetime estimate as a function of the pounds of carbon per 1000 cfm for different isotherm slopes. A linear isotherm has been assumed. The three segments of the graph, from left to right, are in time units of minutes, hours, and days. In order to obtain a maximum filter lifetime of about 10 days for a filter with 45 lb carbon/1000 cfm, a contaminant with a value of $K = 8 \times 10^2$ or higher would be

necessary. This isotherm slope is several orders of magnitude higher than the largest isotherm slope reported in Table 2.7, which was for acetone. Based on the value of K_0 for acetone (rated a 3 on the odor index), the maximum possible filter lifetime for acetone would be only about 5.5 hours.

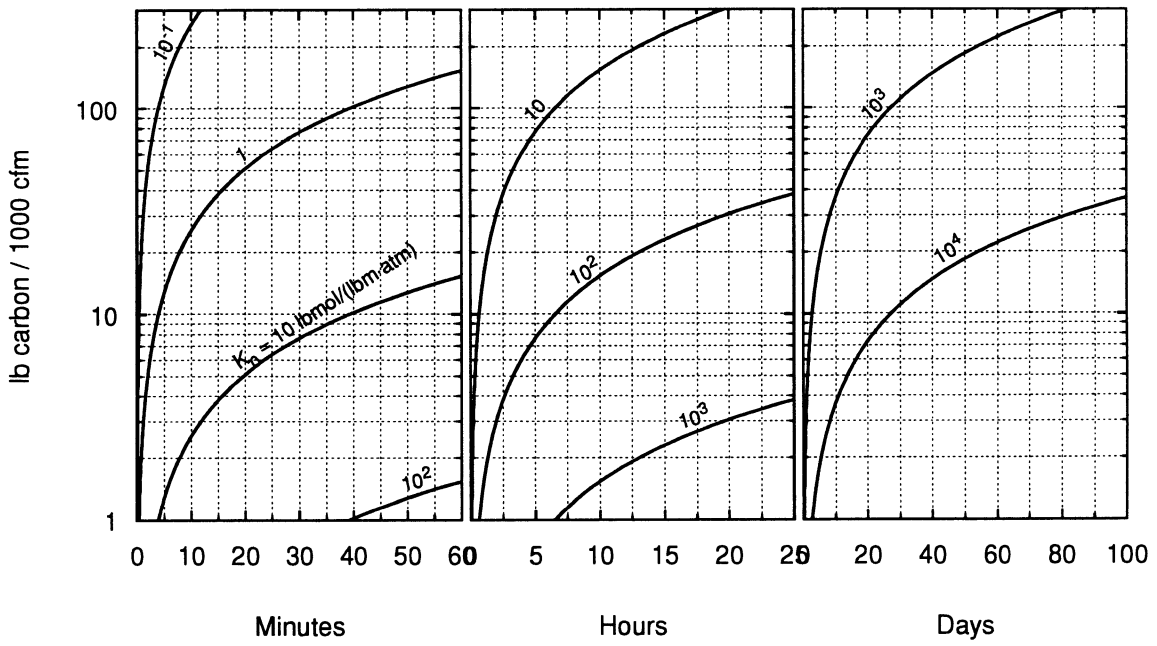

Figure 3.3 Maximum possible lifetime of a fixed-bed activated carbon filter for various isotherm slopes, in minutes, hours, and days.

In reality, breakthrough would occur sooner. The mass transfer effects cause the adsorption wave to spread and become s-shaped, as shown in Figure 3.4. From a mass balance, the area under the actual (s-shaped) breakthrough curve is equal on each side of the step change breakthrough predicted by Equation 3.2.1. The breakthrough curve, however, is not necessarily symmetric, although often it is assumed to be close enough to symmetric so that the breakthrough time predicted by Equation 3.2.1 is approximated as the time at which the outlet concentration reaches 50% of the inlet concentration (referred to as 50% breakthrough).

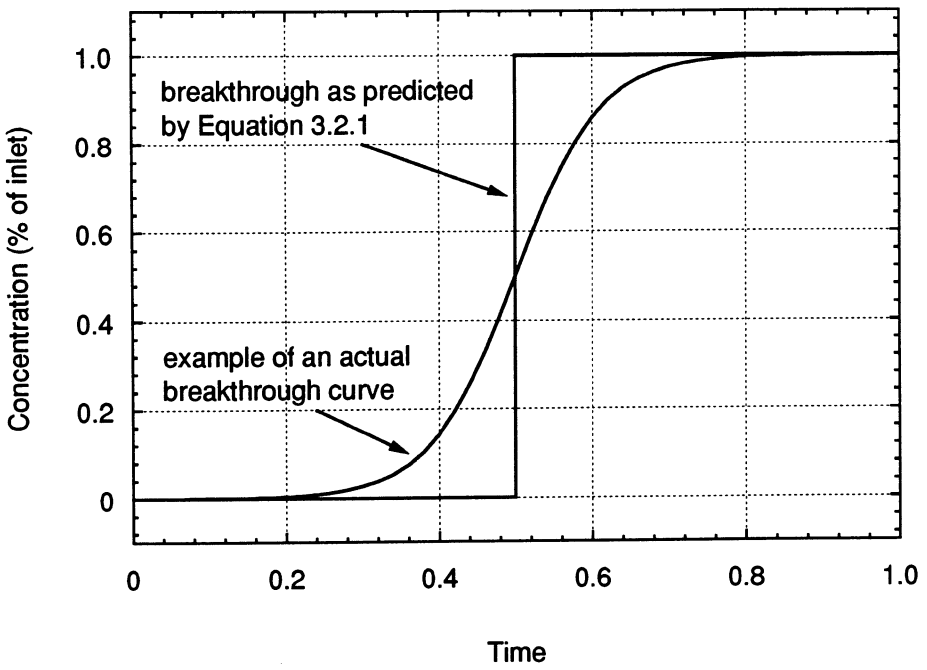

Figure 3.4 Typical breakthrough curves.

The short lifetimes predicted in the above example and illustrated in Figure 3.3 seem incredible; for most of the K_0 values, they are unreasonably short. Even so, they represent the maximum possible lifetime. Some breakthrough will occur before the time predicted by Equation 3.2.1, as illustrated in Figure 3.4. The presence of other contaminants may cause breakthrough to occur sooner.

Equation 3.2.1 is often used in textbooks to estimate activated carbon filter lifetimes, e.g., [110, 114]. However, the retentivity is often used in place of W in the equation [114]; in [110], an average value of 20% retentivity is recommended. By comparing the amount adsorbed in the isotherm plots of Figures 2.2 to 2.8 with the retentivities in Table 3.2, it can be seen that the retentivities are generally much higher than the W value obtained from the isotherm.

Several papers have been published supporting the short lifetimes calculated from Equation 3.2.1. For example, in an article published in the July 1988 *ASHRAE Journal* [125], Sparks states that:

> "The available data indicate that simple activated carbon filters are not likely to be effective for controlling organic vapors at the parts per billion level found in indoor environments. The data show that small activated carbon filters might be able to reduce organic vapor concentrations from short-term spills. Long-term effectiveness of carbon filters requires that the filters be regenerated on a frequent schedule."

Ramanathan et al. [81], based on experimental isotherm data and some modeling results, state that:

> "A 6 inch (15 cm) thick filter, such as those typically marketed for odor control applications, would break through almost immediately after installation, even in the absence of other pollutants or humidity effects, both of which would cause performace to deteriorate further."

In a paper by Clapham, Junker, and Tobias [83], the conclusion is reached that for an air stream with a continuous 10 ppm contaminant concentration, the typical thin filter lifetime would be on the order of hours. However, they claim that if the odor generation is not continuous, odors will desorb during the "clean" periods, such that carbon capacity is recovered. While researching a method to measure carbon filter effectiveness, Mahajan [122] came to the opposite conclusion: that activated carbon filters for indoor air may *not* be practical because of the fact that they desorb when the concentration is reduced. When the contaminants are desorbed, they simply re-enter the space which was earlier cleaned. At room temperature, however, the desorption rate should be very slow. The whole concept of retentivity suggests this, as do experimental studies of desorption.

The short lifetimes of the fixed-bed carbon filters calls into question their practicality. The frequent replacement or regeneration needed for effective use of a

carbon filter indicates that a rotary regenerative configuration, such as used in desiccant air conditioning systems, may be a more practical solution. Traditionally, regenerative carbon systems have been used only in solvent recovery applications.

3.3 Rotary regenerative activated carbon filters

A system diagram for an HVAC system with a rotary regenerative carbon filter is shown in Figure 3.5. The filter may be located in either the return air (location A) or in the supply air (location B), as in the ASHRAE Standard 62-1989. Outdoor air is heated and passed through the regeneration portion of the carbon wheel; the heat required for regeneration could possibly be obtained through solar energy or waste heat reclamation. Although not shown, it may be necessary to modify the temperature and humidity of the airstream both before and after the carbon filter to improve the filter efficiency.

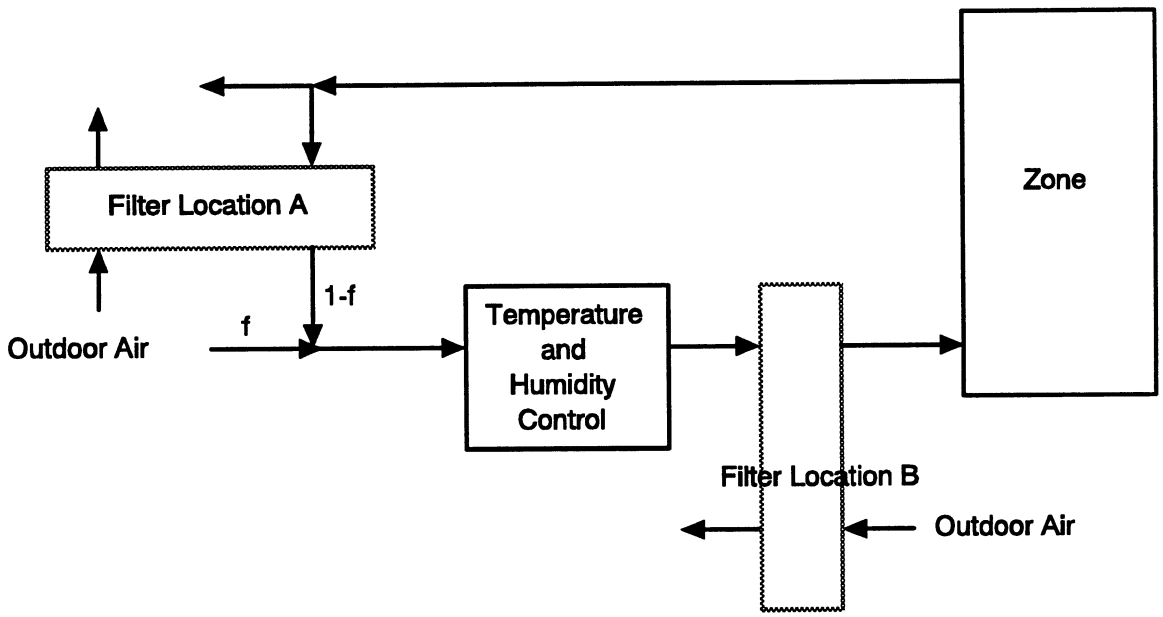

Figure 3.5 Example of an HVAC system with a rotary regenerative activated carbon filter. Two possible locations for the filter are indicated.

The adsorbent bed rotates between two different air streams (see Figure 3.6); the portions of the bed through which the different air streams pass are sealed off from each other to prevent mixing. The air stream from which the controlled component (e.g., water vapor, formaldehyde, etc.) is removed is called the process air stream, and the portion of the wheel through which it flows is called the process section (or process side or process period). The section of the wheel in which the controlled component is cleaned from the rotating adsorbent is called the regeneration section (or side or period); the cleaning is accomplished by heating the air which passes through the regeneration section, thereby desorbing the matrix. Other wheel sections can also be incorporated, such as a purging section to cool the matrix after regeneration and before processing.

The idea of a rotary regenerative system using activated carbon is not new. Many books have pictures of carbon wheels [e.g., 21, 23, 126], although the applications are for solvent recovery and control of VOC emissions from industrial processes (with higher concentrations than encountered in indoor air). Gidaspow and Onischak [160] proposed a type of rotary regenerative sorption system for removing NO from flue gases with silica gel as the adsorbent.

There have also been many studies of rotary regenerative wheels that adsorb water vapor as part of a desiccant air conditioning system, both experimental and computational [e.g., 1, 127-133]. Other studies have examined the effect of contaminants on desiccant performance [134] and the ability of desiccant wheels to remove contaminants [135]. There are several differences between the desiccant system and an activated carbon wheel for removal of trace VOCs from indoor air. The concentrations are much lower and there are multiple adsorbing species with a wide range of isotherm slopes. In addition, the identities of the individual VOCs are most likely unknown.

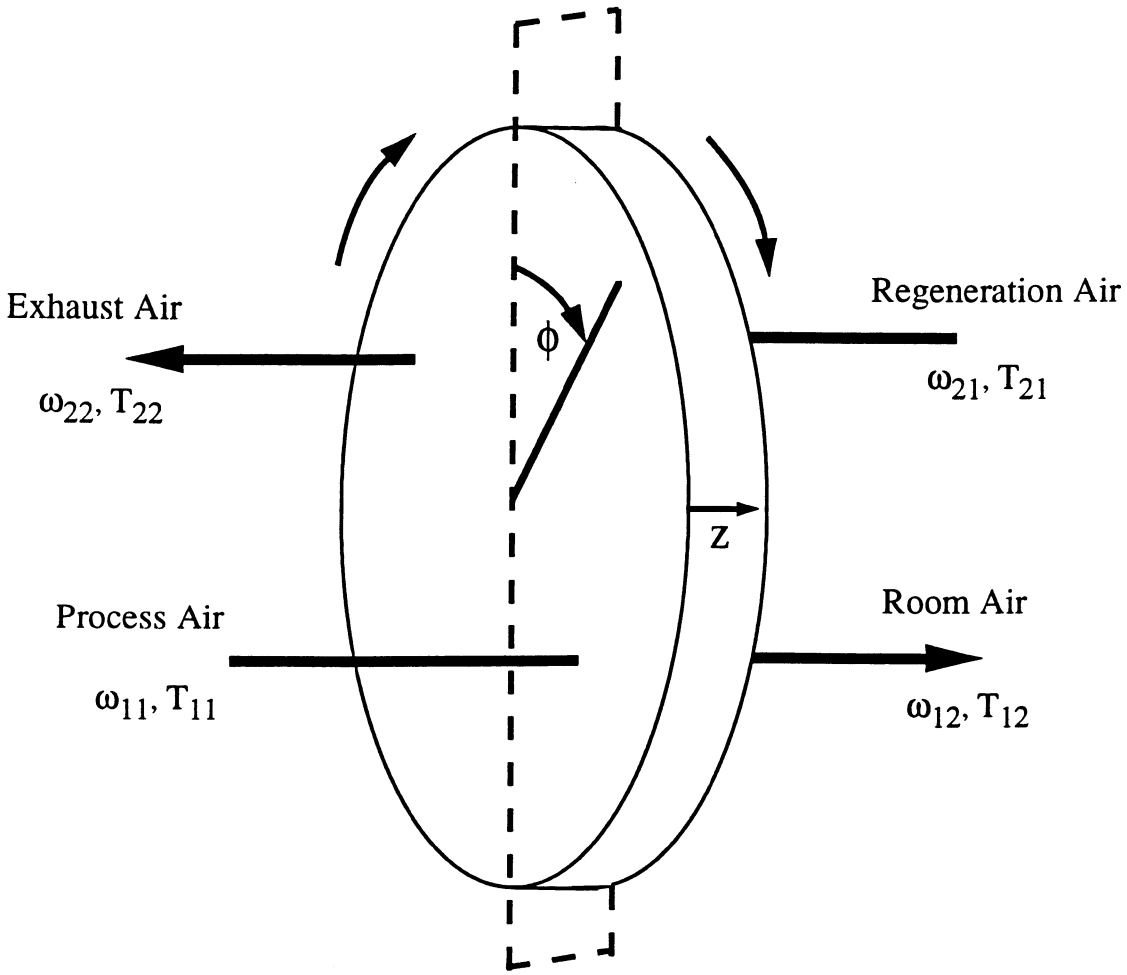

Figure 3.6 Rotary regenerative activated carbon wheel.

3.4 Related applications

There are many applications where activated carbon is used for removing vapor phase contaminants from air. Some of the studies of these applications may contain information relevant to the design of carbon filters for VOC control in indoor air. Some of the related areas include gas masks, respirator cartridges, submarine and spacecraft air quality control and industrial applications (e.g., solvent recovery). Studies of other adsorption systems, such as desiccant air conditioning systems, may also contain useful information. These related applications are briefly described in the following sections.

3.4.1 Residential filters

Daisey and Hodgson [136] examined four different tabletop home air cleaners, and found them to be ineffective for long-term removal of VOCs. These units typically contain several types of filters, one of which is an activated carbon filter for removing VOCs. The manufacturer's recommended lifetimes of the carbon filters ranged from 3 to 6 months. On three of the systems, the weight of the carbon was able to be measured, and operating at their maximum fan speed, the three filters had 1.9, 2.1, and 0.75 lb carbon/1000 cfm. Closed system tests in experimental room-like chambers were conducted to determine the efficiency of the filters. Six VOCs were used in the tests, and the initial concentrations were as follows: *n*-heptane, 170 ± 37 ppb; toluene, 176 ± 35 ppb; dichloromethane, 76 ± 29 ppb; tetrachloroethylene, 53 ± 15 ppb; hexanal, 45 ± 4 ppb; 2-butanone, 45 ± 9 ppb. Effective cleaning rates (in m^3 air cleaned per hour) were computed, and varied from 3-5 m^3/h for the poorest performing filter to 40-50 m^3/h for the best performing filter.

The best performing filter was studied in more detail. After the first 100 minutes, the concentrations of all of the VOCs except dichloromethane were reduced to about 1/10 of their initial levels. 1,1,1-trichloroethane, which was not one of the test vapors, was initially emitted by the filter, although the emission rate decayed after the first hour. After a second test, the effective cleaning rate was reduced to approximately 30-40 m^3/h (it had been 40-50 m^3/h after the first test). This filter was then tested in a home, at the medium speed (3.9 lb carbon/1000 cfm), and after approximately 150 hours of intermittent use in the home, for a total of 160 hours of use, the effective cleaning rate had dropped to about 15-20 m^3/hr. The manufacturer's stated life of the carbon filter was 1000 hours or 3 months. In addition, the residents had complained that the filter emitted an odor; tests indicated that formaldehyde was being emitted from the filter unit, possibly from particleboard contained in the filter housing.

3.4.2 Gas masks

The need for gas masks during World War I, and the ensuing research, increased knowledge about activated carbon considerably. An excellent and thorough discussion of activated carbon is given in a paper published in 1919 [137]. Gas masks used in World War I contained a mixture of 60% 6 to 14 mesh activated coconut shell carbon and 40% 8 to 14 mesh soda-lime-permanganate granules [137]. This mixture was referred to as the "war-gas mixture." Starting from near the end of World War I, impregnated carbons have been used to improve the lifetime of the mask [21, 137].

One of the main requirements of the gas mask was the ability to hold on to a vapor when it was no longer present in the air, a concept later called retentivity. Activated carbon was found to be superior to other adsorbents in this capacity. One of the functions

of the soda-lime was to contain any vapors which did desorb. It was also important that the adsorbent be mechanically strong, able to withstand rough handling. Activated carbon was also found to be very versatile, offering protection against many gases [137].

Average battlefield concentrations were assumed to be roughly 1000 ppm [137]. Inhalation rates for a moderately active man were taken to be 30-32 l/min (about 1 cfm or 1.7 m^3/hr) [137, 138]. The canister contained 42 in^3 (687 cm^3) of the war-gas mixture [138]. Some of the typical war gases include, among others, chlorpicrin, phosgene, hydrocyanic acid, cyanogen chloride, and dichlorodiethyl sulfide (mustard gas) [137, 138]. The research and design work appears to have been primarily experimental; tables of measured cartridge lifetimes appear in [137] and [138].

In comparison with carbon filters for indoor air VOC control, the flowrates through the gas mask cartridges are much smaller. The gases, hopefully, are different. The concentrations are higher for the gas mask. Unfortunately, the weight of the carbon was not given in any of the references consulted, such that it was not possible to compute the lb carbon/1000 cfm to compare with the numbers used for fixed-bed indoor air quality activated carbon filters.

3.4.3 Respirator cartridges

Respirators are used by workers to limit exposures to various pollutants in the workplace. A typical respirator cartridge consists of a plastic or metal case containing 25-40 g of activated carbon; there are usually two cartridges per mask such that there is 50-100 g of carbon in a mask [109]. Human breathing rates range from the sitting rate of 14 l/min (0.5 cfm) to the extremely heavy work rate of 75 l/min (2.6 cfm) [109]. For a cartridge with 50 g of carbon, the range of breathing rates corresponds to 220 lb

carbon/1000 cfm to 42 lb carbon/1000 cfm; for a cartridge with 100 g of carbon, the range of breathing rates corresponds to 440 lb carbon/1000 cfm to 85 lb carbon/1000 cfm. Experimental data in the form of breakthrough curves have been published, e.g., [109, 112, 139-141], along with various attempts to model and predict the breakthrough curves, e.g., [109, 112, 139, 141-145]. The concentrations examined are in the range of 50 to 3000 ppm, mostly around 1000 ppm. These concentration are higher than the "Sick Building Syndrome" type indoor air quality concentrations.

In a series of eight papers, summarized in [109], Nelson et al. reported experimental and modeling results. Included were measured breakthrough curves for 131 different vapors at 1000 ppm [146]. The base conditions for the tests were 1000 ppm inlet concentration, 20-25°C, 53.3 l/min total flowrate (1.88 cfm), 50% relative humidity preconditioning of the cartridge, and 50% relative humidity in the inlet flow. Variations from these conditions, including other concentrations, flowrates, and relative humidities were also studied.

To examine the effect of concentration, breakthrough curves for nine different vapors at concentrations between 50 and 3000 ppm were measured. Both the shape and position of the breakthrough curves were observed to depend on the concentration, with breakthrough occurring sooner and with a sharper wave as the concentration increased. Breakthrough time was inversely proportional to flow rate.

Some examples of breakthrough times are as follows. In [141], 1% breakthrough times are given for acetone in dry air on a dry cartridge at different air flowrates and bed weights. A 1% breakthrough time of 55 minutes was reported for 1020 ppm acetone at an air flowrate of 103 lb carbon/1000 cfm. In [139], 10% breakthrough times for cartridges preconditioned at 50% relative humidity and with an influent air stream at 50%

relative humidity are reported. Some results include: for 1000 ppm acetone at 73 and 83 lb carbon/1000 cfm, 10% breakthrough times of 42.9 min and 66.3 min, respectively; for 100 ppm acetone at 73 and 83 lb carbon/1000 cfm, 10% breakthrough times of 132 and 245 minutes; for 1000 ppm hexane at 62 and 83 lb carbon/1000 cfm, 57.7 and 77.4 minutes, respectively.

The papers dealing with the respirator cartridge application contain some of the most extensive studies of the effect of relative humidity. However, almost no data are reported at zero percent relative humidity, so that unfortunately the data can not be related to dry adsorption studies. Nelson et al. [112] found that increasing relative humidity levels decreased the breakthrough time, and that the effect was more pronounced at low concentrations. They observed little effect of relative humidity at 50% or less, but this would be expected since the beds were preconditioned at 50% relative humidity. They also found the effect of relative humidity in the influent to be more significant than the preconditioning. At high relative humidities, the breakthrough curves were observed to become nonsymmetrical [144].

Several empirical models for the breakthrough curves have been developed. The modified Wheeler and Mecklenburg equations accurately model the breakthrough curve up until only about 40% breakthrough [109]. These models were also considered by many authors to be too complex, requiring too many parameters. Yoon and Nelson [142] proposed a model which more accurately modeled the entire breakthrough curve. All of the models are isothermal, although any effects of the heat of adsorption would be included in the model parameters which are fit to the breakthrough curves. Relative humidity effects are also included in this manner. Equation 2.4.1 has been used to estimate the performance of the respirator cartridges for different vapors [69-71].

3.4.4 Submarines

The introduction of nuclear submarines around 1955 (which can stay submerged for weeks at a time) created a need for an on-board air cleaning system in order to maintain acceptable air quality. The air cleaning system described in [147] consisted of four components: a monoethanolamine scrubber for controlling CO_2, electrostatic precipitators for removing aerosols, catalytic burners for H_2, CO, and some VOCs, and activated carbon beds for also removing VOCs. About 500 lbs of activated carbon in 5 lb cloth bags were stacked like sandbags to form the carbon bed. Leakage through the bed was significant, as much as 50%.

In experimental studies, the catalytic burners removed more VOCs than the carbon bed. For example, on a submarine with two catalytic burners and a carbon bed [147], 680 g/day VOC were generated. 560 g/day were removed by the burners compared with only 120 g/day removed by the carbon bed. The total equilibrium VOC concentration was measured as 40 mg/m^3. In another study, a total VOC concentration of 15-25 mg/m^3 was reported [148]. In [148], they state the activated carbon beds are ineffective for VOCs with less than 6 carbon atoms; a graph in [148] illustrates that there is no noticeable effect on the methane concentration even when the carbon bed is replaced.

There are many contaminants present in the submarine atmosphere. In one case, over 400 vapor phase pollutants were detected [147]. The types of VOCs identified include aliphatic hydrocarbons, aromatic hydrocarbons, unsaturated and alicyclic compounds, some miscellaneous hydrocarbons, chlorinated compounds, refrigerant and propellant gases. Because the carbon beds would become saturated very quickly, source control programs were implemented in order to restrict pollutant generation, e.g., water-thinned paints were used and the use of aerosols (deoderant, shaving cream, etc.)

was restricted [147]. Before the control program, carbon from one submarine contained 23.4% VOCs by weight (practically saturated) after only 11 days. After the control program was initiated, a similar submarine carbon bed contained only 1.7% VOCs by weight after 30 days [148].

Originally no way to determine the useful lifetime of the carbon beds was known, and the carbon beds were simply replaced about every 21 days [148]. An experimental method, described in [148], was developed to estimate the effectiveness of the carbon bed by simultaneously measuring the VOC concentration in the bed influent and effluent. With time, the ratio of the effluent concentration to the influent concentration increases towards one, indicating that the effectiveness of the carbon filter is decreasing.

3.4.5 Spacecraft

Some preliminary work for spacecraft air quality control involved measuring adsorption data. Isotherms of several VOCs and water at multiple temperatures were measured on different mesh sizes of Barneby-Cheney BD activated carbon (some of the data are plotted in Figures 2.7a and b). Heats of adsorption were calculated from the data. Mixed contaminant adsorption data in the low ppm range were measured, illustrating some interference effects (see Figure 2.8). Some experimental data examining the effect of relative humidity were included. Vacuum desorption as a means for carbon regeneration was also studied.

In [149], the design and testing of a gaseous pollutant control system for maintaining acceptable air quality in a spacecraft is described. The system was designed to be small and lightweight, and capable of lasting through a 180 day mission without replacement. 145 different gaseous contaminants were considered, a large portion of

which were VOCs. Maximum allowable concentrations for each contaminant were established by the Air Standards for Manned Space Flight of the Space Science Board. Generation rates for each contaminant were also estimated. The concentrations considered and tested were in the ppm range.

The final system design consisted of three major components: a catalytic oxidizer, a fixed carbon bed, and a regenerative carbon bed. Use of the combination of a regenerative carbon bed and a fixed bed as opposed to just a fixed bed reduced the total amount of carbon required from 500 lb to 59 lb. The catalytic oxidizer was used to remove some of the lighter organics, e.g., methane, acetylene, ethylene, and ethane. The fixed carbon bed was used to remove some of the more strongly adsorbed VOCs, such as toluene, the xylenes, and methyl ethyl ketone. The carbon bed was cylindrical, 17 in. (0.43 m) in diameter, 13.6 in. (0.35 m) long, and contained 56 lb (25.4 kg) of carbon. The flowrate through the fixed bed was 76 cfm (129 m^3/hr).

The regenerative bed was used to remove the rest of the VOCs, including acetone, acetaldehyde, vinyl chloride, and trichloroethylene. It was not continually regenerated, but rather operated in an adsorption mode for 24 hours, after which it was regenerated for 2 to 3 hours by thermal (up to 200°C) and vacuum desorption (10^{-4} mmHg $\approx$ 10^{-7} atm). During the regeneration period, the pollutant removal system does not operate. The regenerative bed is cylindrically shaped, thermally insulated, 7.7 in. (0.20 m) in diameter, 10.5 in. (0.27 m) long and contains 5.2 lb (2.4 kg) of carbon. A 71 W electric heater is contained within the bed. The flow through the regenerative bed was limited to 3 cfm (5.1 m^3/hr).

In comparison with HVAC carbon filters for indoor air quality, which typically contain 45-60 lb carbon/1000 cfm, the fixed bed carbon filter for this spacecraft design

contains approximately 737 lb carbon/1000 cfm, and its lifetime was only designed to be 180 days. The regenerative filter was designed with 1733 lb carbon/1000 cfm; it is only designed to last for 24 hours, at which time it is regenerated.

The potential theory of adsorption, in the form of Equation 2.4.14, was used to estimate the adsorption equilibria. Molar volumes were used to estimate β, such that a plot of ($\tilde{A} = A/v$) versus W (a normalized potential curve) was assumed invariant for different adsorbates. From limited experiments, it was found that relative humidity had a negligible impact on the adsorption of water soluble compounds, but reduced the amount of adsorption for non-water soluble compounds. A different normalized characteristic curve was used for water soluble and non-water soluble compounds. The effect of the relative humidity was more pronounced at higher $\tilde{A}$ values (smaller amounts of contaminant adsorbed). Some experiments with multiple contaminants revealed that a component with a higher $\tilde{A}$ value would displace a lower $\tilde{A}$ value component if the difference in the $\tilde{A}$ values was greater than about 16 (gmol·K)/ml. Breakthrough data for acetone and Freon 11, alone and combined, is also reported.

Desorption studies indicated that components with a molar volume greater than 185 ml/gmol could not be practically desorbed. Components with a molar volume between 80 and 185 ml/gmol were adequately removed by desorption for 2 hours at a pressure of 10^{-4} mmHg and a temperature of 200°C. Components with a molar volume less than 80 ml/gmol were desorbed within 2 hours at 10^{-4} mmHg and 100°C. Desorption occurred at a faster rate as the temperature was increased, for example, to desorb acetone took 8 hours at ambient temperature and only 2 hours at 100°C.

To design the system, the carbon beds were modeled as consisting of a saturated layer and an adsorption zone (the region in which the adsorption wave is located). The

length of the saturated layer was estimated based on the $\tilde{A}$ values of the components, and the length of the adsorption zone was based on a theoretical equation and experimental correlation of adsorption zone length with $\tilde{A}$. The model was not particularly successful, however it was not clear whether the model was at fault or the required input information was inaccurate.

The system was tested by running experiments on a 1/10 scale model. The original design consisted of a shorter fixed carbon bed (8 in.) and a longer cycle time for the regenerative carbon bed (48 hours). The system was connected to a simulated cabin, and a closed loop test was run for 180 days. Only a subset of the 145 pollutants was used in the tests: NH_3, SO_2, Freon 114, and n-propyl alcohol were the contaminants to be removed by the fixed carbon bed; vinyl chloride, Freon 12, Freon 11 and acetone were the contaminants to be removed by the regenerative carbon bed; and CH_4, CO, C_2H_2, C_2H_4, and C_2H_6 were the contaminants to be removed by the catalytic oxidizer.

Monitoring of the fixed carbon bed indicated that n-propyl alcohol broke through on the 85th day. Freon 114 broke through on the 45th day, but was removed by the regenerative carbon bed. The fixed bed was then lengthened for the final design. The regenerative carbon bed worked very well for acetone and Freon 11, with only a few isolated instances where the efficiency dropped from approximately 100%. Freon 12 and vinyl chloride, however, broke through after about 24 hours. As a result, the cycle time was shortened to 24 hours in the final design. Some design modifications and additional testing were undertaken in a later study described in [150].

Another study [151] explored different regeneration techniques. Four different methods included thermal desorption via vacuum, thermal desorption via nitrogen purge, in-situ catalytic oxidation, and in-situ non-catalytic oxidation. The nitrogen-purge

thermal desorption was found to result in the most complete desorption with the least loss of carbon due to oxidation, and therefore was the recommended regeneration technique. Multiple adsorption and desorption cycles with single and mixed contaminants indicated some loss in working capacity of the carbon. Both the rate and amount of desorption were observed to increase with increasing temperature. For example, after desorbing for 76 minutes a carbon bed containing approximately 0.45 g acetone/g carbon via nitrogen purge thermal desorption, at 23°C, only 9% was desorbed; at 75°C, 74% was desorbed; at 105°C, 90% was desorbed; and at 150°C, 97% was desorbed.

3.4.6 Solvent recovery

Regenerated activated carbon beds are commonly used in solvent recovery applications. Low pressure steam is used for regeneration and the condensed vapors are then separated. The advantage of the process of adsorption on carbon is that the vapors become concentrated (as much as 30-50 times [152]). Efficiencies are typically in the range of 92-98%; it becomes too costly to make the process more efficient [21]. The capacity of the carbon beds is known to decrease over many cycles [152]. Design is often accomplished with pilot-scale studies [126]; see, for example, [100].

The activated carbon beds are typically cylindrical, either vertical or horizontal, with depths ranging from 0.5-3 m [21, 110, 152]. The pressure drop through the beds is on the order of 2 to 5 in. of H_2O/ft of bed depth (3.7-9.3 mmHg/ft). Annular carbon beds are an alternative configuration sometimes used.

There are at least two beds, one being used for adsorption while the other is being regenerated. When the solvent vapor begins to break through, the beds are switched. Cycle times are usually on the order of hours [152], and are determined either by

monitoring the outlet or on a time schedule which is usually based on past experience [110]. It is common to use three or four beds, of which two of the beds are used for adsorption. By arranging the two adsorption beds in series, the first bed is allowed to become completely saturated before being regenerated. In some cases, separate drying and cooling stages are added after the regeneration. Often, however, the steam is not removed from the bed prior to adsorption, as the the evaporation of the water vapor from the bed during adsorption helps keep the temperature of the bed down [123].

The concentration of the solvent vapor in the inlet gas is typically in the range of 1 to 20 g/m^3 [21] (for toluene at 30°C and 1 atm total pressure, this corresponds to 270 to 5400 ppm). Sometimes the concentration of solvent in the inlet gas is lowered by dilution in order to decrease the temperature rise resulting from the adsorption. The temperature of the inlet air is usually kept below about 40°C.

Steam has been found to be more effective than hot gases for regeneration [126, 152]. Typically 1 to 4 pounds of steam are used per pound of recovered solvent [152]. The direction of flow for regeneration is always opposite to that of adsorption in order to keep the end of the bed as clean as possible.

Nelson et al. [153] performed field studies of six full-scale activated carbon solvent recovery systems. The systems were all used in the surface coating industry, two representing each of the following areas: rubberized fabric manufacturing, magnetic tape manufacturing, and flexible package manufacturing. Four were horizontal carbon beds and two were annular carbon beds. Adsorption times ranged from 64 to 560 minutes. All of the beds were steam regenerated for times ranging from 25 to 55 minutes. The six systems were designed with 400, 667, two at 909, and 1786 lb carbon/1000 cfm. Inlet concentrations were typically between 1000 ppm and 4000 ppm and inlet temperatures

ranged from 29°C to 49°C. Inlet and outlet concentrations were measured over a two week period. The measured efficiencies for four of the plants were greater then 97%; the other two plants had efficiencies of approximately 85% and 95%. Four of the systems were tested again after 18 months, and from these test results and the known age of the carbon, the lifetimes of the four plants were estimated at 4 to 6 years before a significant reduction in efficiency.

An alternative type of regenerative carbon system used for solvent recovery is a continually regenerated fluidized-bed or moving-bed system [21, 126, 154, 155]. As opposed to a rotary regenerative system, this system involves actual movement of the carbon granules (whereas the rotary regenerative system involves movement of the carbon bed). The carbon typically moves downward and the air to be cleaned flows through the carbon in either a crosscurrent or countercurrent direction. Desorption usually occurs at the bottom before the carbon is transported back to the top. It is important to have a very hard carbon, as attrition of the carbon is a significant problem.

Larsen and Pilat [154, 155] experimentally studied a moving bed activated carbon adsorption system for removing VOCs from air with application to a painting facility. In a pilot plant study [155], a concentration about 30-50 ppm ethanol was to be removed from an air stream. Two carbon flowrates were used, 8 lb/hr (3.63 kg/hr) and 5 lb/hr (2.27 kg/hr). Desorption was accomplished through contact heating at temperatures from 80 to 140°C. The system worked well (almost 100% efficient) for the first 18 hours at which time the efficiency began to drop. After 26 hours, when the study was stopped, the efficiency was about 85%. Attrition of the carbon was significant: after 26 hours of operation, 7.7% of the carbon was reduced to less than 30 mesh (0.59 mm). The carbon had originally consisted of cylindrical pellets 4.4 mm in diameter.

The system was later installed at an actual painting facility [154]. The total VOC concentration was measured as if it were entirely methyl ethyl ketone so that the VOC concentrations were reported in equivalent units of methyl ethyl ketone ppm. Due to the variable nature of the painting, the VOC concentration varied widely, from less than 0.01 ppm to 20 ppm. Carbon flowrates of 5 and 8 lb/hr (2.27 kg/hr and 3.63 kg/hr) were used and air flowrates were between 5.3 and 36 cfm (9 and 61.2 m^3/hr). The average desorption temperature was about 80°C. The VOC collection efficiency was in the range of 75 to 100%. After 48 hours, 13.5% of the carbon had been reduced to less than 30 mesh.

Klobucar and Pilat [156] studied the desorption of ethanol from an activated carbon countercurrent moving bed adsorption system. As regeneration temperatures were increased from 20 to 60°C, the desorber efficiency, defined as the gas phase outlet ethanol flowrate divided by the solid phase ethanol inlet flowrate, was observed to increase from about 25% to 80%. Mass transfer cofficients were also estimated.

3.4.7 Food storage

Activated carbon has been used in fruit and other food storage, ostensibly to slow ripening and decay by adsorbing VOCs emitted by the food [157, 158]. Although studies did indicate that carbon reduced the cross-transfer of food odors between different foods [157], Gerhardt [158] found that using an activated carbon air cleaning system did not prolong the storage life of fruit. In an experiment, fruit was stored in two test rooms, one with an activated carbon air purifier and the other without. Measurements were taken over a six month period. Ethylene, a gas suspected to promote ripening, was not significantly reduced by the carbon. The carbon room did exhibit lower levels of VOCs,

but the carbon system, although larger than specified by the manufacturer, was saturated after three months; the manufacturer had indicated that it would last for an entire season. Studies of commercial fruit storage rooms with and without activated carbon air purifying systems showed no significant effect of the carbon on VOC concentrations. Tests on the fruit (e.g., firmness), for the most part indicated no advantage to storing the fruit in the room with the carbon system.

3.4.8 Chromatography

In chromatography, activated carbon is not usually used as an adsorbent. Chromatography is used primarily to identify different components of a mixture; it is an analytical tool. The mixture is passed through an adsorbent which separates the components based on their different adsorptivities. A chromatograph consists of a column, which contains the adsorbent, inside of a temperature controlled oven. An inert gas, such as nitrogen, flows through the column to a detector, e.g., a flame ionization detector. The mixture is added as a pulse input to the inert carrier gas. As the pulse of the mixture moves through the adsorbent column, different components of the mixture are delayed by different amounts of time. The individual components of the mixture are identified by matching the time that it takes for them to transverse the system with known times for different species. The area of the peak can be used to estimate the concentration. Activated carbon is not used very often in chromatographic columns because it does not do a good job of separating the different mixture components. This feature of activated carbon is one of the main reasons that it is used in air pollution control applications.

3.4.9 Desiccant studies

Activated carbon is not usually used as a desiccant, however, there have been many studies of rotary regenerative adsorbent wheels for use in desiccant air conditioning systems, e.g., [1, 128-132, 159]. The modeling techniques are applicable to the carbon filter design, i.e., the same equations with similar type solutions. The results, however, are not especially relevant; they are applicable to only a tiny portion of the VOC filtration problem.

Desiccant studies for air conditioning applications involve adsorption of water vapor (one known vapor with well-documented properties) on an adsorbent which is typically silica gel, a molecular sieve, lithium chloride, or lithium bromide. More recently, polymers have also been investigated for use as a desiccant adsorbent. Activated carbon is not used as a desiccant because it does not adsorb water vapor well at low relative humidities, which is one of the main reasons that carbon is suitable for VOC removal. The adsorption and desorption characteristics of activated carbon are somewhat different, e.g., activated carbon has higher retentivites than other adsorbents.

Many of the applied results of the desiccant studies, e.g., optimization of the wheel rotation speed, are strongly tied to the isotherm slope. For the desiccants, the range of the isotherm slope is very limited. The range of isotherm slopes for the different VOCs on activated carbon spans at least five orders of magnitude. In addition, the concentrations are very different, e.g., 5% relative humidity corresponds to 1500 ppm.

Some of the more relevant work is that involving adsorption of different pollutants on desiccant wheels. An experimental study of the pollutant removal capabilities of a commercial rotary regenerative desiccant unit was conducted by Relwani and Moschandreas [135]. The pollutants considered were CO, NO_2, and SO_2. Two different

adsorbents, a silica gel and a molecular sieve, were used. In all, 65 different experiments were conducted, including two regeneration temperatures, three pollutant concentrations, and different relative humidity levels. Inlet and outlet concentrations and temperatures were measured for both the process and regeneration sides of the wheel. System specifications include a wheel speed of 3.2 rotations per hour, a wheel diameter of 2 ft, a wheel thickness of 2 in., and an air flowrate of 150 cfm. Approximately 2/3 of the wheel was used for processing and 1/3 for regeneration.

Removal efficiency, defined as the change in concentration between the process inlet and outlet divided by the process inlet concentration, for silica gel ranged from 10 to 36% for CO, 15 to 33% for NO_2, and 9 to 18% for SO_2. Removal efficiencies for molecular sieve 5A ranged from 10 to 61% for CO, 27 to 43% for NO_2, and 73 to 95% for SO_2. Data on the concentration change across the regeneration side of the wheel were also reported.

Unfortunately, many of the conclusions in [135], which result from comparisons of experimental runs, are unfounded. There appeared to be no control on the concentration in the regeneration inlet air for different runs; sometimes it was greater than the process side inlet concentration and sometimes it was less. For example, for the five different CO runs on silica gel at the high regeneration temperature (≈135-150°C), the process and regeneration inlet concentrations in units of $\mu g/m^3$ were (784,929), (1124,1182), (1365,1503), (11731,605), and (12924,556), where the first number of each pair is the process inlet concentration and the second number is the regeneration inlet concentration. These numbers correspond to ratios of regeneration inlet concentration to process inlet concentration ranging from 1.185 to 0.043.

In addition, many of the graphs presented for the regeneration side analyses do not agree with the tabulated data (e.g., the data for CO on the molecular sieve at the low regeneration temperatures). The graphs are supposed to plot the increase in concentration across the regeneration side of the wheel versus the regeneration inlet concentration. In most cases, the concentration increase appears to have been plotted versus the wrong inlet concentration (i.e., the inlet concentration from a different run). The concentration increase values appear to have been plotted by assuming that the regeneration inlet concentration increased with the table row number, however the regeneration inlet concentration varied inconsistently with row number. Adding to the confusion is the fact that the values of the regeneration inlet concentrations in the plots (in any order) do not match those in the table. Because these graphs were used by Relwani and Moschandreas for their regeneration analyses, many of the conclusions are incorrect.

Chapter 4

Model Development

This chapter describes the adsorption problem from a modeling point of view. Included are the assumptions, nomenclature, and model equations. Previous modeling work is summarized.

4.1 Assumptions

The development of the model equations for the rotary regenerative carbon wheel is based on the modeling of desiccant wheels by Van den Bulck [130]. The following assumptions, made by Van den Bulck, are also used in this work:

1. plug flow;
2. negligible pressure drop;
3. uniform packing;
4. no leakage between process and regeneration sides;
5. adsorption is completely reversible;
6. constant specific heats;
7. ideal gas;
8. gas phase storage of energy and mass is negligible;
9. no convection in the solid phase;
10. no axial conduction or diffusion;
11. fluid and matrix states are uniform in the radial direction;
12. inlet concentrations and temperatures are uniform and constant;
13. lumped transfer coefficients are adequate to model heat and mass transfer effects;
14. adiabatic operation of the wheel.

An additional assumption used in modeling the carbon wheel is that there is no competitive adsorption between the different contaminants. For the very low VOC concentrations being considered, and considering the number of uncertainties involved regarding the VOCs, this is a reasonable first assumption.

For this project, only the periodic steady-state solution was considered. The steady-state solution, combined with the above assumptions, means that for a stationary observer (Eulerian coordinate system) the concentration and temperature within the wheel vary with axial position and with angular position, but not with time. At the outlet of the wheel, the concentrations and temperatures are a function of angular position, and thus to calculate the filter's effect on, e.g., the process air stream, the angular-average concentrations and temperatures are required.

To an observer riding on the wheel (Lagrangian coordinate system), the steady-state operation is periodic. The concentrations and temperatures vary with axial position and change with time, although each time the wheel goes around, the same concentrations and temperatures are observed at the same angular position as on the previous rotation. Thus, the "time" referred to throughout this work is for a specific rotating piece of the wheel. For a rotating observer at the outlet of the wheel the concentrations and temperatures are a function of time only.

Since the concentration and temperature variations with time of a rotating piece of the wheel are identical to the angular variations seen by a stationary observer, the angular-average outlet concentration and temperature is the same as the rotating observer's time-average outlet concentration and temperature.

The duration of the process period is defined as the time it takes to rotate through the process side of the wheel; the duration of the regeneration period is similarly defined. If the wheel rotation speed is slow enough that the outlet state (i.e., concentration and temperature) at the end of the process period is equal to the process inlet state, the wheel is considered to be fully or completely processed. Similarly, if the outlet state at the end of the regeneration period is equal to the regeneration inlet state, the wheel is referred to as fully or completely regenerated.

4.2 Nomenclature

The gas phase concentration of a contaminant is denoted by the symbol ω. The concentration is actually the mole ratio with units of [kgmol i/kgmol clean air]. By assuming an ideal gas, the mole ratio is equivalent to the volume ratio, and thus the parts per million (ppm) and part per billion (ppb) units, which are usually volume based, can be used as molar units. The solid phase concentration of contaminant i is denoted by the symbol W; it is a mixed ratio, with units of [kgmol i/kg clean adsorbent matrix]. The adsorbent matrix, for this work, is the activated carbon, and does not include any additional mass of a support system, frame, etc. The gas phase concentration of contaminant i in equilibrium with the solid phase concentration, which because of mass transfer effects is not the same as the actual gas phase concentration, is denoted by ω^*. Thus the isotherm equations of Chapter 2 should really be written as functions of W and ω^* instead of W and ω.

The temperature of the gas phase is denoted by t, and the temperature of the solid phase by T. The total enthalpy of the gas and solid phases is denoted by the symbols h and H, respectively. The gas phase enthalpy is the total molar enthalpy on a clean air

basis, i.e., it is in units of [J/kgmol clean air]. The solid phase total enthalpy is mass based, with units of [J/kg clean matrix]. The total enthalpy of the ideal gas phase can be expressed as the sum of the enthalpy of the clean air and the enthalpy of the contaminant, i.e.,

$$h = h_{air} + \omega h_i \tag{4.2.1}$$

where h_i is the enthalpy of the vapor phase contaminant in [J/kgmol i]. The convention of using a molar basis for the gas phase and a mass basis for the solid phase is used consistently throughout, so that quanities like specific heats and densities will be either molar or mass based depending on whether they refer to the gas or the solid phase.

Some of the nomenclature used to decribe the rotary wheel is indicated in Figure 3.6. z is the distance along the length of the wheel in the air flow direction, varying from 0 to L. For each period, z=0 is at the edge of the wheel where the air enters. The angular coordinate, ϕ, increases in the direction of rotation, from 0 at the start of the process period to 2π at the end of the regeneration period.

The different airstreams entering and leaving the rotary filter are denoted by a two-number subscript, the first number indicating which period (1=process, 2=regeneration) and the second number indicating which end of the flow (1=inlet, 2=outlet). For example, ω_{21} is the regeneration side inlet gas phase concentration.

4.3 Non-equilibrium model equations

The governing equations for the adsorbent system, taking into account the assumptions listed in Section 4.1, are as follows:

contaminant mass conservation equation:

$$\dot{n}_{air}\frac{\partial \omega}{\partial z}+\frac{m_m}{L}\frac{\partial W}{\partial \theta}=0 \tag{4.3.1}$$

contaminant mass transfer rate equation:

$$\dot{n}_{air}\frac{\partial \omega}{\partial z}=\frac{\kappa_m A}{L}(\omega^*-\omega) \tag{4.3.2}$$

energy conservation equation:

$$\dot{n}_{air}\frac{\partial h}{\partial z}+\frac{m_m}{L}\frac{\partial H}{\partial \theta}=0 \tag{4.3.3}$$

energy transfer rate equation:

$$\dot{n}_{air}\frac{\partial h}{\partial z}=\frac{\kappa_t A}{L}(T-t)+h_i\frac{\kappa_m A}{L}(\omega^*-\omega) \tag{4.3.4}$$

adsorption equilibrium equation:

$$\omega^*=\omega^*(W,T) \tag{4.3.5}$$

enthalpy equations:

$$h=h(\omega,t)=h_{air}(t)+\omega h_i(t) \tag{4.3.6}$$

$$H=H(W,T)=H_{mtx}(T)+WH_i(T) \tag{4.3.7}$$

The conservation equations (4.3.1 and 4.3.3) consist of a gas phase convection term and a solid phase storage term. Storage in the gas phase is neglected.

Normalized space and time variables are introduced to simplify the equations:

$$x = \frac{z}{L} \tag{4.3.8}$$

$$\tau = \frac{\theta \dot{n}_{air}}{m_m} \tag{4.3.9}$$

where the normalized time variable, τ, is equal to the ratio of the air flowrate to the matrix "flowrate". The maximum value of τ occurs at $\theta = \theta_j$, where θ_j is the duration of period j (j=1 indicates the process period and j=2 indicates the regeneration period). The parameter $1/\Gamma_j$ is introduced as the upper bound on τ, i.e., $1/\Gamma_j$ is the normalized duration of period j:

$$\frac{1}{\Gamma_j} = \frac{\theta_j \dot{n}_{air}}{m_{mtx}} \tag{4.3.10}$$

Note that τ can also be defined as:

$$\tau = \frac{\theta}{\theta_j}\frac{1}{\Gamma_j} \tag{4.3.11}$$

For a given matrix mass, $1/\Gamma_j$ is directly proportional to the air mass flowrate and inversely proportional to the wheel rotation speed. Also, *NTU*s are defined for mass and heat transfer as follows:

$$NTU_m = \frac{\kappa_m A}{\dot{n}_{air}} \tag{4.3.12}$$

$$NTU_t = \frac{\kappa_t A}{\dot{n}_{air}\left(\frac{\partial h}{\partial t}\right)_\omega} \tag{4.3.13}$$

For an ideal gas, the partial derivative of the total gas enthalpy with respect to temperature at constant ω, $(\partial h/\partial t)_{\omega}$, is equal to the constant pressure specific heat of air, so that Equation 4.3.13 can be reduced to:

$$NTU_t = \frac{\kappa_t A}{\dot{n}_{air} c_{air}} \tag{4.3.14}$$

Using these normalized variables, Equations 4.3.1 through 4.3.4 can be rewritten as:

$$\frac{\partial W}{\partial \tau} + \frac{\partial \omega}{\partial x} = 0 \tag{4.3.15}$$

$$\frac{\partial \omega}{\partial x} = NTU_m(\omega^* - \omega) \tag{4.3.16}$$

$$\frac{\partial H}{\partial \tau} + \frac{\partial h}{\partial x} = 0 \tag{4.3.17}$$

$$\frac{\partial h}{\partial x} = c_{air} NTU_t(T - t) + h_i NTU_m(\omega^* - \omega) \tag{4.3.18}$$

These equations along with the property relations of Equations 4.3.5 to 4.3.7 form a system of seven equations and seven unknowns: ω, ω*, W, t, T, h, and H.

4.4 Equilibrium equations

As a first approximation, modeling studies are often performed with infinite heat and mass transfer coefficients. Infinite transfer coefficients mean that equilibrium between the gas and solid phases is reached instantaneously; such analyses are often called equilibrium analyses. For example, in an infinite transfer coefficient analysis, an

addition of thermal energy to a gas-solid adsorption system would result in instantaneous identical changes in the gas and solid temperatures and instantaneous changes in the gas and solid phase contaminant concentrations (to values given by the isotherm for the new temperature). Equilibrium analyses are often used to obtain qualitative estimates of system performance.

In an equilibrium analysis,

$$\omega^* = \omega \tag{4.4.1}$$

and

$$T = t \tag{4.4.2}$$

and the rate equations (Equation 4.3.16 and 4.3.18) disappear. The governing equations are thus reduced to:

$$\frac{\partial W}{\partial \tau} + \frac{\partial \omega}{\partial x} = 0 \tag{4.4.3}$$

$$\frac{\partial H}{\partial \tau} + \frac{\partial h}{\partial x} = 0 \tag{4.4.4}$$

For the rotary regenerative configuration, the initial conditions are as follows:

$$\omega(x=0,\tau) = \begin{cases} \omega_{11} & 0 < \tau < 1/\Gamma_1 \\ \omega_{21} & 1/\Gamma_1 < \tau < 1/\Gamma_2 \end{cases} \tag{4.4.5}$$

$$T(x=0,\tau) = \begin{cases} T_{11} & 0 < \tau < 1/\Gamma_1 \\ T_{21} & 1/\Gamma_1 < \tau < 1/\Gamma_2 \end{cases} \tag{4.4.6}$$

where for each period $x = 0$ indicates the inlet side. The step change occurs at the boundaries between the process and regeneration sides. By using the property relations:

$$\omega = \omega(W,T) \tag{4.4.7}$$

$$h = h(\omega,T) \tag{4.4.8}$$

$$H = H(W,T) \tag{4.4.9}$$

Equations 4.4.3 and 4.4.4 can be rewritten with T and ω as the dependent variables, where the notation f_x is used to indicate $(\partial f/\partial x)_y$ where $f = f(x,y)$:

$$\frac{\partial \omega}{\partial \tau} + \left[\frac{\omega_W H_T + \omega_T(h_\omega - H_W)}{H_T}\right]\frac{\partial \omega}{\partial x} + \left[\frac{\omega_T h_T}{H_T}\right]\frac{\partial T}{\partial x} = 0 \tag{4.4.10}$$

$$\frac{\partial T}{\partial \tau} + \left[\frac{h_\omega - H_W}{H_T}\right]\frac{\partial \omega}{\partial x} + \left[\frac{h_T}{H_T}\right]\frac{\partial T}{\partial x} = 0 \tag{4.4.11}$$

Introducing the quantities b_1 through b_5 as defined below:

$$b_1 = \omega_T \tag{4.4.12}$$

$$b_2 = \omega_W \tag{4.4.13}$$

$$b_3 = H_T \tag{4.4.14}$$

$$b_4 = h_T \tag{4.4.15}$$

$$b_5 = h_\omega - H_W \tag{4.4.16}$$

Equations 4.4.10 and 4.4.11 can be rewritten as

$$\frac{\partial \omega}{\partial \tau} + \left[\frac{b_2 b_3 + b_1 b_5}{b_3}\right]\frac{\partial \omega}{\partial x} + \left[\frac{b_1 b_4}{b_3}\right]\frac{\partial T}{\partial x} = 0 \tag{4.4.17}$$

$$\frac{\partial T}{\partial \tau} + \left[\frac{b_5}{b_3}\right]\frac{\partial \omega}{\partial x} + \left[\frac{b_4}{b_3}\right]\frac{\partial T}{\partial x} = 0 \tag{4.4.18}$$

Equations 4.4.17 and 4.4.18 form a coupled system of two nonlinear partial differential equations. They are nonlinear because the coefficients (the terms in brackets) are functions of T and ω. Explicit expressions for the enthalpies and the adsorption isotherms are required to evaluate h_T, h_ω, H_T, H_W, W_ω, and W_T. In the following sections, such expressions are developed along with the partial derivatives.

4.4.1 Enthalpies

Assuming an ideal gas, the total enthalpy of the gas phase can be expressed as

$$h = \int_{T_{ref}}^{T} c_{p,air}\,dy + \omega\left[\int_{T_{ref}}^{T_{dp}} c_{p,l}\,dy + \Delta h_{fg(T_{dp})} + \int_{T_{dp}}^{T} c_{p,v}\,dy\right] \tag{4.4.19}$$

or alternatively as

$$h = \int_{T_{ref}}^{T} c_{p,air}\,dy + \omega\left[\Delta h_{fg(T_{ref})} + \int_{T_{ref}}^{T} c_{p,v}\,dy\right] \tag{4.4.20}$$

and, assuming constant specific heats, reduces to

$$h = c_{p,air}(T - T_{ref}) + \omega[\Delta h_{fg(T_{ref})} + c_{p,v}(T - T_{ref})] \tag{4.4.21}$$

The partial derivatives with respect to temperature and concentration are as follows:

$$h_T = \left(\frac{\partial h}{\partial T}\right)_\omega = c_{p,air} + \omega c_{p,v} \tag{4.4.22}$$

$$h_\omega = \left(\frac{\partial h}{\partial \omega}\right)_T = \Delta h_{fg(T_{ref})} + c_{p,v}(T - T_{ref}) \tag{4.4.23}$$

The enthalpy of the solid phase consists of contributions from the solid matrix and the adsorbed contaminant:

$$H = \int_{T_{ref}}^{T} c_{p,mtx}dy + W\left[\int_{T_{ref}}^{T_{dp}} c_{p,l}dy + \Delta h_{fg(T_{dp})} + \int_{T_{dp}}^{T} c_{p,v}dy\right] - \int_{0}^{W} \Delta h_s dW \tag{4.4.24}$$

where the heat of adsorption is the isosteric heat of adsorption and has been assumed independent of temperature. Using the same approximation for the enthalpy of the contaminant vapor as in Equation 4.4.20, and assuming constant specific heats, the solid phase enthalpy can be expressed as:

$$H = c_{p,mtx}(T - T_{ref}) + W[\Delta h_{fg(T_{ref})} + c_{p,v}(T - T_{ref})] - \int_{0}^{W} \Delta h_s dW \tag{4.4.25}$$

The partial derivatives with respect to temperature and solid phase concentration are:

$$H_T = \left(\frac{\partial H}{\partial T}\right)_W = c_{p,mtx} + W c_{p,v} \tag{4.4.26}$$

$$H_W = \left(\frac{\partial H}{\partial W}\right)_T = \Delta h_{fg(T_{ref})} + c_{p,v}(T - T_{ref}) - \Delta h_s \tag{4.4.27}$$

4.4.2 The linear isotherm

The linear isotherm, as indicated in Chapter 2, is:

$$W = K\omega \tag{4.4.28}$$

and the temperature dependence of the constant K was shown (Equation 2.4.3) to be:

$$K = K_0 \exp\left[\frac{\Delta h_s}{R}\left(\frac{1}{T} - \frac{1}{T_0}\right)\right] \tag{4.4.29}$$

Solving for ω and evaluating the partial derivatives ω_T and ω_W:

$$\omega = \frac{W}{K} \tag{4.4.30}$$

$$\omega_T = \left(\frac{\partial \omega}{\partial T}\right)_W = \frac{\omega \Delta h_s}{RT^2} \tag{4.4.31}$$

$$\omega_W = \left(\frac{\partial \omega}{\partial W}\right)_T = \frac{1}{K} \tag{4.4.32}$$

4.4.3 The Langmuir isotherm

From Chapter 2, recall the form of the Langmuir isotherm (Equation 2.4.9):

$$W = \frac{W_0 K \omega}{W_0 + K\omega} \tag{4.4.33}$$

or, solving for ω:

$$\omega = \frac{W W_0}{K(W_0 - W)} \tag{4.4.34}$$

The partial derivatives with respect to temperature and solid phase concentration are:

$$\omega_T = \left(\frac{\partial \omega}{\partial T}\right)_W = \frac{W W_0 \Delta h_s}{KRT^2(W_0 - W)} = \frac{\omega \Delta h_s}{RT^2} \tag{4.4.35}$$

$$\omega_W = \left(\frac{\partial \omega}{\partial W}\right)_T = \frac{W_0^2}{K(W_0 - W)^2} = \frac{(W_0 + K\omega)^2}{KW_0^2} \tag{4.4.36}$$

Table 4.1 summarizes the quantities b_1 through b_5 for Equations 4.4.17 and 4.4.18 for the linear and Langmuir isotherms.

Table 4.1 Equilibrium equations for the linear and Langmuir isotherms.

Mass conservation equation:

$$\frac{\partial \omega}{\partial \tau}+\left[\frac{b_2 b_3+b_1 b_5}{b_3}\right]\frac{\partial \omega}{\partial x}+\left[\frac{b_1 b_4}{b_3}\right]\frac{\partial T}{\partial x}=0$$

Energy conservation equation:

$$\frac{\partial T}{\partial \tau}+\left[\frac{b_5}{b_3}\right]\frac{\partial \omega}{\partial x}+\left[\frac{b_4}{b_3}\right]\frac{\partial T}{\partial x}=0$$

	Linear isotherm $W = K\omega$	Langmuir isotherm $W = W_0 K\omega/(W_0 + K\omega)$
$b_1 = \omega_T$	$\frac{\omega \Delta h_s}{RT^2}$	$\frac{\omega \Delta h_s}{RT^2}$
$b_2 = \omega_W$	$\frac{1}{K}$	$\frac{(W_0 + K\omega)^2}{K W_0^2}$
$b_3 = H_T$	$c_{mtx} + \omega K c_v$	$c_{mtx} + \left[\frac{W_0 K \omega}{W_0 + K\omega}\right] c_v$
$b_4 = h_T$	$c_{air} + \omega c_v$	$c_{air} + \omega c_v$
$b_5 = h_\omega - H_W$	Δh_s	Δh_s

4.5 Low concentration assumption

Equations 4.4.17 and 4.4.18 form a system of coupled one-dimensional nonlinear hyperbolic partial differential equations, also known as a 2 x 2 system of conservation laws. These equations can be solved using Riemann invariants or other similar techniques and result in changes in temperature and concentration propagating through the matrix as either rarefaction waves or shock waves. The solution, which is presented in Chapter 5, is rather complex, requiring an iterative numerical integration procedure.

For the trace contaminant concentrations with which this research is concerned, an assumption in the energy equation greatly simplifies the equilibrium solution. The contribution to the total enthalpy from the contaminant, both in the gas phase and in the solid phase, is assumed to be negligible due to the very low concentrations. The gas and solid phase concentrations are approximated as follows:

$$h \approx c_{air}(T - T_{ref}) \tag{4.5.1}$$

$$H \approx c_{mtx}(T - T_{ref}) \tag{4.5.2}$$

Physically, this assumption means that the adsorption and desorption processes do not change the temperature of the system since the amount of contaminant adsorbed and desorbed is so small. The enthalpy partial derivatives with this assumption are as follows:

$$h_T = c_{air} \tag{4.5.3}$$

$$H_T = c_{mtx} \tag{4.5.4}$$

$$h_\omega = 0 \tag{4.5.5}$$

$$h_T = 0 \tag{4.5.6}$$

4.5.1 Non-equilibrium equations with the low concentration assumption

The non-equilibrium equations (Equations 4.3.15 to 4.3.18), using the low concentration assumption, reduce to:

$$\frac{\partial W}{\partial \tau} + \frac{\partial \omega}{\partial x} = 0 \tag{4.5.7}$$

$$\frac{\partial \omega}{\partial z} = NTU_m(\omega^* - \omega) \tag{4.5.8}$$

$$\frac{\partial T}{\partial \tau} + \frac{1}{\sigma}\frac{\partial t}{\partial x} = 0 \tag{4.5.9}$$

$$\frac{\partial t}{\partial z} = NTU_t(T - t) \tag{4.5.10}$$

where σ is defined as:

$$\sigma = \frac{c_{mtx}}{c_{air}} \tag{4.5.11}$$

4.5.2 Equilibrium equations with the low concentration assumption

The equilibrium equations (Equations 4.4.3 and 4.4.4), using the low concentration assumption, reduce to:

$$\frac{\partial W}{\partial \tau}+\frac{\partial \omega}{\partial x}=0 \tag{4.5.12}$$

$$\frac{\partial T}{\partial \tau}+\frac{1}{\sigma}\frac{\partial T}{\partial x}=0 \tag{4.5.13}$$

or, in terms of ω and T:

$$\frac{\partial \omega}{\partial \tau}+\omega_W\frac{\partial \omega}{\partial x}+\left[\frac{\omega_T}{\sigma}\right]\frac{\partial T}{\partial x}=0 \tag{4.5.14}$$

$$\frac{\partial T}{\partial \tau}+\frac{1}{\sigma}\frac{\partial T}{\partial x}=0 \tag{4.5.15}$$

Table 4.2 lists the definitions of b_1 through b_5 for use in the original equations, i.e., Equations 4.4.17 and 4.4.18, for the low concentration assumption. Table 4.3 lists the simplified version of the equilibrium conservation equations that result from the low concentration assumption.

Table 4.2 Equilibrium equations for the linear and Langmuir isotherms with the low concentration parameters.

Mass conservation equation:

$$\frac{\partial \omega}{\partial \tau}+\left[\frac{b_2 b_3+b_1 b_5}{b_3}\right]\frac{\partial \omega}{\partial x}+\left[\frac{b_1 b_4}{b_3}\right]\frac{\partial T}{\partial x}=0$$

Energy conservation equation:

$$\frac{\partial T}{\partial \tau}+\left[\frac{b_5}{b_3}\right]\frac{\partial \omega}{\partial x}+\left[\frac{b_4}{b_3}\right]\frac{\partial T}{\partial x}=0$$

	Linear isotherm $W=K\omega$	Langmuir isotherm $W=W_0 K\omega/(W_0+K\omega)$
$b_1=\omega_T$	$\frac{\omega \Delta h_s}{RT^2}$	$\frac{\omega \Delta h_s}{RT^2}$
$b_2=\omega_W$	$\frac{1}{K}$	$\frac{(W_0+K\omega)^2}{KW_0^2}$
$b_3=H_T$	c_{mtx}	c_{mtx}
$b_4=h_T$	c_{air}	c_{air}
$b_5=h_\omega-H_W$	0	0

The energy equation, because of the low concentration assumption, can be solved independently of the mass conservation equation. In addition, because the specific heats have been assumed constant, Equation 4.5.15 is a linear partial differential equation. The mass conservation equation, however, because of the temperature dependence of the adsorption isotherm, is dependent on the solution of the energy equation.

Table 4.3 Low concentration equilibrium equations for the linear and Langmuir isotherms.

	Linear isotherm $W = K\omega$	Langmuir isotherm $W = \frac{W_0 K\omega}{W_0 + K\omega}$
Contaminant mass conservation equation:	$\frac{\partial\omega}{\partial\tau} + \frac{1}{K}\frac{\partial\omega}{\partial x} + \left[\frac{\omega\Delta h_s}{RT^2}\right]\frac{\partial T}{\partial x} = 0$	$\frac{\partial\omega}{\partial\tau} + \left[\frac{(W_0 + K\omega)^2}{KW_0^2}\right]\frac{\partial\omega}{\partial x} + \left[\frac{\omega\Delta h_s}{RT^2}\right]\frac{\partial T}{\partial x} = 0$
Energy conservation equation:	$\frac{\partial T}{\partial\tau} + \frac{1}{\sigma}\frac{\partial T}{\partial x} = 0$	$\frac{\partial T}{\partial\tau} + \frac{1}{\sigma}\frac{\partial T}{\partial x} = 0$

4.6 Application to fixed-bed configurations

The equations presented in this chapter can also be applied for analysis of a fixed-bed. The fixed-bed problem is a transient problem, and in this case the time variable represents time in an Eulerian coordinate system. The rotary regenerative configuration, because of the assumptions made, can be thought of as a fixed-bed which operates as an adsorber for a period of time (the process period duration), after which it is desorbed for a period of time (the regeneration period duration).

4.7 Modeling studies

Many authors have attempted to model the adsorption process using equations similar to Equations 4.3.1 to 4.3.4, or for equilibrium analyses, Equations 4.4.3 and 4.4.4. Often there are slight variations in the assumptions, e.g., the gas phase storage terms or axial diffusion terms are included. A detailed analysis of the different modeling approaches is beyond the scope of this work, and the list of authors included here is not complete.

Although some authors have considered "low concentrations", the concentrations are still higher than the VOC concentrations in indoor air. In addition, virtually all low concentration studies have been isothermal (which supports the low concentration assumption of Section 4.5). For the rotary regenerative carbon filter, however, the non-isothermal solution must be considered because of the step change in the inlet gas temperature that occurs between process and regeneration sides of the wheel.

A goal of this project was not to simply solve the equations, but rather to explore the design and potential of a rotary regenerative activated carbon filter. A way to examine many different possibilities and draw conclusions was necessary. Although the solution of the full equations (Equations 4.3.1 to 4.3.4) could have been used in the filter design, the simplicity of the solution with the low concentration assumption facilitates the filter design. The effect of the assumption on the solution is shown in Chapter 5 to be negligible.

In the next chapter, a method for solving the full equations is presented, and the solution of the low concentration equations is developed as a special case of the full equation solution. Also included is a discussion of some of the more relevant modeling work.

Table 4.4 lists references which either develop or use equilibrium models. Table 4.5 lists references which either develop or use non-equilibrium models. Also included are some references in which the modeling is of heat transfer only, as the equations are analogous to isothermal mass transfer. Several references provide an overview of much of the modeling work, e.g., [24] and [161]. The solutions are both analytical and numerical, e.g., the isothermal single component non-equilibrium solution with an overall mass transfer coefficient has a well known analytic solution (although it does require numerical integration of an integral). The multi-component non-equilibrium adiabatic solutions, on the other hand, are all numerical. The majority of the modeling work has been for the fixed-bed configuration.

Table 4.4 Equilibrium modeling of adsorption processes.

	Isothermal	Adiabatic & Non-isothermal
Single component	159, 162-169, 170	1, 128, 130, 133, 159, 165, 174-183
Multi-component	163, 167, 171-173	165, 182-184

Table 4.5 Non-equilibrium modeling of adsorption processes.

	Isothermal	Adiabatic & Non-isothermal
Single component	80, 82, 127, 159, 162, 164, 185-199	1, 127, 129, 130, 132, 159, 185, 196, 201-212
Multi-component	193, 200	213-218

4.8 Model parameters

Table 4.1 gives an indication of the many parameters which must be assigned values during the modeling. A base set of parameter values, listed in Table 4.6, will be used throughout. Variations from this base case will also be explored.

Table 4.6 Base parameter values.

Parameter	Base values
Δh_s	10 kcal/gmol = 41860000 J/kgmol
R	8314.4 J/(kgmol·K)
c_m	1300 J/(kg·K)
c_{air}	29163 J/(kgmol·K)
$\sigma = c_m/c_{air}$	1300/29163 = 0.044577 kgmol/kg
c_v	60000 J/(kgmol·K)
T_0	25°C
W_0	0.005 kgmol/kg

Using these parameter values, the isotherms can be examined more closely. Figure 4.1 shows the temperature dependence of the linear isotherm slope for three different values of the heat of adsorption. For Δh_s = 10 kcal/gmol, increasing the temperature from 20°C to 60°C results in an increase in the isotherm slope of almost ten times. The variation with temperature is more pronounced for larger values of Δh_s. In the limit as the temperature increases to infinity, the isotherm slope approaches a constant value, i.e.,

$$\lim_{T \to \infty} (K/K_0 P) = \exp[-\Delta h_s/(RT_0)]$$

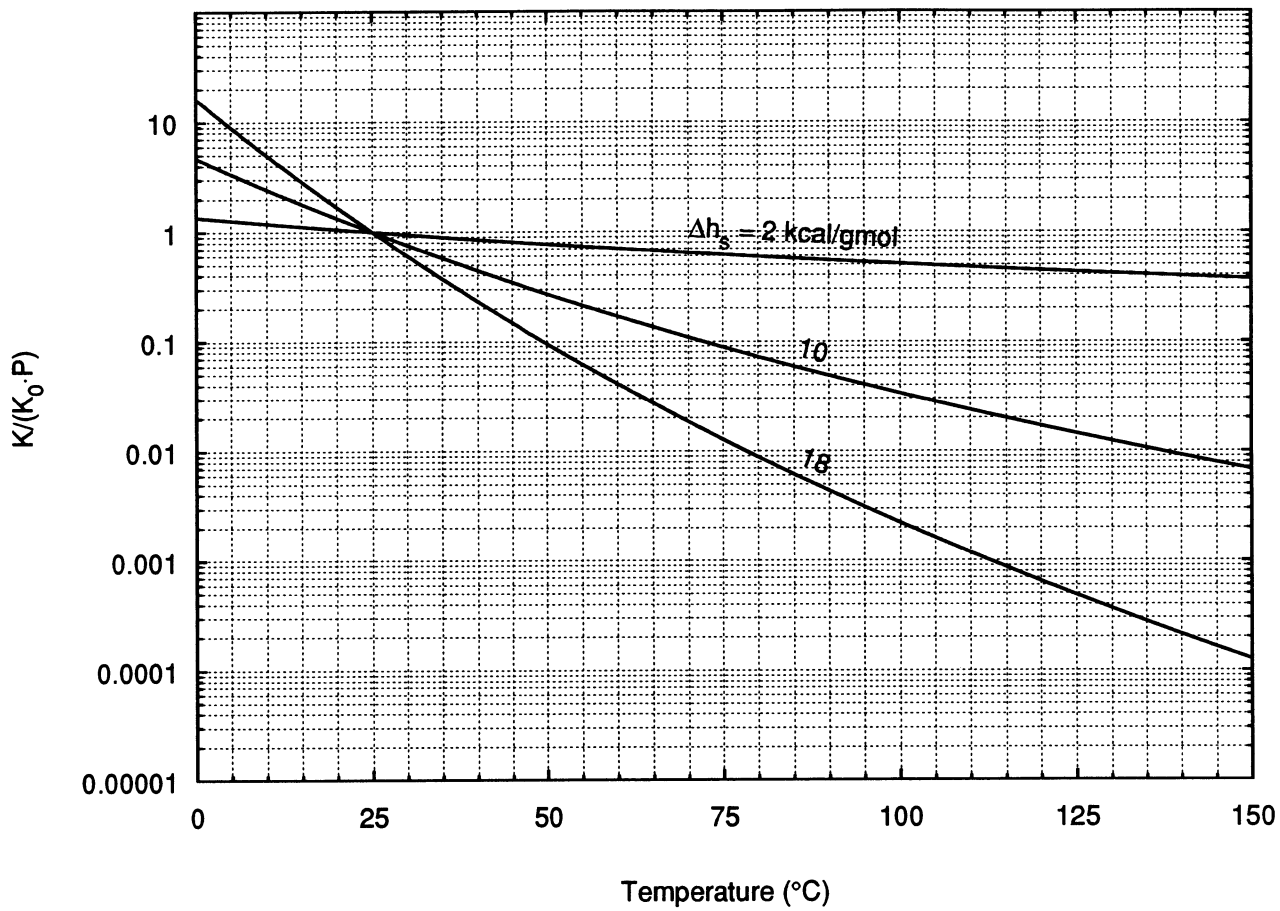

Figure 4.1 Linear isotherm slope as a function of temperature.

Figure 4.2 illustrates the linear and the Langmuir isotherm at 60°C for K_0=1x10^1 kgmol/(kg·atm). In the ppb range the two isotherms are virtually identical. The percent difference between the two isotherms, defined as $(W_{linear} - W_{Langmuir})/W_{Langmuir}$, is shown in Figure 4.3 as a function of gas phase concentration for different K_0 values at 60°C. The value of W_0 was fixed at 0.005 kgmol/kg. For the particular conditions chosen and the range of K_0 values shown, the difference between the linear and Langmuir isotherms is less than 0.1% at 1 ppm and at 10 ppb is less than 0.001%. As K_0 increases, the percent difference increases, e.g. a tenfold increase in K_0 results in a tenfold increase in percent difference. Equation 4.8.1 shows why.

$$\% \text{ diff} = \frac{W_{linear} - W_{Langmuir}}{W_{Langmuir}} = \frac{K\omega}{W_0} \tag{4.8.1}$$

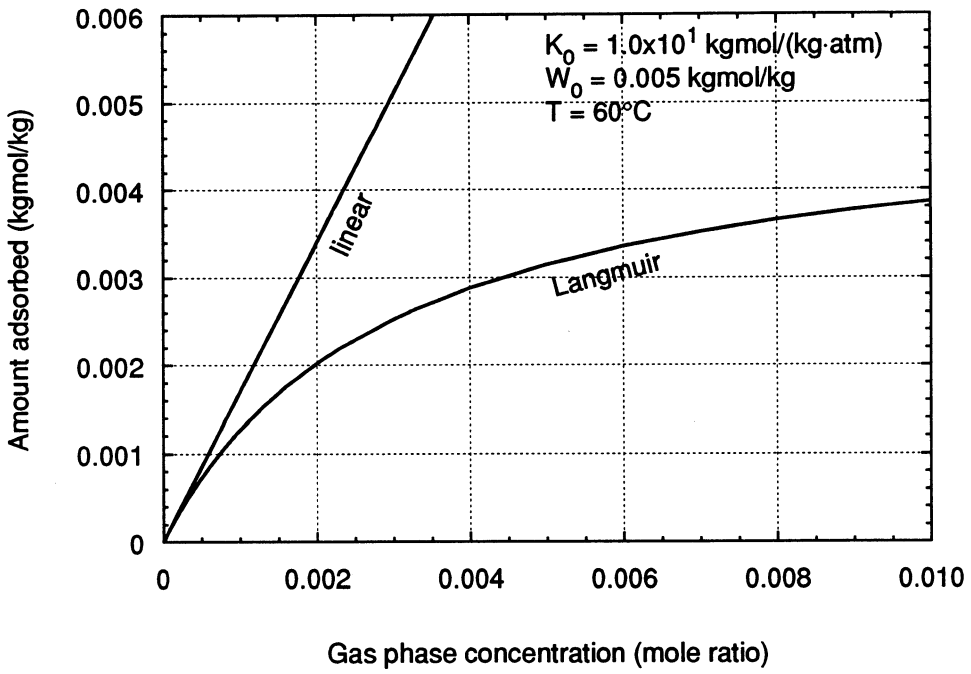

Figure 4.2 Comparison of the linear and the Langmuir isotherm.

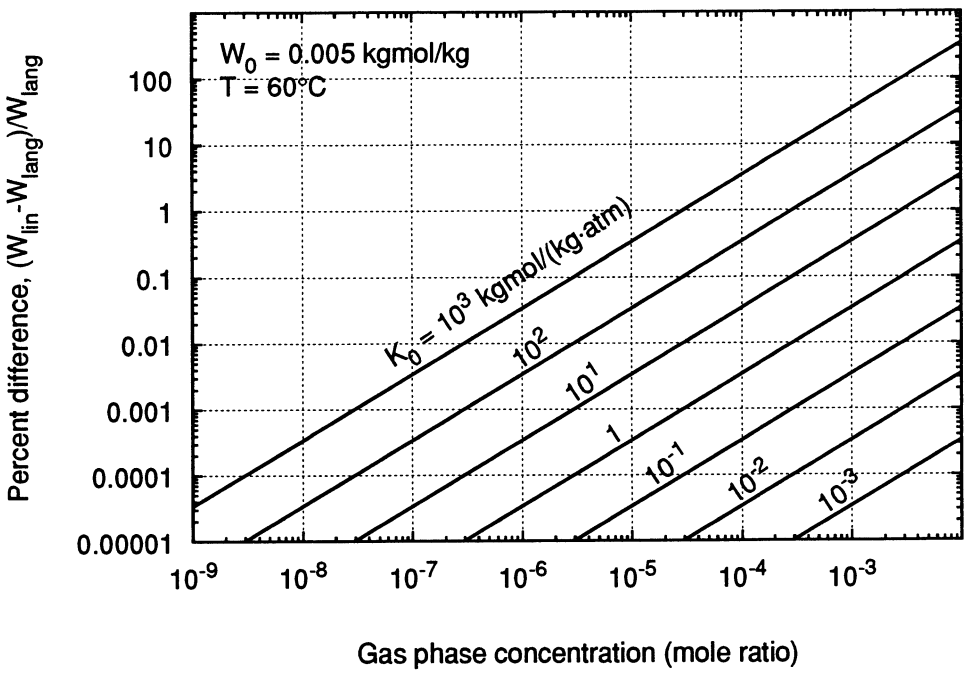

Figure 4.3 Percent difference between the linear and the Langmuir isotherms.

Chapter 5

Solution of the equilibrium model equations

In this chapter, the solution to the model equations is developed. Evaluation of the solution and the significance of different aspects of the solution wil be discussed in the following chapter.

5.1 The model equations

The governing differential equations for adsorption of one component from a gaseous stream flowing through an adiabatic adsorber, for the case of infinite transfer coefficients, were shown in Section 4.4 to be:

$$\frac{\partial W}{\partial \tau}+\frac{\partial \omega}{\partial x}=0 \tag{5.1.1}$$

$$\frac{\partial H}{\partial \tau}+\frac{\partial h}{\partial x}=0 \tag{5.1.2}$$

By making the low concentration assumption (Section 4.5), the equations reduce to:

$$\frac{\partial W}{\partial \tau}+\frac{\partial \omega}{\partial x}=0 \tag{5.1.3}$$

$$\frac{\partial T}{\partial \tau}+\frac{\partial (T/\sigma)}{\partial x}=0 \tag{5.1.4}$$

All of the above equations are in the form of

$$\frac{\partial u}{\partial \tau}+\frac{\partial f(u)}{\partial x}=0 \tag{5.1.5}$$

which, by using the chain rule, can alternatively be written as

$$\frac{\partial u}{\partial \tau}+f'(u)\frac{\partial u}{\partial x}=0 \tag{5.1.6}$$

where $f'(u)$ indicates the total derivative of f with respect to u. Equation 5.1.5 is often called the flux form of the conservation law, consisting of the storage term and the $f(u)$ flux term.

The system of conservation equations (either 5.1.1-5.1.2 or 5.1.3-5.1.4) can be concisely written in matrix form, i.e.,

$$\frac{\partial U}{\partial \tau}+\frac{\partial F(U)}{\partial x}=0 \tag{5.1.7}$$

or

$$\frac{\partial U}{\partial \tau}+F'(U)\frac{\partial U}{\partial x}=0 \tag{5.1.8}$$

where U and $F(u)$ are 2x1 column vectors and $F'(U)$ is a 2x2 matrix. The $F'(U)$ matrix is called the Jacobian.

5.2 The classical Riemann problem

Equations 5.1.1-5.1.2 or 5.1.3-5.1.4 are a 2 x 2 system of conservation laws of the form:

$$U_\tau + F(U)_x = 0 \tag{5.2.1}$$

with initial data:

$$U(x,0) = U_0(x) = \begin{Bmatrix} U_L, & x < 0 \\ U_R, & x > 0 \end{Bmatrix} \tag{5.2.2}$$

where

$$U = \begin{bmatrix} u \\ v \end{bmatrix}; \qquad F(U) = \begin{bmatrix} f(u,v) \\ g(u,v) \end{bmatrix} \tag{5.2.3}$$

and where the notation f_x is used to indicate $(\partial f/\partial x)_y$ where $f = f(x,y)$. Equations 5.2.1 and 5.2.2 are known as the Riemann problem. The method for solving these equations is outlined in the following sections. Some useful references include [219-222].

The classical solution (i.e., a solution which is differentiable) to Equations 5.2.1 and 5.2.2 is not globally defined; instead, to solve the problem for all $\tau > 0$, one must consider the weak solution, which permits jump discontinuities.

5.2.1 The single conservation law

First, consider the classical solution of a single conservation law,

$$u_\tau + f(u)_x = 0 \tag{5.2.4}$$

It is convenient to find a curve, Σ, in x,τ-space along which u is constant and also a solution to Equation 5.2.4. That is,

$$\frac{du}{d\Sigma}=0=\frac{\partial u}{\partial \tau}+f'(u)\frac{\partial u}{\partial x} \tag{5.2.5}$$

where $f'(u)$ indicates df/du. Using the chain rule, $du/d\Sigma$ can be expressed as:

$$\frac{du}{d\Sigma}=\frac{\partial u}{\partial \tau}\frac{d\tau}{d\Sigma}+\frac{\partial u}{\partial x}\frac{dx}{d\Sigma}=0 \tag{5.2.6}$$

so that Equation 5.2.4 is satisfied if

$$\frac{d\tau}{d\Sigma}=1 \qquad \text{and} \qquad \frac{dx}{d\Sigma}=f'(u) \tag{5.2.7}$$

The curve, Σ, is defined by

$$\frac{dx}{d\tau}=\left(\frac{dx}{d\Sigma}\right)\left(\frac{d\Sigma}{d\tau}\right)=f'(u) \tag{5.2.8}$$

Along Σ, u is constant, so that Equation 5.2.8 can be integrated to yield:

$$\frac{x}{\tau}=f'(u) \tag{5.2.9}$$

Given x and τ, Equation 5.2.9 is used to determine the u value at that point. 5.2.9 defines a straight line of slope $1/f'(u)$ in x,τ-space along which u is constant; also, note that for different u values, the slope of the line is different. These lines are often called characteristics. The solution of an equation such as 5.2.4 is often displayed on a x,τ graph, called a wave diagram. The left hand side of Equation 5.2.8 is a velocity,

specifically the velocity of a particular value of u. This is often called the wavespeed, denoted by the symbol λ, and is equal to the inverse of the slope of the characteristic on a wave diagram.

As an example, consider the simple case in which $f'(u) = c$ = constant. For this special case, the speed at which all u values propagate is identical. Therefore, on a wave diagram, lines of slope $1/c$ indicate propagation paths of constant u. For example, consider the following initial condition, shown in Figure 5.1:

$$u(x,\tau=0)=u_0(x)=\left\{\begin{array}{ll} 0, & x<0 \\ \frac{1}{2}[1-\cos(2\pi x)], & 0<x<1 \\ 0, & x>1 \end{array}\right\} \tag{5.2.10}$$

Each u value of the initial curve propagates at speed c, i.e., on a wave diagram (Figure 5.2(a)), each u value moves along a line of slope $1/c$ (the dotted lines). Since in this case the wavespeed is not a function of u, at times greater than zero the curve of u versus x retains its original shape, but is translated in space, as shown in Figure 5.2(b).

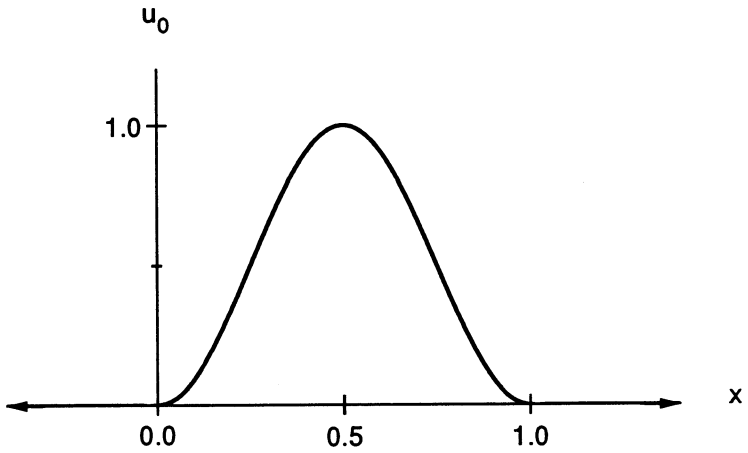

Figure 5.1. Initial condition given by Equation 5.2.10.

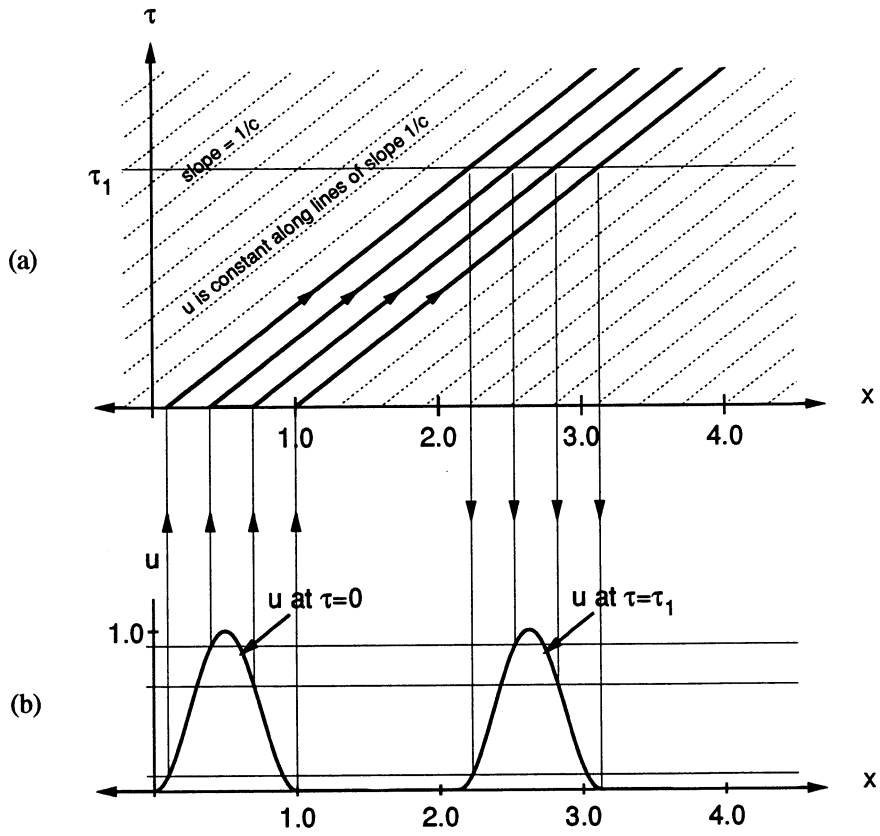

Figure 5.2. (a) Characteristics drawn on a wave diagram for a single conservation law where $f'(u)$ is constant. (b) Wave profiles at time equal to zero and at a later time, τ_1.

Usually the wavespeed is not constant, but is instead a function of u. Typically, the initial conditions consist of a step change at time zero, such as shown in Figure 5.3.

The characteristics resulting from these initial conditions might look like those in Figure 5.4. At time zero, u is equal to u_R for $x > 0$ and u is equal to u_L for $x < 0$. The dotted lines (which represent the characteristics) originating from any point where $u = u_R$ all have a slope equal to $1/f'(u_R)$; those originating from any point where $u = u_L$ have a slope of $1/f'(u_L)$.

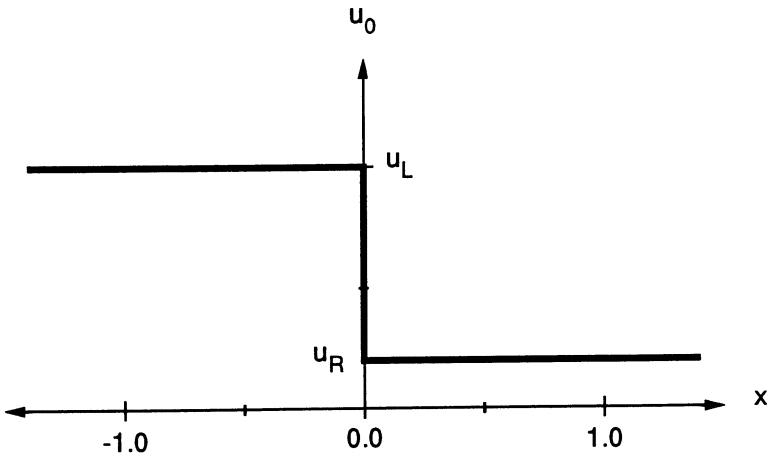

Figure 5.3. Step change initial condition.

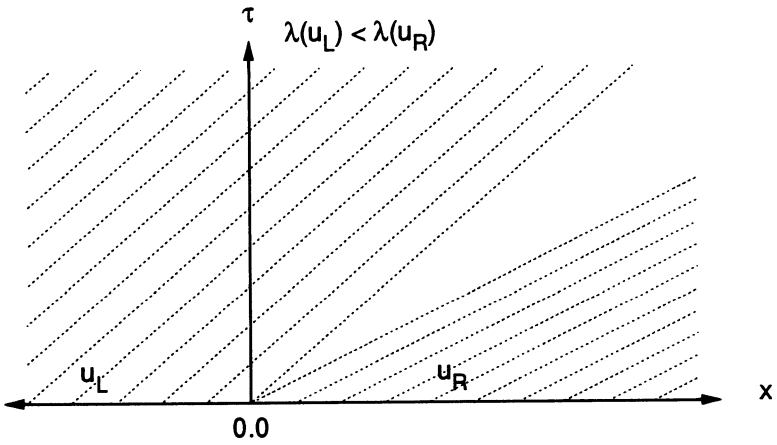

Figure 5.4. Characteristics on a wave diagram where $\lambda(u_L) < \lambda(u_R)$.

In this example, $u_L > u_R$ and $f'(u) = \lambda(u)$ has been assumed to be a non-increasing function of u, so that the slope of the characteristics is greater for the state u_L than for u_R, or, in other words, u_R values move faster than u_L values. In Figure 5.4, there is a gap between the u_L and u_R characteristics; an infinite number of lines of varying slope τ/x fill this region, and from Equation 5.2.9, it can be seen that u varies continuously between u_L

and u_R in this region. The result is a wave; this type of wave is called a rarefaction wave, and on a wave diagram is indicated by a "fan" such as in Figure 5.5. Note that the wave spreads as it moves. Figure 5.6 illustrates the solution at the times τ_1 and τ_2.

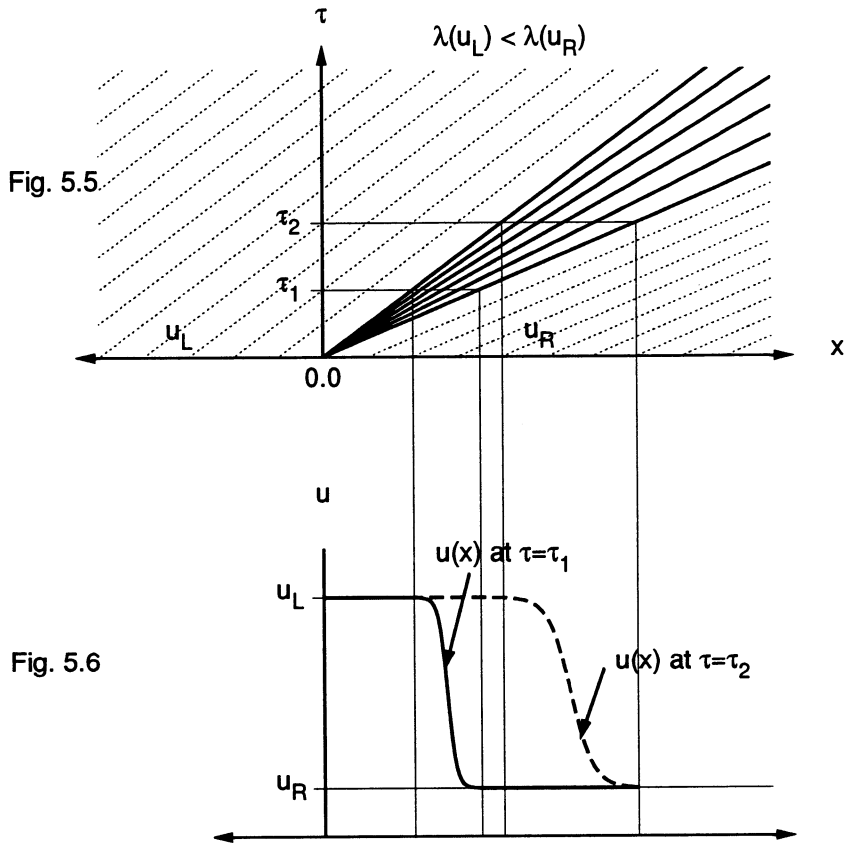

Fig. 5.5

Fig. 5.6

Figure 5.5 Rarefaction wave; Figure 5.6 Wave profiles.

If, however, $f'(u) = \lambda(u)$ is a non-decreasing function of u, then the characteristics associated with u_L have a slope less than those associated with u_R (the u_R values move slower than the u_L values). In this case, the characteristics intersect, as shown in Figure 5.7. In the region where the lines intersect, the solution seems to imply that there are two u values at each x at a time. This is physically impossible - the classical solution is

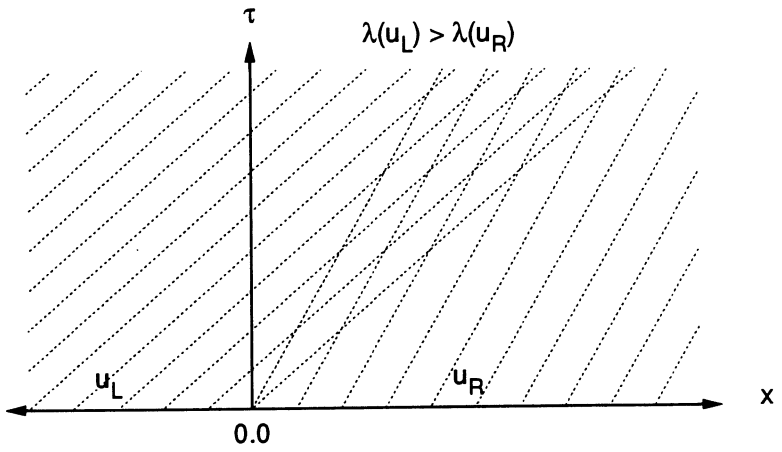

Figure 5.7. Characteristics on a wave diagram where $\lambda(u_L) > \lambda(u_R)$.

overdetermined in this region. The solution in this case is a jump discontinuity, called a shock wave, which satisfies an integral form of the conservation law (Equation 5.2.4). This is called the Rankine-Hugoniot condition or sometimes simply the jump condition:

$$s[u] = [f(u)] \tag{5.2.11}$$

where the boldface brackets indicate a difference across the shock, i.e.:

$$[u] = u_R - u_L \tag{5.2.12}$$

and s is the speed of the shock. Notice that the flux form of the equations is used in Equation 5.2.11. The solution admitted by Equation 5.2.11 is not unique and a stability condition is required:

$$\lambda(u_R) \leq s \leq \lambda(u_L) \tag{5.2.13}$$

The stability condition is often called the entropy condition from the requirement that entropy must increase across a shock in the study of gas dynamics. On a wave diagram, a shock wave is indicated by a single line, as in Figure 5.8. The solution at times τ_1 and τ_2

is illustrated in Figure 5.9. Often on a wave diagram the only characteristics drawn are those which actually indicate a change in u, and throughout the rest of this work, this will be the case.

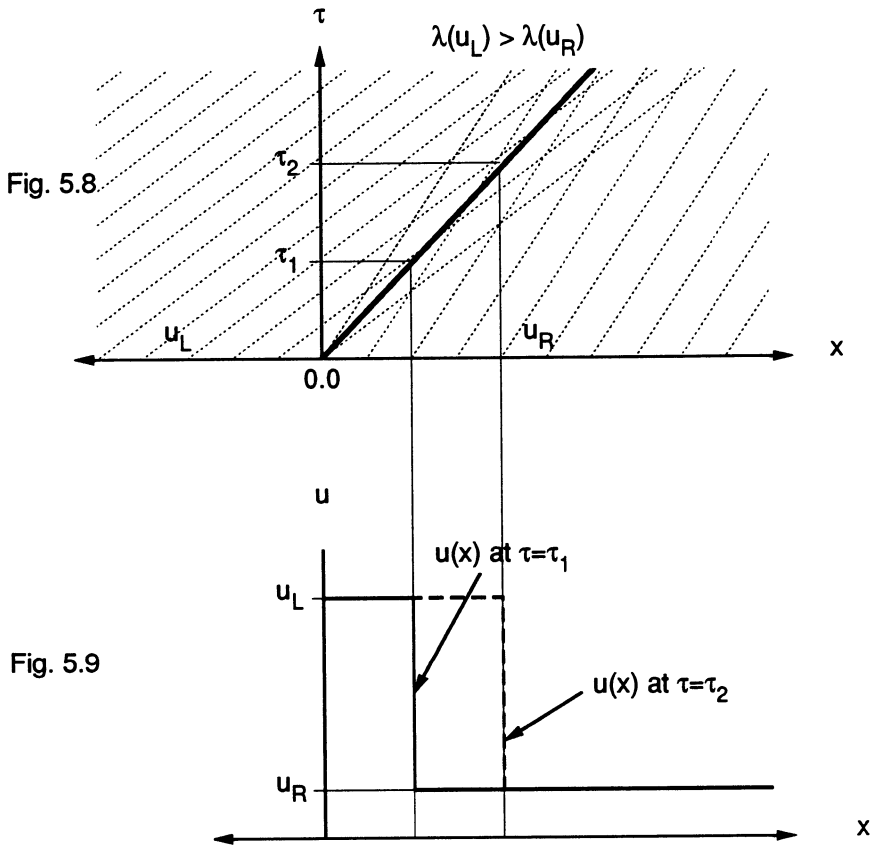

Fig. 5.8

Fig. 5.9

Figure 5.8 Shock wave; Figure 5.9 Wave profiles.

For both the rarefaction wave and the shock wave solutions, an assumption was made that the wavespeed was monotonic with respect to u. This condition is called the convexity condition, i.e.:

$$\lambda'(u) = f''(u) \neq 0 \tag{5.2.14}$$

There will be equations for which Equation 5.2.14 is not satisfied. In this case, the solution is more complex, and may consist of a combination of waves. For example, consider the function $f(u)$ and the corresponding $\lambda(u) = f'(u)$ shown in Figure 5.10, where in this case $u_L < u_R$.

Between state u_L and u_1, λ is non-decreasing, leading to rarefaction type wave behavior. Between state u_1 and u_R, λ is non-increasing, leading to shock wave type behavior. The result is a rarefaction wave between u_L and u_*, and a discontinuity, called a contact discontinuity, between u_* and u_R. The state u_* is determined by the requirement that $\lambda(u_*) = s$.

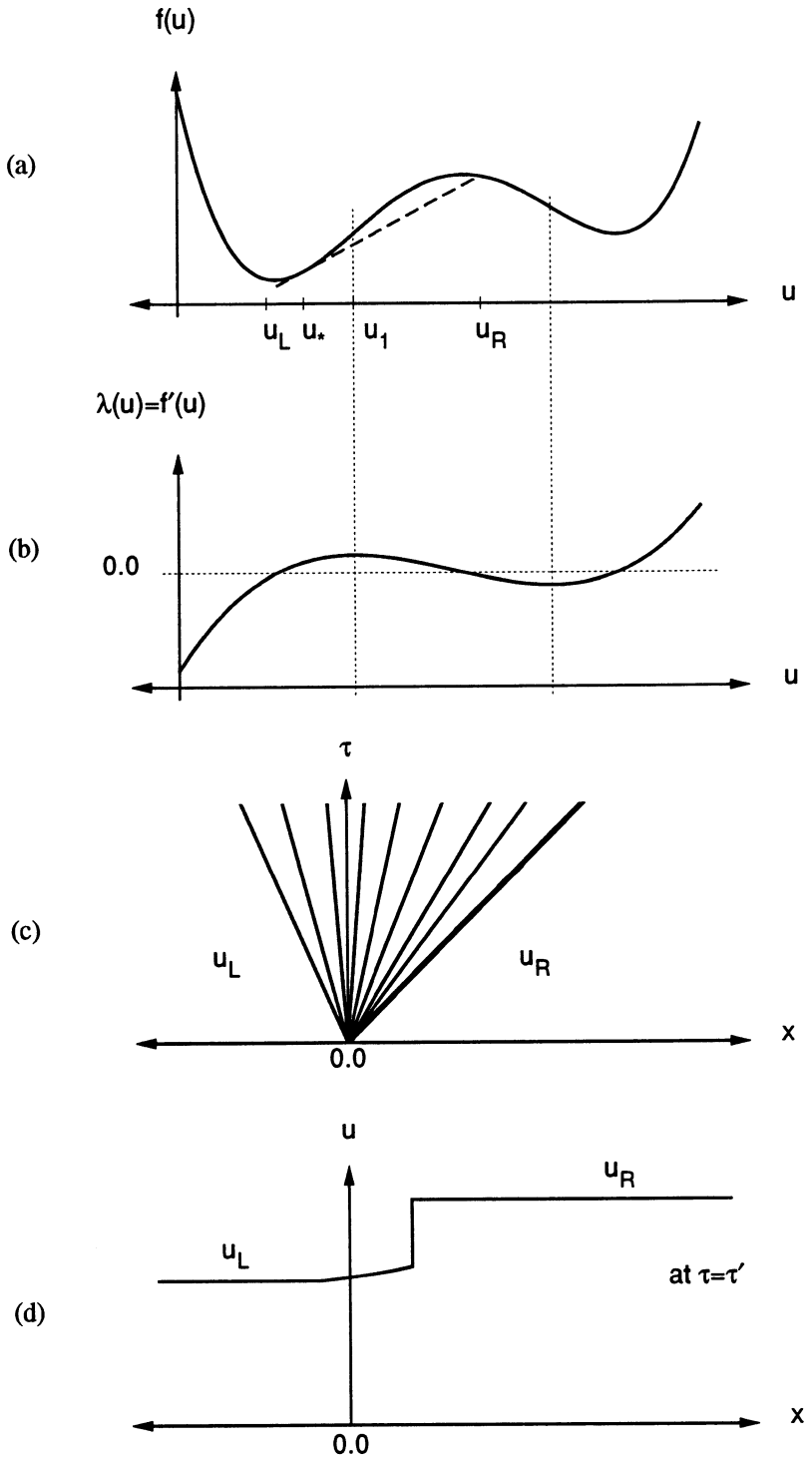

Figure 5.10. (a) Plot of a hypothetical f(u) function. (b) Plot of $f'(u) = \mathrm{d}f(u)/\mathrm{d}u = \lambda(u)$. (c) The corresponding wave diagram, indicating a rarefaction wave and a contact discontinuity. (d) The wave profile at time $\tau = \tau'$.

A brief note on the classical solution of Equation 5.2.4: the solution, $u = u(x,\tau)$, is known to be a function of $\xi = x/\tau$ only, such that

$$\frac{\partial u}{\partial \tau} = \frac{\partial u}{\partial \xi}\frac{\partial \xi}{\partial \tau} = \frac{-\xi}{\tau}\frac{\partial u}{\partial \xi} \tag{5.2.15}$$

$$\frac{\partial f(u)}{\partial x} = \frac{\partial f(u)}{\partial \xi}\frac{\partial \xi}{\partial x} = \frac{1}{\tau}\frac{\partial f(u)}{\partial \xi} \tag{5.2.16}$$

substituting into Equation 5.2.4 yields:

$$(f'(u) - \xi)\frac{du}{d\xi} = 0 \tag{5.2.17}$$

The solution of Equation 5.2.17 is therefore either

$$\frac{du}{d\xi} = 0, \quad \text{i.e.,} \quad u = \text{constant} \tag{5.2.18}$$

or

$$\xi = \frac{x}{\tau} = f'(u) \tag{5.2.19}$$

This is the same result as stated earlier, namely, constant regions separated by rarefaction waves. An analogous derivation will be used in the solution of systems of conservation laws.

5.2.2 The 2 x 2 system of conservation laws

Now, with an understanding of the solution of the single conservation law, consider the 2 x 2 system of conservation laws specified in Equation 5.2.1:

$$U_\tau + F(U)_x = U_\tau + F'(U)U_x = 0 \tag{5.2.20}$$

with initial conditions:

$$U(x,0) = U_0(x) = \begin{Bmatrix} U_L, & x < 0 \\ U_R, & x > 0 \end{Bmatrix} \tag{5.2.21}$$

where U, F', and F are matrices, i.e., Equation 5.5.20 can be written as:

$$\begin{bmatrix} u \\ v \end{bmatrix}_\tau + \begin{bmatrix} f_u & f_v \\ g_u & g_v \end{bmatrix} \begin{bmatrix} u \\ v \end{bmatrix}_x = 0 \tag{5.2.22}$$

Again, the weak solution must be considered in order to globally define a solution. The system is considered to be *strictly hyperbolic* if the eigenvalues of the Jacobian matrix (F') are everywhere real and distinct. Solutions where this is not the case will be discussed in the next section.

For the strictly hyperbolic system of n conservation laws, the solution consists of at most n wave groups separated by constant states [219]. The waves may be either rarefaction waves (which satisfy Equation 5.2.1 in the classical sense), shock waves, or contact discontinuities. Therefore, for the 2 x 2 system, the solution consists of at most three constant states (U_L, U_R, and an intermediate state, $\overline{U}$) separated by waves. For the system of equations, the "state" refers to a (u,v) pair; both u and v change as a wave passes.

Figure 5.11 illustrates an example of a wave diagram and wave profiles for the solution to a 2 x 2 system. In this example, there is a region where U is equal to the initial value, U_R. A rarefaction wave separates this region from a region in which U is constant at the intermediate value, $\overline{U}$. A shock wave then separates the intermediate state from a region in which U is constant at the final U value, U_L. In this case, the rarefaction

wave would pass an observer before the shock wave; the wave which separates the initial state from the intermediate state is therefore called the fast wave and the wave separating the intermediate state from the final state is called the slow wave. In general, the state in front of any wave will be designated U_+ and the state behind a wave will be called U_-.

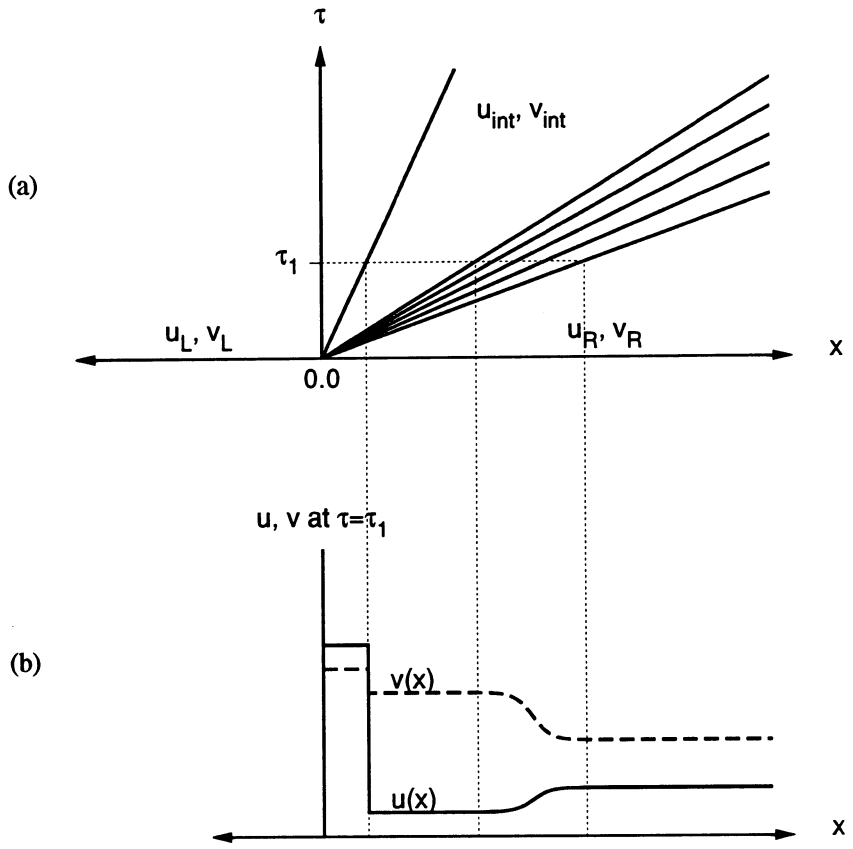

Figure 5.11. (a) Example wave diagram for a 2x2 system of conservation laws, showing a rarefaction wave followed by a shock wave. (b) Wave profiles.

Two questions arise: first, what is the U value of the intermediate state, and second, what type of wave separates each of the constant U regions?

As in the solution of the single equation, the solution of the 2 x 2 system is known to be a function of $\lambda = x/\tau$ only. Consider the classical solution; rewriting Equation 5.2.20 in terms of λ yields:

$$-\lambda U_\lambda + F'(U)U_\lambda = 0 \tag{5.2.24}$$

or, rearranging,

$$(F'(U) - \lambda I)\, U_\lambda = 0 \tag{5.2.25}$$

This equation is analogous to Equation 5.2.17 for the single conservation law. The solution is also similar in that either

$$U_\lambda = 0, \quad \text{i.e.,} \quad U = \text{constant} \tag{5.2.26}$$

or else

$$F'(U) - \lambda I = 0 \tag{5.2.27}$$

From Equation 5.2.25, it can be seen that λ is equal to the eigenvalues of the Jacobian, $F'(U)$, and U_λ evaluated at the eigenvalues gives the right eigenvectors. Therefore, for a system of conservation laws, the speeds of the rarefaction waves ($\lambda = x/\tau$) are equal to the eigenvalues of the Jacobian matrix. The condition of strict hyperbolicity is equivalent to the condition that the two wavespeeds can not be equal at any point.

Evaluating the eigenvalues, i.e.,

$$\det(F' - \lambda I) = 0 \tag{5.2.29}$$

yields a quadratic equation,

$$\lambda^2 - (f_u + g_v)\lambda + f_u g_v - f_v g_u = 0 \tag{5.2.30}$$

indicating that there are two eigenvalues, one representing the faster wave and the other representing the slower wave. Traditionally, they are numbered such that $\lambda_1 < \lambda_2$ [219]. This means that the first wave has speeds λ_2 (or s_2 for a shock), while the second wave has speeds λ_1 or s_1. Thus, the slow waves are sometimes referred to as 1-rarefaction waves or 1-shock waves (or back shocks) and the fast waves as 2-rarefaction waves or

2-shock waves (or front shocks). This is slightly confusing, since for a stationary observer at some fixed point x, the first wave to pass is the 2-wave, while the second wave is the 1-wave.

As in the analysis of a single equation, if the corresponding $\lambda_k(u,v)$ increases from the state behind the wave (u_-, v_-) to that in front of the wave (u_+, v_+), a rarefaction wave will result. If, on the other hand, the corresponding eigenvalue decreases from behind the wave to in front of the wave, a shock wave will result. For example, in Figure 5.11, $\lambda_2(u,v)$ must be a non-decreasing function of U between $\overline{U}$ and U_R, while λ_1 must be a non-increasing function of U between U_L and $\overline{U}$.

For a rarefaction wave, the position of the k^{th} wave is given by:

$$\frac{x}{\tau} = \lambda_k(U) \tag{5.2.31}$$

An expression for the intermediate U values is obtained from the integral curve of the right eigenvector, for example, for the rarefaction wave of Figure 5.11:

$$u_R - \overline{u} = \int_{\overline{v}}^{v_R} \frac{du}{dv} dv = \int_{\overline{v}}^{v_R} \frac{(du/d\lambda)}{(dv/d\lambda)} dv \tag{5.2.32}$$

Equation 5.2.32 is one equation in two unknowns, $\overline{u}$ and $\overline{v}$. To evaluate the intermediate state, it is also necessary to consider the equations for the other wave. For the example of Figure 5.11, this is a shock wave.

Any shock waves in the solution satisfy the Rankine-Hugoniot condition:

$$s_k[U] = [F(U)] \tag{5.2.33}$$

with the classical Lax entropy conditions [219]:

$$\lambda_k(U_+) \le s_k \le \lambda_k(U_-) \tag{5.2.34}$$

$$\lambda_{k-1}(U_-) \le s_k \le \lambda_{k+1}(U_+) \tag{5.2.35}$$

For example, for the shock in Figure 5.11:

$$\begin{aligned} s_1[\bar{u} - u_L] &= [f(\bar{u},\bar{v}) - f(u_L, v_L)] \\ s_1[\bar{v} - v_L] &= [g(\bar{u},\bar{v}) - g(u_L, v_L)] \end{aligned} \tag{5.2.36}$$

where

$$\begin{aligned} \lambda_1(\bar{u},\bar{v}) \le s_1 \le \lambda_1(u_L, v_L) \\ s_1 \le \lambda_2(\bar{u},\bar{v}) \end{aligned} \tag{5.2.37}$$

Equations 5.2.36 can be solved to eliminate s_1:

$$(\bar{g} - g_L)(\bar{u} - u_L) = (\bar{f} - f_L)(\bar{v} - v_L) \tag{5.2.38}$$

Equations 5.2.32 and 5.2.38 are two equations in two unknowns, $\bar{u}$ and $\bar{v}$, thus determining the intermediate state. Once the intermediate state is known, either of the Equations 5.2.36 can be solved for the shock speed. The positions of the waves are then known, since $s_1 = x/\tau$ and $\lambda_2(U) = x/\tau$.

The example considered consisted of one rarefaction wave and one shock wave. For a given problem there could be two rarefaction waves, resulting in two equations like 5.2.32, or two shock waves requiring the solution of two equations like 5.2.38.

As mentioned previously, there is a third type of wave which may occur in a system of conservation laws: the contact discontinuity. The k^{th} characteristic field of Equation 5.2.20 is considered to be *genuinely nonlinear* if for all $U = (u, v)$:

$$\nabla\lambda_k \cdot r_k \neq 0 \tag{5.2.39}$$

and it is *linearly degenerate* if for all $U = (u, v)$:

$$\nabla\lambda_k \cdot r_k = 0 \tag{5.2.40}$$

where r_k is the k^{th} right eigenvector. If, on the other hand, $\nabla\lambda_k \cdot r_k = 0$ only at isolated points along the integral curve, then the charateristic field is neither genuinely nonlinear or linearly degenerate. Systems of equations with at least one characteristic field where this is the case are called *general systems* [223]. Liu [224] has extended Lax's original admissibility condition (Equations 5.2.34-5.2.35) to include systems of this type (some of the admissible solutions would not be admissible under Equations 5.2.34-5.2.35).

The condition of genuine nonlinearity assures that the λ_k are either strictly increasing or decreasing as they vary between the constant states, i.e., it corresponds to the convexity condition for the single conservation law. If one of the characteristic fields is linearly degenerate, then λ_k is constant along the characteristic curve. Instead of a rarefaction wave or a shock wave, the constant states will be separated by a contact discontinuity. The contact discontinuity is not a self-sharpening shock wave, but rather is a discontinuity reflecting the initial conditions. The equations describing a contact discontinuity are the same as those for a shock wave, i.e.,

$$s[U] = [F(U)] \tag{5.2.41}$$

In general, consider a wave with state $U_+ = (u_+, v_+)$ in front of it and state $U_- = (u_-, v_-)$ behind it. Whereas for the single conservation law, any two u values could be separated by some type of wave, for the 2 x 2 system of conservation laws, the solution is more restricted. Considering each wave independently, relative to the waves there are four ways of looking at the constant states: a state may be 1) in front of the fast

wave, 2) behind the fast wave, 3) in front of the slow wave, or 4) behind the slow wave.

Consider a state, U', and first consider it as case 2, i.e., behind the fast wave. There is a locus of states, U_+, to which $U' = U_-$ may be connected by a fast rarefaction wave. These states are indicated by the line R_2 in Figure 5.12(a). For this wave to be a rarefaction wave, λ_2 must increase as you move along R_2 away from U'; that is, the wavespeed of the state behind the wave must be slower than the wavespeed in front of the wave. An arrowhead is used to indicate the direction of U_+, and for the R curves, this corresponds to the direction of increasing λ. Similarly, for case 4, there is a set of U_+ states to which $U' = U_-$ may be connected by a slow rarefaction wave, indicated by the line R_1 in Figure 5.12(a). It will be the convention in this work to show the fast waves (2-waves) as dashed or dotted lines and the slow waves (1-waves) as solid lines.

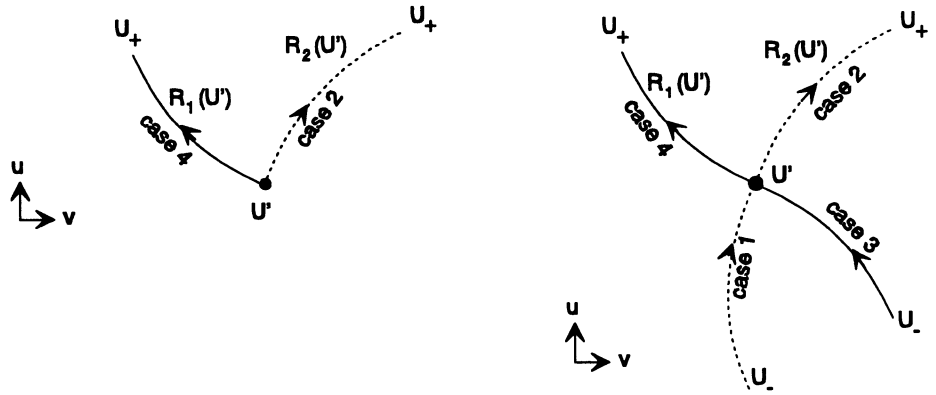

Figure 5.12. (a) Integral curves through a state U' behind a fast wave (R_2) and behind a slow wave (R_1). (b) Integral curves through a state U' in front of a fast wave and in front of a slow wave, in addition to the curves from part (a).

For cases 1 and 3, in which U' is the state in front of a wave, a line representing those states behind the wave which could be connected to $U' = U_+$ by either a fast or slow rarefaction wave could be drawn. Along these lines, the appropriate λ would increase as

you move towards the state $U' = U_+$. These lines are a continuation of the R_2 and R_1 curves already drawn, and extend to the other side of U', as in Figure 5.12(b). The R lines, called the integral curves or rarefaction curves, are a graphical representation of Equation 5.2.32. The states U_- and U_+ both lie somewhere along this line, and the arrowhead points away from U_- and towards U_+.

Again, consider case 2; as for the rarefaction wave, there is a locus of states U_+ to which the state $U' = U_-$ may be connected by a shock wave. These states are represented by the line S_2 in Figure 5.13. The arrowheads again point away from U_- and towards U_+. Those states U_+ which may be connected to $U' = U_-$ by a slow shock wave (case 4) are represented by the line S_1. As for the rarefaction waves, cases 1 and 3 are represented by a continuation of the S_2 and S_1 curves through the point U'. The S lines, called the Hugoniot loci or shock curves, are a graphical representation of Equation 5.2.33. It can be shown [221] that the first two derivatives of the curves R_1 and S_1 are equal at the point U', and likewise those of R_2 and S_2. Through any point in the u-v plane, the curves R_1, R_2, S_1, and S_2 may be drawn to yield a map of the solution. This graph is called a hodograph plot.

For known states U_R and U_L, where U_R is the initial state and U_L is the final state, the solution can be illustrated on a hodograph plot. All four curves (R_2, R_1, S_2, and S_1) could be drawn for each state U_R and U_L, however, the only relevant curves are the 1-curves through state U_L, where U_L is the state behind the waves (i.e., the portion of the R_1 and S_1 curves for case 3) and the 2-curves through state U_R, where U_R is the state in front of the waves (i.e., the portion of the R_2 and S_2 curves for case 1). Figure 5.14 illustrates the states U_R and U_L and the relevant curves through them. Notice that, as previously mentioned, the R_k and S_k curves have equal first and second derivatives. The

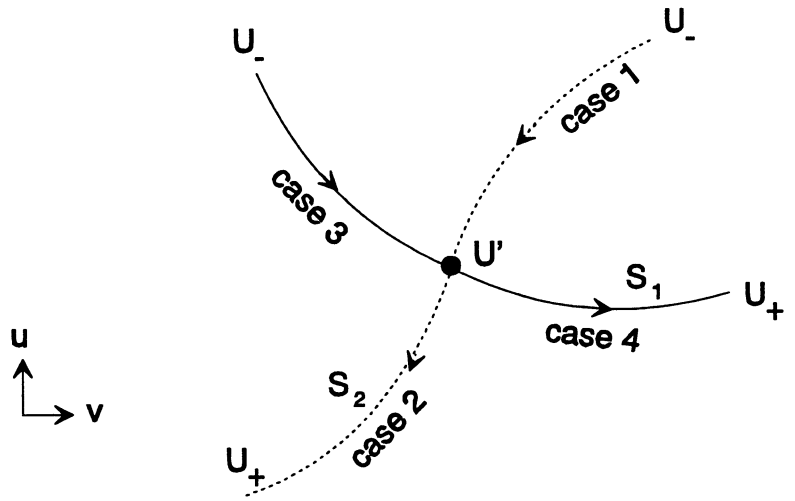

Figure 5.13. Hugoniot loci through the state U', i.e., those states which may be connected to U' by a shock wave.

combined curve, $R_k \cup S_k$, is sometimes called the wave curve. These curves represent all of the U_- states which may be connected to the state $U_+ = U_R$ and all of the U_+ states which may be connected to the state $U_- = U_L$.

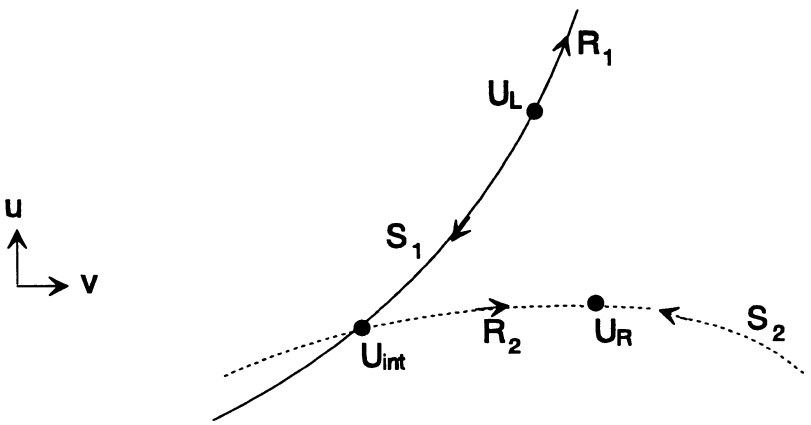

Figure 5.14. Hodograph plot illustrating U_L and U_R, the 1 and 2-curves through U_L and U_R, and the determination of the intermediate state.

The intermediate state must lie on a 1-curve through U_L and on a 2-curve through U_R, and thus will be the state at which the 1-curve and the 2-curve intersect. Sometimes the intermediate state is referred to as the intersection point state. From Figure 5.14, it

can be seen that for this case, the curves R_2 and S_1 intersect while curves R_1 and S_2 do not. Therefore, the solution consists of a front rarefaction wave and a back shock wave, such as in Figure 5.11.

Often the hodgraph plot is drawn with only the R curves, because the R curves can be used to obtain a qualitative estimate of the solution. In this case, a shock is indicated by moving along an R curve against the direction of the arrows.

5.3 Extension to non-strictly hyperbolic systems

For a system of conservation laws to be strictly hyperbolic, all of the eigenvalues must be real and distinct. If the eigenvalues are equal at some point, then the system is non-strictly hyperbolic. Non-strictly hyperbolic systems can be classified further. If $\lambda_1 = \lambda_2$ along a curve, Σ, and F' is not diagonizable, this is called a parabolic degeneracy [223, 225]. If $\lambda_1 = \lambda_2$ along Σ and F' is diagonizable, the system is hyperbolic, but not strictly hyperbolic [225]. If $\lambda_1 = \lambda_2$ at isolated points, these points are called umbilic points [226]. Ths solution of non-strictly hyperbolic conservation laws is more complex than for strictly hyperbolic conservation laws, particularly for the point singularities [223].

The theory of non-strictly hyperbolic systems of conservation laws was described in 1985 by Keyfitz [223] as "still far away from being guided by a general theory". This is still the case. Some references which include discussions of non-strictly hyperbolic systems of conservation laws include [223-234].

Although there is no general theory for non-strictly hyperbolic conservation laws, solutions to specific problems have been shown to consist of more than n wave groups

(where n is the number of conservation laws), whereas for strictly hyperbolic systems, the solution was limited to n wave groups. Transitional waves, which are not associated with a unique characteristic family, can also result [230]. As an example, Bohannon [229] studied at a 2x2 system of conservation laws which had a parabolic degeneracy along the lines u=0 and v=0 and was linearly degenerate in one characteristic family. The solution, which was shown to be unique, consisted of as many as seven waves.

5.4 Comparison of the model equations

In this section, the adsorption equations will be analyzed using the theory of Sections 5.2 and 5.3. In particular, differences between the four different equation sets will be examined.

Equations 4.4.17 and 4.4.18 can be written in matrix form:

$$\begin{bmatrix} \omega \\ T \end{bmatrix}_\tau + \begin{bmatrix} \left(\frac{b_2b_3+b_1b_5}{b_3}\right) & \left(\frac{b_1b_4}{b_3}\right) \\ \left(\frac{b_5}{b_3}\right) & \left(\frac{b_4}{b_3}\right) \end{bmatrix} \begin{bmatrix} \omega \\ T \end{bmatrix}_x = 0 \tag{5.4.1}$$

where b_1 through b_5 are defined in Table 4.1 for the full equations and in Table 4.2 for the low concentration equations. The characteristic equation is:

$$[b_3]\,\lambda^2 + [-(b_4 + b_2b_3 + b_1b_5)]\,\lambda + [b_2b_4] = 0 \tag{5.4.2}$$

and, solving for the eigenvalues:

$$\lambda_k = \frac{b_2b_3 + b_4 + b_1b_5}{2b_3} \pm \sqrt{\frac{(b_1b_5 + b_2b_3 + b_4)^2 - 4b_2b_3b_4}{4b_3^2}} \tag{5.4.3}$$

The right eigenvectors are:

$$r_k = \begin{bmatrix} \dfrac{b_1 b_4}{b_3} \\ \left(\lambda_k - b_2 - \dfrac{b_1 b_5}{b_3}\right) \end{bmatrix} \tag{5.4.4}$$

and the integral curves of the eigenvectors are found by integrating:

$$\left[\frac{d\omega}{dT}\right]_k = \frac{b_1 b_4}{(b_3\lambda_k - b_2 b_3 - b_1 b_5)} \tag{5.4.5}$$

For the low concentration assumption, the above equations can be used with the b_1 through b_5 values given in Table 4.2. Alternatively, identical equations can be derived from the simplified version of the conservation equations, i.e. Equations 4.5.14 and 4.5.15:

$$\begin{bmatrix} \omega \\ T \end{bmatrix}_\tau + \begin{bmatrix} \omega_W & \dfrac{\omega_T}{\sigma} \\ 0 & \dfrac{1}{\sigma} \end{bmatrix} \begin{bmatrix} \omega \\ T \end{bmatrix}_x = 0 \tag{5.4.6}$$

$$\lambda_k = \omega_W, \frac{1}{\sigma} \tag{5.4.7}$$

$$r_k = \begin{bmatrix} \dfrac{\omega_T}{\sigma} \\ \lambda_k - \omega_W \end{bmatrix} \tag{5.4.8}$$

$$\left[\frac{d\omega}{dT}\right]_k = \frac{\omega_T}{\sigma(\lambda_k - \omega_W)} \tag{5.4.9}$$

In particular, for the linear isotherm with the low concentration assumption, the eigenvalues and eigenvectors are equal to:

$$\lambda_k = \frac{1}{K}, \frac{1}{\sigma} \tag{5.4.10}$$

$$r_k = \left[\frac{\omega \Delta h_s}{\sigma R T^2} \right] \left(\lambda_k - \frac{1}{K} \right) \tag{5.4.11}$$

$$\left[\frac{d\omega}{dT} \right]_k = \frac{\omega \Delta h_s}{\sigma R T^2 \left(\lambda_k - \frac{1}{K} \right)} \tag{5.4.12}$$

and since, by convention, $\lambda_2 \geq \lambda_1$,

$$\lambda_1 = \min\left(\frac{1}{K}, \frac{1}{\sigma} \right); \quad \lambda_2 = \max\left(\frac{1}{K}, \frac{1}{\sigma} \right) \tag{5.4.13}$$

Throughout this work, the terms "concentration" wave and "thermal" wave will be used, and will be indicated by the subscripts C and T respectively, e.g., λ_C and λ_T. The terms "concentration" and "thermal" refer to the conservation equations with which the waves are associated, i.e.:

$$\lambda_C = \frac{1}{K} \tag{5.4.14}$$

$$\lambda_T = \frac{1}{\sigma} \tag{5.4.15}$$

Depending on the temperature, λ_C may be either greater than or less than λ_T, so that the concentration wave can be either λ_1 or λ_2, and vice versa for the thermal wave. Similarly, concentration and thermal integral curves can be defined:

$$\left[\frac{d\omega}{dT} \right]_C = \infty \tag{5.4.16}$$

$$\left[\frac{d\omega}{dT}\right]_T = \frac{\omega K \Delta h_s}{RT^2(K-\sigma)} \tag{5.4.17}$$

5.4.1 Hyperbolic classification

In this section, the full equations and the low concentration assumption equations with both the linear and the Langmuir isotherm will be examined to determine whether each set of equations is strictly hyperbolic. The system of equations is strictly hyperbolic if the eigenvalues are real and distinct. The eigenvalues are real (from Equation 5.4.3) if

$$(b_4 + b_2 b_3 + b_1 b_5)^2 - 4 b_2 b_3 b_4 \geq 0 \tag{5.4.18}$$

and they are distinct if

$$(b_4 + b_2 b_3 + b_1 b_5)^2 - 4 b_2 b_3 b_4 \neq 0 \tag{5.4.19}$$

Starting with the low concentration equations and the linear isotherm, it is obvious from Equation 5.4.10 that both eigenvalues are real. Since K is a function of temperature, there is a temperature at which the eigenvalues are equal and the equations are parabolic:

$$T_{par} = \frac{1}{\frac{1}{T_0} + \frac{R}{\Delta h_s} \ln\left(\frac{\sigma}{K_0 P}\right)} \tag{5.4.20}$$

At this temperature, the eigenvalues are equal for all values of ω. Equation 5.4.20 is plotted in Figure 5.15(a) for the base parameter values of c_m = 1300 J/(kg·K) and Δh_s = 10 kcal/gmol; Figure 5.15(b) illustrates the dependence of T_{par} on σ and Δh_s. Since K_0 values range from about 1×10^{-3} to 1×10^{2} kgmol/(kg·atm) and higher, there are contaminants for which T_{par} is within the working temperature range.

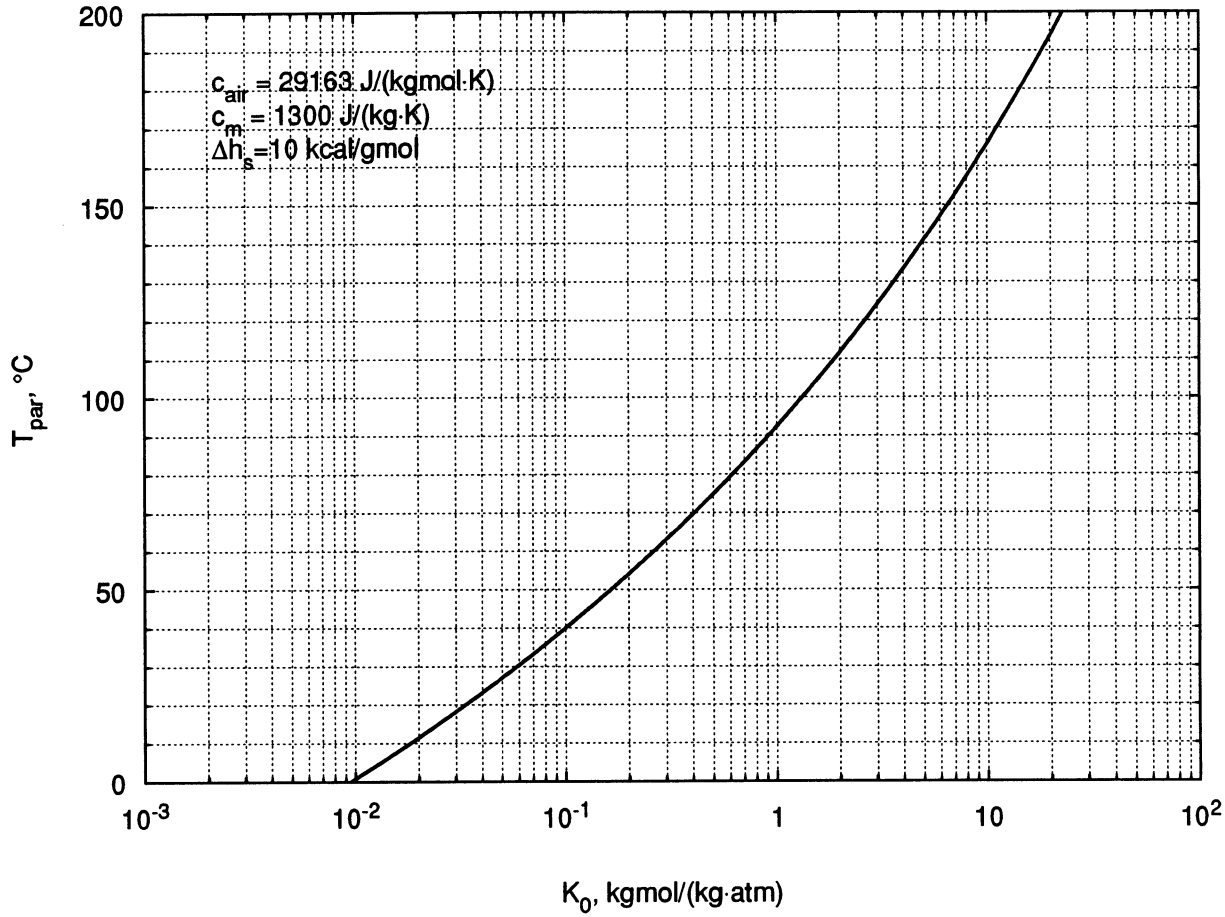

Figure 5.15(a) Temperature at which $\lambda_1 = \lambda_2$ as a function of K_0 for the base parameter values of Δh_s and σ given in Table 4.6.

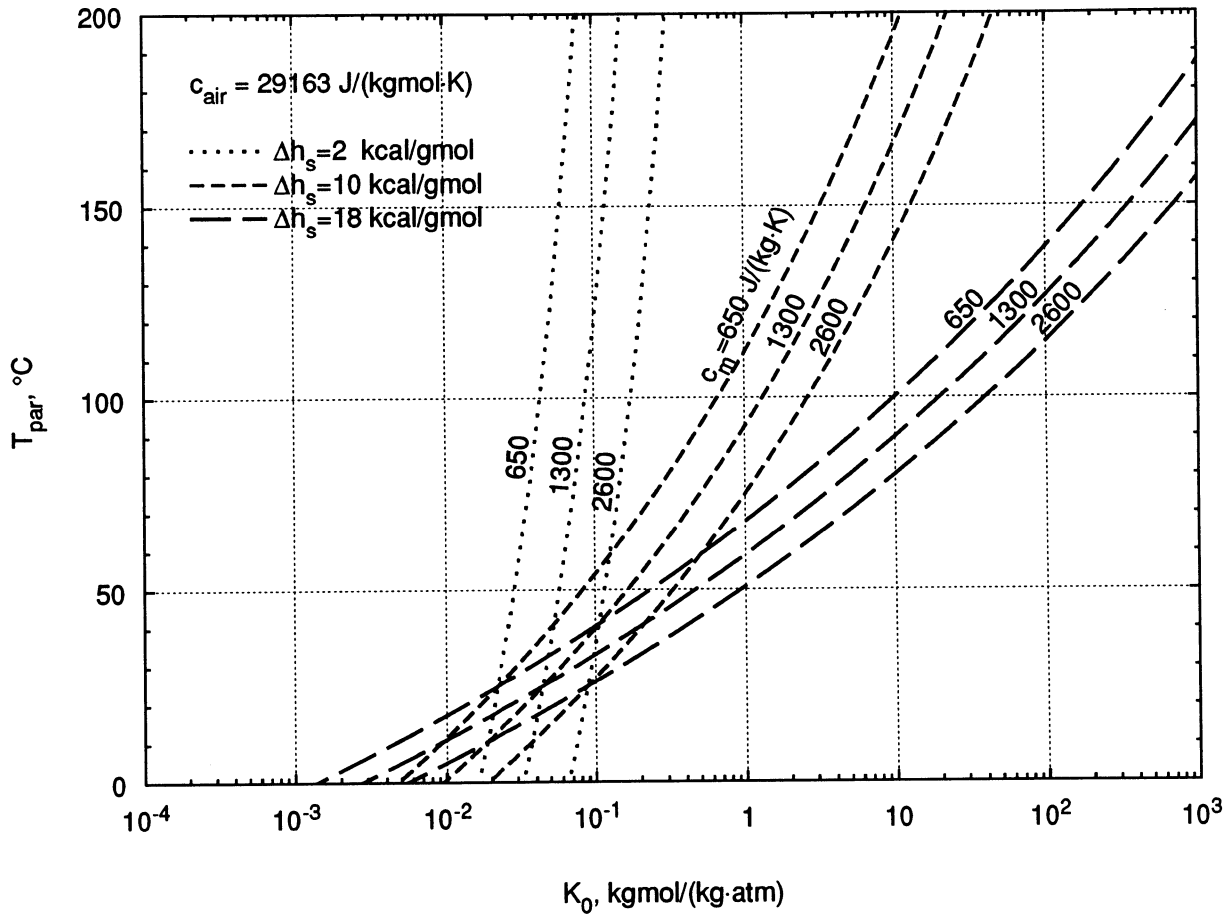

Figure 5.15(b) Temperature at which $\lambda_1 = \lambda_2$ as a function of K_0 for a range of Δh_s and σ values.

The temperature given by Equation 5.4.20 is particularly significant because this is the temperature at which the "concentration" wavespeed and the "thermal" wavespeed are equal. Above this temperature, for a given K_0, the concentration wave is faster than the thermal wave ($\lambda_1 = \lambda_T$, $\lambda_2 = \lambda_C$) and below this temperature the concentration wave is slower than the thermal wave ($\lambda_1 = \lambda_C$, $\lambda_2 = \lambda_T$). The solution of the equations is very different depending on whether the process and regeneration temperatures are both below or both above T_{par} or if one temperature is below and one is above.

Next, the hyperbolicity of the full equations with the linear isotherm is evaluated. Substituting the definitions of b_1 through b_5 from Table 4.1 into Equation 5.4.18, the eigenvalues for the full equations with the linear isotherm will be real if

$$[K^2\xi^2(\xi + 4c_v)]\omega^2 + [2K\xi(c_m + Kc_{air})]\omega + [(c_m - Kc_{air})^2] \geq 0 \tag{5.4.21}$$

where

$$\xi = \frac{\Delta h_s^2}{RT^2} \tag{5.4.22}$$

Since all of the coefficients in Equation 5.4.21 are positive, it is apparent that in the physically realistic range of ω, i.e., for $\omega \geq 0$, the eigenvalues are real.

If Equation 5.4.21 is equal to zero for some values of ω and T, then the eigenvalues are not everywhere distinct and the problem is non-strictly hyperbolic. Equation 5.4.21 is itself a quadratic equation in ω; the values of ω, at a given temperature, for which the eigenvalues are not distinct are:

$$\omega_{\lambda_1=\lambda_2} = \frac{-\xi(c_m + Kc_{air}) \pm \sqrt{4\xi[Kc_m c_{air}\xi - c_v(c_m - Kc_{air})^2]}}{K\xi(\xi + 4c_v)} \tag{5.4.23}$$

The only values of $\omega_{\lambda_1=\lambda_2}$ which are of interest are those where $\omega_{\lambda_1=\lambda_2}$ is real and $\omega_{\lambda_1=\lambda_2} \geq 0$. For $\omega_{\lambda_1=\lambda_2}$ to be real, the quantity under the square root sign must be positive and for $\omega_{\lambda_1=\lambda_2}$ to be non-negative, since the denominator is positive, the numerator of Equation 5.4.23 must be non-negative. This eliminates one root immediately, since the root obtained using the negative sign will always be negative. For the root obtained with the positive sign to be greater than or equal to zero, the following condition must be true:

$$-\xi(c_m + Kc_{air}) + \sqrt{4\xi[Kc_m c_{air}\xi - c_v(c_m - Kc_{air})^2]} \geq 0 \tag{5.4.24}$$

This equation can be manipulated into the following form:

$$\xi(c_m - Kc_{air})^2 \leq -4c_v(c_m - Kc_{air})^2 \tag{5.4.25}$$

and if $(c_m - Kc_{air}) \neq 0$ this reduces to:

$$\xi = \frac{\Delta h_s^2}{RT^2} \quad \leq \quad -4c_v \tag{5.4.26}$$

Since ξ and c_v are both always positive, the inequality of Equation 5.4.26 is never true, and therefore when $(c_m - Kc_{air}) \neq 0$ the second root is always negative. When $(c_m - Kc_{air}) = 0$, i.e., substituting $K = c_m/c_{air} = \sigma$ into Equation 5.4.23, it turns out that $\omega_{\lambda_1=\lambda_2} = 0$. Since the specific heats have been assumed constant and K is a function only of temperature, the only place where the governing equations are not hyperbolic is at $\omega = 0$ and the temperature is such that $K = \sigma$, i.e.,

$$\omega = 0, \qquad T = \frac{1}{\left[\frac{1}{T_0} + \frac{R}{\Delta h_s}\ln\left(\frac{\sigma}{K_0 P}\right)\right]} \tag{5.4.27}$$

The equations are parabolic at this point.

This temperature is the same as that given by Equation 5.4.20. Thus the difference between the full equations and the low concentration equations for the linear isotherm is that the full equations are parabolic at the point ($\omega = 0, T_{par}$) while the low concentration equations are parabolic at T_{par} for all ω.

The full equations and the low concentration equations with the Langmuir isotherm are more difficult to directly evaluate. Instead, the value of $(\lambda_2 - \lambda_1)$ was minimized with respect to temperature for $K_0 = 1\text{x}10^{-1}$ kgmol/(kg·atm) and the base values of the parameters given in Table 4.6. The computer equation solving program EES [EES] was used for the minimization. Figure 5.16 illustrates the temperature at which the minimum value of $(\lambda_2 - \lambda_1)$ was determined for all four cases and Figure 5.17 is a plot of the minimum value of $(\lambda_2 - \lambda_1)$ normalized by λ_2 for all four cases.

From Figure 5.17 it can be seen that for the low concentration equations, the eigenvalues are equal at some temperature at all concentrations; the temperature at which the eigenvalues are equal is seen in Figure 5.16 to be constant for the linear isotherm and a decreasing function of concentration for the Langmuir isotherm. For the full equations, the eigenvalues are equal only at $\omega = 0$, although the difference becomes very small as the concentration decreases. The temperature at which the difference in the eigenvalues is minimized is a decreasing function of concentration, and the effect is stronger for the Langmuir isotherm. It is apparent from Figures 5.16 and 5.17 that the low concentration equations are the limiting form of the full equations at $\omega = 0$.

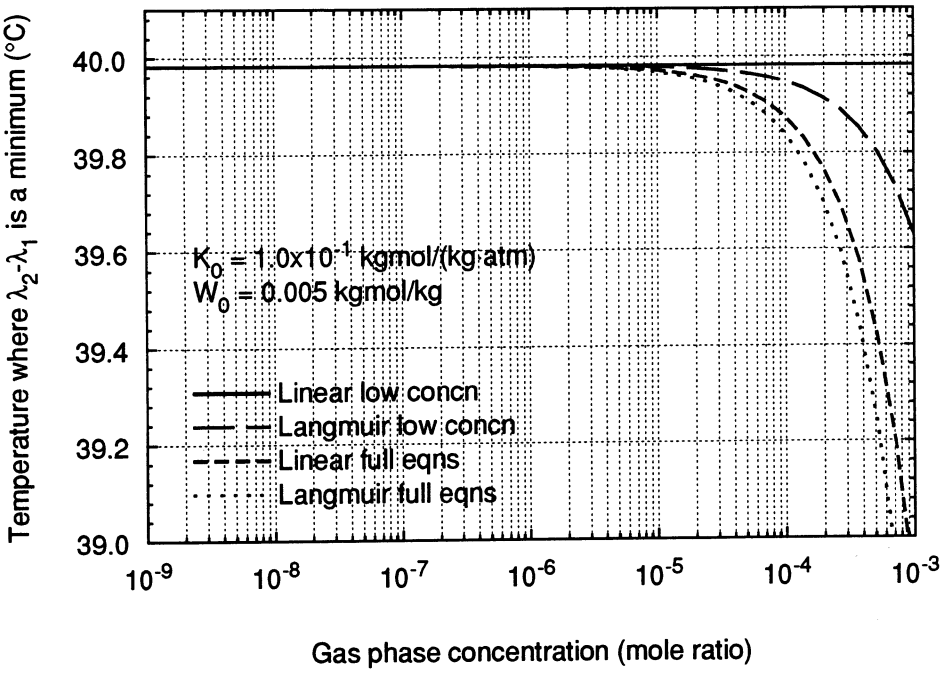

Figure 5.16 Temperatures at which the difference in the eigenvalues (wavespeeds) is minimized for $K_0 = 1\text{x}10^{-1}$ and the parameter values of Table 4.6.

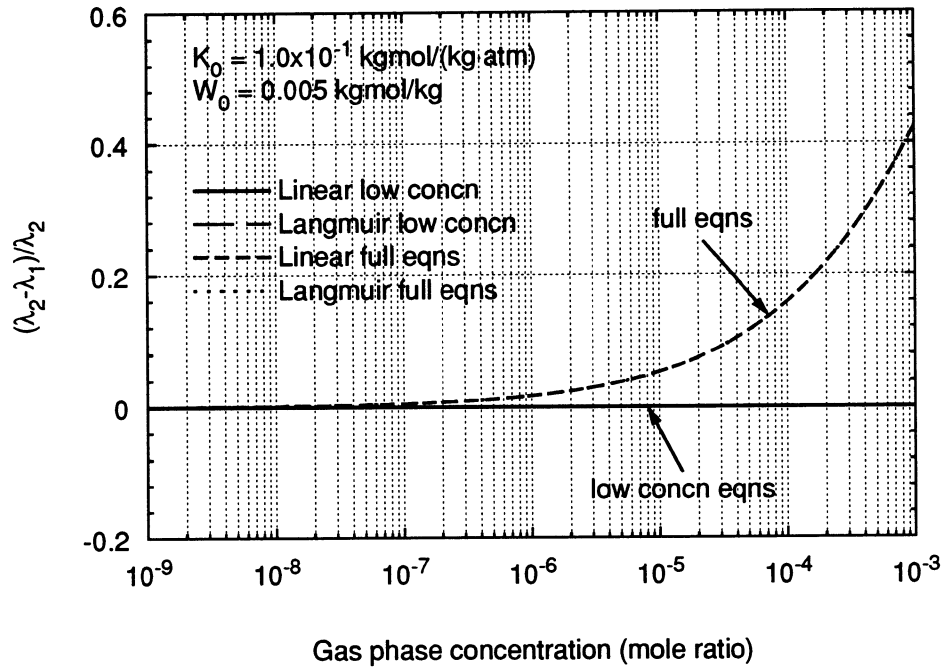

Figure 5.17 The minimum difference between the eigenvalues (wavespeeds) for $K_0 = 1\text{x}10^{-1}$ and the parameter values of Table 4.6.

5.4.2 Linear classification

To determine whether the conservation equations are genuinely nonlinear, linearly degenerate, or a general system, the quantity $\nabla\lambda_k \cdot r_k$ is examined. For the low concentration equations with the linear isotherm, in terms of the concentration and thermal waves,

$$\nabla\lambda_C \cdot r_C = \begin{bmatrix} 0 \\ \dfrac{\Delta h_s}{KRT^2} \end{bmatrix} \cdot \begin{bmatrix} \dfrac{\omega\Delta h_s}{\sigma RT^2} \\ 0 \end{bmatrix} = 0 \tag{5.4.28}$$

$$\nabla\lambda_T \cdot r_T = \begin{bmatrix} 0 \\ 0 \end{bmatrix} \cdot \begin{bmatrix} \dfrac{\omega\Delta h_s}{\sigma RT^2} \\ \left(\dfrac{1}{\sigma} - \dfrac{1}{K}\right) \end{bmatrix} = 0 \tag{5.4.29}$$

and thus the characteristics associated with the concentration wave and the thermal wave are both linearly degenerate.

For the low concentration equations with the Langmuir isotherm,

$$\nabla\lambda_C \cdot r_C = \begin{bmatrix} \dfrac{(W_0 + K\omega)^2}{KW_0^2} \\ \dfrac{\Delta h_s[W_0^2 - (K\omega)^2]}{KW_0^2RT^2} \end{bmatrix} \cdot \begin{bmatrix} \dfrac{\omega\Delta h_s}{\sigma RT^2} \\ 0 \end{bmatrix} = \frac{\omega\Delta h_s(W_0 + K\omega)^2}{\sigma KW_0^2RT^2} \tag{5.4.30}$$

$$\nabla\lambda_T \cdot r_T = \begin{bmatrix} 0 \\ 0 \end{bmatrix} \cdot \begin{bmatrix} \dfrac{\omega\Delta h_s}{\sigma RT^2} \\ \dfrac{1}{\sigma} - \dfrac{(W_0 + K\omega)^2}{KW_0^2} \end{bmatrix} = 0 \tag{5.4.31}$$

The characteristics associated with the thermal wave are linearly degenerate. For the concentration wave, $\nabla\lambda_C \cdot r_C$ is equal to zero at $\omega = 0$. At all other physically meaningful

values of ω, $\nabla\lambda_C \cdot r_C \neq 0$. Since the characteristics associated with the concentration wave are neither genuinely nonlinear or linearly degenerate, the low concentration equations with the Langmuir isotherm can be classified as a general system.

It is considerably more difficult to determine an expression which can be analyzed for $\nabla\lambda_k \cdot r_k$ for the full equations. Instead, the value of $\nabla\lambda_k \cdot r_k$ was calculated as a function of temperature for $\omega = 1$ ppm and the parameter values of Table 4.6. Figure 5.18 shows the values of $\nabla\lambda_1 \cdot r_1$ and $\nabla\lambda_2 \cdot r_2$ for the full equations with the linear and the Langmuir isotherms. Nowhere is $\nabla\lambda_k \cdot r_k$ equal to zero. The values were plotted as 1 and 2-curves rather than concentration and thermal curves; the concentration curve is the 1-curve below T_{par} (approximately 40°C) and the 2-curve above T_{par}. The differences in $\nabla\lambda_k \cdot r_k$ between the linear and the Langmuir isotherm are very small at this concentration, and the linear isotherm values of $\nabla\lambda_k \cdot r_k$ are hidden underneath the Langmuir values in Figure 5.18.

For comparison, the values of $\nabla\lambda_1 \cdot r_1$ and $\nabla\lambda_2 \cdot r_2$ for the low concentration equations with the linear and the Langmuir isotherm at $\omega = 1$ ppm are shown in Figure 5.19. As expected, the values of $\nabla\lambda_1 \cdot r_1$ and $\nabla\lambda_2 \cdot r_2$ are equal to zero for the linear isotherm. Below T_{par}, $\nabla\lambda_1 \cdot r_1$ corresponds to $\nabla\lambda_C \cdot r_C$, whereas above T_{par}, $\nabla\lambda_2 \cdot r_2$ corresponds to $\nabla\lambda_C \cdot r_C$. Thus, as predicted by Equations 5.4.30 and 5.4.31, $\nabla\lambda_C \cdot r_C \neq 0$ and $\nabla\lambda_T \cdot r_T = 0$ for the low concentration equations with the Langmuir isotherm.

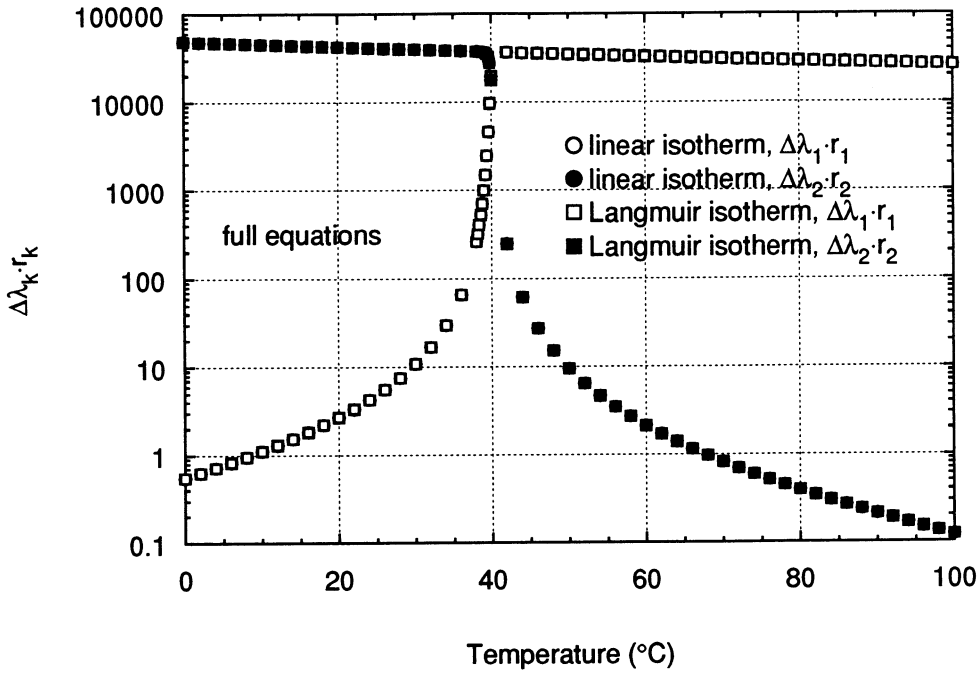

Figure 5.18 The values of $\nabla\lambda_1 \cdot r_1$ and $\nabla\lambda_2 \cdot r_2$ for the full equations with the linear and the Langmuir isotherm as a function of temperature for $\omega = 1$ ppm and the parameter values of Table 4.6.

5.4.3 Integral curves

Integral curves for the full equations and the low concentration equations with both linear and Langmuir isotherms are shown in Figures 5.20 to 5.23. All parameters are at the base values given in Table 4.6. The starting point for the integration was 5 ppm at 20, 60, 100, 140, and 180°C; the equation for the integral curve was numerically integrated in both directions from this point. The arrows point in the direction of increasing wavespeeds. Therefore, when moving along an integral curve from the state behind a wave to the state in front of a wave, moving in the direction of the arrows indicates a rarefaction wave while moving against the arrow direction indicates a shock wave. Since

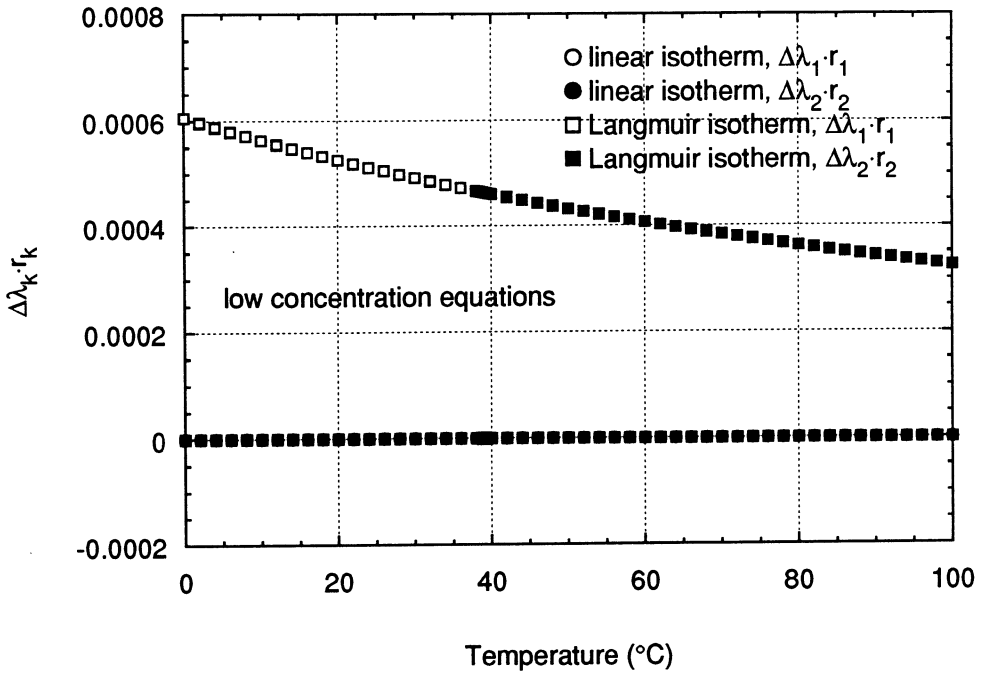

Figure 5.19 The values of $\nabla\lambda_1 \cdot r_1$ and $\nabla\lambda_2 \cdot r_2$ for the low concentration equations with the linear and the Langmuir isotherm as a function of temperature for $\omega = 1$ ppm and the parameter values of Table 4.6.

these hodoplots consist only of integral curves, any shock solutions as predicted by the diagrams are only approximate. Before discussing these plots, however, an example helps indicate their usefulness.

Figure 5.24 is the hodograph plot (consisting of integral curves) for the full equations with the linear isotherm and K_0=1x10^1 kgmol/(kg·atm). A process inlet state of (20°C, 8 ppm) and a regeneration inlet state of (60°C, 5 ppm) are indicated on the plot. Dashed lines have been used for the 2-curves and solid lines for the 1-curves. Considering the process side of the wheel, the state behind the 1-wave (the slow wave) is the process inlet state, and therefore the intermediate state lies somewhere along the 1-curve through the process state. Assuming that the matrix were fully regenerated, the state in front of the 2-wave (the fast wave) is the regeneration state, and therefore the

intermediate state must lie somewhere along the 2-curve through the regeneration state. The only point at which the 1-curve through the process state and the 2-curve through the regeneration state intersect is the process side intermediate state, as indicated in Figure 5.24.

The concentration of the intermediate state is less than either the process or the regeneration concentration. As the first wave (the 2-wave) passes, the concentration decreases from the regeneration value of 5 ppm to less than 1 ppm. The temperature also decreases, and it appears to decrease to the process temperature. As the second wave (the 1-wave) passes, the concentration increases to the process concentration while the temperature, which is already at the process temperature, remains constant. In reality, there is a slight temperature decrease from the intermediate state to the process state: the intermediate temperature is 20.011°C. Both waves are rarefaction waves.

For the regeneration side of the wheel, the role of the process and regeneration states is reversed: the regeneration state is behind the slower wave and the process state is in front of the faster wave. This means that the regeneration side intermediate state will be at the intersection of a 1-wave through the regeneration state and a 2-wave through the process state. This intermediate state is off the graph in Figure 5.24. Both waves are shock waves.

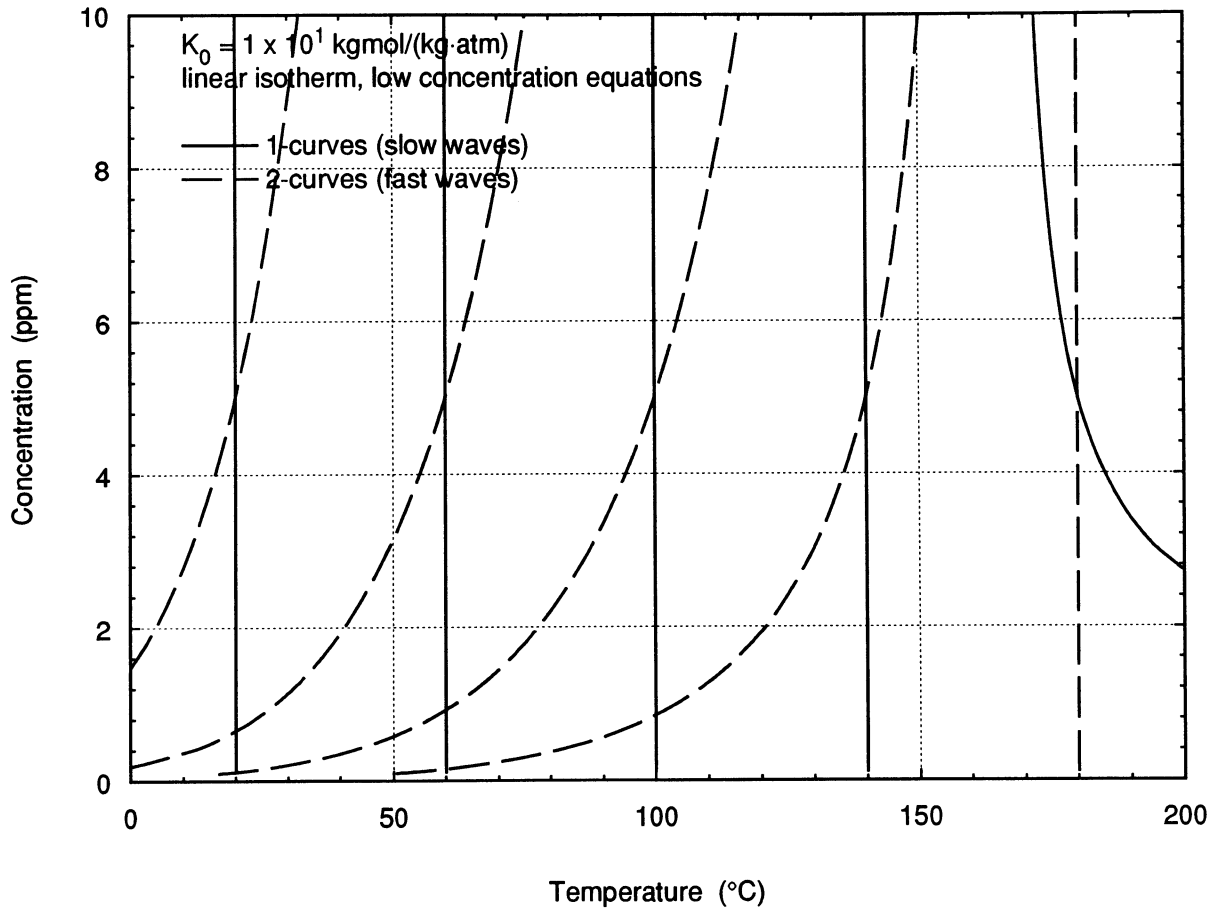

Figure 5.20 Integral curves for the low concentration equations with the linear isotherm in the ppm range, K_0=1x10^1 kgmol/(kg·atm), and the base parameter values of Table 4.6.

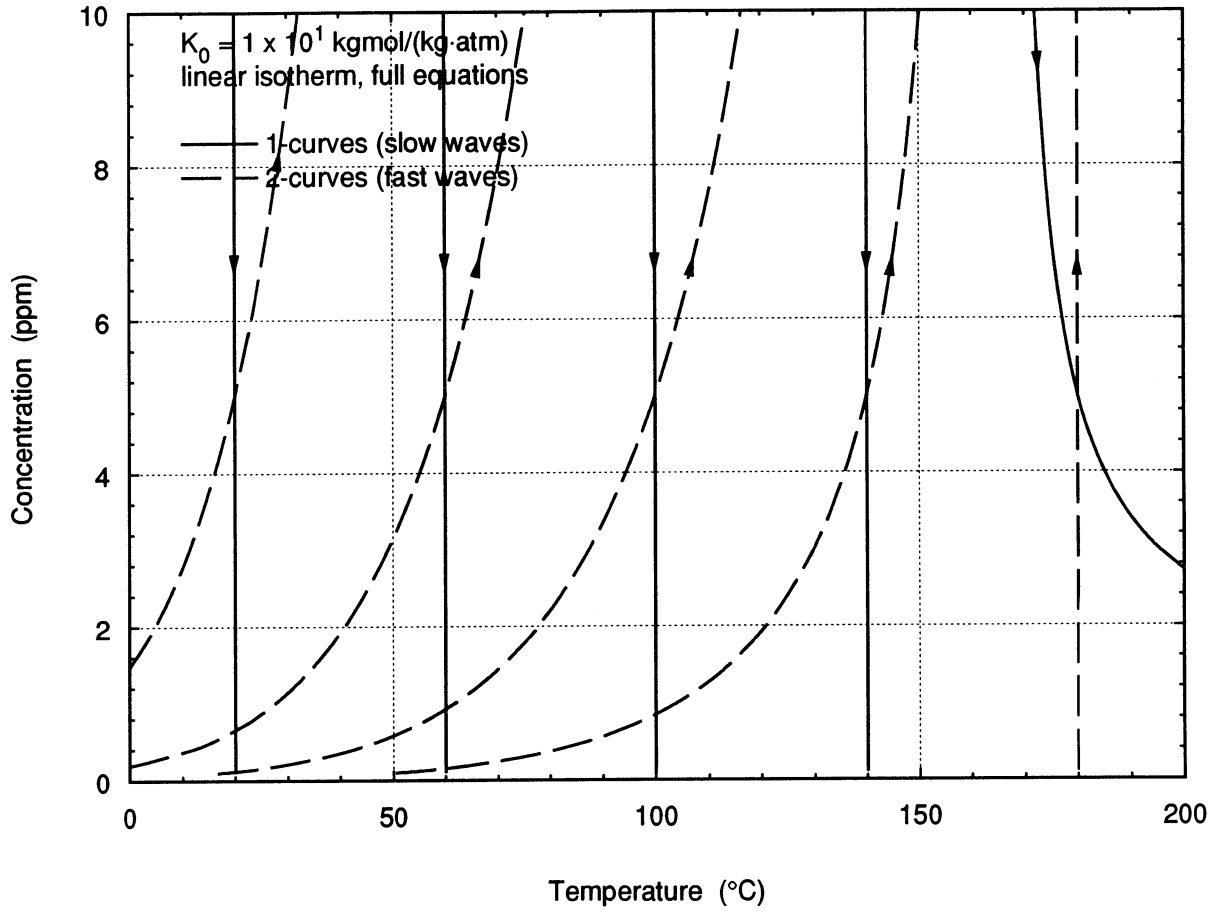

Figure 5.21 Integral curves for the full equations with the linear isotherm in the ppm range, K_0=1x10^1 kgmol/(kg·atm), and the base parameter values of Table 4.6.

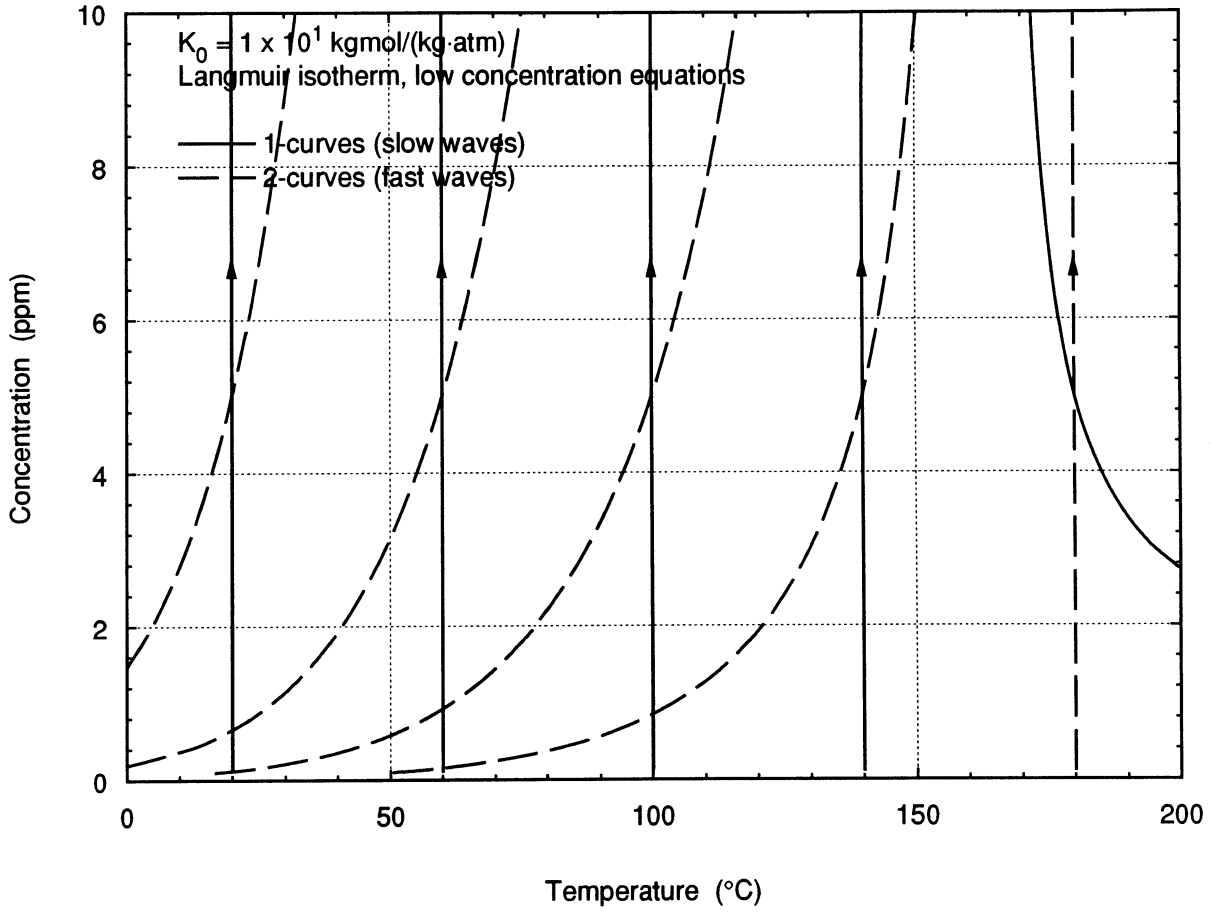

Figure 5.22 Integral curves for the low concentration equations with the Langmuir isotherm in the ppm range, K_0=1x10^1 kgmol/(kg·atm), and the base parameter values of Table 4.6.

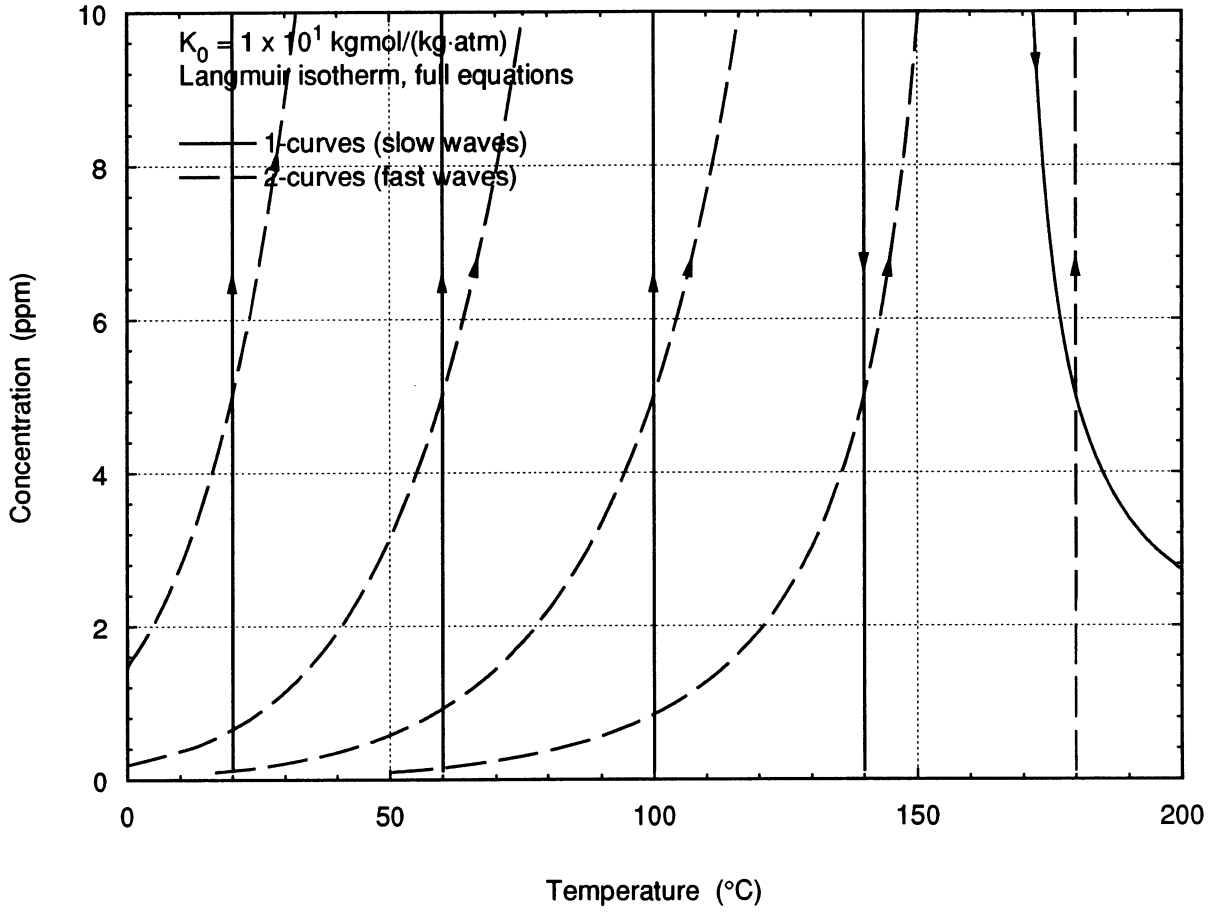

Figure 5.23 Integral curves for the full equations with the Langmuir isotherm in the ppm range, K_0=1x10^1 kgmol/(kg·atm), and the base parameter values of Table 4.6.

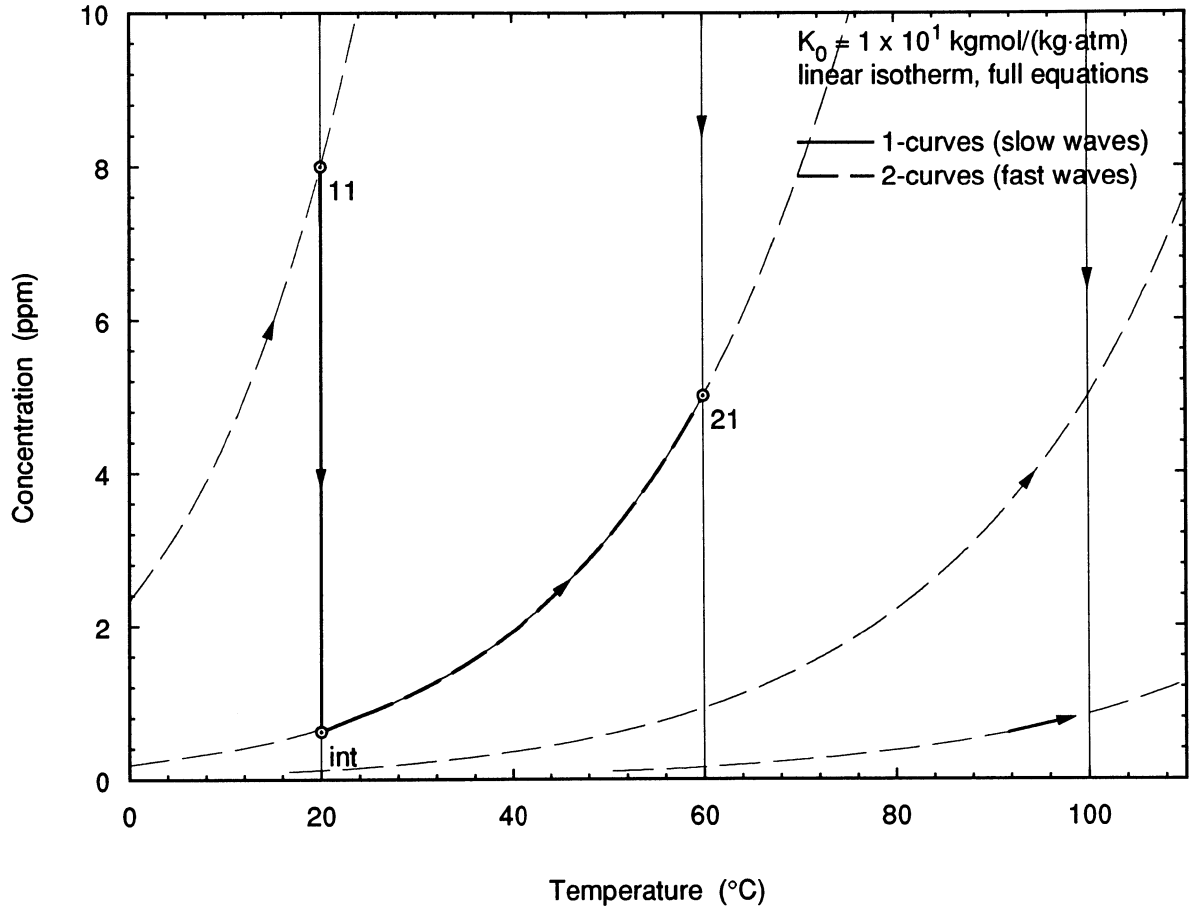

Figure 5.24 Example of process (11), regeneration (21), and intermediate states on a plot of integral curves for the low concentration equations with the linear isotherm, K_0=1x10^1 kgmol/(kg·atm), and the base parameter values of Table 4.6.

Integral curves for the linear isotherm low concentration equations are plotted in Figure 5.20 for $K_0=1x10^1$ kgmol/(kg·atm) up to 10 ppm. There are no arrows because both of the characteristic families in this case are linearly degenerate and the wavespeeds (eigenvalues) are constant along the integral curve. Both waves are therefore contact discontinuities. For this case, the vertical characteristics (which are the concentration characteristics) have infinite slopes (Equation 5.4.16). The parabolic temperature, T_{par}, is equal to 165.67°C for the parameter values used in Figure 5.20, and the behavior of the 1 and 2-curves reverses around this temperature. The concentration curves, along which there is no change in temperature, are represented by the vertical curves in Figure 5.20. Below T_{par}, these are the 1-curves (the slow waves) wheras above T_{par}, the concentration curves are the 2-curves (the fast waves). The reverse is true for the thermal curves.

Comparison with the plots for the other isotherm and assumption combinations indicates that there is no significant difference between the curves in this concentration range. The types of the curves (i.e., rarefaction, shock, or contact discontinuity), however, are different, as indicated by the different arrow directions. For example, considering the process side of the wheel for the process and regeneration inlet states of (8 ppm, 20°C) and (5 ppm, 60°C) respectively, the linear isotherm low concentration waves would consist of two contact discontinuities; the linear isotherm full equation waves would consist of two rarefaction waves; the Langmuir isotherm low concentration waves would consist of one contact discontinuity and one shock wave; the Langmuir isotherm full equation waves would consist of one shock wave and one rarefaction wave. For comparison, Table 5.1 lists the temperature, concentration, and wavespeed at 0.1 ppm and 10 ppm for the 1 and 2-curves through the point (5 ppm, 100°C). The difference in the temperature values between the four equation sets is less than 0.01%, and the difference in the wavespeeds is less than 0.3%.

Table 5.1 Comparison of the end points of the 1 and 2-curves through (5 ppm, 100°C) for the different equations sets.

	T (°C)	ppm	λ_1	T (°C)	ppm	λ_2
Linear, low concn	100.0000	0.1	2.9785	16.6693	0.1	22.433
	100.0000	10	2.9785	116.4139	10	22.433
Linear, full eqns	100.0081	0.1	2.9793	16.6691	0.1	22.432
	99.9917	10	2.9758	116.4153	10	22.446
Langmuir, low concn	100.0000	0.1	2.9785	16.6709	0.1	22.433
	100.0000	10	2.9825	116.4114	10	22.433
Langmuir, full eqns	100.0081	0.1	2.9794	16.6706	0.1	22.432
	99.9917	10	2.9798	116.4128	10	22.446

The hodoplots in the range of 0 to 10 ppb look virtually identical to those in the range of 0 to 10 ppm illustrated in Figures 5.20 to 5.23; for comparison, the low concentration linear isotherm integral curves in the range of 0 to 10 ppb are plotted in Figure 5.25. The differences between the four different assumption/isotherm combinations in the ppb range are even smaller than in the ppm range. On the other hand, as the concentration level increases, the trends in Table 5.1 become more pronounced, and the differences become larger. Figure 5.26 shows the integral curves in the range of 0 to 1000 ppm for the full equations with the Langmuir isotherm.

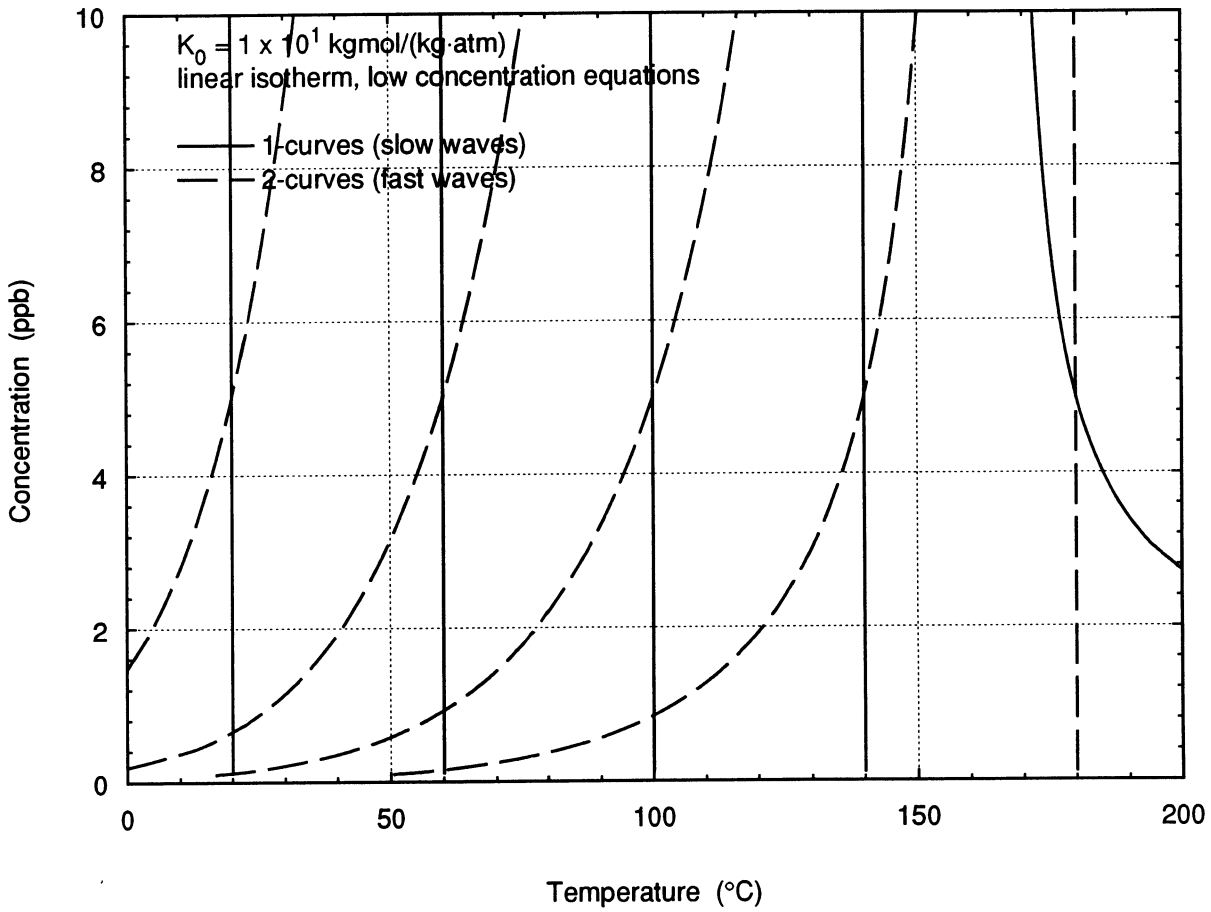

Figure 5.25 Integral curves for the low concentration equations with the linear isotherm in the ppb range, K_0=1x10^1 kgmol/(kg·atm), and the base parameter values of Table 4.6.

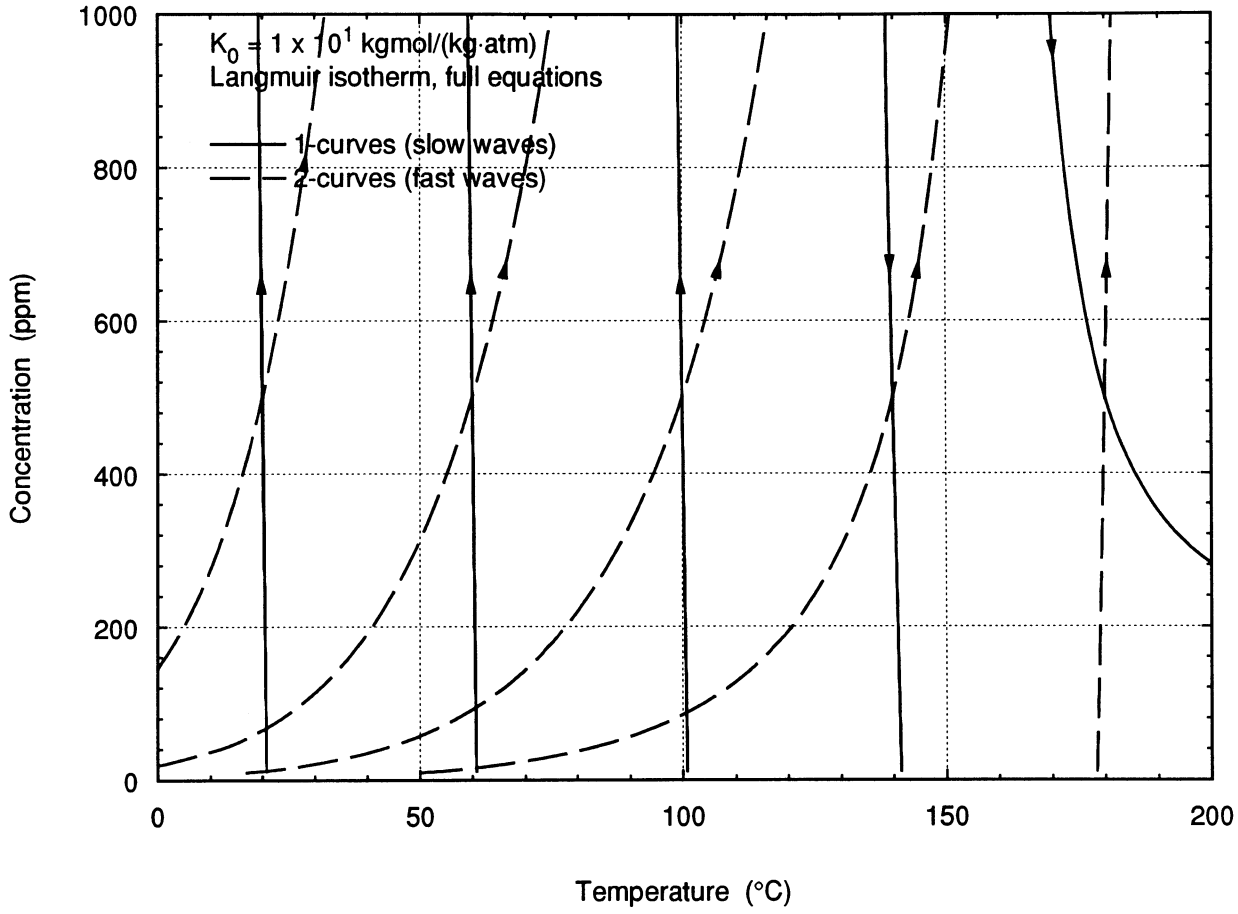

Figure 5.26 Integral curves for the full equations with the Langmuir isotherm in the high ppm range, K_0=1x10^1 kgmol/(kg·atm), and the base parameter values of Table 4.6.

Figure 5.27 compares the intermediate concentration for the low concentration equations and the full equations with the linear isotherm as a function of the concentration order of magnitude. Multiplying the y-axis value by the x-axis value gives the concentration, e.g., the leftmost point represents ω_{int}=0.621x10^{-9} kgmol/kgmol which is equivalent to 0.621 ppb. Parameters were set to the base values of Table 4.6. The process and regeneration temperature were equal to 20°C and 60°C, respectively. The process and regeneration concentrations were equal to 8 and 5 times the appropriate order of magnitude, e.g., for the leftmost point, ω_{11} = 8 ppb and ω_{21} = 5 ppb. Figure 5.28 compares the intermediate temperatures for the same conditions. These figures support the validity of the low concentration assumption for the ppb range of indoor air contaminants; it would also be valid in the lowppm range.

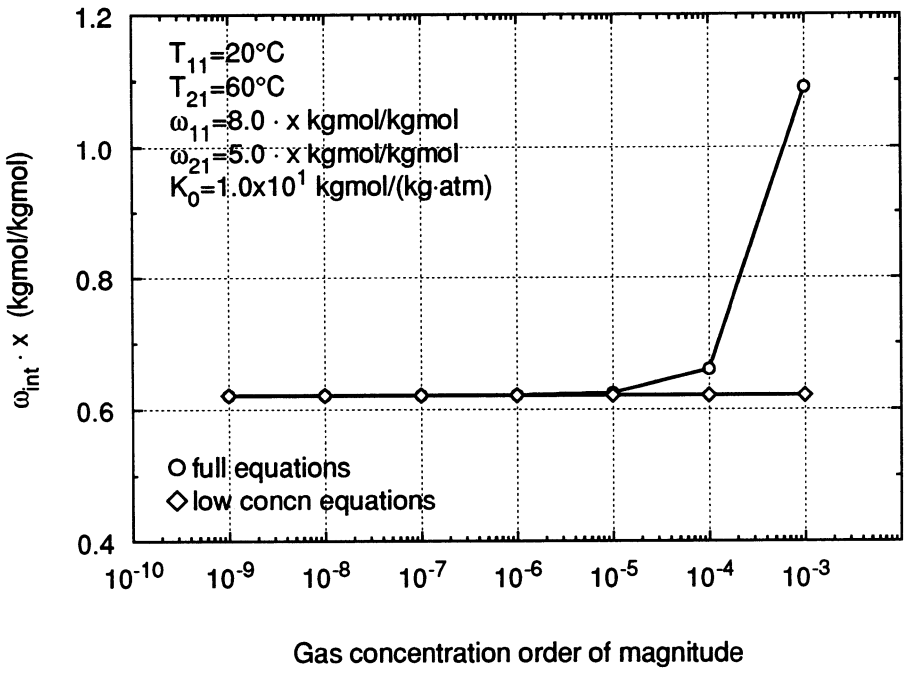

Figure 5.27 Intermediate concentration for the full equations and the low concentration equations with the linear isotherm, as a function of concentration order of magnitude.

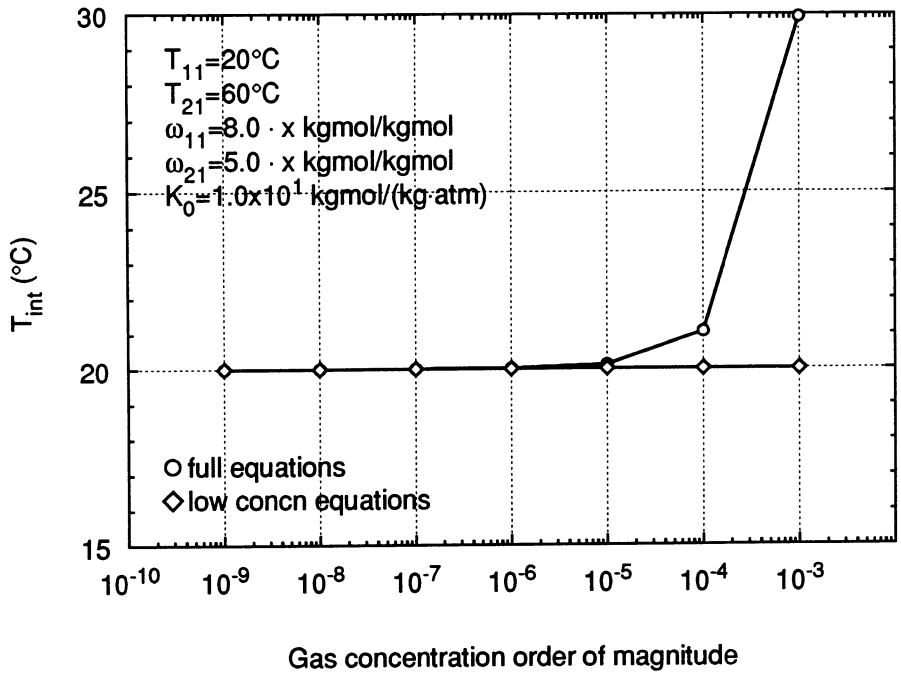

Figure 5.28 Intermediate temperature for the full equations and the low concentration equations with the linear isotherm, as a function of concentration order of magnitude.

5.5 The low concentration equations, linear isotherm solution

The simplified equations for the low concentration assumption, in flux form, are as follows:

$$\frac{\partial W}{\partial \tau}+\frac{\partial \omega}{\partial x}=0 \tag{5.5.1}$$

$$\frac{\partial T}{\partial \tau}+\frac{\partial (T/\sigma)}{\partial x}=0 \tag{5.5.2}$$

Recall that both characteristic fields are linearly degenerate (Section 5.4.2) so that in regions where the equations are strictly hyperbolic, the solution consists of two contact discontinuities separated by a constant state. Figure 5.29 illustrates an example wave diagram. State *R* is the state to the right of the waves; this is the initial state (the term

"state" is used to describe an ω, T pair). When analyzing the process period of a completely regenerated rotary wheel, this would be the regeneration inlet state, state 21. State L is the state to the left of the waves, which is the inlet state. For the process period, this corresponds to the process inlet state, state 11.

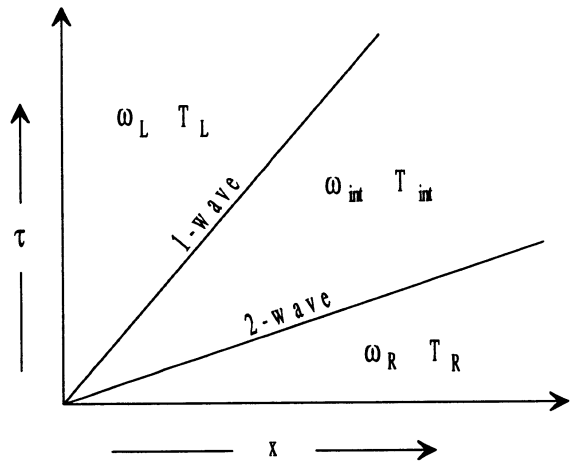

Figure 5.29 Example wave diagram. State R is to the right of all of the waves and state L is to the left of all of the waves. Both waves are contact discontinuities.

The solution is determined from the Rankine-Hugoniot conditions which are based on the flux form of the conservation equations. The equations for the fast wave are as follows:

$$s_2(W_R - W_{int}) = (\omega_R - \omega_{int}) \tag{5.5.3}$$

$$s_2(T_R - T_{int}) = \frac{1}{\sigma}(T_R - T_{int}) \tag{5.5.4}$$

and the equations for the slow wave are:

$$s_1(W_{int} - W_L) = (\omega_{int} - \omega_L) \tag{5.5.5}$$

$$s_1(T_{int} - T_L) = \frac{1}{\sigma}(T_{int} - T_L) \tag{5.5.6}$$

with the entropy conditions:

$$\lambda_{2(R)} \le s_2 \le \lambda_{2(\text{int})} \tag{5.5.7}$$

$$\lambda_{1(\text{int})} \le s_2 \tag{5.5.8}$$

$$\lambda_{1(\text{int})} \le s_1 \le \lambda_{1(L)} \tag{5.5.9}$$

$$s_1 \le \lambda_{2(L)} \tag{5.5.10}$$

For now consider only the range of (ω, T) such that $\lambda_C < \lambda_T$, which means that the temperatures (both the process temperature and the regeneration temperature) are restricted so that $T < T_{par}$ and consequently $\frac{1}{K} < \frac{1}{\sigma}$. In this case,

$$\lambda_1 = \lambda_C = \frac{1}{K} \tag{5.5.11}$$

$$\lambda_2 = \lambda_T = \frac{1}{\sigma} \tag{5.5.12}$$

and the entropy conditions become:

$$\frac{1}{\sigma} \le s_2 \le \frac{1}{\sigma} \tag{5.5.13}$$

$$\frac{1}{K_{\text{int}}} \le s_2 \tag{5.5.14}$$

$$\frac{1}{K_{\text{int}}} \le s_1 \le \frac{1}{K_L} \tag{5.5.15}$$

$$s_1 \le \frac{1}{\sigma} \tag{5.5.16}$$

In order to satisfy Equation 5.5.6, either $s_1 = \frac{1}{\sigma}$ or $T_{int} = T_L$. From the entropy condition of Equation 5.5.15, it can be seen that the first condition is not possible, i.e., $s_1 \neq \frac{1}{\sigma}$ since $s_1 \leq \frac{1}{K_L}$ and the problem has been constrained such that $\frac{1}{K_L} < \frac{1}{\sigma}$. Therefore, the following must be true:

$$T_{int} = T_L \tag{5.5.17}$$

This agrees with the low concentration assumption, namely that there is no temperature change resulting from the adsorption or desorption of the contaminant.

From Equation 5.5.5, either $s_2 = \frac{1}{\sigma}$ or $T_R = T_{int}$. The entropy condition of Equation 5.5.13 indicates that in this case the first condition is true, i.e.,

$$s_2 = \frac{1}{\sigma} \tag{5.5.18}$$

and therefore, in general $T_R \neq T_{int}$. The concentration of the intermediate state can be solved for from Equation 5.5.3, using Equations 5.5.17 and 5.5.18:

$$\omega_{int} = \omega_R \left[\frac{K_R - \sigma}{K_L - \sigma} \right] \tag{5.5.19}$$

Substituting this result into Equation 5.5.5, the shock speed s_1 can be solved for:

$$s_1 = \frac{1}{K_L} \tag{5.5.20}$$

which satisfies the entropy conditions (Equation 5.5.15 and 5.5.16). Again, these results support the condition of linear degeneracy, since the shock speeds are equal to the eigenvalue of one of the surrounding constant states. Figure 5.30 illustrates an example wave diagram for this case.

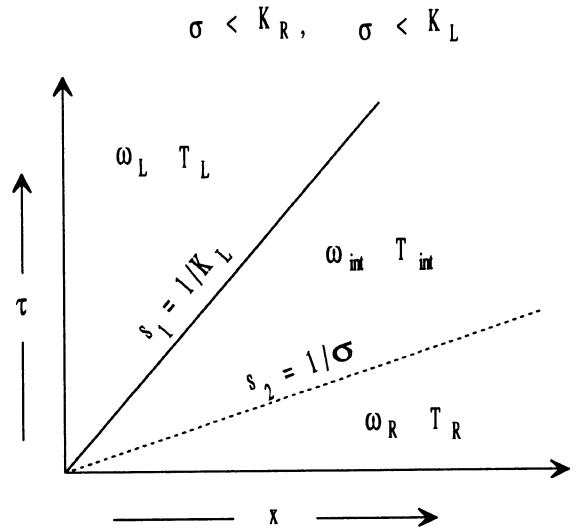

Figure 5.30 Example wave diagram where the thermal wave (dashed line) is the fastest wave. The concentration wave is shown by the solid line.

Next, consider the range of (ω, T) such that $\lambda_T < \lambda_C$, which means that the temperature is restricted so that $T > T_{par}$ and consequently $\frac{1}{\sigma} < \frac{1}{K}$. In this case,

$$\lambda_1 = \lambda_T = \frac{1}{\sigma} \tag{5.5.21}$$

$$\lambda_2 = \lambda_C = \frac{1}{K} \tag{5.5.22}$$

and $\frac{1}{\sigma} < \frac{1}{K}$. An analysis similar to that for the region where $\lambda_C < \lambda_T$ yields the results that

$$s_1 = \lambda_T = \frac{1}{\sigma} \tag{5.5.23}$$

$$s_2 = \lambda_C = \frac{1}{K_R} \tag{5.5.24}$$

$$T_{int} = T_R \tag{5.5.25}$$

$$\omega_{int} = \omega_L \left[\frac{K_L - \sigma}{K_R - \sigma} \right] \tag{5.5.26}$$

Figure 5.31 illustrates an example wave diagram for this case.

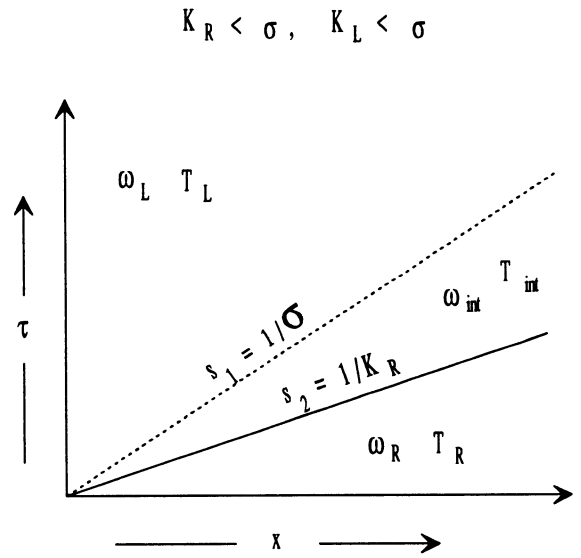

Figure 5.31 Example wave diagram where the thermal wave (dashed line) is the slowest wave. The concentration wave is shown by the solid line.

Translating these mathematical results (Equations 5.5.17-5.5.20 and 5.5.23-5.5.26) into physical terms, the thermal wave propagates at a speed of $1/\sigma$, which is constant and independent of the mass balance. Both the temperature and the concentrations change across the thermal wave. The concentration wave propagates at a speed equal to $1/K$, where $K = K(T)$. Therefore, when the temperature changes, the speed of the

concentration wave changes. Within a region of constant temperature the speed of the concentration wave is constant. Across the concentration wave there is no change in temperature, only a change in concentration.

So far, only two cases have been examined: that where the process and regeneration temperatures are less than T_{par} and that where the process and regeneration temperatures are greater than T_{par}. It is possible, however, to have a process temperature below T_{par} and a regeneration temperature above T_{par}.

First examine the case where $T_R > T_{par} > T_L$. This corresponds to a process period analysis where the regeneration temperature, which is the initial temperature, is greater than T_{par} while the process temperature (the inlet temperature) is less than T_{par}. The thermal wave, as always, propagates at speed $1/\sigma$ and the temperature changes across the wave from T_R in front of the wave to T_L behind the wave. It is not obvious, however, whether the thermal or the concentration wave is the faster wave. Evaluating $\lambda_C = 1/K$ at T_R gives a concentration wave faster than the thermal wave, while evaluating $\lambda_C = 1/K$ at T_L gives a concentration wave slower than the thermal wave.

In the previous analyses, there was no such contradiction. For example, for the case where all $T < T_{par}$, the concentration wavespeed evaluated at either T_R or T_L resulted in a concentration wave slower than the thermal wave. Since the concentration wave was slower than the thermal wave and since the region behind the thermal wave was entirely at the temperature T_L, the appropriate concentration wavespeed was $\lambda_C = 1/K_L$.

So, of the two possible concentration wavespeeds, which one will the concentration wave "pick" ? Initially, it was suspected that this represents some initial instability, and that one of the concentration wavespeeds would be more or less randomly "selected". A

mass balance, however, shows that this scenario is not correct. Picking one of the concentration wavespeeds (either one) results in an intermediate concentration less than zero. The other possibility was that there were two concentration waves, one at each speed, i.e., $\lambda_{C2} = 1/K_R$ and $\lambda_{C1} = 1/K_L$, where $\lambda_{C2} > \lambda_T > \lambda_{C1}$. From a mass balance, evaluation of the two intermediate states (between the fast concentration wave and the thermal wave and between the thermal wave and the slow concentration wave) for this scenario yields identical intermediate state concentrations, both of which are equal to zero. The proposed solution, in the form of a wave diagram is illustrated in Figure 5.32.

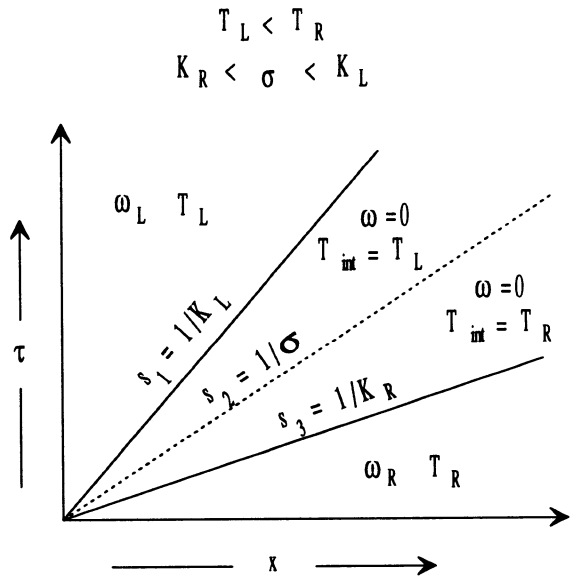

Figure 5.32 Example wave diagram where the thermal wave (dashed line) propagates at a speed between the two concentration wavespeeds (solid line).

This solution consists of three waves separating four different constant states. Initially, this seemed to be a violation of the rule that the solution of a system of 2x2 conservation laws consists of at most two wave groups and three constant states. This apparent contradiction lead to a reconsideration of the original equations, at which time it became apparent that the equations were not strictly hyperbolic. Further investigation (summarized in Section 5.3) indicated that when the solution involves the region in which

the equations are not strictly hyperbolic, then the solution can consist of other combinations of wave groups than the traditional two waves and three constant states for the strictly hyperbolic equations.

Next examine the case where $T_R < T_{par} < T_L$. This corresponds to a regeneration period analysis where the process temperature, which is the initial temperature, is less than T_{par} while the regeneration temperature (the inlet temperature) is greater than T_{par}. The thermal wave propagates at speed $1/\sigma$ and the temperature changes across the wave from T_R in front of the wave to T_L behind the wave. In this case, the low temperature concentration wavespeed is less than the thermal wavespeed and the high temperature concentration wavespeed is greater than the thermal wavespeed.

Since the region behind the thermal wave is at the high temperature, a concentration wave in this region will intersect the thermal wave at some point. Similarly, concentration waves in the region in front of the thermal wave, which move slower than the thermal wave, will also intersect the thermal wave at some point. Neither concentration wave can cross over into the other region because it will be immediately propagated back. The result is that once a concentration wave intersects the thermal wave, it then follows the thermal wave. A mass balance reveals that when the concentration wave is following the thermal wave, the concentration wave is of infinite concentration and zero width. Figure 5.33 illustrates a wave diagram for this case for a matrix initially uniform at state R.

The general solution for the low concentration equations with the linear isotherm and uniform initial conditions is summarized in Table 5.2.

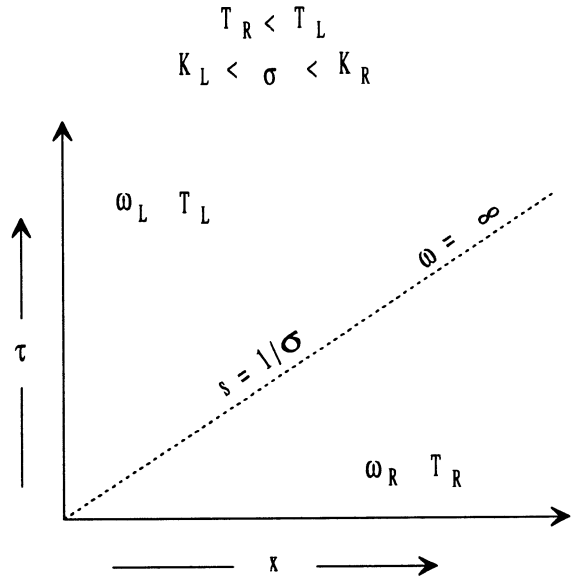

Figure 5.33 Example wave diagram where the concentration waves follow the thermal wave (dashed line).

Table 5.2 Equilibrium solution of the low concentration equations with the linear isotherm with uniform initial conditions. R is the state to the right of the waves (the initial state) and L is the state to the left of the waves (the inlet state).

	$T < T_{par}$	$T > T_{par}$	$T_R > T_{par} > T_L$	$T_R < T_{par} < T_L$
Wavespeeds	$\lambda_1 = \lambda_C = \frac{1}{K_L}$ $\lambda_2 = \lambda_T = \frac{1}{\sigma}$	$\lambda_1 = \lambda_T = \frac{1}{\sigma}$ $\lambda_2 = \lambda_C = \frac{1}{K_R}$	$\lambda_1 = \lambda_{C(L)} = \frac{1}{K_L}$ $\lambda_2 = \lambda_T = \frac{1}{\sigma}$ $\lambda_3 = \lambda_{C(R)} = \frac{1}{K_R}$	$\lambda_1 = \lambda_2 = \lambda_T = \frac{1}{\sigma}$
T_{int}	$T_{int} = T_L$	$T_{int} = T_R$	T_L and T_R	-
ω_{int}	$\omega_R \left[\frac{K_R - \sigma}{K_L - \sigma} \right]$	$\omega_L \left[\frac{K_L - \sigma}{K_R - \sigma} \right]$	0	∞

5.5.1 Process period (completely regenerated matrix)

For the process period in which the matrix is initially in equilibrium with the regeneration state, $T_R = T_{21}$ and $T_L = T_{11}$. The regeneration temperature is assumed to be higher than the process temperature, so that $K_R < K_L$, where $K_R = K_{21}$ and $K_L = K_{11}$. Depending on the values of K_0 and σ, there are three different wave combinations which may result, corresponding to the first three columns of Table 5.2. These three cases, which will be referred to as Case 1, Case 2, and Case 3, are as follows:

Case 1: $\sigma < K_{21} < K_{11}$

$$\lambda_2 = \frac{1}{\sigma} \tag{5.5.27}$$

$$\lambda_1 = \frac{1}{K_{11}} \tag{5.5.28}$$

$$\omega_{int} = \omega_{21}\left[\frac{K_{21} - \sigma}{K_{11} - \sigma}\right] \tag{5.5.29}$$

Case 2: $K_{21} < \sigma < K_{11}$

$$\lambda_3 = \frac{1}{K_{21}} \tag{5.5.30}$$

$$\lambda_2 = \frac{1}{\sigma} \tag{5.5.31}$$

$$\lambda_1 = \frac{1}{K_{11}} \tag{5.5.32}$$

$$\omega_{int} = 0 \tag{5.5.33}$$

Case 3: $K_{21} < K_{11} < \sigma$

$$\lambda_2 = \frac{1}{K_{21}} \tag{5.5.34}$$

$$\lambda_1 = \frac{1}{\sigma} \tag{5.5.35}$$

$$\omega_{int} = \omega_{11}\left[\frac{K_{11} - \sigma}{K_{21} - \sigma}\right] \tag{5.5.36}$$

Table 5.3 lists the temperatures and concentrations of the process period as a function of x and τ, assuming that the matrix is initially in equilibrium with the regeneration state. The three columns on the right side of the table indicate, for each case, the region in which the temperature or concentration is as specified in the left column. The bottom section of Table 5.3 lists the value of the intermediate concentration for each case.

The wave diagram is a very useful tool for illustrating the operation of the rotary regenerative filter. Figure 5.34(a) shows the wave diagram for the Case 1 conditions, Figure 5.35(a) for the Case 2 conditions, and Figure 5.36(a) for the Case 3 conditions. The x-axis represents the axial position, so that the left side of the diagram is the inlet and the right side is the outlet. The process air blows from left to right. The y-axis represents the time (for a rotating observer) or the rotation angle (for a stationary observer). The bottom edge of the wave diagram represents the initial conditions, and the top edge is the conditions at the end of the period, i.e., the state of the matrix at the last instant before it rotates into the other section of the wheel.

The lines indicating the waves represent jumps in the concentration and temperature. If you were to cut out the wave diagram and place it on the circumferential

Table 5.3
Process period solution for a fully regenerated matrix.

	Case 1P $\sigma < K_{21} < K_{11}$	Case 2P $K_{21} < \sigma < K_{11}$	Case 3P $K_{21} < K_{11} < \sigma$
Temperatures:			
$T = T_{21}$	$\frac{\tau}{x} < \sigma$	$\frac{\tau}{x} < \sigma$	$\frac{\tau}{x} < \sigma$
$T = T_{11}$	$\sigma < \frac{\tau}{x}$	$\sigma < \frac{\tau}{x}$	$\sigma < \frac{\tau}{x}$
Concentrations:			
$\omega = \omega_{21}$	$\frac{\tau}{x} < \sigma$	$\frac{\tau}{x} < K_{21}$	$\frac{\tau}{x} < K_{21}$
$\omega = \omega_{int}$	$\sigma < \frac{\tau}{x} < K_{11}$	$K_{21} < \frac{\tau}{x} < K_{11}$	$K_{21} < \frac{\tau}{x} < \sigma$
$\omega = \omega_{11}$	$\frac{\tau}{x} > K_{11}$	$\frac{\tau}{x} > K_{11}$	$\frac{\tau}{x} > \sigma$
Intermediate Concentration:			
ω_{int}	$\omega_{21}\left[\frac{K_{21}-\sigma}{K_{11}-\sigma}\right]$	0	$\omega_{11}\left[\frac{K_{11}-\sigma}{K_{21}-\sigma}\right]$

surface of the process portion of the wheel, it would be a map of the regions of different concentration and temperature. The outlet concentration and temperature profiles can be obtained from the right edge of the wave diagram (x=1).

As an example, consider the Case 1 conditions of Figure 5.34(a). For someone rotating on the wheel at x=1, during the initial portion of the process period the outlet concentration would be equal to that in the bottom portion of the right edge of the wave

diagram, ω_{21}. At rotation time $\tau = \sigma$, the outlet concentration would change to ω_{int}, and at time $\tau = K_{11}$, the concentration would change to the process inlet concentration, ω_{11}. Figure 5.34(b) shows the concentration and temperature outlet profiles as a function of time, where the "time" is the rotation time within a period, so that Figure 5.34(b) is also represents the angular variation of the concentration and temperature at the wheel outlet.

The slope of the waves as drawn on the wave diagram is equal to one over the wavespeed. Therefore, faster waves have lower slopes on the wave diagram. For a wave originating from $x = 0$, $\tau = 0$, the time at which the wave breaks through, i.e., reaches the end of the wheel (x=1), is also equal to the inverse of the wavespeed. Thus the thermal wave of Figure 5.34(a) breaks through at time $\tau = \sigma$ and the concentration wave breaks through at time $\tau = K_{11}$.

It is interesting to examine the integral curves once again, particularly for the Case 2 scenario. Case 2 means that the regeneration temperature is above the parabolic temperature (the temperature at which $K = \sigma$) and the process temperature is below T_{par}. The portion of Figure 5.20 between 100°C and 200°C has been reproduced in Figure 5.37. A process state of (5 ppm, 140°C) and a regeneration state of (5 ppm, 180°C) have been marked on the graph. The 1-curve through the process state and the 2-curve through the regeneration state do not intersect at any point, and thus there is not a single intermediate state. The path between the process and regeneration states is as follows: move along the 1-curve through the process state to where the 1-curve intersects the x-axis. This is the second intermediate state (0 ppm, 140°C). Then move along the x-axis to the point where the 2-curve throught the regeneration state intersects the x-axis. This is the first intermediate state (0 ppm, 180°C). A 2-curve connects this point to the regeneration state.

For the regeneration period analysis, in which the process state is the initial state and the regeneration state is the inlet state, the intermediate state should be at the intersection of the 1-curve through the regeneration state and the 2-curve through the process state. It can be seen in Figure 5.37 that these two curves will never intersect, and unlike the process period analysis, there is no axis for the curves to end on. The intermediate concentration in this case is infinity, as shown in Section 5.5.2.

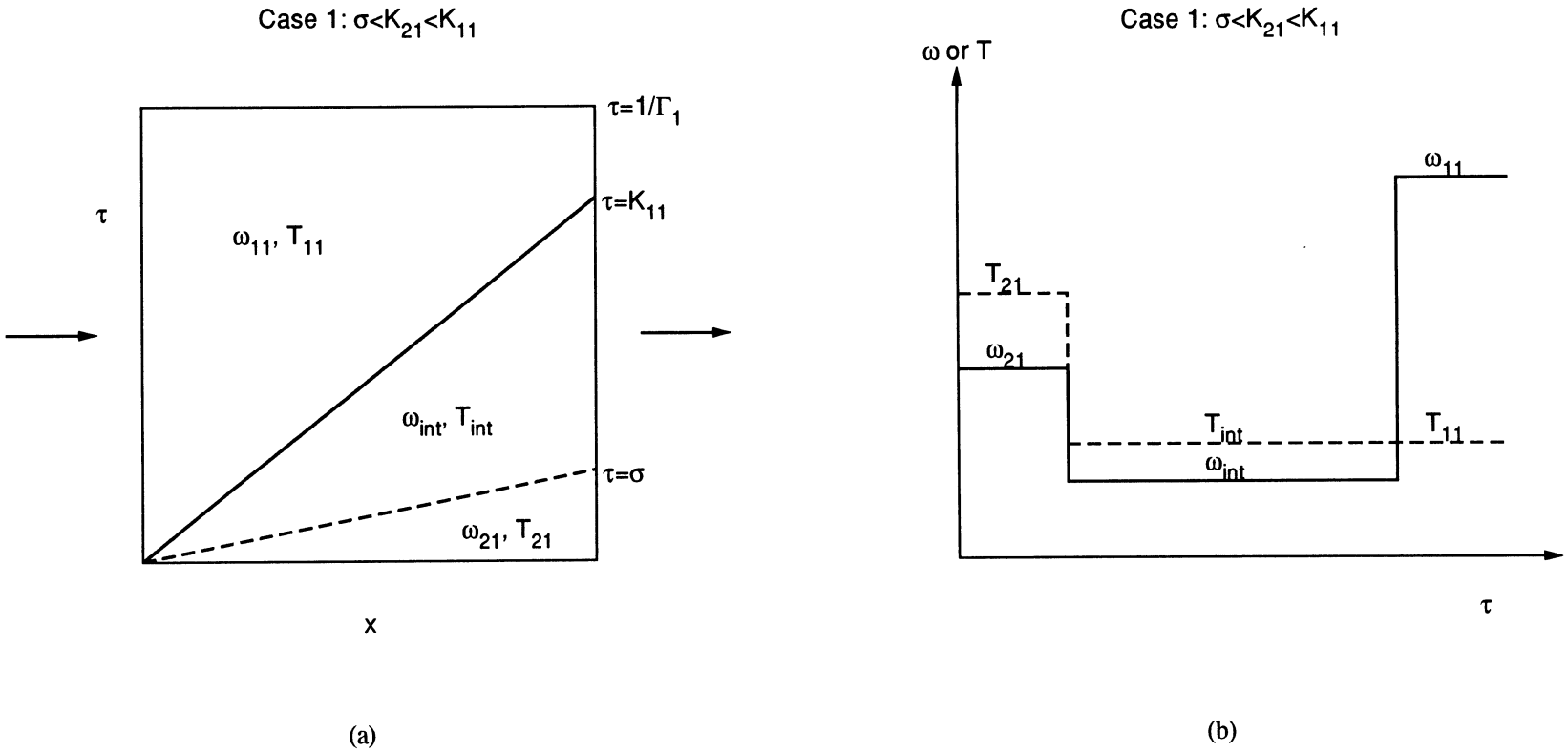

Figure 5.34 Wave diagram (a) and outlet concentration and temperature profiles (b) for a Case 1 process period.

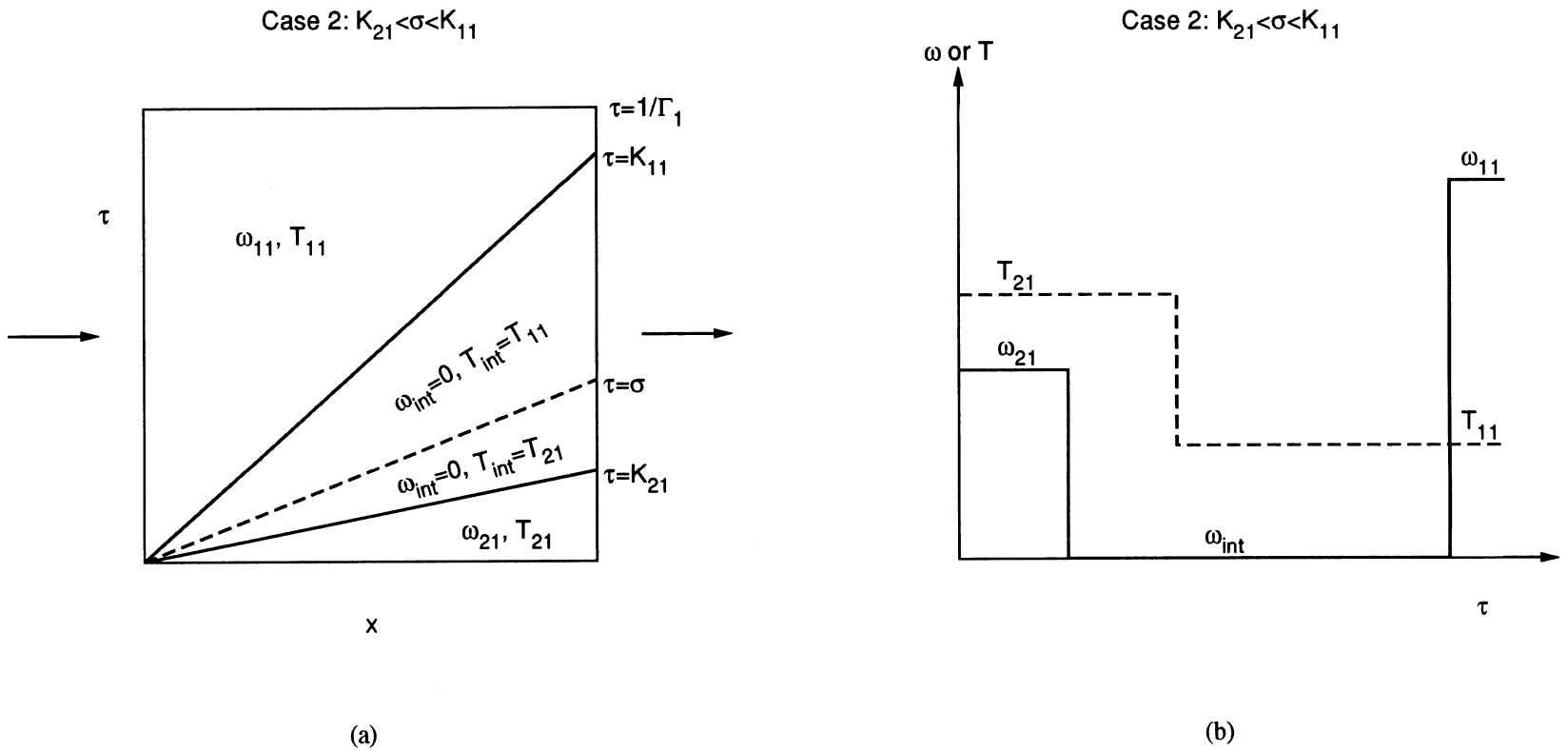

Figure 5.35 Wave diagram (a) and outlet concentration and temperature profiles (b) for a Case 2 process period.

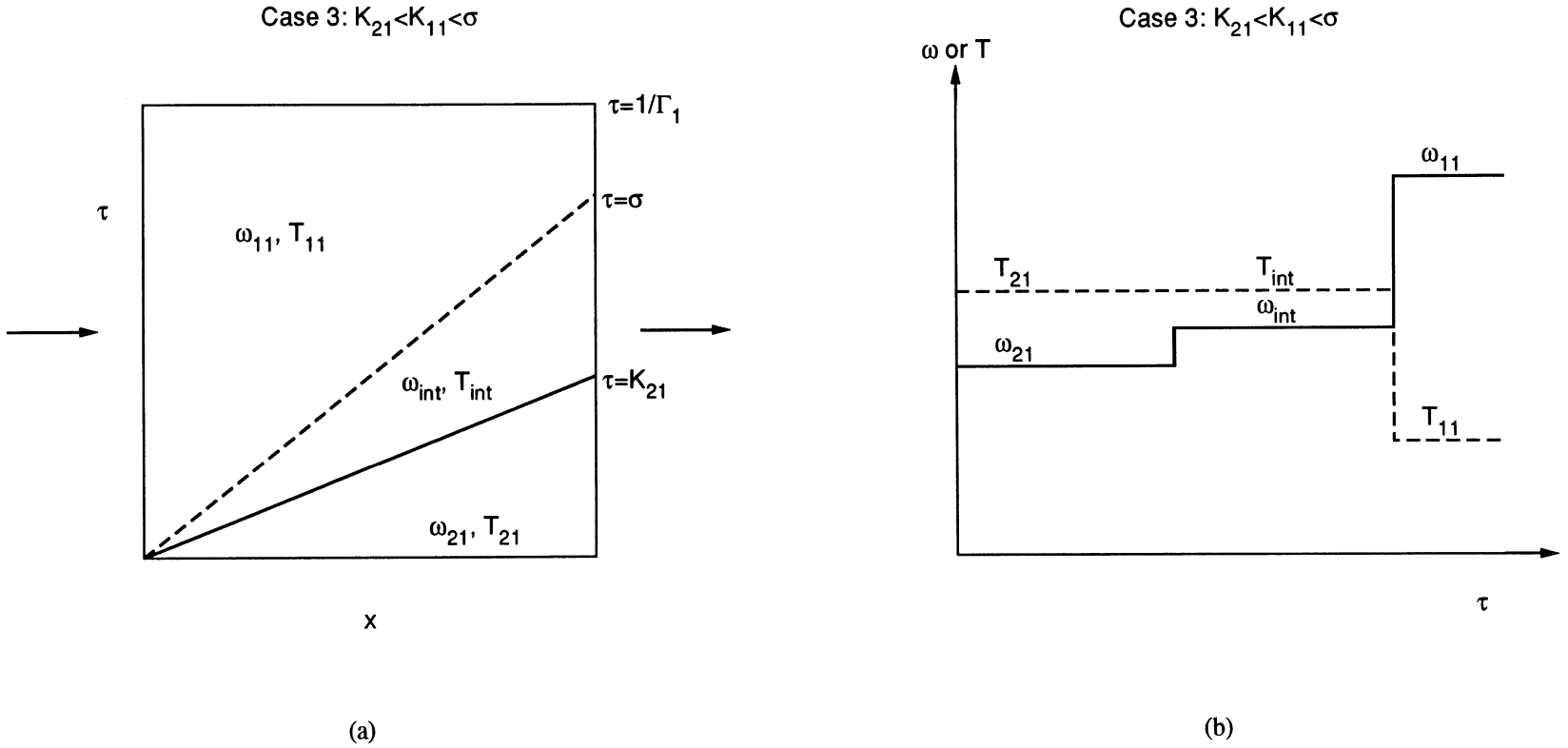

Figure 5.36 Wave diagram (a) and outlet concentration and temperature profiles (b) for a Case 3 process period.

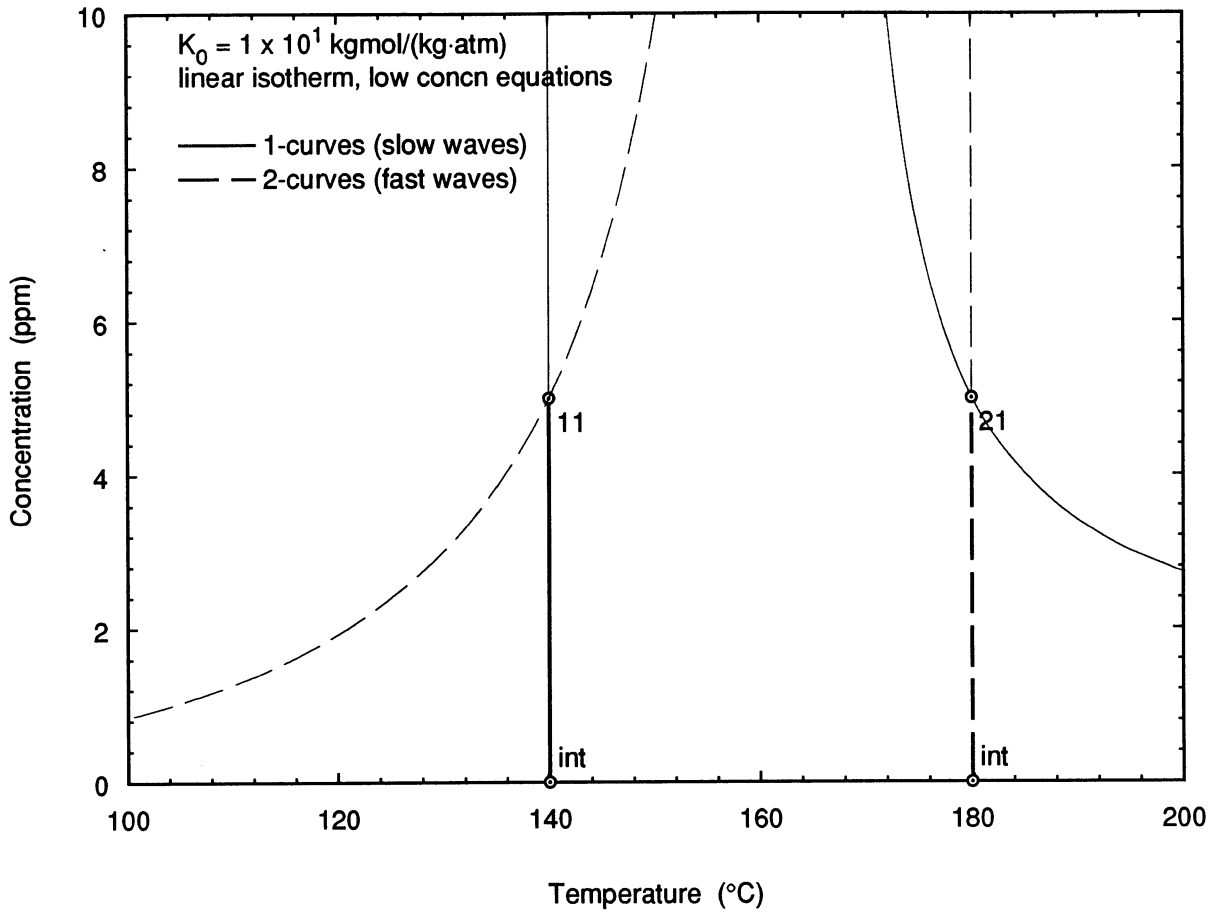

Figure 5.37 Integral curves through process and regeneration states in which $T_{11} < T_{par} < T_{21}$.

5.5.2 Regeneration period (completely processed matrix)

For the regeneration period in which the matrix is initially in equilibrium with the process state, $T_R = T_{11}$ and $T_L = T_{21}$. The regeneration temperature is assumed to be higher than the process temperature, so that $K_L < K_R$, where $K_R = K_{11}$ and $K_L = K_{21}$. Depending on the values of K_0 and σ, there are, as for the process period, three different wave combinations which may result: the first, second, and fourth columns of Table 5.2. These three cases, which will also be referred to as Case 1, Case 2, and Case 3, are as follows:

Case 1: $\sigma < K_{21} < K_{11}$

$$\lambda_2 = \frac{1}{\sigma} \tag{5.5.37}$$

$$\lambda_1 = \frac{1}{K_{21}} \tag{5.5.38}$$

$$\omega_{int} = \omega_{11}\left[\frac{K_{11} - \sigma}{K_{21} - \sigma}\right] \tag{5.5.39}$$

Case 2: $K_{21} < \sigma < K_{11}$

$$\lambda_2 = \lambda_1 = \frac{1}{\sigma} \tag{5.5.40}$$

$$\omega_{int} = \infty \tag{5.5.41}$$

Case 3: $K_{21} < K_{11} < \sigma$

$$\lambda_2 = \frac{1}{K_{11}} \tag{5.5.42}$$

$$\lambda_1 = \frac{1}{\sigma} \tag{5.5.43}$$

$$\omega_{int} = \omega_{21}\left[\frac{K_{21} - \sigma}{K_{11} - \sigma}\right] \tag{5.5.44}$$

Table 5.4 lists the temperatures and concentrations of the regeneration period in the same format as Table 5.3 for the process period. Throughout this thesis, the wave diagrams for the regeneration period will be drawn backwards, i.e., the inlet will be on the right side and the outlet on the left side. The purpose is twofold. First, a wave diagram can be immediately identified as process or regeneration by looking at the direction of the wave propagation, and second, this convention is convenient when considering the operation of the process and regeneration periods together (Section 5.6). Figures 5.38 through 5.40 illustrate the wave diagrams and outlet profiles for the three cases.

Table 5.4
Regeneration period solution for a fully processed matrix.

	Case 1R $\sigma < K_{21} < K_{11}$	Case 2R $K_{21} < \sigma < K_{11}$	Case 3R $K_{21} < K_{11} < \sigma$
Temperatures:			
$T = T_{11}$	$\frac{\tau}{x} < \sigma$	$\frac{\tau}{x} < \sigma$	$\frac{\tau}{x} < \sigma$
$T = T_{21}$	$\sigma < \frac{\tau}{x}$	$\sigma < \frac{\tau}{x}$	$\sigma < \frac{\tau}{x}$
Concentrations:			
$\omega = \omega_{11}$	$\frac{\tau}{x} < \sigma$	$\frac{\tau}{x} < \sigma$	$\frac{\tau}{x} < K_{11}$
$\omega = \omega_{int}$	$\sigma < \frac{\tau}{x} < K_{21}$	$\frac{\tau}{x} = \sigma$	$K_{11} < \frac{\tau}{x} < \sigma$
$\omega = \omega_{21}$	$\frac{\tau}{x} > K_{21}$	$\frac{\tau}{x} > \sigma$	$\frac{\tau}{x} > \sigma$
Intermediate Concentration:			
ω_{int}	$\omega_{11}\left[\frac{K_{11}-\sigma}{K_{21}-\sigma}\right]$	∞	$\omega_{21}\left[\frac{K_{21}-\sigma}{K_{11}-\sigma}\right]$

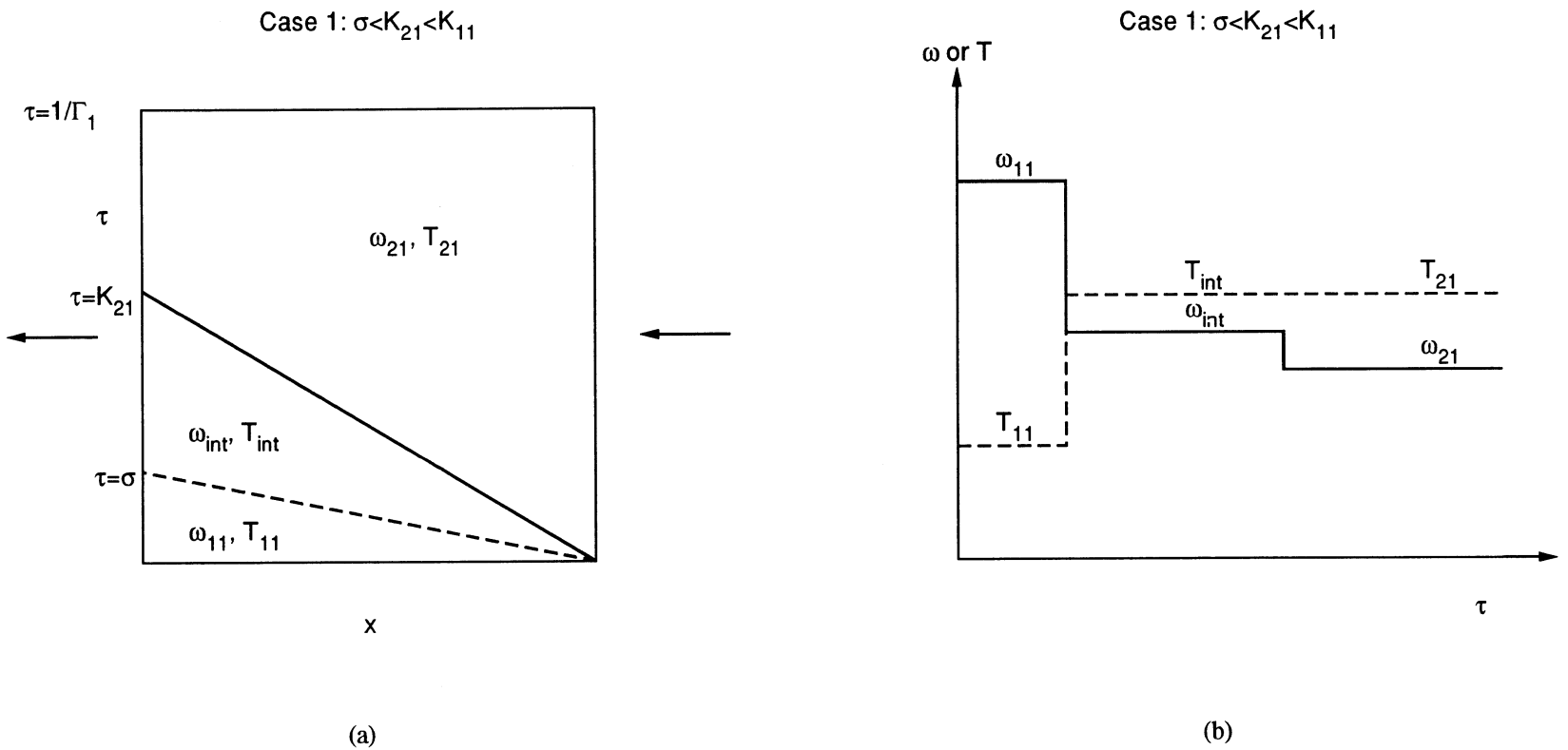

Figure 5.38 Wave diagram (a) and outlet concentration and temperature profiles (b) for a Case 1 regeneration period.

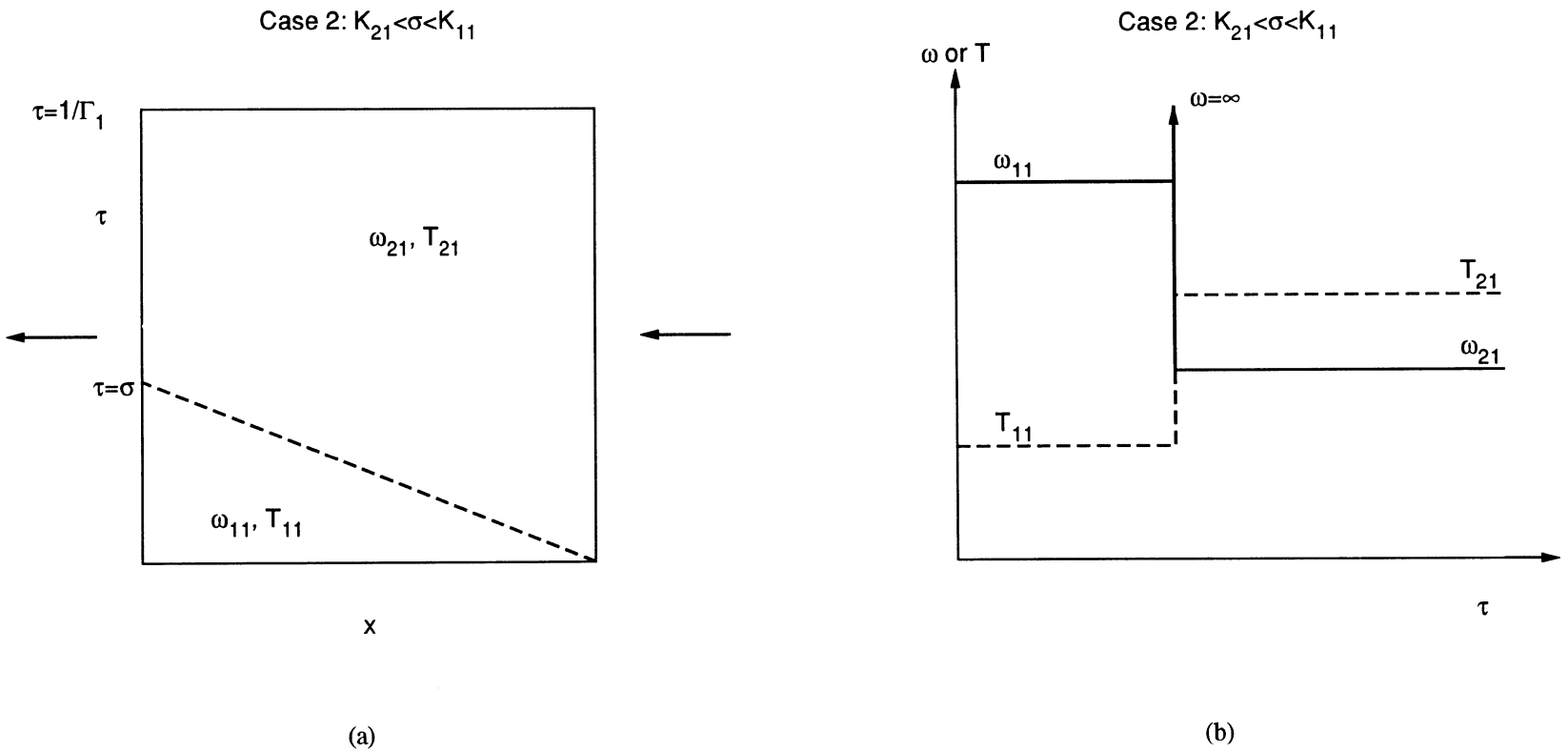

Figure 5.39 Wave diagram (a) and outlet concentration and temperature profiles (b) for a Case 2 regeneration period.

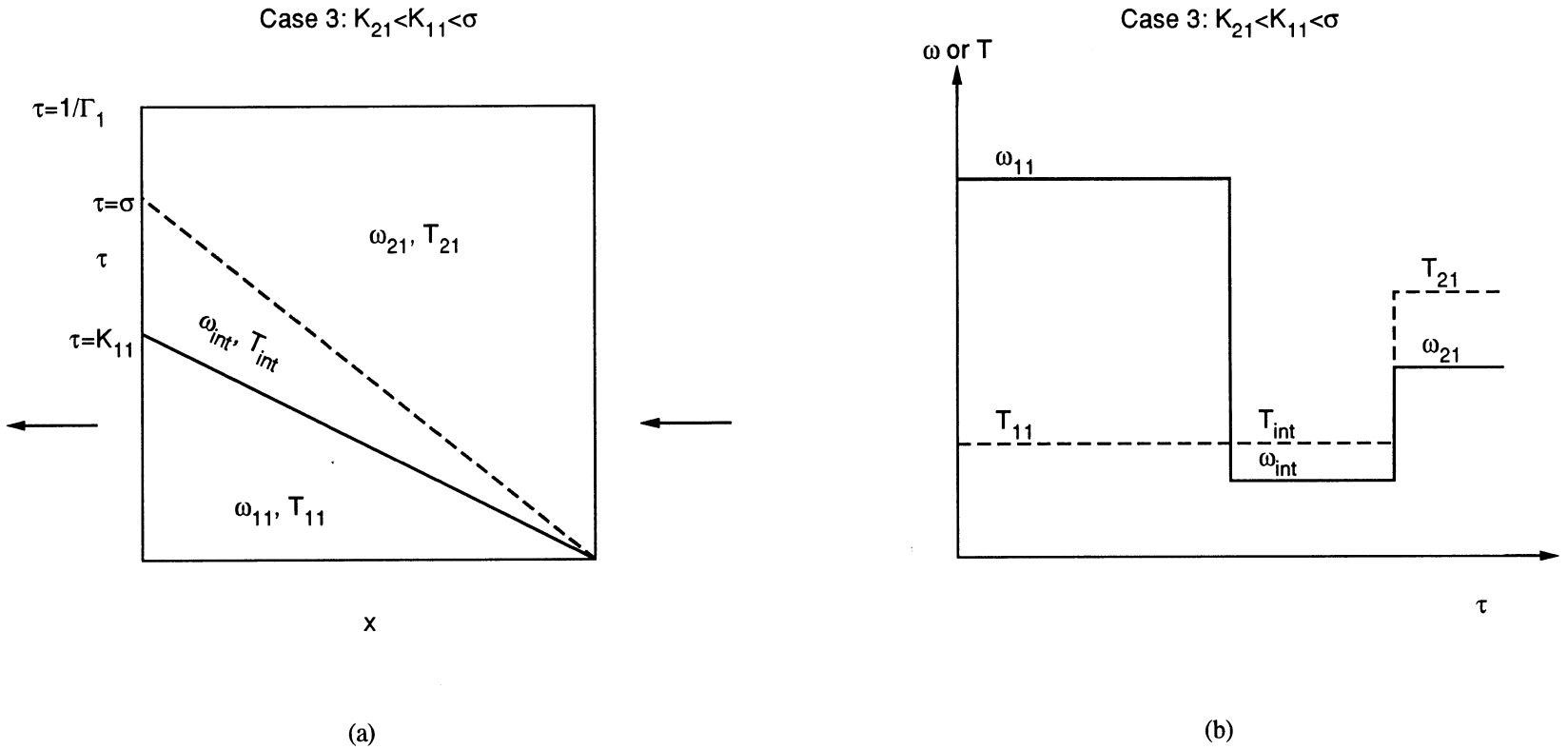

Figure 5.40 Wave diagram (a) and outlet concentration and temperature profiles (b) for a Case 3 regeneration period.

5.6 Steady-state filter operation

The process period and regeneration period solutions presented in Tables 5.3 and 5.4 are for a single period in which the matrix is uniform at the start of the period. To obtain the steady-state process and regeneration period wave positions, an iterative process is used. Several "rules" for wave propagation were established in Section 5.5. Thermal waves always propagate at a constant velocity of $1/\sigma$. Within a region of constant temperature, concentration waves propagate at the speed $1/K(T)$. To find the steady-state wave positions, given an initial matrix state for the process period, the positions of the concentration and thermal waves at the end of the process period are computed and then used as the starting wave positions for the regeneration period. The positions of the waves at the end of the regeneration period are then used in the next iteration as the positions of the waves at the start of the process period. This process is continued until the wave positions in both periods do not change.

A computer program was written to calculate the steady-state wave positions using the wave propagation rules described above. The matrix is assumed to be initially uniform at the regeneration inlet state. The program, EQSOL2.C, is listed in Appendix A.

Figures 5.41 through 5.43 are all examples of the wave diagrams from the iteration process. Concentration waves are indicated by solid lines and thermal waves are shown as dashed lines. The wave positions in each period were calculated with the program EQSOL2.C. Every other iteration has been shaded for clarity. Within an iteration, the

wave diagram for the regeneration period is on top of the wave diagram for the process period. The wave diagrams have been drawn such that the waves propagate to the right in the process period and to the left in the regeneration period.

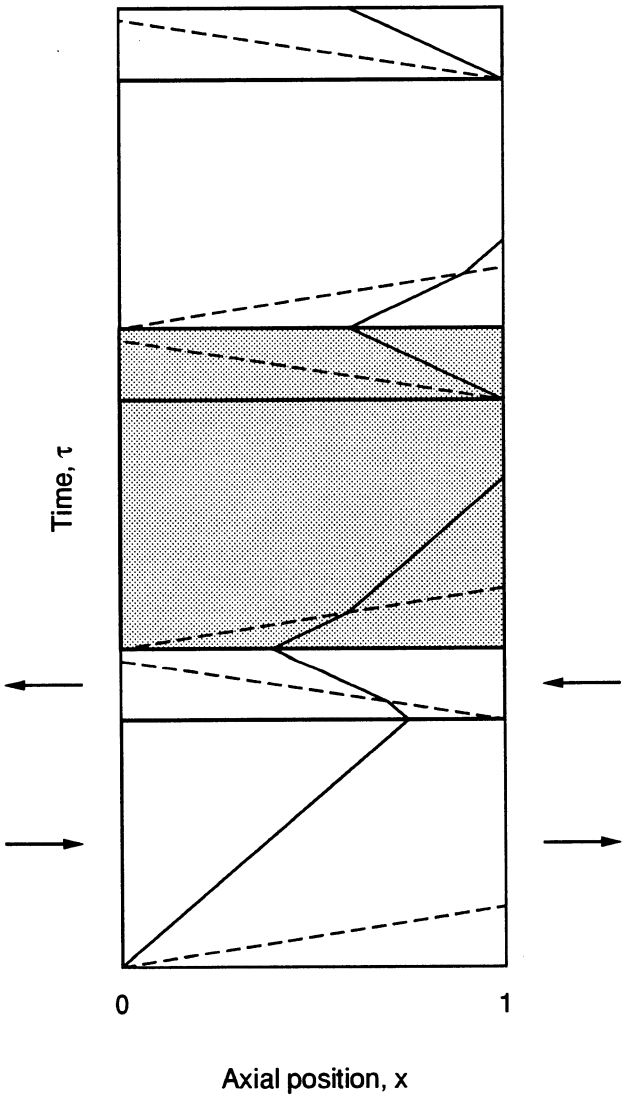

Figure 5.41 An example of the iteration process required to obtain the steady-state solution. This is an example in which the thermal wave (dashed line) is faster than the concentration waves (solid lines), i.e., $\sigma < K_{21} < K_{11}$ (Case 1).

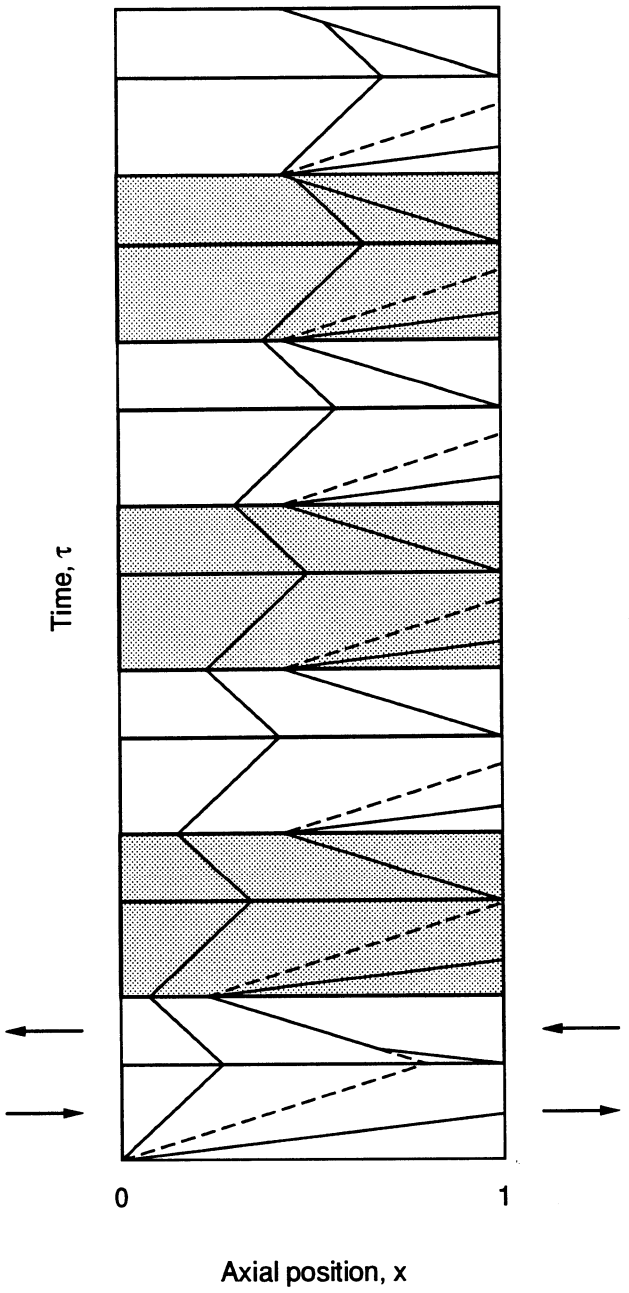

Figure 5.42 An example of the iteration process required to obtain the steady-state solution. This is an example in which the thermal wavespeed (dashed line) is between the concentration wavespeeds (solid lines), i.e., $K_{21} < \sigma < K_{11}$ (Case 2).

Complete regeneration occurs when all of the waves in the regeneration period break through (i.e., reach the end of the matrix) before the end of the regeneration period.

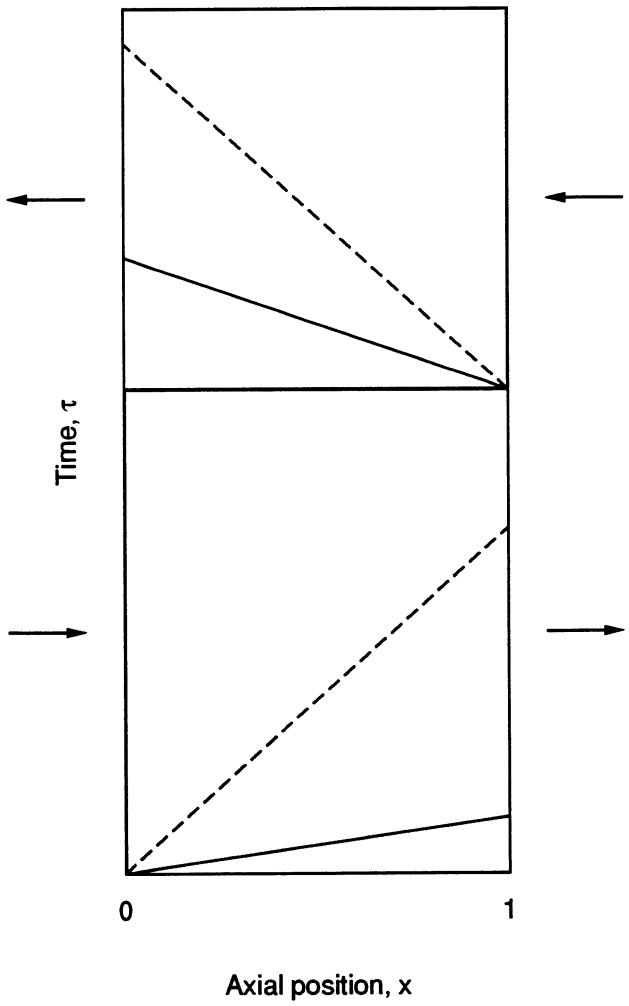

Figure 5.43 An example of the iteration process required to obtain the steady-state solution. This is an example in which the thermal wave (dashed line) is slower than the concentration waves (solid lines), i.e., $K_{21} < K_{11} < \sigma$ (Case 3).

In this case, the entire matrix is in equilibrium with the regeneration inlet conditions at the end of the regeneration period. The minimum regeneration period duration required for complete regeneration is equal to the time at which the last wave breaks through. This period duration is a function of the process period duration, the process and regeneration temperatures, σ, and K_0. Similar definitions apply for the process period.

Using wave diagrams, expressions for the minimum regeneration period duration required for complete regeneration, $1/\Gamma_{1R}$, can be derived. The results are as follows:

Case 1: $\sigma \le K_{21} \le K_{11}$

$$\frac{1}{\Gamma_{2R}} = \begin{cases} \dfrac{1}{\Gamma_1} & , \quad \dfrac{1}{\Gamma_1} \le \sigma \\ \dfrac{\frac{1}{\Gamma_1}(K_{21}-\sigma)+\sigma(K_{11}-K_{21})}{K_{11}-\sigma} & , \quad \sigma \le \dfrac{1}{\Gamma_1} \le K_{11} \\ K_{21} & , \quad \dfrac{1}{\Gamma_1} \ge K_{11} \end{cases} \tag{5.6.1}$$

Case 2: $K_{21} \le \sigma \le K_{11}$

$$\frac{1}{\Gamma_{2R}} = \begin{cases} \dfrac{1}{\Gamma_1} & , \quad \dfrac{1}{\Gamma_1} \le \sigma \\ \sigma & , \quad \dfrac{1}{\Gamma_1} \ge \sigma \end{cases} \tag{5.6.2}$$

Case 3: $K_{21} < K_{11} < \sigma$

$$\frac{1}{\Gamma_{2R}} = \begin{cases} \dfrac{1}{\Gamma_1} & , \quad \dfrac{1}{\Gamma_1} \le \sigma \\ \sigma & , \quad \dfrac{1}{\Gamma_1} \ge \sigma \end{cases} \tag{5.6.3}$$

Similarly, expressions for the minimum process period duration required for complete processing, $1/\Gamma_{1P}$, can be derived and are as follows:

Case 1: $\sigma \le K_{21} \le K_{11}$

$$\frac{1}{\Gamma_{1P}} = \begin{cases} \dfrac{1}{\Gamma_2} & , \quad \dfrac{1}{\Gamma_2} \le \sigma \\ \dfrac{\frac{1}{\Gamma_2}(K_{11}-\sigma)+\sigma(K_{21}-K_{11})}{K_{21}-\sigma} & , \quad \sigma \le \dfrac{1}{\Gamma_2} \le K_{21} \\ K_{11} & , \quad \dfrac{1}{\Gamma_2} \ge K_{21} \end{cases} \tag{5.6.4}$$

Case 2: $K_{21} \le \sigma \le K_{11}$

$$\frac{1}{\Gamma_{1P}} = \begin{cases} \dfrac{K_{11}}{\sigma}\dfrac{1}{\Gamma_2} & , \quad \dfrac{1}{\Gamma_2} \le \sigma \\ K_{11} & , \quad \dfrac{1}{\Gamma_2} \ge \sigma \end{cases} \tag{5.6.5}$$

Case 3: $K_{21} < K_{11} < \sigma$

$$\frac{1}{\Gamma_{1P}} = \begin{cases} \dfrac{1}{\Gamma_2} & , \quad \dfrac{1}{\Gamma_2} \le \sigma \\ \sigma & , \quad \dfrac{1}{\Gamma_2} \ge \sigma \end{cases} \tag{5.6.6}$$

Solving the second part of Equation 5.6.4 for $1/\Gamma_2$ as a function of $1/\Gamma_{1P}$ reveals that the line described by the second part of Equation 5.6.4 is identical to the line of complete regeneration described by the second part of Equation 5.6.1.

Equations 5.6.1-5.6.6 are plotted in Figures 5.44 to 5.46. Any $1/\Gamma_1$, $1/\Gamma_2$ pair which are above the complete regeneration line indicate operation in the region of complete regeneration. Any $1/\Gamma_1$, $1/\Gamma_2$ pair which are to the right of the complete processing line indicate operation in the region of complete processing. For Case 1 and Case 3, it can be

seen from Figure 5.44 and 5.46 that for all values of $1/\Gamma_1$ and $1/\Gamma_2$, the steady-state operation involves either complete regeneration, complete processing, or both. For Case 2 (Figure 5.45), there is a region in which steady-state operation of the wheel can be achieved without either complete regeneration or complete processing.

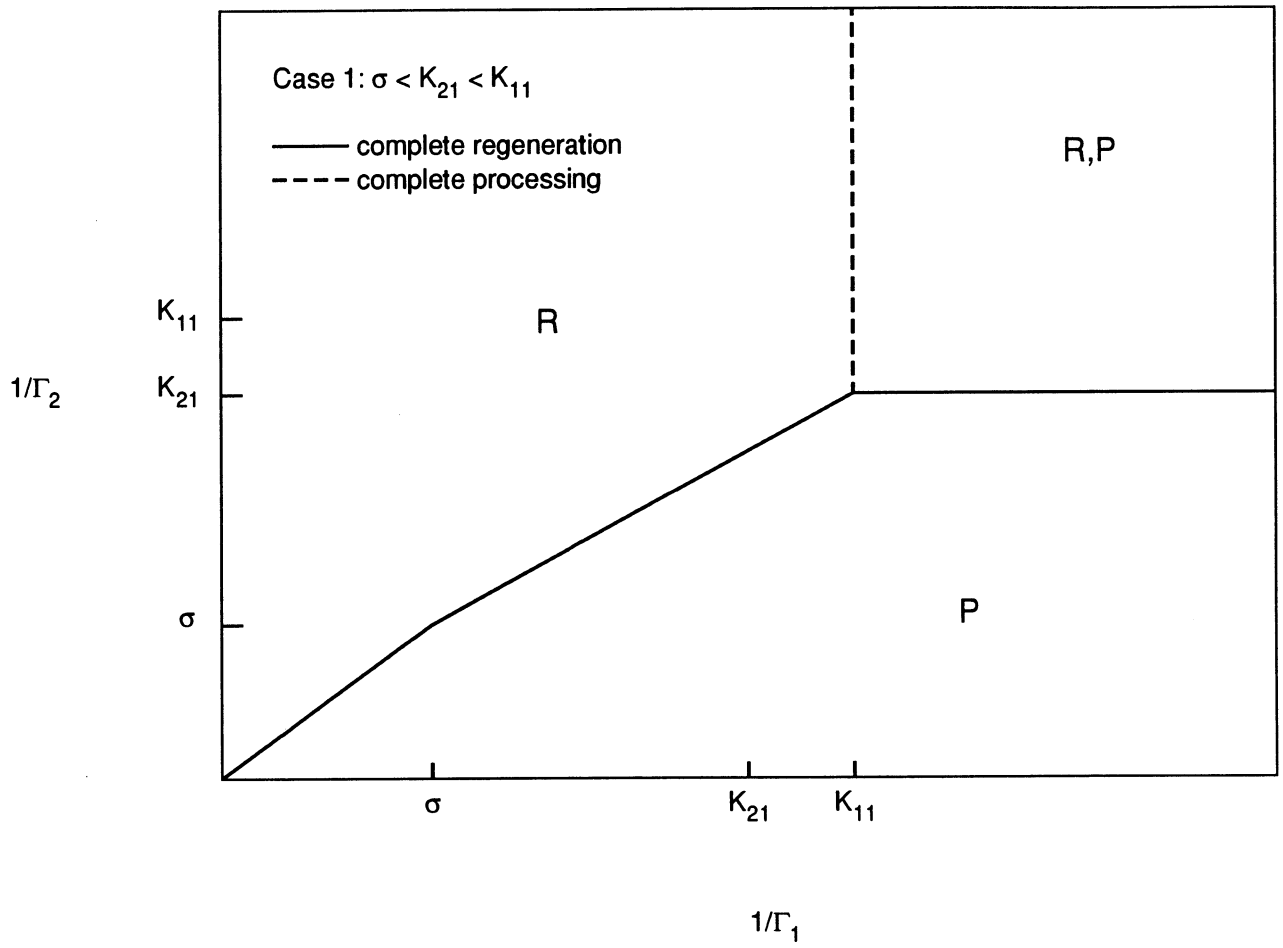

Figure 5.44 Diagram showing regions of complete processing and complete regeneration (indicated by P and R, respectively) for Case 1 conditions, i.e., $\sigma \leq K_{21} \leq K_{11}$.

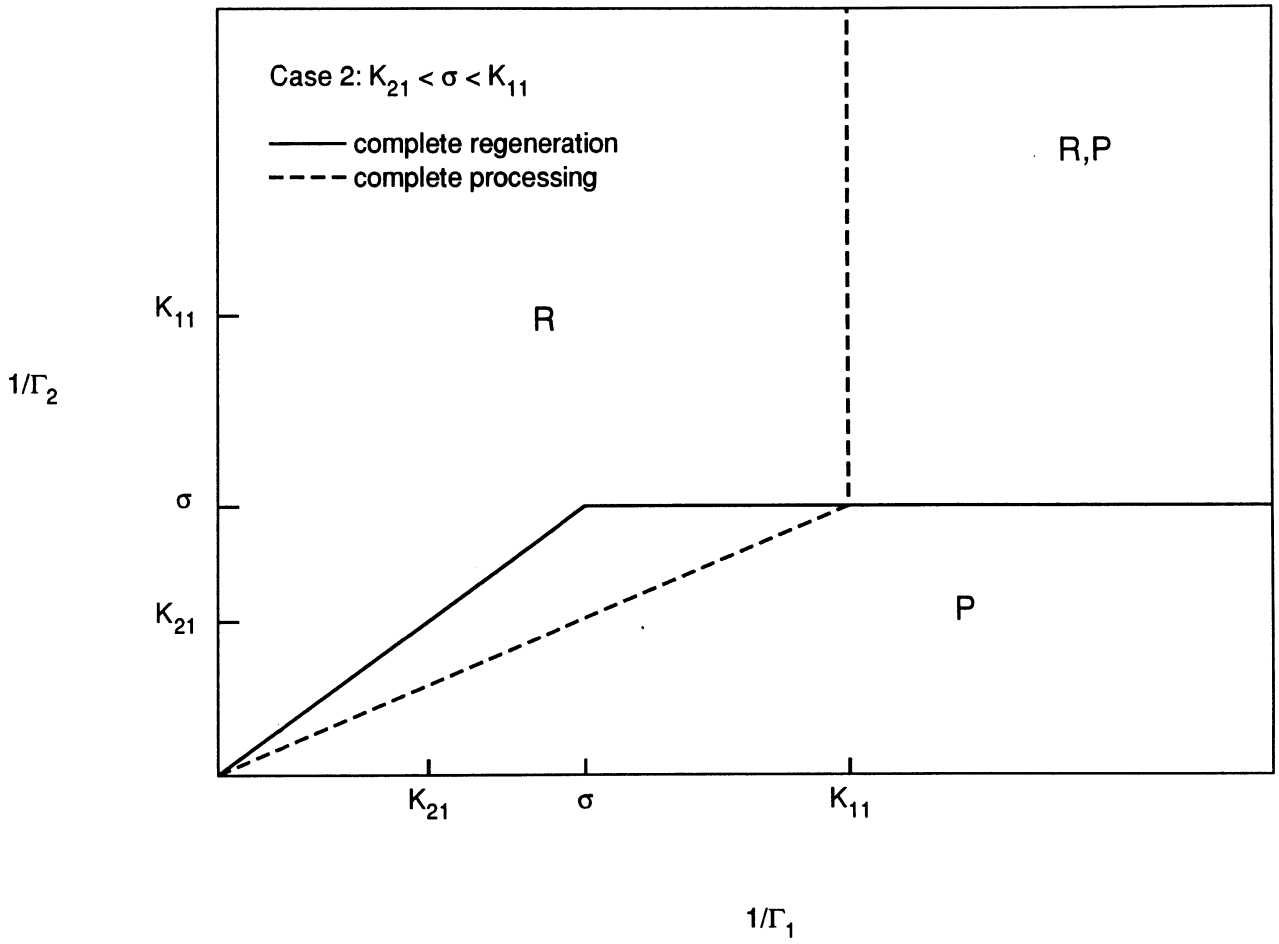

Figure 5.45 Diagram showing regions of complete processing and complete regeneration (indicated by P and R, respectively) for Case 2 conditions, i.e., $K_{21} \leq \sigma \leq K_{11}$.

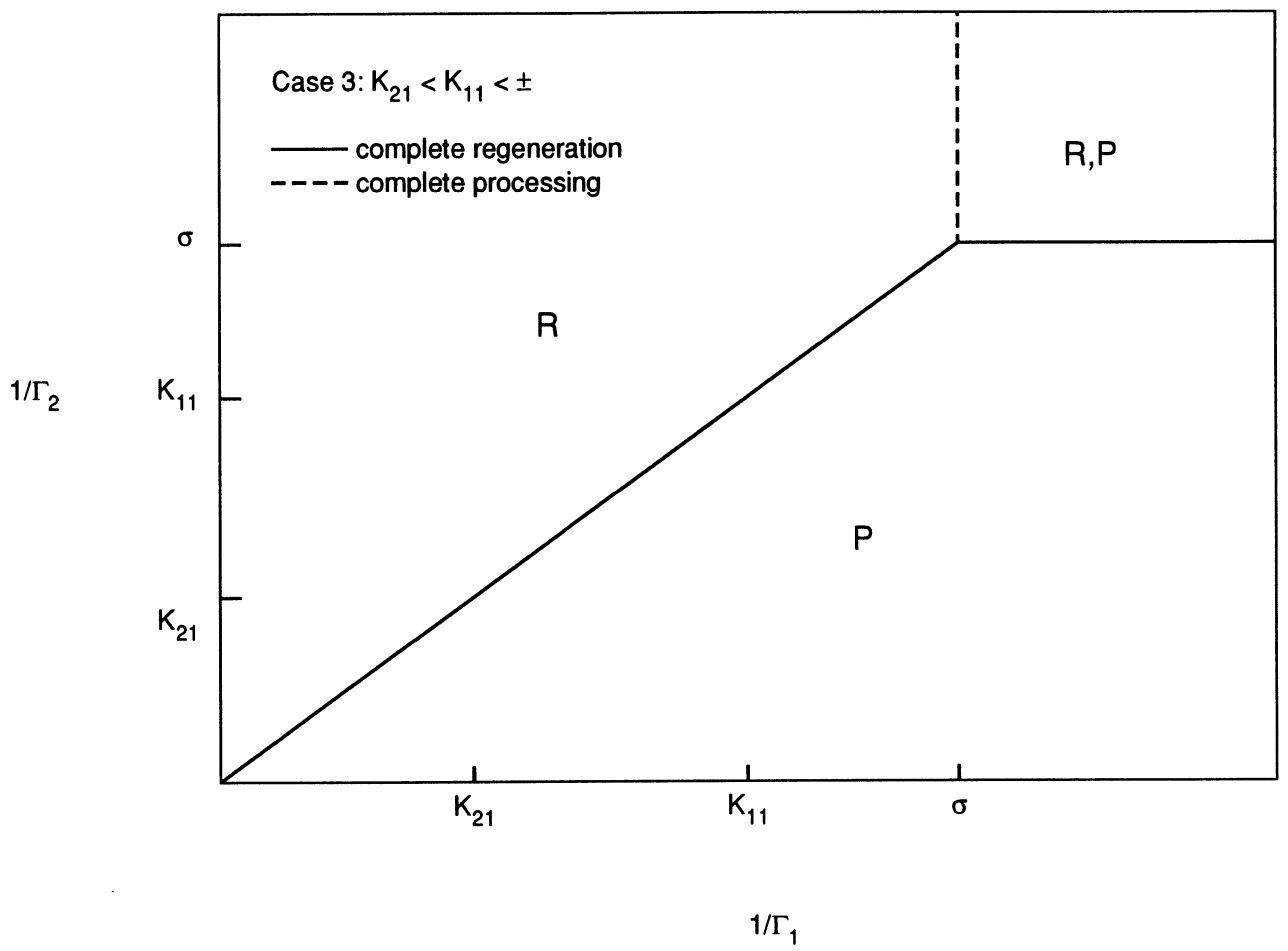

Figure 5.46 Diagram showing regions of complete processing and complete regeneration (indicated by P and R, respectively) for Case 3 conditions, i.e., $K_{21} \leq K_{11} \geq \sigma$.

5.7 Model reviews

Most of the modeling work listed in Tables 4.4 and 4.5 is limited to regions where the equations are strictly hyperbolic. For example, past desiccant analyses, e.g., [1, 128-130, 159] were always limited to the range where all temperatures were less than T_{par} and thus the equations were strictly hyperbolic. This made the analysis of the desiccant systems more straightforward. Several sets of authors, however, have considered solutions which encompass non-strictly hyperbolic regions, although they do not define them as such.

First, some general notes. In the engineering literature, the convention that $\lambda_2 > \lambda_1$ is generally not followed, and instead the fast wave is the 1-wave and the slow wave is the 2-wave. The modeling work discussed below was all based on the analysis of fixed-bed adsorption systems, which as pointed out in Section 4.6, is analogous to the rotary regenerative adsorber operating at steady-state. The terms process and regeneration are used in the following discussion, although these are not the terms used by the authors in the papers; terms such as purge, feed, elution, saturation, etc. are used in the papers.

A group of authors which includes Pan, Basmadjian, Ha, and Proulx has published papers [174, 175, 177, 178, 204] in which the full version of the adiabatic adsorption equilibrium equations are solved. The technique is essentially the same as presented in this work, in that expressions for the slopes of the integral curves are derived and integrated to obtain the integral curves. The qualitative behavior for different types of isotherms over a wide range of conditions was considered in [178], and a table listing the

types of waves which result for favorable (Langmuir-type) isotherms is presented in [174]. For a Langmuir isotherm under conditions where the intermediate concentration is less than both the process and regeneration concentrations, the front wave will be a rarefaction wave and the rear wave can be either a rarefaction or a shock wave [174]. This agrees with the results presented earlier in this chapter.

Although they do not consider the concepts of linear degeneracy and strict hyperbolicity, they do examine the solution in the non-strictly hyperbolic region and they do consider waves which are not genuinely nonlinear. Two types of pure thermal waves are described [178], along with approximate conditions for predicting the occurrence of the pure thermal waves.

The first type of pure thermal wave occurs, under certain conditions, when either the initial or inlet concentration is equal to zero. In terms of the low concentration linear isotherm analysis presented in Section 5.5, this type of pure thermal wave corresponds to the either the leading thermal wave which would result when the the bed was initially at zero concentration and the contaminant was Case 1 (both concentration waves slower than the thermal wave) or the trailing thermal wave which would result when the inlet concentration was equal to zero and the contaminant was Case 3 (both concentration waves faster than the thermal wave). In fact, the approximate conditions set forth in [PB3] for the occurrence of this type of thermal wave are identical to those just stated, except that since the general isotherm form is nonlinear, the isotherm slope at zero concentration is used.

The second type of pure thermal wave, which appears as a footnote in [178] and as part of the analysis in [174], corresponds to the process period Case 2 thermal wave, i.e., a thermal wave surrounded by states of zero concentration in between two concentration

waves. The conditions for the occurrence of this type of wave are identical to the Case 2 conditions, i.e., $K_{21} < \sigma < K_{11}$, except that the isotherm slope at zero concentration is used in place of the linear isotherm slope. This behavior is all inferred from the integral curves, and there is no formal discussion of the fact that the equations are not strictly hyperbolic.

The Case 2 regeneration period result presented in Section 5.5 does not occur for the full equations. The infinite concentration is an artifact of the low concentration assumption. For the full equations the integral curves intersect at higher concentrations.

Experimental concentration and temperature profiles for CO_2 on 5A molecular sieves [175, 178], CO_2 on carbon [175], and C_2H_6 on carbon [175] show excellent qualitative agreement with the predictions of the equilibrium theory, although as expected, the presence of finite heat and mass transfer coefficients cause the wave fronts to spread out more than predicted by the equilibrium theory. Conditions in which a pure thermal wave of the first type was supposed to occur were tested, and the pure thermal wave did indeed appear, although not as a discontinuity (there was significant spreading of the wave due to the finite transfer coefficients) [175].

Another group of authors which includes Rhee, Aris, Amundson, and Heerdt have published a series of papers [176, 181-184] in which a variation of the full equations was solved with a Langmuir isotherm. Specific examples were presented to indicate the different types of behavior which would result in different regions of the solution space, and the occurrence of pure thermal waves was also noted [183]. Adsorption of two components was also studied [184], where the intereference effects were accounted for by the multicomponent form of the Langmuir isotherm.

A series of papers describing the equilibrium modeling of parametric pumps [235-239] was discovered after the development of the low concentration linear isotherm solution presented in Chapter 5. The assumptions used in the parametric pump models are virtually identical, including the low concentration assumption. The solution of the equations presented in Section 5.5 agrees with the results developed in [235], including the Case 2 solutions. Parametric pumps are used for separating mixtures, and consist of a fixed-bed through which the mixture flows in alternate directions during periods of different temperature. Wankạt [240] pointed out that the alternating flow fixed-beds are analagous to the rotary regenerative configuration.

Chapter 6

Equilibrium Design

The design of an adsorption filter will be considered in this chapter by using the low concentration linear isotherm equilibrium model. The solution was outlined in Section 5.5 and 5.6. It is simple enough algebraically that a wide range of conditions and parameters can be considered, giving insight into the potential and limitations of such a filter.

6.1 Intermediate concentration

The value of the intermediate concentration is important in the design of an adsorption filter. A big advantage of the filter is that the intermediate concentration can be lower than the concentration of either inlet air stream, thus providing cleaner air than possible without the filter. In Sections 5.5 and 5.6, expressions for the intermediate concentration were derived. For the process and regeneration periods they are as follows:

Table 6.1 Intermediate concentrations.

	Process side	Regeneration side
Case 1: $\sigma < K_{21} < K_{11}$	$\omega_{int} = \omega_{21}\left[\frac{K_{21}-\sigma}{K_{11}-\sigma}\right]$	$\omega_{int} = \omega_{11}\left[\frac{K_{11}-\sigma}{K_{21}-\sigma}\right]$
Case 2: $K_{21} < \sigma < K_{11}$	$\omega_{int} = 0$	$\omega_{int} = \infty$
Case 3: $K_{21} < K_{11} < \sigma$	$\omega_{int} = \omega_{11}\left[\frac{K_{11}-\sigma}{K_{21}-\sigma}\right]$	$\omega_{int} = \omega_{21}\left[\frac{K_{21}-\sigma}{K_{11}-\sigma}\right]$

The intermediate concentration depends on either the process inlet concentration (ω_{11}) or the regeneration inlet concentration (ω_{21}), but not both. For example, for the process side when the thermal wave is the fastest (Case 1), the intermediate concentration depends on the regeneration inlet concentration and is independent of the process inlet concentration. Thus, for this case, variations in the process inlet concentration do not affect the intermediate concentration.

Figure 6.1 shows the normalized intermediate concentration as a function of K_0 for the process period with $T_{11} = 20°C$ and $T_{21} = 60°C$. Different x-values, i.e., K_0 values, represent different contaminants. The regions corresponding to Case 1, 2, and 3 are indicated on the graph. In the Case 3 region the intermediate concentration has been normalized by the process inlet concentration (ω_{int}/ω_{11}), and in the Case 1 region the intermediate concentration has been normalized by the regeneration inlet concentration, i.e., ω_{int}/ω_{21}. In the Case 2 region, $\omega_{int} = 0$. The border between the Case 3 and Case 2 regions is at the K_0 value such that $K_{11} = \sigma$. For smaller values of K_0, both mass waves will be faster than the thermal wave. The border between the Case 2 and Case 1 regions is at the value of K_0 such that $K_{21} = \sigma$. At larger K_0 values, both mass waves will be slower than the thermal wave.

In the limit as $K_0 \rightarrow 0$ (i.e., no adsorption), the normalized process period intermediate concentration (ω_{int}/ω_{11}) approaches 1. On the other hand, as K_0 increases, the normalized intermediate concentration for the process period (ω_{int}/ω_{21}) approaches a limiting value of $\exp[\Delta h_s/R\,(1/T_{21} - 1/T_{11})]$, plotted in Figure 6.2. The quantity $\exp[\Delta h_s/R\,(1/T_{21} - 1/T_{11})]$ decreases as T_{21} increases and as T_{11} decreases. Larger heats of adsorption also result in lower values of $\exp[\Delta h_s/R\,(1/T_{21} - 1/T_{11})]$.

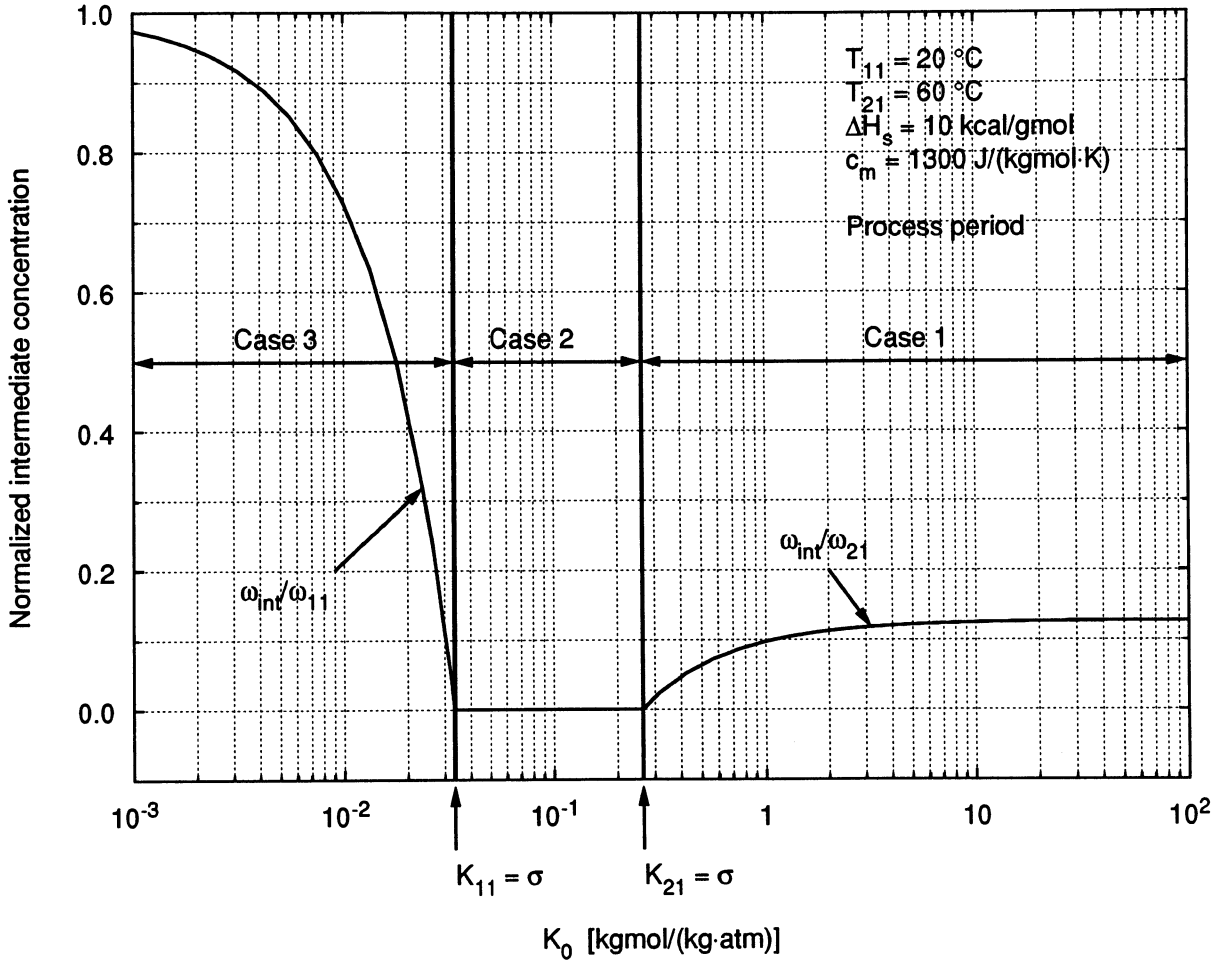

Figure 6.1 Normalized process period intermediate concentration (ω_{int}/ω_{21} or ω_{int}/ω_{11}) as a function of K_0.

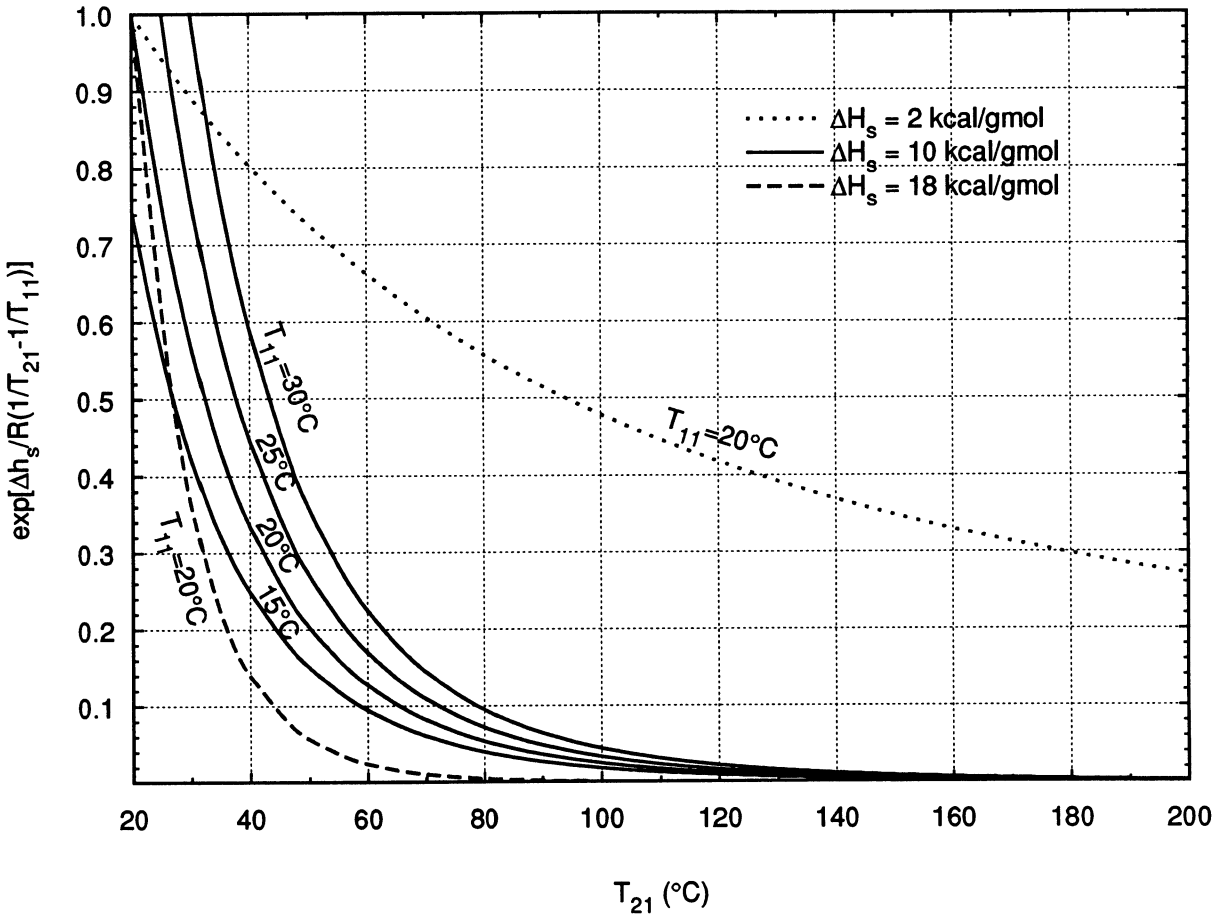

Figure 6.2 Limiting value of ω_{int}/ω_{21} as $K_0 \to \infty$.

Figure 6.1 shows that for contaminants with very low K_0 values, the ability of an adsorption filter to reduce the concentrations is limited because the intermediate concentration will not be much less than the process inlet concentration. Thus even for a continually regenerated filter, the lower K_0 contaminants will not be as effectively removed from the air. For contaminants with K_0 values which place them in the Case 2 region, the potential of the adsorption filter is very promising because the intermediate concentration is zero. For the larger K_0 contaminants, the intermediate concentration (for these particular conditions) is less than or equal to 0.1272 times the regeneration inlet concentration. Even if this were 0.1272 times the process inlet concentration, it would represent a significant reduction in concentration, but because it is relative to the regeneration inlet concentration, which should be less than the process inlet concentration, the reduction is even greater. Figure 6.2 shows the limiting value of the contaminant concentration reduction as $K_0 \rightarrow \infty$ at other conditions.

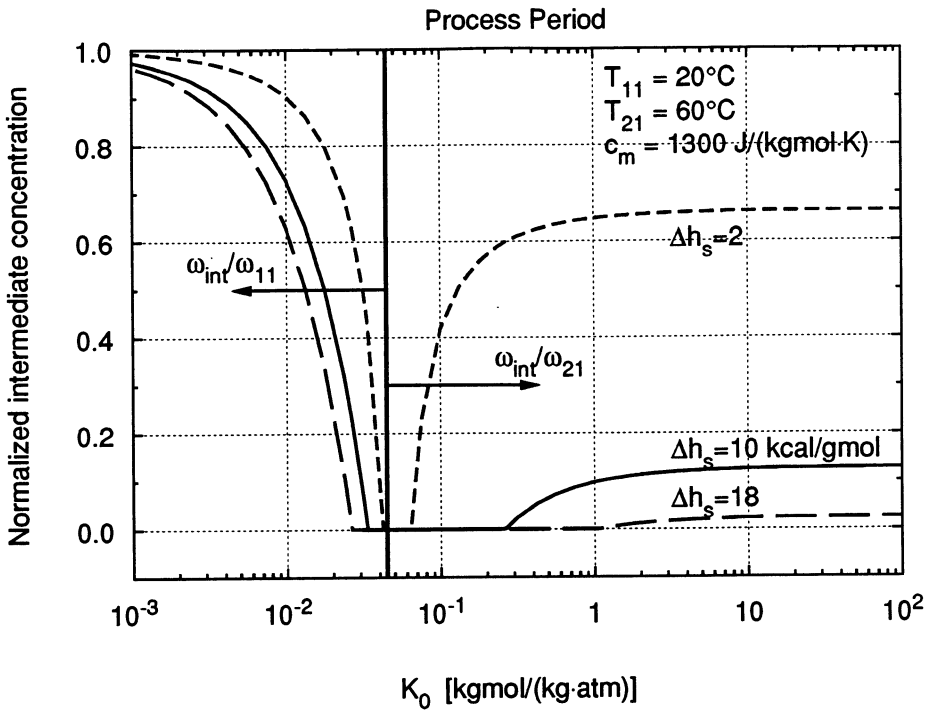

Figure 6.3 Normalized process period intermediate concentration as a function of K_0 for different values of Δh_s.

Figure 6.3 illustrates the effect of the heat of adsorption on the process period intermediate concentration. Higher heats of adsorption increase the temperature sensitivity of the isotherm slope, and as such result in lower intermediate concentrations. The range of K_0 values in the Case 2 region also increases as Δh_s increases. Thus contaminants with higher heats of adsorption should be more effectively removed from the air.

Figure 6.4 shows the effect of σ on the process period intermediate concentration through the variation of c_m ($\sigma = c_m/c_{air}$). The behavior is different depending on whether a contaminant is Case 1 or Case 3. For Case 3 (low K_0) contaminants, increasing σ increases the intermediate concentration, whereas for Case 1 (large K_0) contaminants,

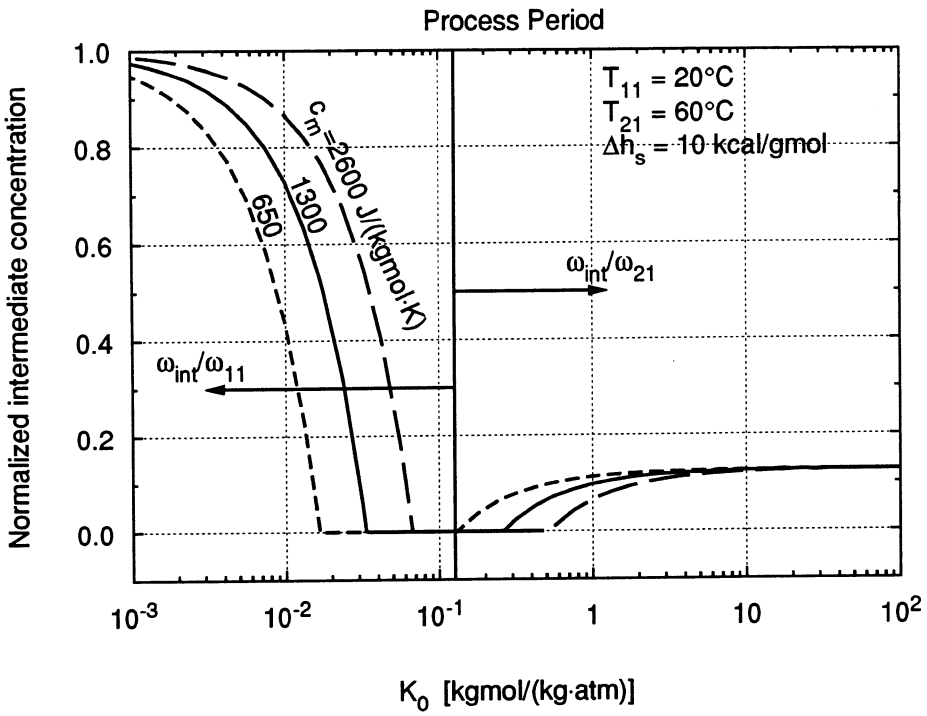

Figure 6.4 Normalized process period intermediate concentration as a function of K_0 for different values of c_m.

increasing σ decreases the intermediate concentration. The width of the Case 2 region remains constant as σ is varied, however, the region shifts towards lower K_0 values σ decreases and shifts towards higher K_0 values as σ increases.

The effect of process temperature on the intermediate concentration is shown in Figure 6.5. Lower process temperatures decrease the intermediate concentration for all K_0 values. The upper edge of the Case 2 region does not depend on T_{11}, but the lower edge, which does, moves towards lower K_0 values as T_{11} decreases. The width of the Case 2 region thus becomes greater for lower T_{11} values, and the effect is to improve the concentration reduction in the low K_0 contaminant region.

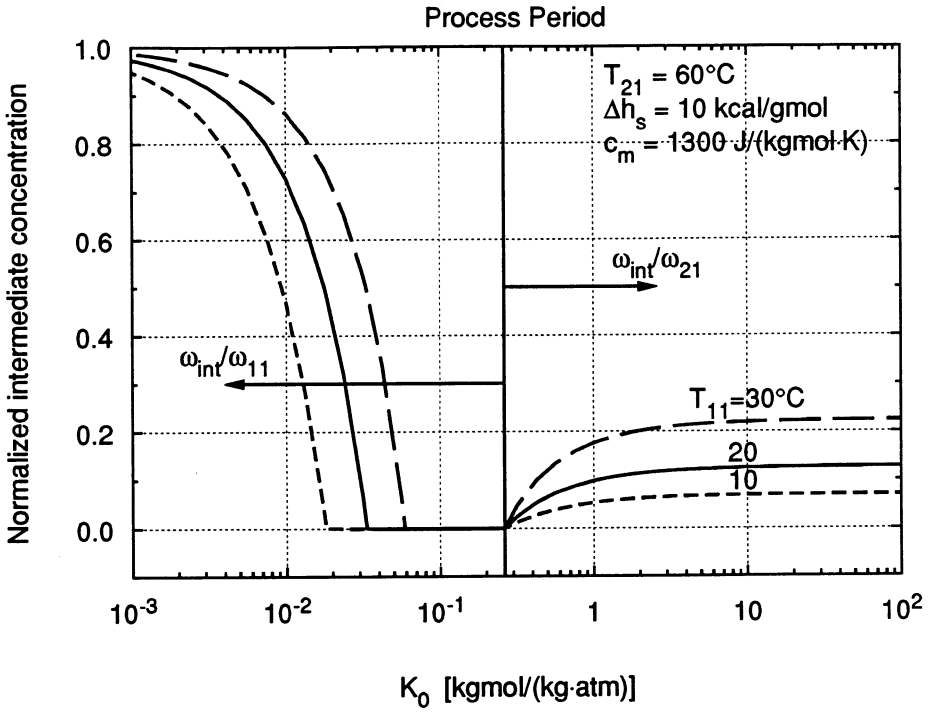

Figure 6.5 Normalized process period intermediate concentration as a function of K_0 for different values of T_{11}.

The effect of regeneration temperature is just the opposite of the effect of process temperature. Figure 6.6 shows that higher regeneration temperatures decrease the intermediate concentration at all K_0 values. The Case 2 region expands as T_{21} is increased, but in the direction of larger K_0 values. Figure 6.6 suggests that in system studies, when considering the concentration reduction as a function of energy required to heat the regeneration air, there will be an optimum regeneration temperature since the amount of additional concentration reduction diminishes as the temperature increases. Although the different T_{21} lines are close together in the Case 3 (low K_0) region, the effect of the regeneration temperature is significant for the larger K_0 values in the Case 3 region. For example, at K_0=2.5x10^{-2}, $\omega_{int}/\omega_{11} = 0.57$ at $T_{21} = 25°C$ and $\omega_{int}/\omega_{11} = 0.28$ at

$T_{21} = 60°C$, a 50% reduction. In the limit as $T_{21} \rightarrow \infty$, in the Case 1 region $\omega_{int}/\omega_{21} \rightarrow \exp[-\Delta h_s/(RT_{11})]$ which is equal to 3.48×10^{-8} for $T_{11} = 20°C$ and Δh_s=10 kcal/gmol. In the Case 3 region, in the limit as $T_{21} \rightarrow \infty$, $\omega_{int}/\omega_{11} \rightarrow \exp[\Delta h_s/(RT_{11})]$.

Figure 6.7 plots the process period intermediate concentration as a function of the regeneration temperature, T_{21}, for different K_0 values. Each curve in Figure 6.7 represents a vertical slice out of Figure 6.6. It is apparent from Figure 6.7 that the effect of increasing the regeneration temperature past about 60°C is limited (with T_{11}=20°C, Δh_s=10 kcal/gmol, and c_m=1300 J/(kgmol·K).

The regeneration period intermediate concentration as a function of K_0 (different contaminants) is shown in Figure 6.8. For the regeneration period, the Case 3 intermediate concentration is normalized by ω_{21} and the Case 1 intermediate concentration is normalized by ω_{11}. In the Case 2 region, the intermediate concentration is equal to infinity. This study is not concerned with the concentrations in the regeneration outlet air; the air is assumed to be exhausted to the outdoors. Therefore, attention will be focused on analysis of the process period outlet air.

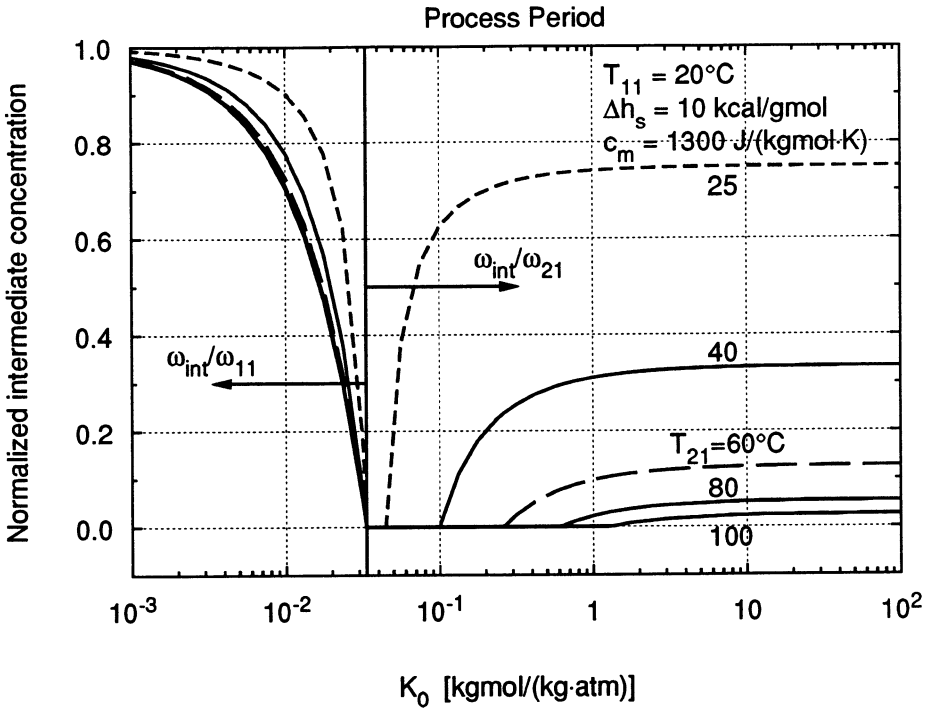

Figure 6.6 Normalized process period intermediate concentration as a function of K_0 for different values of T_{21}.

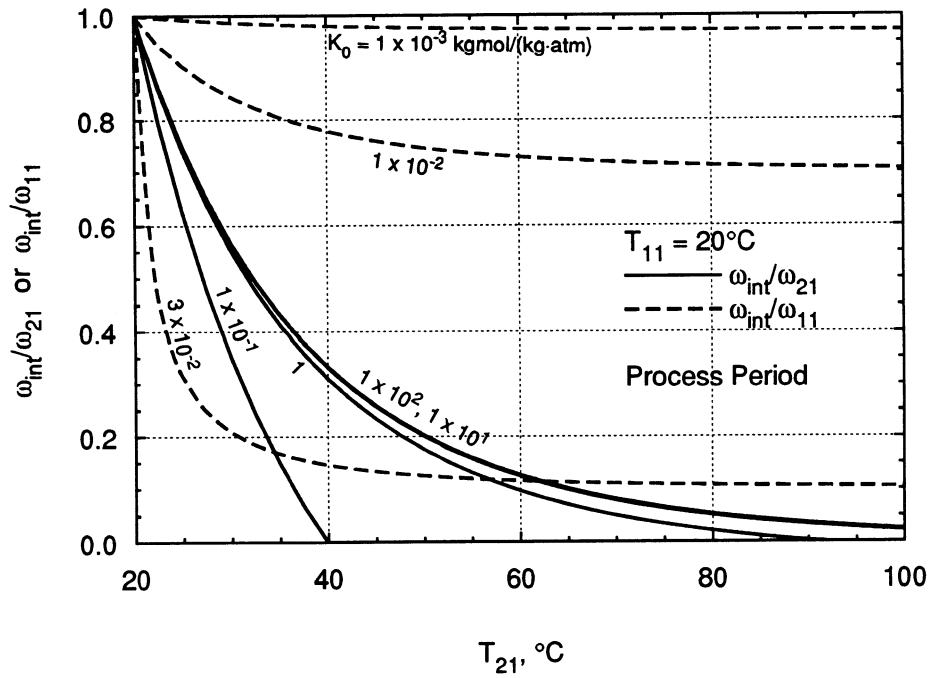

Figure 6.7 Normalized process period intermediate concentration as a function of T_{21} for different values of K_0.

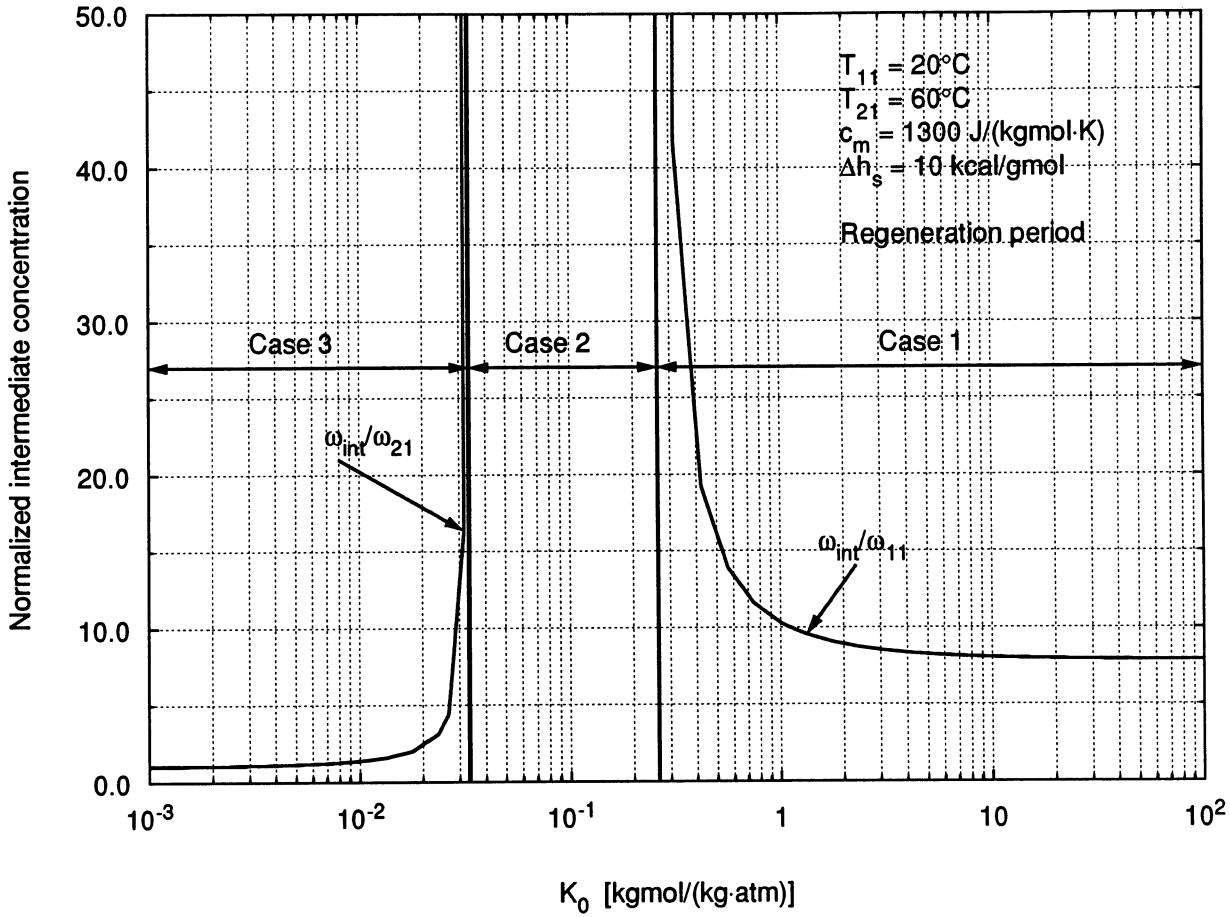

Figure 6.8 Normalized regeneration period intermediate concentration as a function of K_0.

6.2 Process period average outlet concentration

Since the purpose of the filter is to clean the air, low intermediate concentrations are desirable. However, the intermediate concentration is the effluent concentration for only a portion of the process period (see, for example, the outlet concentration profiles of Figures 5.34(b), 5.35(b), and 5.36(b)). It is ultimately the average outlet concentration over the entire process period which determines the reduction capability of the filter. If the intermediate concentration is output for only a small portion of the process period, a higher intermediate concentration output over a larger portion of the process period may result in a lower average concentration.

The process period average outlet concentration is equal to:

$$\omega_{12} = \frac{\int_0^{1/\Gamma_1} \omega(x=1,\tau)d\tau}{\int_0^{1/\Gamma_1} d\tau} \tag{6.2.1}$$

which for a completely regenerated matrix can be broken down into:

$$\omega_{12} = \frac{\int_0^{\tau=\min(\tau_A,\,1/\Gamma_1)} \omega_{21}(x=1,\tau)d\tau + \int_{\tau=\min(\tau_A,\,1/\Gamma_1)}^{\tau=\min(\tau_B,\,1/\Gamma_1)} \omega_{\text{int}}(x=1,\tau)d\tau + \int_{\tau=\min(\tau_B,\,1/\Gamma_1)}^{\tau=1/\Gamma_1} \omega_{11}(x=1,\tau)d\tau}{\int_0^{\tau=1/\Gamma_1} d\tau} \tag{6.2.2}$$

where τ_A and τ_B are the times at which the first and second waves with which a change in concentration is associated reach $x = 1$. If these times are less than the process period

duration ($1/\Gamma_1$), then they are the times at which the waves break through. Otherwise, these are the times at which the waves would break through in an infinitely long process period. Integrating Equation 6.2.2 gives the following expression:

$$\omega_{12} = \frac{\omega_{21}\min\left(\tau_A, \frac{1}{\Gamma_1}\right) + \omega_{int}\left(\min\left(\tau_B, \frac{1}{\Gamma_1}\right) - \tau_A\right)^+ + \omega_{11}\left(\frac{1}{\Gamma_1} - \tau_B\right)^+}{\frac{1}{\Gamma_1}} \tag{6.2.3}$$

where the + superscripts indicate inclusion of the term only if it is positive. Similarly, the process period average outlet temperature is given by:

$$T_{12} = \frac{T_{21}\min\left(\tau_T, \frac{1}{\Gamma_1}\right) + T_{11}\left(\frac{1}{\Gamma_1} - \tau_T\right)^+}{\frac{1}{\Gamma_1}} \tag{6.2.4}$$

where τ_T is the time at which the thermal wave reaches $x = 1$. For a matrix which has been completely regenerated, τ_A, τ_B and τ_T are defined as follows:

$$\tau_A = \min(\sigma, K_{21}) \tag{6.2.5}$$

$$\tau_B = \max(\sigma, K_{11}) \tag{6.2.6}$$

$$\tau_T = \sigma \tag{6.2.7}$$

Only the process period average outlet concentration for a matrix which is completely regenerated for all contaminants will be examined. Quantities influencing the average outlet states include the duration of the process period ($1/\Gamma_1$), the various concentrations ($\omega_{11}, \omega_{21}, \omega_{int}$), and the breakthrough times of the various waves (σ, K_{21}, K_{11}). The intermediate concentration, however, can be expressed as a function of the other quantities.

Figure 6.9 shows the quantity ω_{12}/ω_{21} plotted versus process period duration. The process period average outlet temperature is also shown. A longer process period

duration is equivalent to a slower rotation speed. Each curve represents a different K_0 value (a different contaminant). The process and regeneration temperatures are 20°C and 60°C, respectively. The process inlet concentration has been assumed to be twice the regeneration inlet concentration.

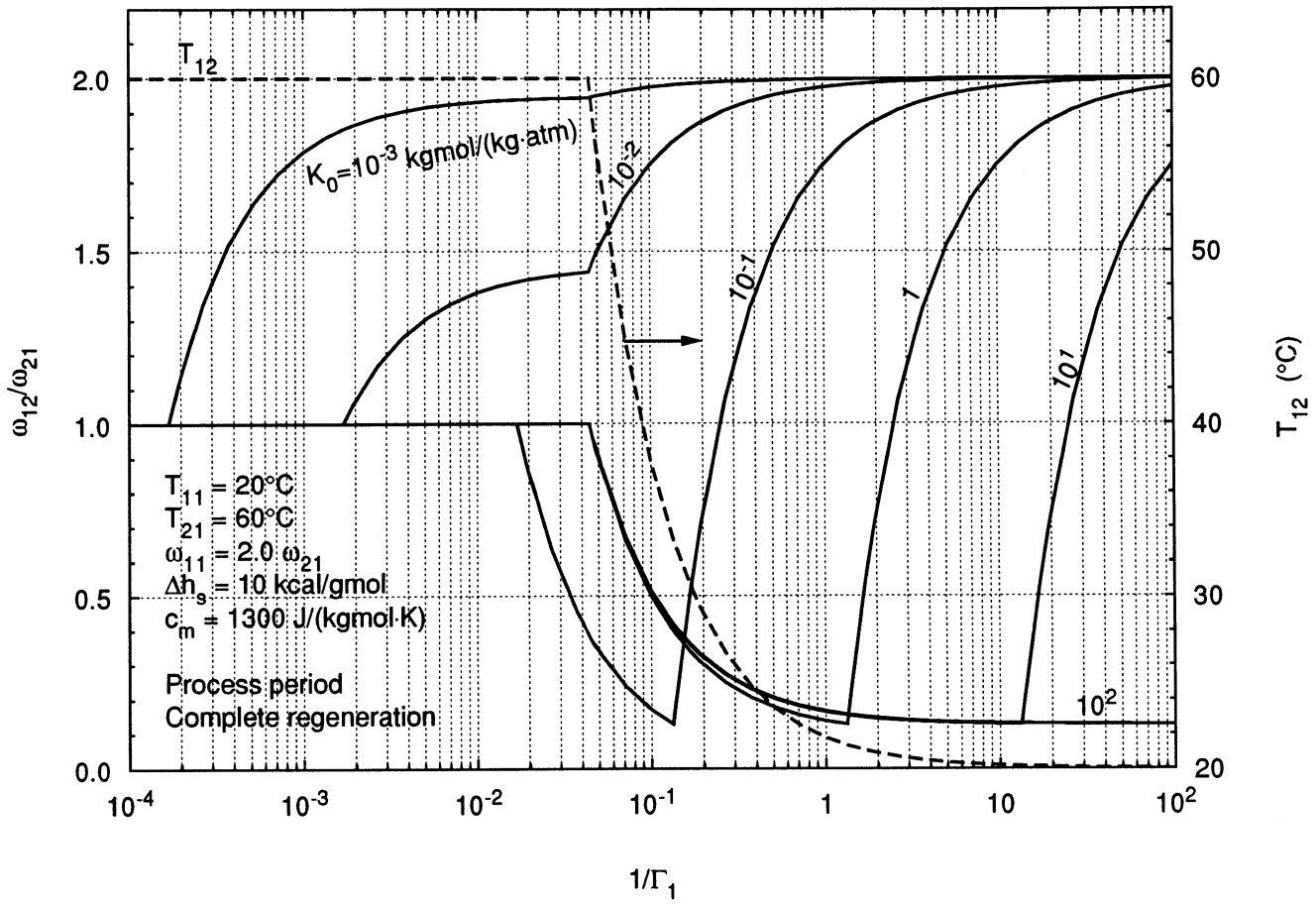

Figure 6.9 Process period average outlet concentration and temperature for a completely regenerated matrix as a function of process period duration.

The abrupt changes in the slope of the curves indicate a wave breaking through, so that sudden changes in the instantaneous outlet concentration occur. For example, the curve for $K_0 = 1x10^{-2}$ kgmol/(kg·atm) represents a Case 3 contaminant. The concentration wave breaks through at $\tau = K_{11} = 1.696x10^{-3}$ kgmol/kg and the thermal wave breaks through at $\tau = \sigma = 4.458x10^{-2}$ kgmol/kg. In Figure 6.9, the curves for $K_0 = 1x10^{-3}$ and $1x10^{-2}$ represent Case 3 contaminants, $K_0 = 1x10^{-1}$ represents a Case 2 contaminant, and $K_0 = 1$, $1x10^{1}$, and $1x10^{2}$ represent Case 1 contaminants.

By rotating the wheel very fast, ($1/\Gamma_1$ very small), none of the waves have a chance to break through and the average process outlet concentration is equal to the regeneration inlet concentration, i.e., $\omega_{12}/\omega_{21} \rightarrow 1$. Rotating the wheel very slow ($1/\Gamma_1$ large) results in all of the waves breaking through very quickly, and the average process outlet concentration approaches the process inlet concentration, i.e., $\omega_{12}/\omega_{21} \rightarrow \omega_{11}/\omega_{21}$, which for the example of Figure 6.9 is equal to 2. Thus the limiting value of all the K_0 curves on the left side of the graph represents an average outlet concentration equal to the regeneration inlet concentration. The upper bound on the right side of the graph represents an average outlet concentration equal to the process inlet concentration. Assuming that outdoor air is used for the regeneration air, ω_{12}/ω_{21} values below 1 indicate an average outlet concentration below the outdoor concentration.

To achieve any significant reduction in the concentration of the low K_0 contaminants, the filter must be rotated very fast (small $1/\Gamma_1$). However, operating at a very fast rotation speed hurts the filter's performance for the large K_0 contaminants: they are only reduced to the outdoor concentration. Also, the average outlet temperature at fast rotation speeds is nearly equal to the regeneration temperature, so that additional cooling of the process air would be required before it enters the zone. Operating at a

rotation speed of about $1/\Gamma_1$, on the other hand, results in a significant reduction in the concentration of contaminants with large K_0 values ($K_0 \geq 1$) at the expense of the smaller K_0 contaminants. The temperature change through the filter in this case is small.

Figure 6.10 shows ω_{12}/ω_{21} plotted as a function of K_0. Each curve, in this case, represents a different process period duration. As in Figure 6.9, T_{11}=20°C, T_{21}=60°C, $\omega_{11} = 2\omega_{21}$, and the matrix is assumed to be completely regenerated for all contaminants. For comparison, the intermediate concentration has also been plotted; the entire intermediate concentration curve is plotted as ω_{int}/ω_{21} (unlike the curves in Figures 6.1 and 6.3-6.8). The range of K_0 values for which $\omega_{int} = 0$ has been shaded. A comparison of the intermediate concentration curve with the other curves indicates that a low intermediate concentration is only useful if the wheel is rotated at a speed to take advantage of the low concentration.

Also shown in Figure 6.10 is the minimum possible average outlet concentration for each K_0 (contaminant), which was obtained by minimizing ω_{12}/ω_{21} as a function of $1/\Gamma_1$, i.e., at each K_0 value, $1/\Gamma_1$ was chosen to minimize ω_{12}/ω_{21}. This curve illustrates that there are three groups of contaminants: 1) contaminants for which the concentration can be reduced significantly below the outdoor concentration if the wheel is rotated at the optimal speed, 2) contaminants for which the concentration can only be reduced to the outdoor concentration when the wheel is rotated at the optimal speed, and 3) some contaminants in between. To some extent these regions are dependent on the operating conditions and parameters (e.g., Δh_s, T_{11}), but for any given set, these three regions exist.

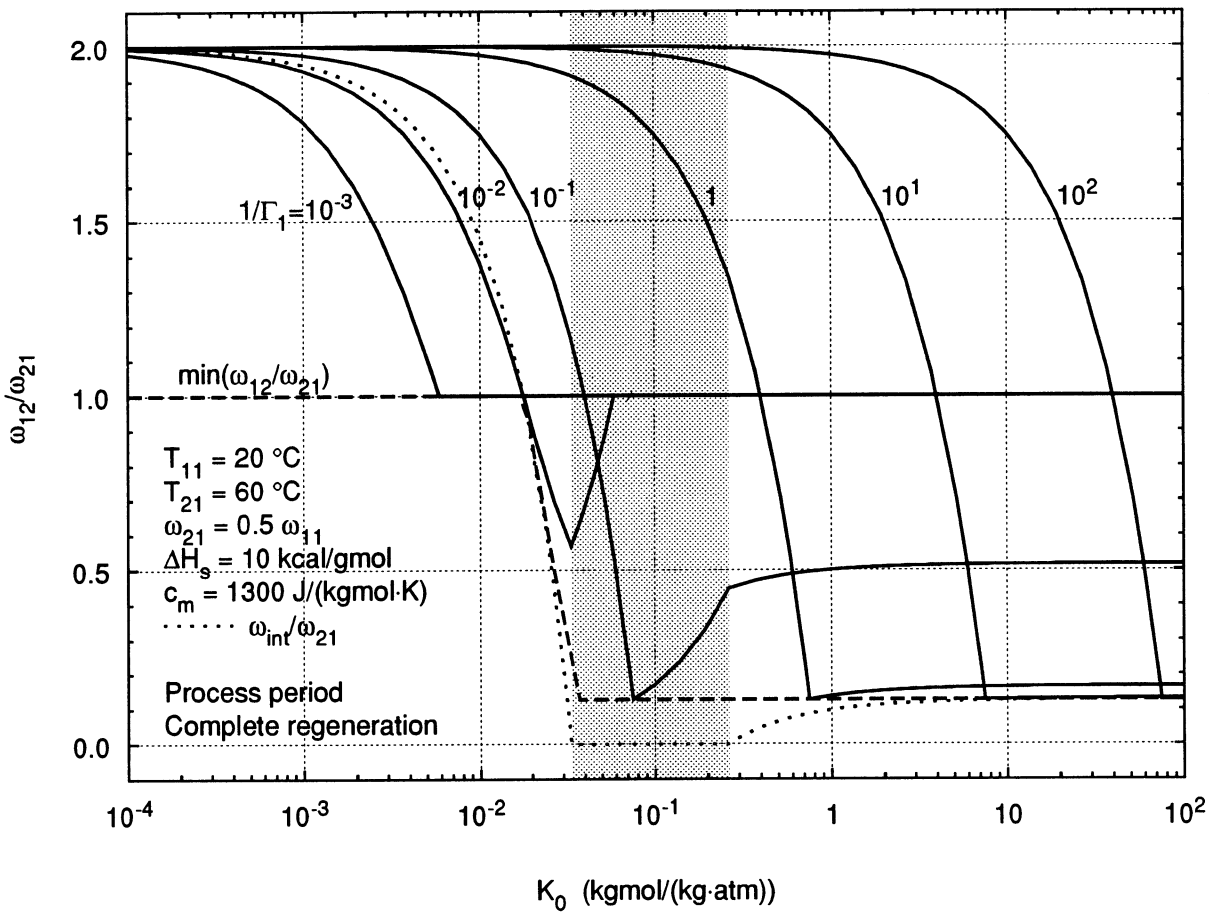

Figure 6.10 Process period average outlet concentration as a function of K_0 for different values of $1/\Gamma_1$. The matrix is assumed to be completely regenerated.

Figures 6.11 and 6.12 show the effect of σ (by changing c_m). Minimizing the value of σ improves the filter operation for all contaminants. The effect is only significant, however, on the average outlet concentrations obtained when operating near $1/\Gamma_1 = \sigma$ ($\sigma = 2.229\text{x}10^{-2}$ for $c_m = 650$ J/(kgmol·K), $\sigma = 4.458\text{x}10^{-2}$ for $c_m = 1300$ J/(kgmol·K), and $\sigma = 8.915\text{x}10^{-2}$ for $c_m = 2600$ J/(kgmol·K)).

Figures 6.13 and 6.14 show the effect of changing T_{11}. Lower process temperatures reduce the filter outlet concentration for all contaminants, and higher process temperature increase the filter outlet concentration for all contaminants. This behavior is a consequence of the temperature dependence of the isotherm: at lower temperatures, more contaminant is adsorbed.

The effect of the regeneration temperature as shown in Figures 6.15 and 6.16, however, is different. For the higher K_0 values, increasing the regeneration temperature decreases the average outlet temperature whereas decreasing the regeneration temperature has the opposite effect. This seems reasonable, since less contaminant is adsorbed at higher temperatures and thus the wheel will be better "cleaned" at high regeneration temperatures. For the low K_0 (Case 3) contaminants, however, the effect is just the opposite. The reason for this behavior is that for the Case 3 contaminants, the first wave which breaks through is the concentration wave at time $\tau = K_{21}$. For the Case 3 contaminants (see Figure 6.1), the intermediate concentration can be greater than the regeneration inlet concentration, which means that delaying the breakthrough of the concentration wave (i.e., lower values of T_{21}) decreases the average outlet concentration. For the conditions of Figure 6.17 and 6.18, $\omega_{11}/\omega_{21} = 2$, and therefore when $\omega_{int}/\omega_{11} \geq 0.5$ (see Figure 6.1), $\omega_{int} > \omega_{21}$.

Figures 6.17 and 6.18 show the effect of different values of the heat of adsorption on the process period average outlet concentration. The effect of Δh_s is very similar to that of T_{21}. That is, larger values of Δh_s improve the filter performance for the higher K_0 (Case 1 and 2) contaminants and decrease the filter performance for the smaller K_0 (Case 3) contaminants. The reasons for this behavior are the same as for the effect of T_{21}.

Figure 6.19 illustrates the effect of ω_{11}/ω_{21}. Different values of ω_{11}/ω_{21} move the top portion of the graph while leaving the bottom anchored. Thus larger values of ω_{11}/ω_{21} decrease the concentration reduction through the filter.

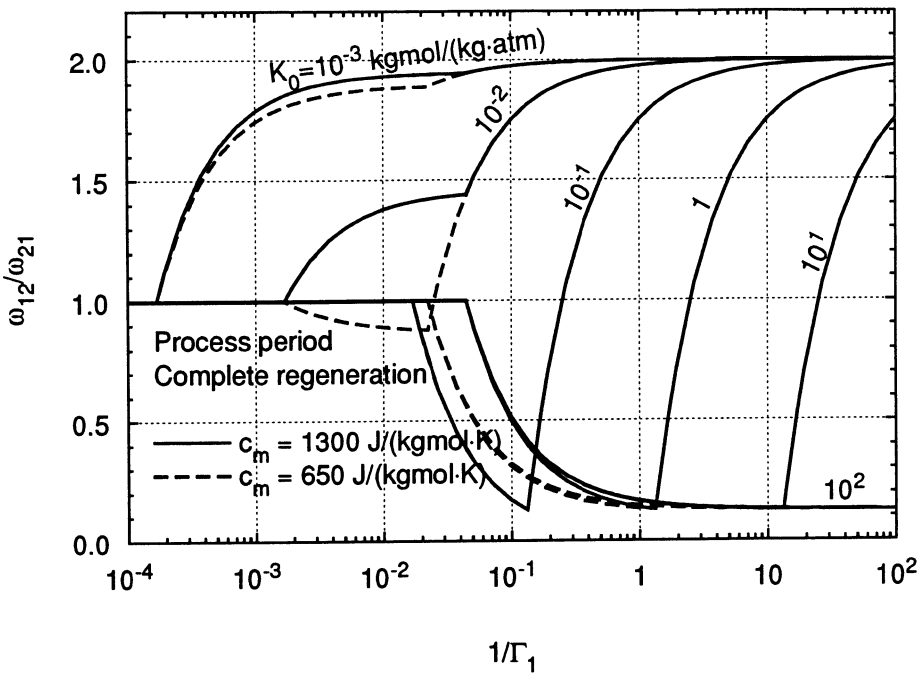

Figure 6.11 Effect of smaller c_m on the process period average outlet concentration.

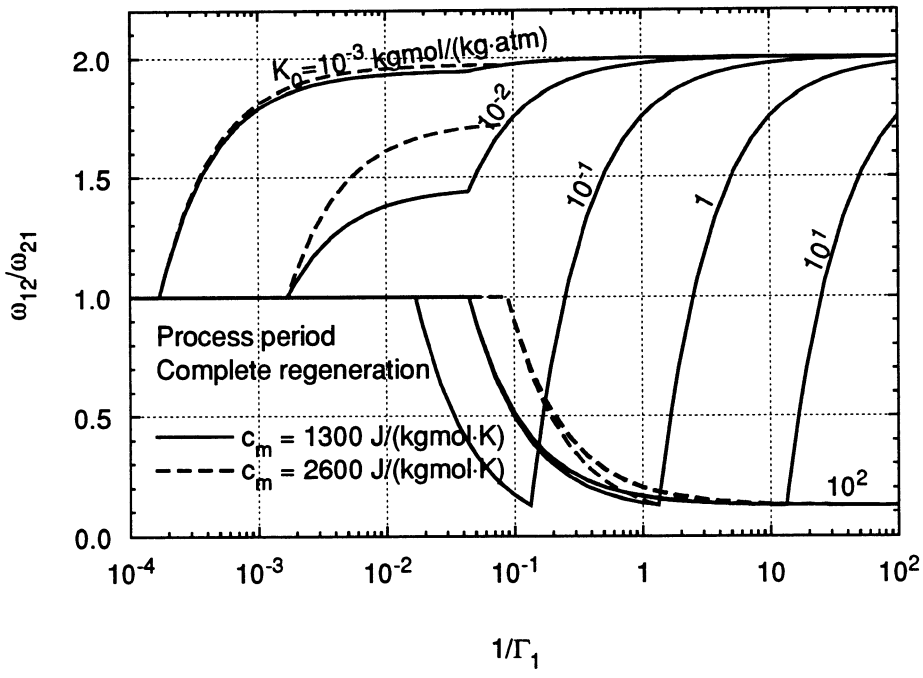

Figure 6.12 Effect of larger c_m on the process period average outlet concentration.

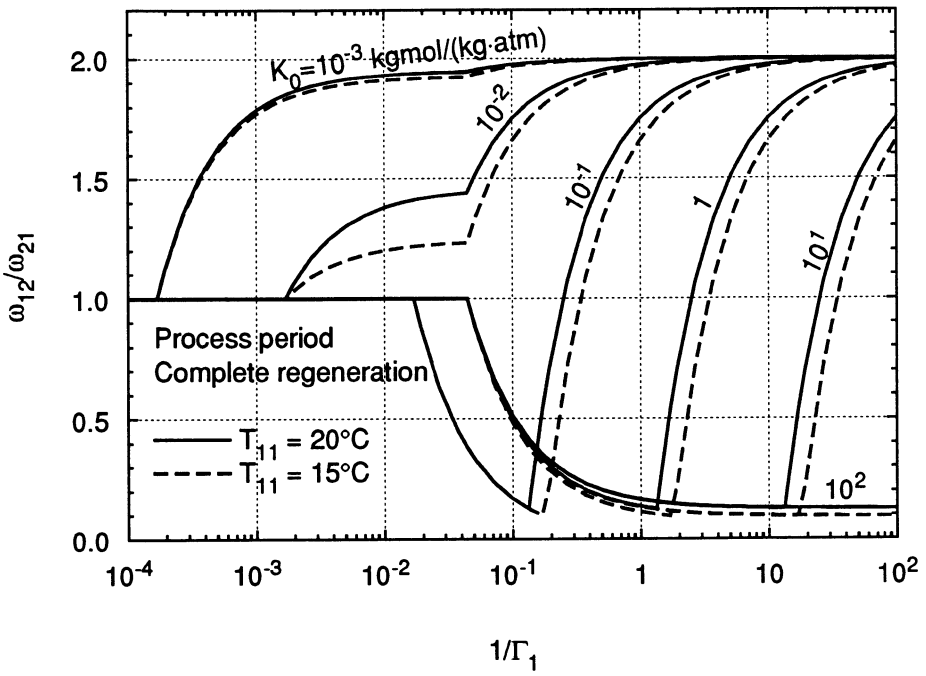

Figure 6.13 Effect of lower T_{11} on the process period average outlet concentration.

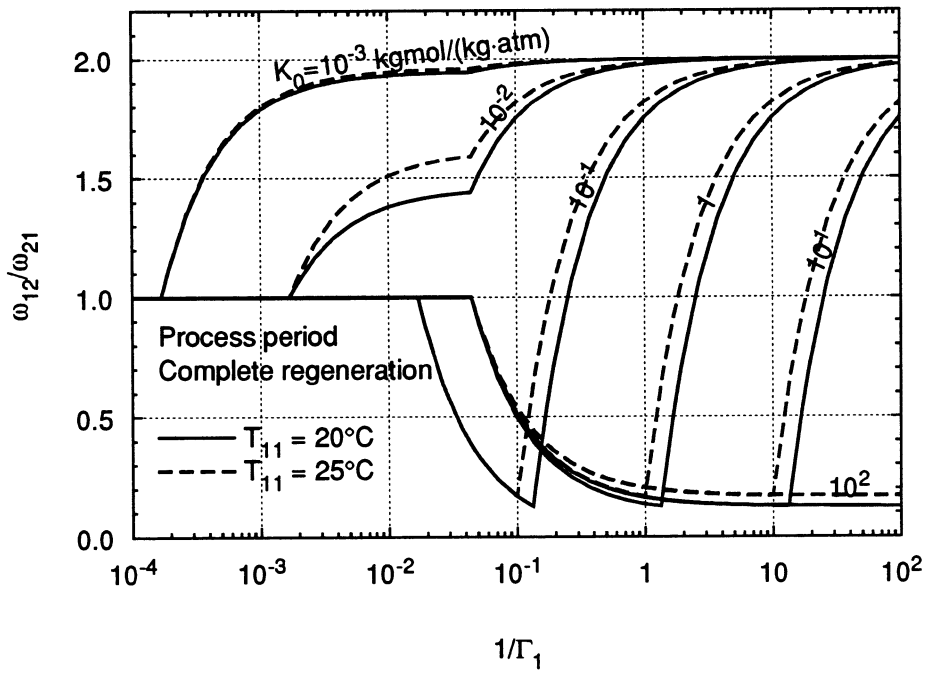

Figure 6.14 Effect of higher T_{11} on the process period average outlet concentration.

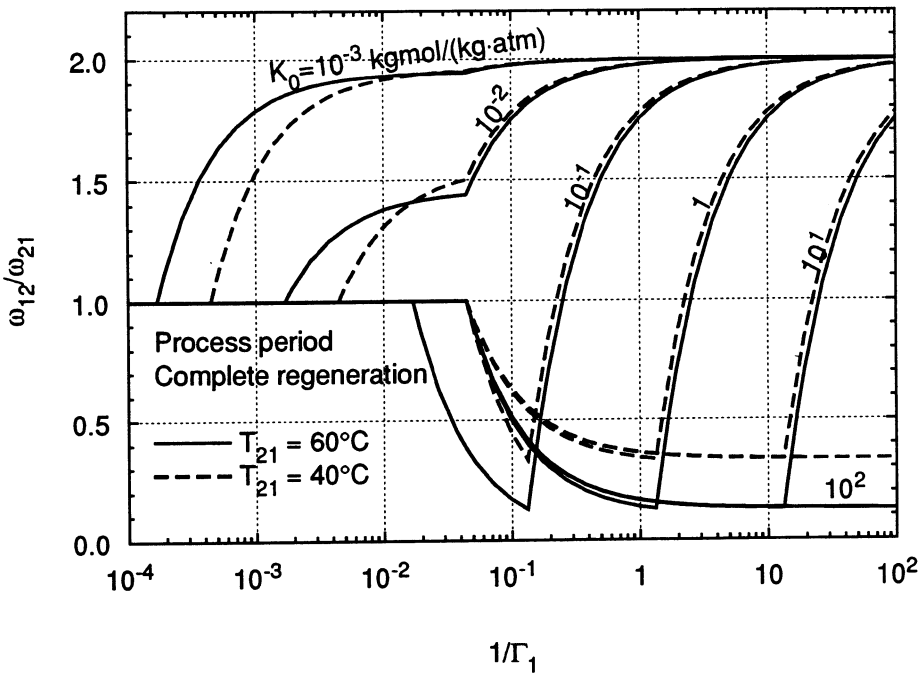

Figure 6.15 Effect of lower T_{21} on the process period average outlet concentration.

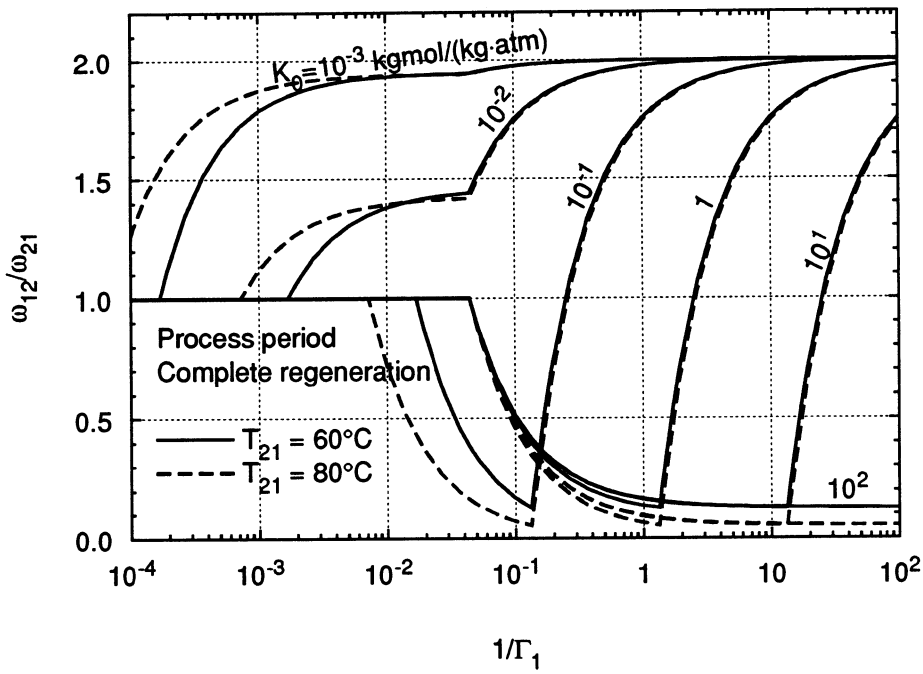

Figure 6.16 Effect of higher T_{21} on the process period average outlet concentration.

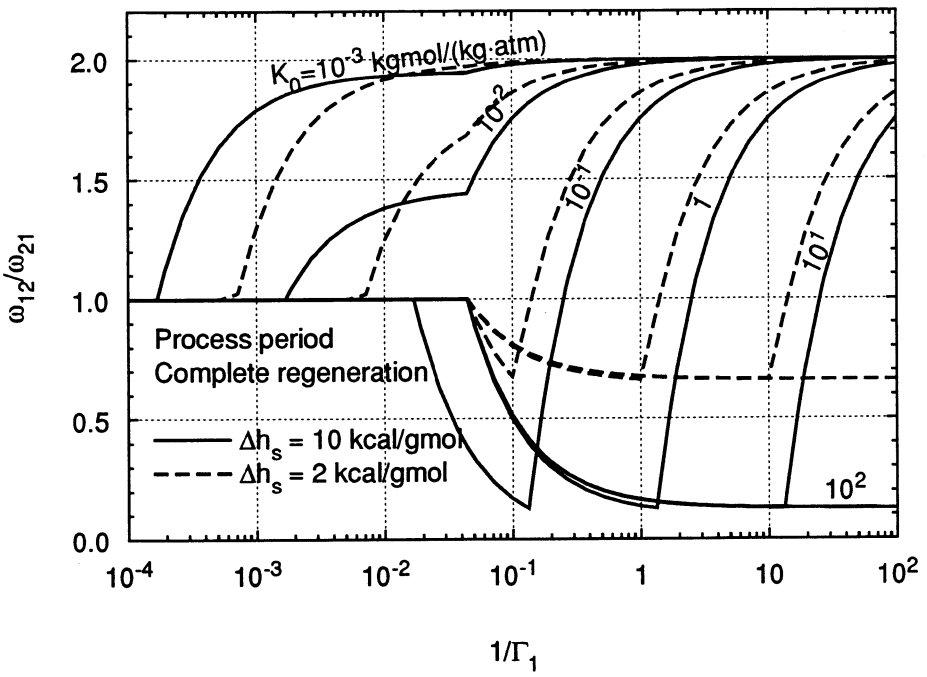

Figure 6.17 Effect of smaller Δh_s on the process period average outlet concentration.

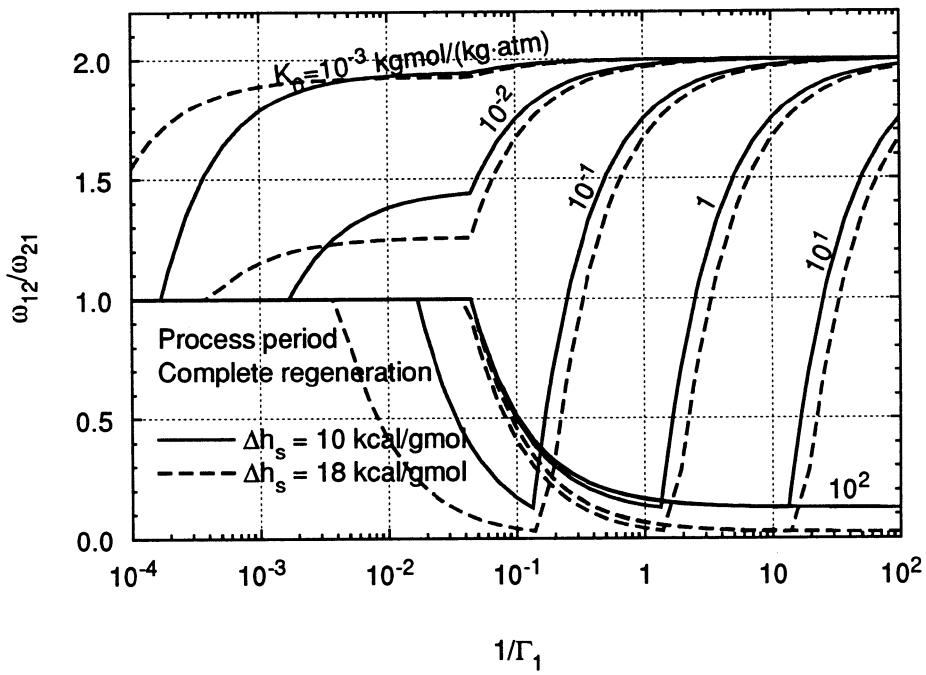

Figure 6.18 Effect of larger Δh_s on the process period average outlet concentration.

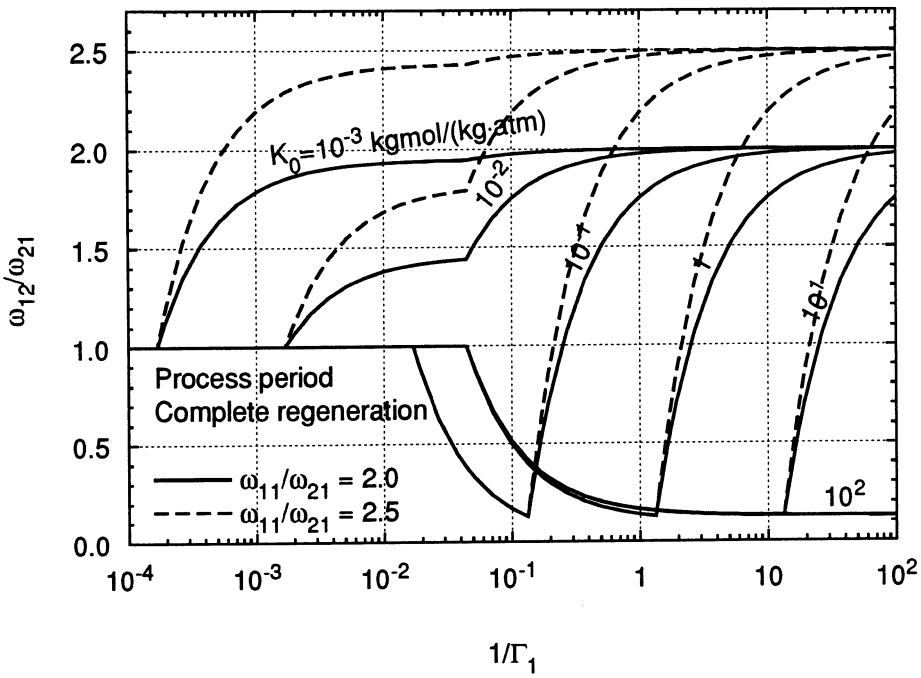

Figure 6.19 Effect of ω_{11}/ω_{21} on the process period average outlet concentration.

All of the graphs of the process average outlet concentration shown so far were for a matrix which was completely regenerated for all contaminants. This can be achieved by making the duration of the regeneration period sufficiently long. Figure 6.20 shows the lines of complete regeneration as a function of $1/\Gamma_1$ for different K_0 values. To obtain complete regeneration for all of the contaminants (K_0 values) shown, the duration of the regeneration period would have to be greater than or equal to the value of $1/\Gamma_2$ given by the line for K_0=1x10^2.

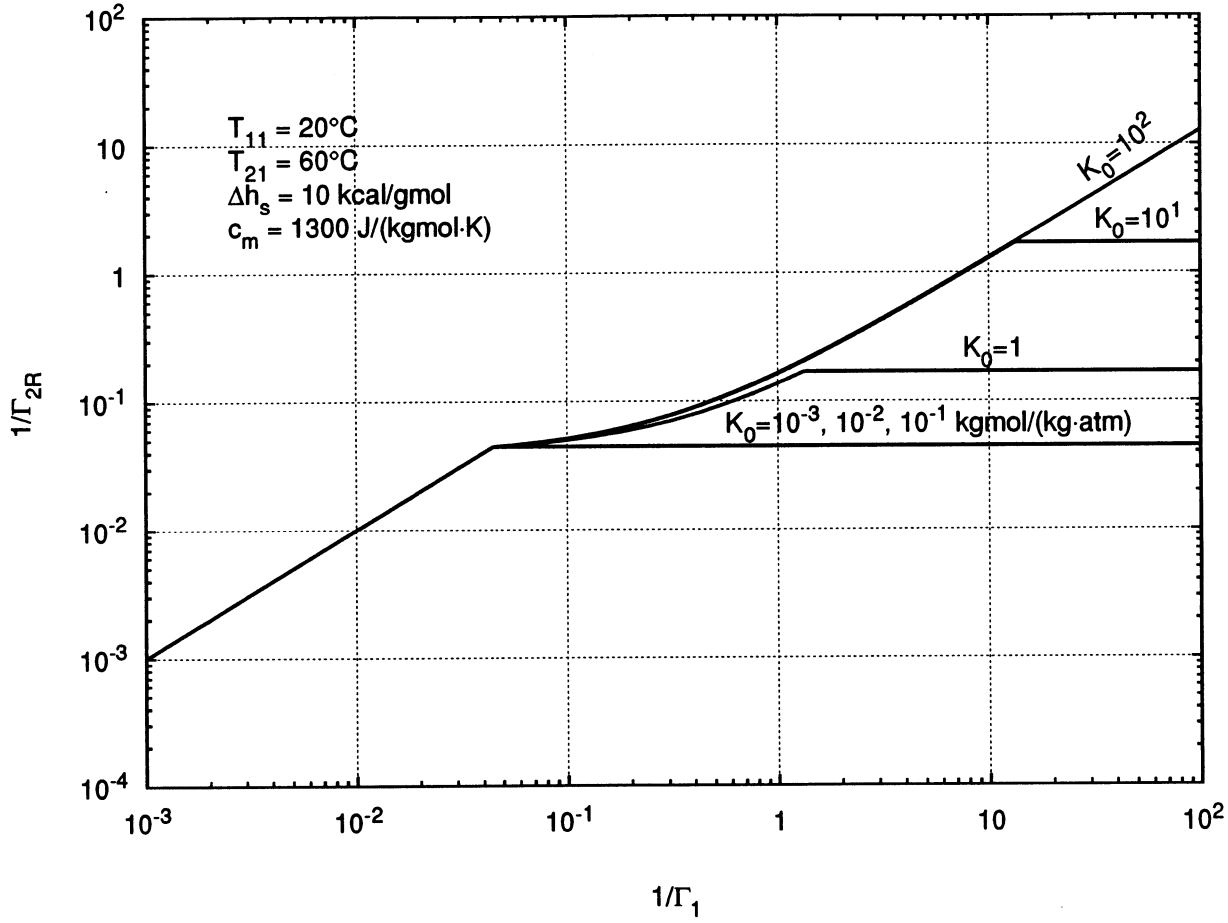

Figure 6.20 Complete regeneration lines for different K_0 values. Any value of $1/\Gamma_2$ above the complete regeneration line results in complete regeneration of the matrix.

6.3 Zone concentration

In the figures shown so far, the process inlet concentration has been assumed to be independent of the process outlet concentration. In the operation of a filter in an HVAC system such as shown in Figure 3.5, changes in the outlet concentration affect the inlet concentration. By considering the entire system of Figure 3.5, and assuming outdoor air (of concentration ω_o) is used to regenerate the filter (i.e., $\omega_{21} = \omega_o$), expressions for the steady-state zone concentration (relative to the outdoor concentration) for filters placed in either location A or B can be developed from system mass balances and the equation for the average outlet concentration (Equation 6.2.3). These equations apply only for a completely regenerated matrix with infinite heat and mass transfer coefficients. A constant pollutant generation rate and perfect mixing within the zone are assumed. The equations are as follows:

Filter Location A:

$$\frac{\omega_z}{\omega_o} = \frac{\dot{P}}{\dot{m}_r \omega_o} + f + (1-f)\Gamma_1 \left[\min\left(\tau_A, \frac{1}{\Gamma_1}\right) + \left(\min\left(\tau_B, \frac{1}{\Gamma_1}\right) - \tau_A \right)^+ \alpha_{int}\alpha_1 + \left(\frac{1}{\Gamma_1} - \tau_B\right)^+ \frac{\omega_z}{\omega_o} \right] \tag{6.3.1}$$

Filter Location B:

$$\frac{\omega_z}{\omega_o} = \frac{\dot{P}}{\dot{m}_r \omega_o} + \Gamma_1 \left[\min\left(\tau_A, \frac{1}{\Gamma_1}\right) + \left(\min\left(\tau_B, \frac{1}{\Gamma_1}\right) - \tau_A \right)^+ \alpha_{int}\alpha_1 + \left(\frac{1}{\Gamma_1} - \tau_B\right)^+ \left(f + (1-f)\frac{\omega_z}{\omega_o} \right) \right] \tag{6.3.2}$$

where $\tau_A, \tau_B, \alpha_1, \alpha_{int}$ are defined in Table 6.2. f is the fraction of outdoor air and $\dot{P}/\dot{m}_r\omega_o$ is a dimensionless contaminant generation rate. Notice that ω_z/ω_o appears on both sides of the equations, so that the equations can not be solved explicitly.

Table 6.2 Definitions of τ_A, τ_B, α_1, and α_{int} for use in Equations 6.3.1 and 6.3.2 (the zone concentration equations).

Case	τ_A	τ_B	α_1		α_{int}
			Location A	Location B	
1: $\sigma < K_{21} < K_{11}$	σ	K_{11}	1	1	$\frac{K_{21}-\sigma}{K_{11}-\sigma}$
2: $K_{21} < \sigma < K_{11}$	K_{21}	K_{11}	1	1	0
3: $K_{21} < K_{11} < \sigma$	K_{21}	σ	$\frac{\omega_z}{\omega_o}$	$f+(1-f)\frac{\omega_z}{\omega_o}$	$\frac{K_{11}-\sigma}{K_{21}-\sigma}$

To estimate the magnitude of the dimensionless generation rate, $\dot{P}/(\dot{m}_r\omega_o)$, mass balances for a system with no filter were used to relate the generation rate to the zone to outdoor concentration ratio:

$$\frac{\dot{P}}{\dot{m}_r\omega_o} = f\left[\left(\frac{\omega_z}{\omega_o}\right)_{no\,filter} - 1\right] \tag{6.3.3}$$

Figure 6.21 illustrates Equation 6.3.3 for different amounts of outdoor air.

The zone concentration for a filter at location B, as computed from Equation 6.3.2, is shown in Figure 6.22 as a function of process period duration for $\dot{P}/(\dot{m}_r\omega_o) = 0.1$, $T_{11} = 20°C$, $T_{21} = 60°C$, and the parameter values listed in Table 4.6. Each curve represents a different K_0 value (a different contaminant). K_0=1, 10, and 100

kgmol/(kg·atm) are Case 1, K_0=1x10^{-1} kgmol/(kg·atm) is Case 2, and K_0=1x10^{-2} and 1x10^{-3} kgmol/(kg·atm) are Case 3. The dashed line represents the filter average outlet temperature.

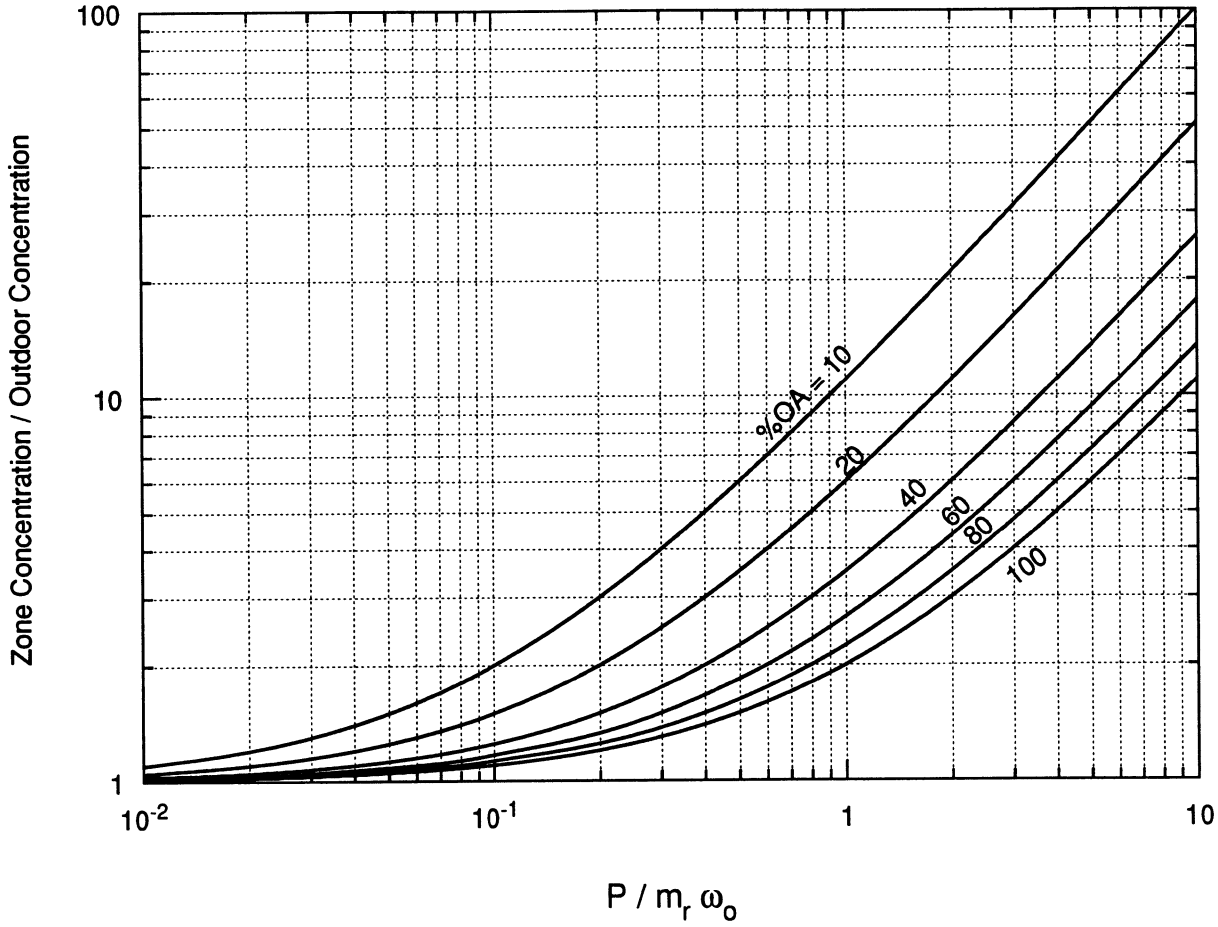

Figure 6.21 Zone concentration relative to outdoor concentration with no filter, as a function of pollutant generation rate.

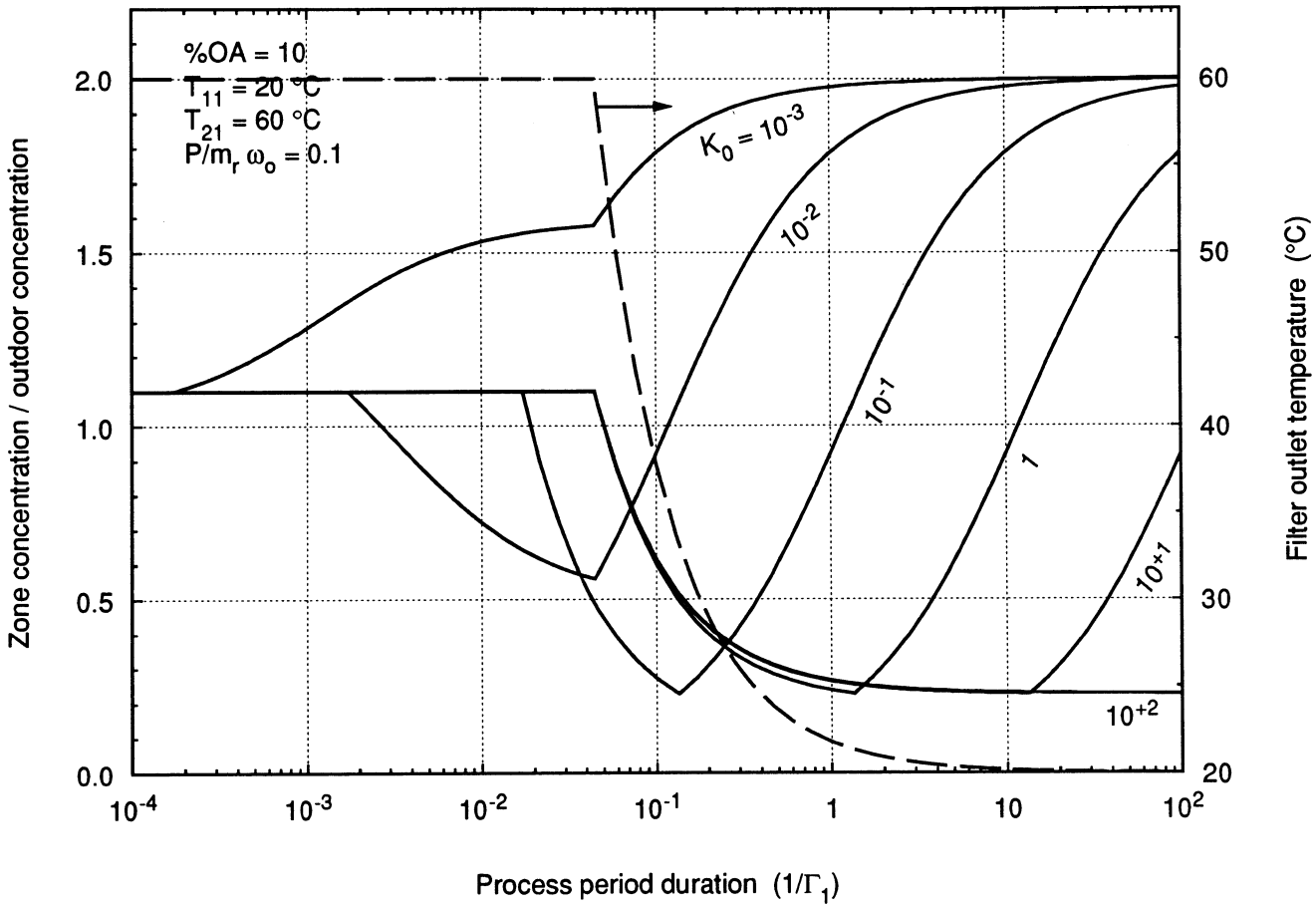

Figure 6.22 Zone concentration and average filter outlet temperature as a function of process period duration for filter at location B. The filter is assumed to be completely regenerated for all contaminants.

For very fast rotation speeds (small $1/\Gamma_1$), none of the waves have a chance to break through and the filter outlet concentration is equal to the outdoor concentration, so that the zone concentration is equal to that obtained with no filter at 100% outdoor air. For example, from Figure 6.21, for $\dot{P}/(\dot{m}_r\omega_o) = 0.1$, the zone to outdoor concentration for no filter at 100% outdoor air is 1.10. In Figure 6.22, the concentration value for small $1/\Gamma_1$ is 1.10. While at first glance this seems to be a good speed at which to operate the wheel, the average outlet temperature from the filter will be very close to the regeneration temperature, so that the temperature change through the filter is large. This temperature change will increase the load on the air conditioning system. The other aspect to consider is that for many of the contaminants, much lower concentrations can be obtained by rotating at a slower speed.

For slow rotation speeds (large $1/\Gamma_1$) and small K_0 values, the waves will break through very quickly and the filter average outlet concentration is nearly equal to the filter inlet concentration. The resulting zone concentration is therefore approximately equal to that obtained with no filter at the specified amount of outdoor air. In Figure 6.22, which is for 10% outdoor air, the concentration values at large $1/\Gamma_1$ for the $K_0 = 10^{-2}$ and $K_0 = 10^{-3}$ kgmol/(kg·atm) curves are equal to 2.0. In Figure 6.21, 2.0 is the zone to outdoor concentration value for no filter at 10% outdoor air. The point of minimum concentration for the high K_0 (Case 1) contaminants is equal to $\dot{P}/(\dot{m}_r\omega_o) + K_{21}/K_{11}$ and occurs at $1/\Gamma_1 = K_{11}$. The ratio K_{21}/K_{11} is equal to $\exp[\Delta h_s/R\,(1/T_{21} - 1/T_{11})]$, which is plotted in Figure 6.2.

The time that it takes for the first wave to break through (τ_A in Equation 6.3.2) is indicated by the point at which the zone concentration deviates from the no filter 100%

outdoor air value. For the Case 3 contaminants, this is at $1/\Gamma_1 = K_{21}$; for the Case 1 and 2 contaminants, this is at σ. Moving along a K_0 curve, the second point at which the slope is discontinuous is the time at which the second wave which affects the concentration breaks through, τ_B. For Case 3 contaminants, this is at σ; for Case 1 and 2, at K_{11}. These are the same points at which the sharp changes in the average outlet concentration curves occur (e.g., Figure 6.9).

By operating at a rotation speed such that $1/\Gamma_1 > \sigma$, the zone concentration of the some of the contaminants (those with larger K_0 values) can be reduced below that possible with no filter at 100% outdoor air. Contaminants with smaller K_0 values will have zone concentrations between the values obtained with no filter at 100% outdoor air and no filter at the specified amount of outdoor air.

At rotation speeds such that $1/\Gamma_1 < \sigma$, all of the Case 1 (large K_0) contaminants will have zone concentrations equal to that obtained with no filter at 100% outdoor air. The Case 2 contaminant zone concentrations will be equal to the no filter 100% outdoor air zone concentration for $1/\Gamma_1 < K_{21}$ and less than the no filter 100% outdoor air zone concentration for $K_{21} < 1/\Gamma_1 < \sigma$. Case 3 concentrations can be either greater than or less than the no filter 100% outdoor zone concentration at rotation speeds less than σ.

For example, if the wheel were operated such that $1/\Gamma_1 = 1$, for the parameters used in Figure 6.22, contaminants with $K_0 = 1, 10, 100$ kgmol/(kg·atm) (and larger) will have a zone concentration equal to roughly a quarter of the outdoor concentration - this is less than possible with no filter at 100% outdoor air. For a contaminant with $K_0 = 1\text{x}10^{-3}$ kgmol/(kg·atm), the filter would have virtually no effect. For $K_0 = 1\text{x}10^{-1}$ kgmol/(kg·atm), the zone concentration would be slightly less than that obtained with no

filter at 100% outdoor air. For K_0=1x10^{-2} kgmol/(kg·atm) the zone concentration would be roughly equal to 1.75 times the outdoor concentration, a value between that obtained with no filter at 100% outdoor air and that obtained with no filter at 10% outdoor air.

The zone concentration graph of Figure 6.22 is for a dimensionless pollutant generation rate of 0.1 and 10% outdoor air, which corresponds to a zone concentration to outdoor air concentration ratio of 2.0 with no filter. When there is no filter, the concentration of the air supplied to the zone is determined by mixing the outdoor air and the return air, and for f=0.10, $\dot{P}/(\dot{m}_r\omega_o) = 0.1$, and $\omega_z/\omega_o = 2.0$, the concentration of the supply air is equal to 1.9 times the outdoor air concentration. If a filter were placed in the supply air duct (filter location B), the initial value of $\omega_{11}/\omega_{21} = \omega_{11}/\omega_o$ would be equal to this ratio of 1.9. At the system steady-state, however, ω_{11}/ω_o would be different. Figure 6.23 is a filter average outlet concentration graph for $\omega_{11}/\omega_{21} = 1.9$.

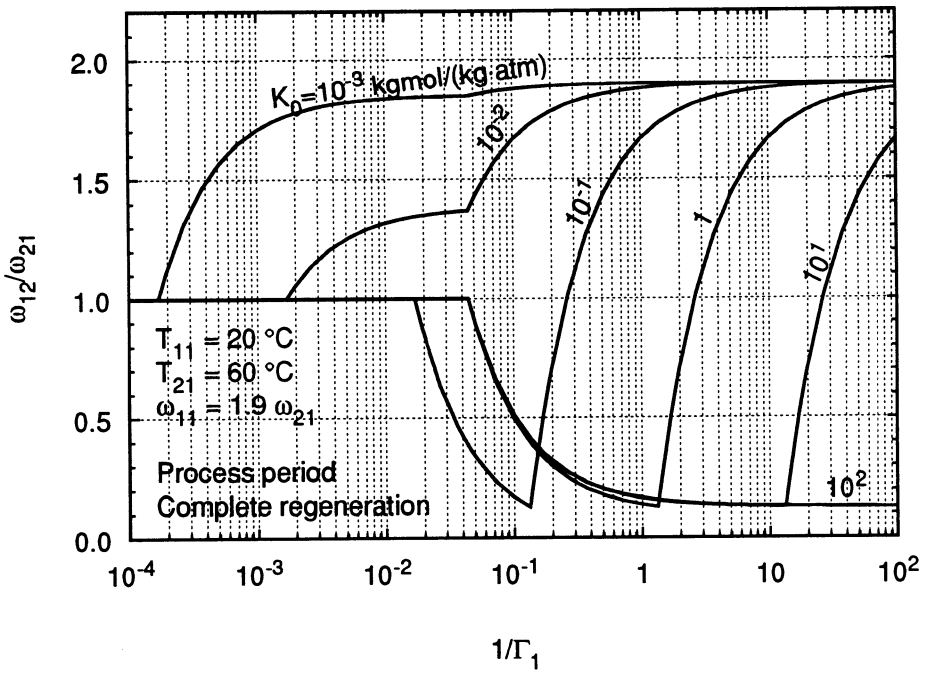

Figure 6.23 Average outlet concentration as a function of process period duration for $\omega_{11}/\omega_{21} = 1.9$.

Comparing the average outlet concentration graph of Figure 6.23 with the zone concentration graph of Figure 6.22, it can be seen that the curves are similar. There are, however, some differences. The most striking difference, and perhaps the most surprising, is that the zone concentration of the K_0=1x10^{-2} contaminant is *less* than the outdoor concentration for rotation speeds between about 2x10^{-3} and 1.5x10^{-1}. On the average outlet concentration graph, the concentration in this range is *higher* than the outdoor (regeneration inlet) concentration. Thus the zone concentration graph indicates that some of the contaminants may be removed more effectively than expected based on the average outlet concentration graphs.

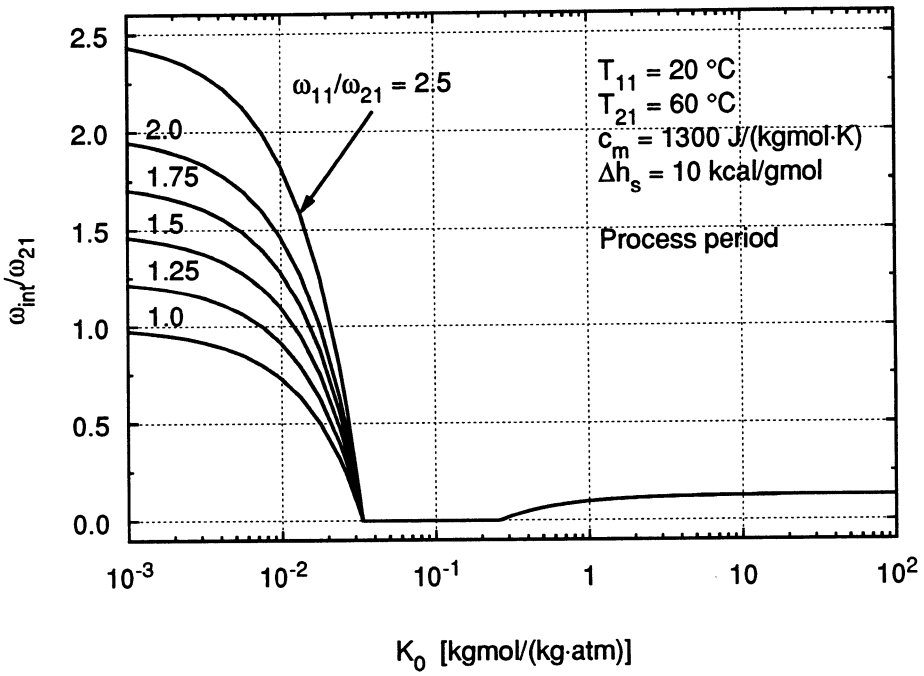

Figure 6.24 Ratio of the intermediate concentration to the regeneration inlet concentration for different ratios of ω_{11}/ω_{21}.

The reason for this rather dramatic change is related to the intermediate concentration. The ratio ω_{11}/ω_{21} with no filter correpsonds to the initial state of the system before the filter is added. Once the filter is turned on, the zone concentration will

be reduced during an initial transient period, and eventually reach a steady-state value. At the initial state ($\omega_{11}/\omega_{21} = 1.9$), the intermediate concentration for the K_0=1x10^{-2} contaminant is greater than the outdoor concentration, resulting in the behavior seen in the average outlet concentration graph. However, because the average outlet concentration is less than the process inlet concentration, on the next "iteration" through the HVAC system, the process inlet concentration will be lower, i.e., ω_{11}/ω_{21} is reduced. Each "iteration" until the system reaches steady-state, the process inlet concentration is reduced even farther, and eventually it becomes low enough that the intermediate concentration becomes less than the outdoor concentration. Figure 6.24 is a graph of ω_{int}/ω_{21} for different values of ω_{11}/ω_{21}. For K_0=1x10^{-2}, once ω_{11}/ω_{21} drops below 1.37, the intermediate concentration becomes less than the outdoor concentration. Continuing the "iterations" until the system reaches steady-state results in the behavior seen in Figure 6.22. The time it would take the system to reach steady-state would depend on the transient behavior of the carbon wheel, an area which is not covered in this thesis. Only the steady-state solution of the system and the wheel are considered.

In general, for all of the contaminants, the zone concentration to outdoor concentration ratio of Figure 6.22 is less than the average outlet concentration to outdoor concentration ratio of Figure 6.23. This outcome is not surprising, since at the system steady-state the value of ω_{11}/ω_{21} is less than it was initially.

Figure 6.25 compares the effect on the zone concentration when the filter is placed at either location A or B. Location B offers a slight advantage in concentration reduction, although it does require processing a larger amount of air and thus a larger filter. As such, in some cases, location A may be preferable. For higher percentages of outdoor air, the effect becomes more pronounced.

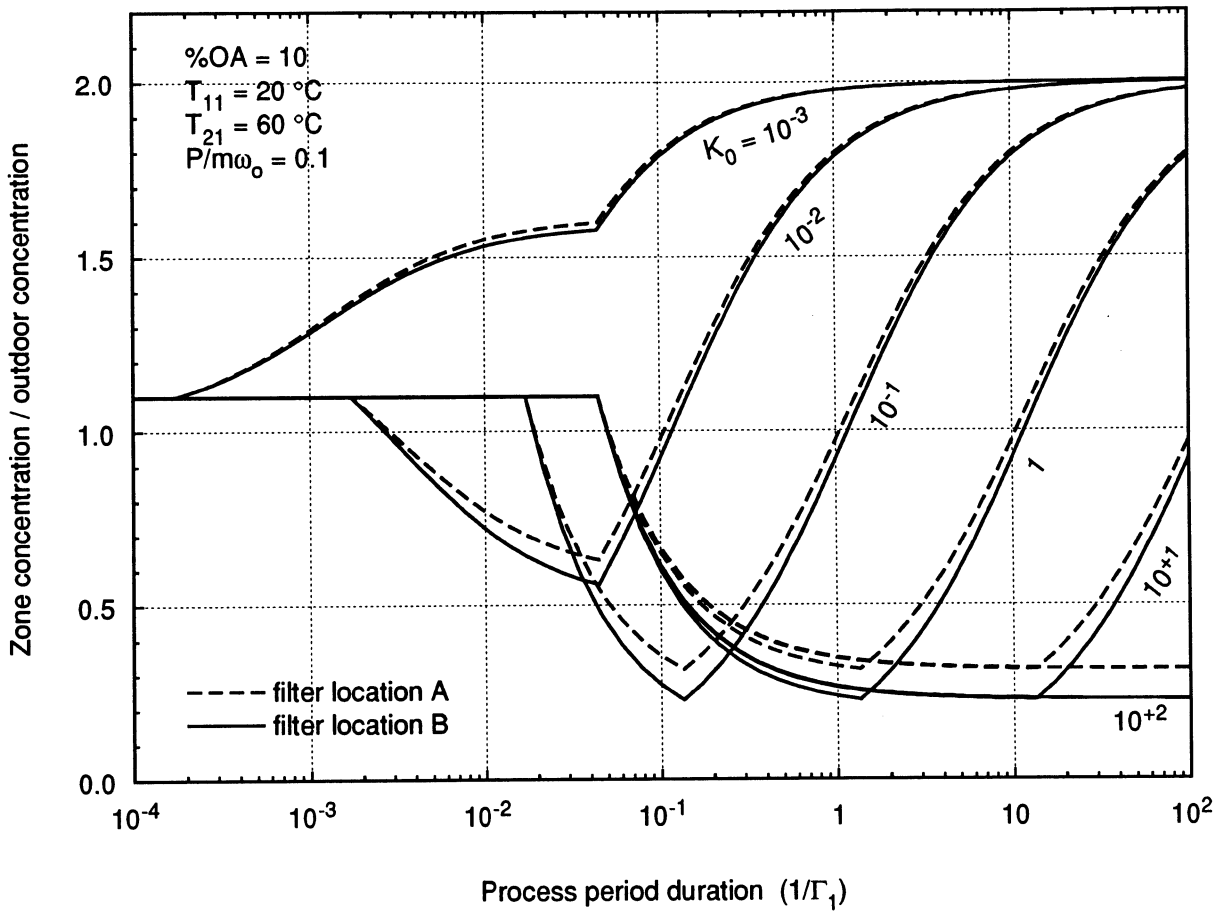

Figure 6.25 Comparison of zone concentration as a function of process period duration for filters at location A and location B.

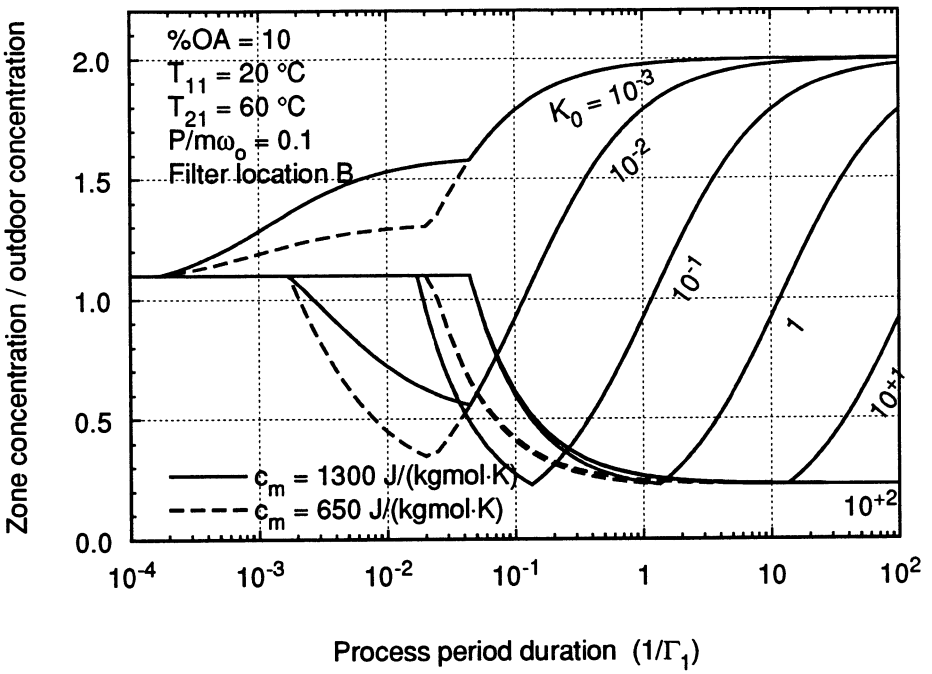

Figure 6.26 Effect of smaller c_m on the zone concentration.

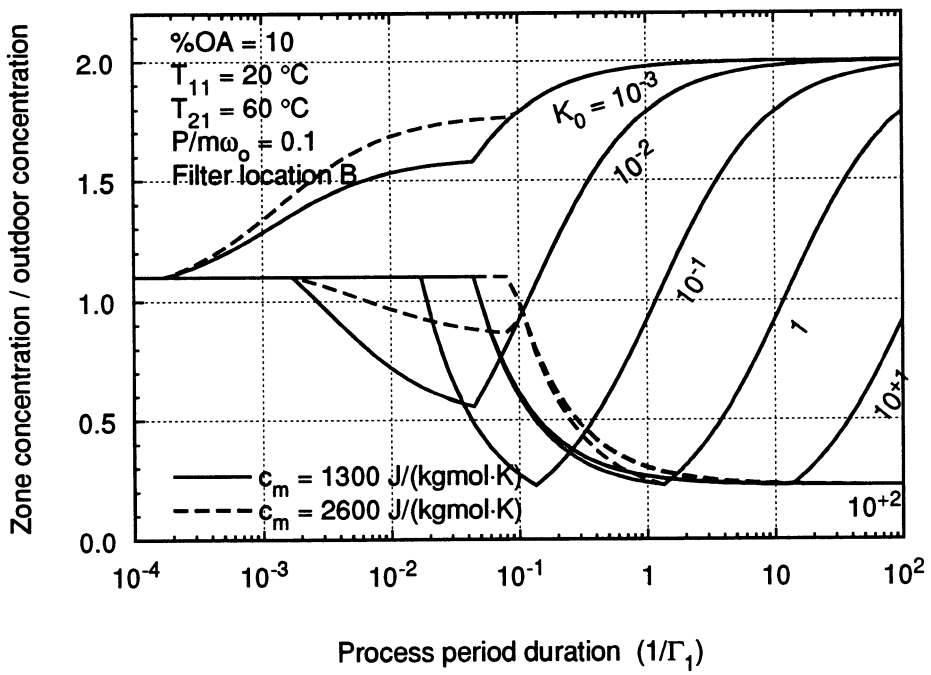

Figure 6.27 Effect of larger c_m on the zone concentration.

Figures 6.26 and 6.27 illustrate the effect on the zone concentrations of varying c_m, which assuming a constant specific heat of air is equivalent to varying σ. As for the average outlet concentrations, the effect becomes more significant as the process period duration approaches $1/\Gamma_1 = \sigma$. Smaller values of c_m lower the zone concentration for all of the contaminants, and therefore c_m should be minimized.

Figures 6.28 and 6.29 ilustrate the effect of Δh_s on the zone concentrations. Again, the effect is very similar to that of Δh_s on the average outlet concentration. Lower Δh_s values reduce the zone concentration only for the lowest K_0 contaminants at very fast rotation speeds (low $1/\Gamma_1$). Otherwise, lower values of Δh_s increase the zone concentrations. Increasing Δh_s has the opposite effect.

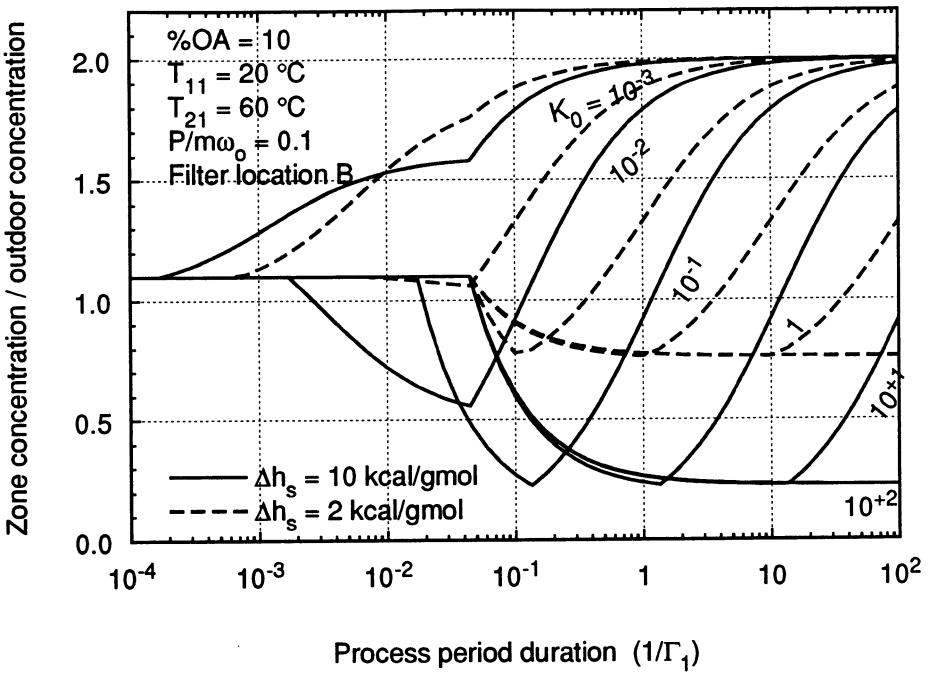

Figure 6.28 Effect of smaller Δh_s on the zone concentration.

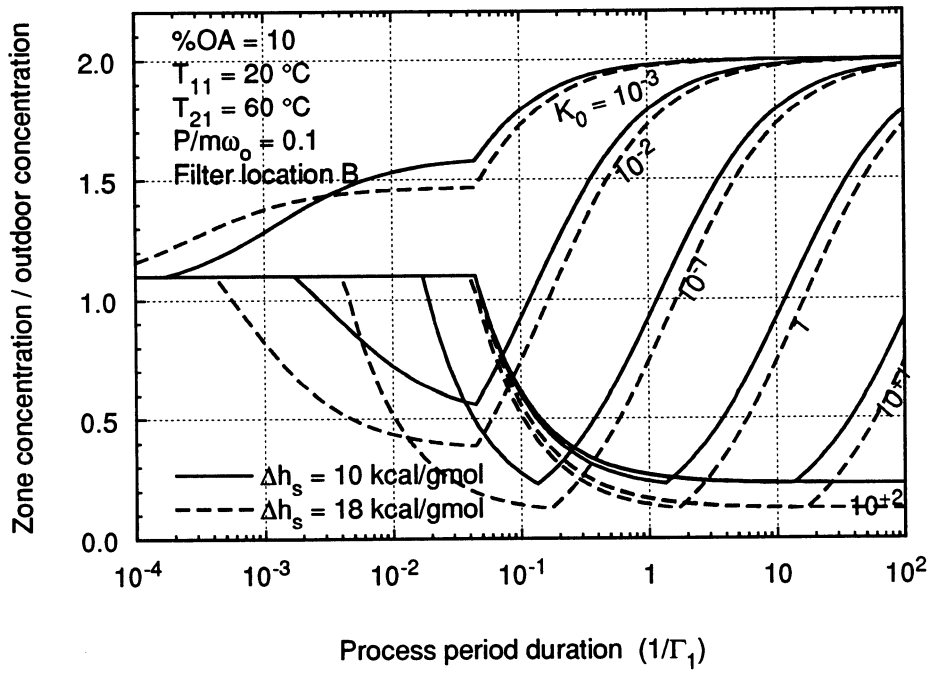

Figure 6.29 Effect of larger Δh_s on the zone concentration.

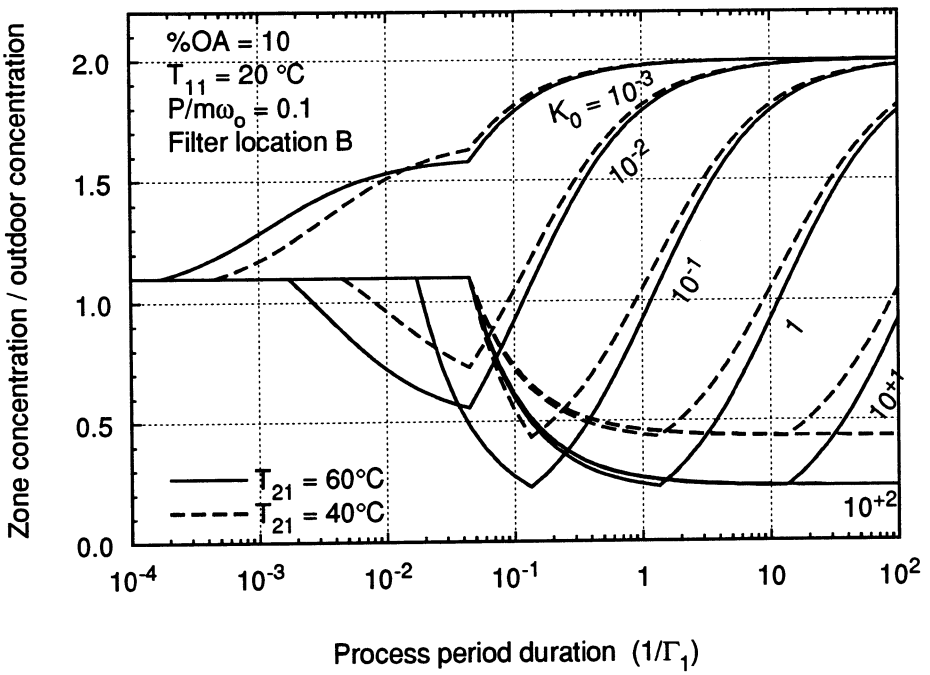

Figure 6.30 Effect of lower T_{21} on the zone concentration.

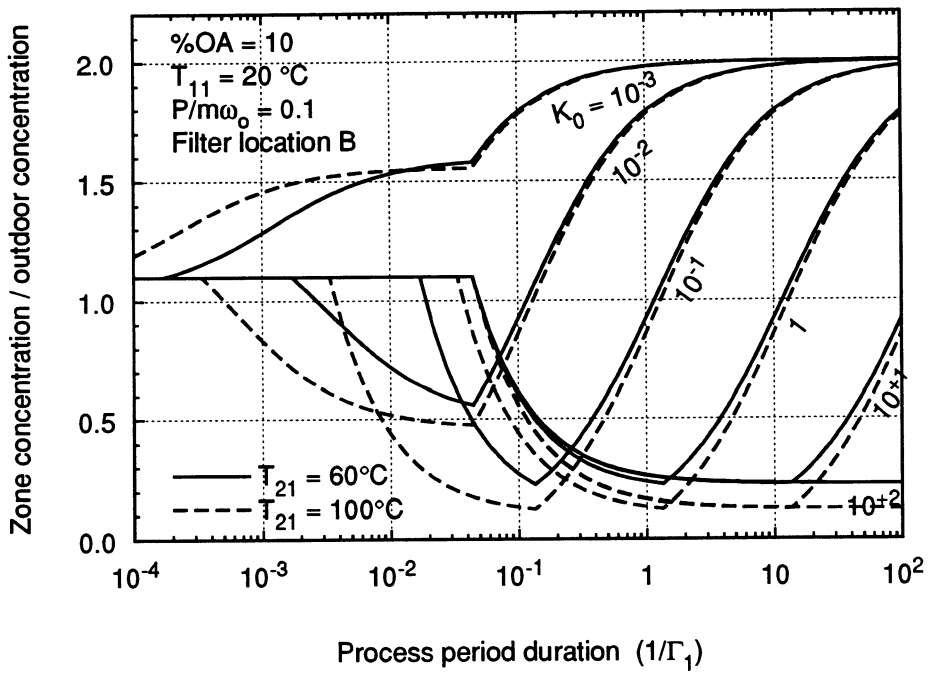

Figure 6.31 Effect of higher T_{21} on the zone concentration.

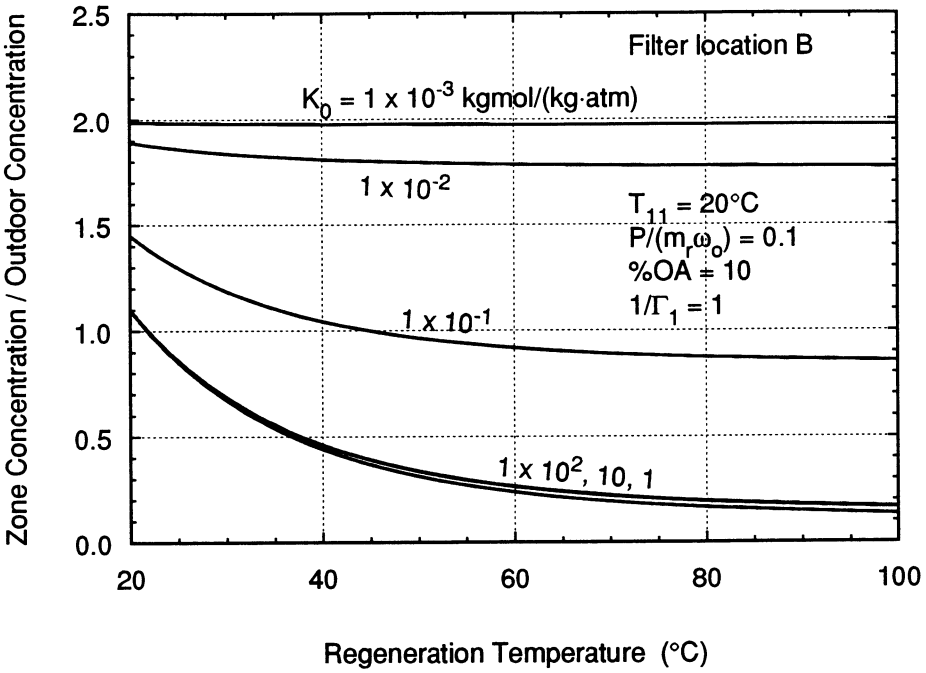

Figure 6.32 Effect of regeneration temperature on the zone concentration for a process period duration of $1/\Gamma_1 = 1$.

Figures 6.30 and 6.31 show the zone concentrations at different regeneration temperatures. Once again, the effect is analogous to the effect of the regeneration temperature on the average outlet concentration. However, since the curve for K_0=1x10^{-2} drops below $\omega_z/\omega_o = 1$, increasing the regeneration temperature reduces the zone concentration for this contaminant. Figure 6.32 shows the effect of regeneration temperature on the zone concentrations at a process period duration of $1/\Gamma_1 = 1$. Even at high regeneration temperatures, the filter's ability to remove contaminants with $K_0 = 1\text{x}10^{-3}$ kgmol/(kg·atm) is negligible at this particular rotation speed. The temperature effect is more pronounced for the larger K_0 values, but it is small for temperatures greater than about 60°C.

Figure 6.33 illustrates the effect of increasing the pollutant generation rate to 0.6. Without a filter, this corresponds to a zone to outdoor concentration ratio of 7.0 at 10%

outdoor air and 1.6 at 100% outdoor air. The fast rotation speed (low $1/\Gamma_1$) zone concentration has therefore changed from 1.0 to 1.6 and the limiting slow rotation speed (high $1/\Gamma_1$) zone concentration has changed from 2.0 to 7.0. The curve for K_0=1x10^{-2} has moved above the line of $\omega_z/\omega_o = 1$ because the generation rate is large enough that system steady-state is reached before ω_{11} decreases to a point at which the intermediate concentration drops below the outdoor concentration. For the other K_0 curves, the effect of the increase in pollutant generation rate is to shift the curves upward and stretch them in the vertical direction.

Figure 6.34 illustrates the effect of increasing the percent of outdoor air. The bottom of the curves remain fixed while they are vertically compressed. The fast rotation speed zone concentration is equal to the zone concentration obtained with no filter at 100% outdoor air and is thus independent of the percent of outdoor air. The limiting value on the upper right side of the graph, however, is equal to the zone concentration obtained with no filter at the given percent of outdoor air, and thus as the amount of outdoor air increases, the limiting value decreases.

The actual conditions that a filter would see are much more complicated than assumed in this analysis. Each contaminant would be generated at a different rate, which would most likely not be constant. The heat of adsorption would be different for different contaminants. Finite heat and mass transfer coefficients would smear the wave fronts.

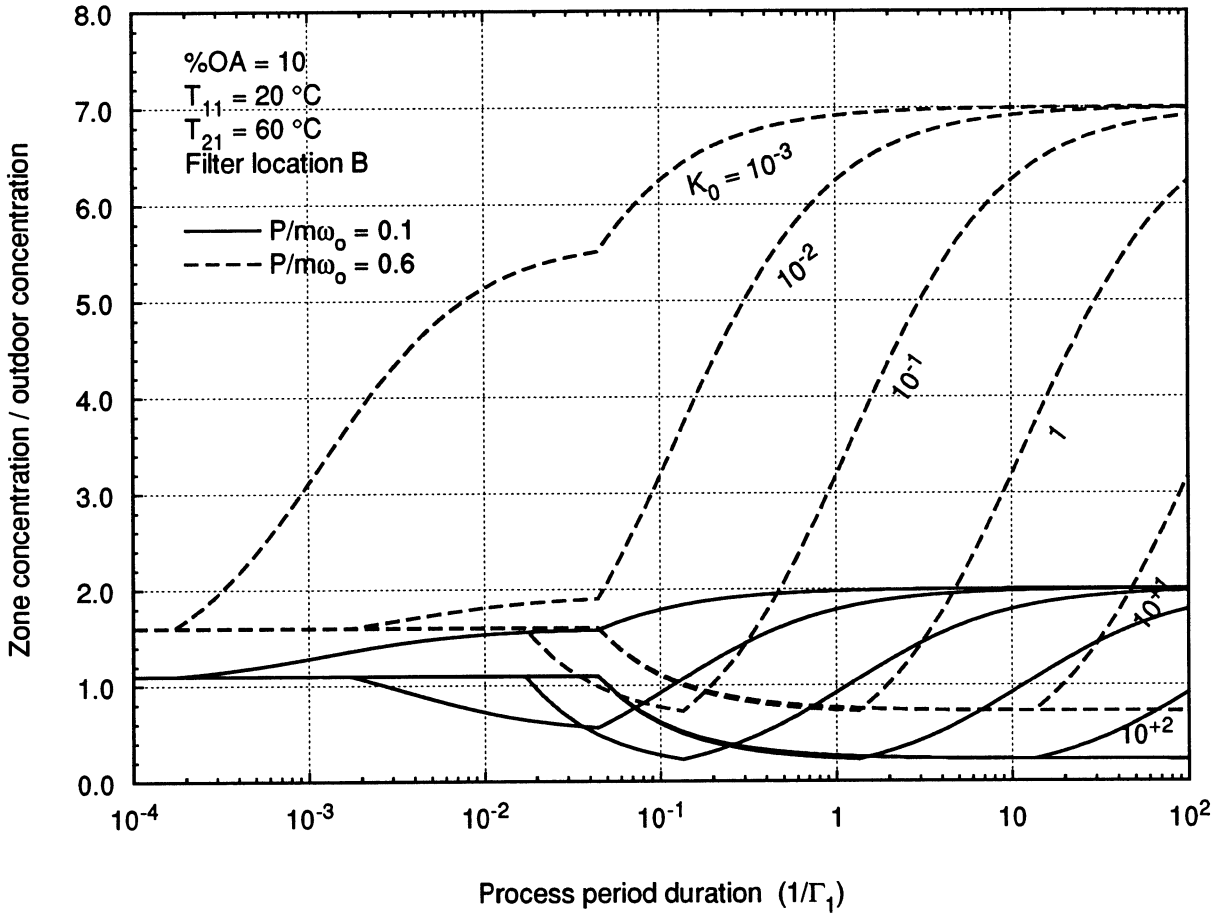

Figure 6.33 Zone concentration at different pollutant generation rates.

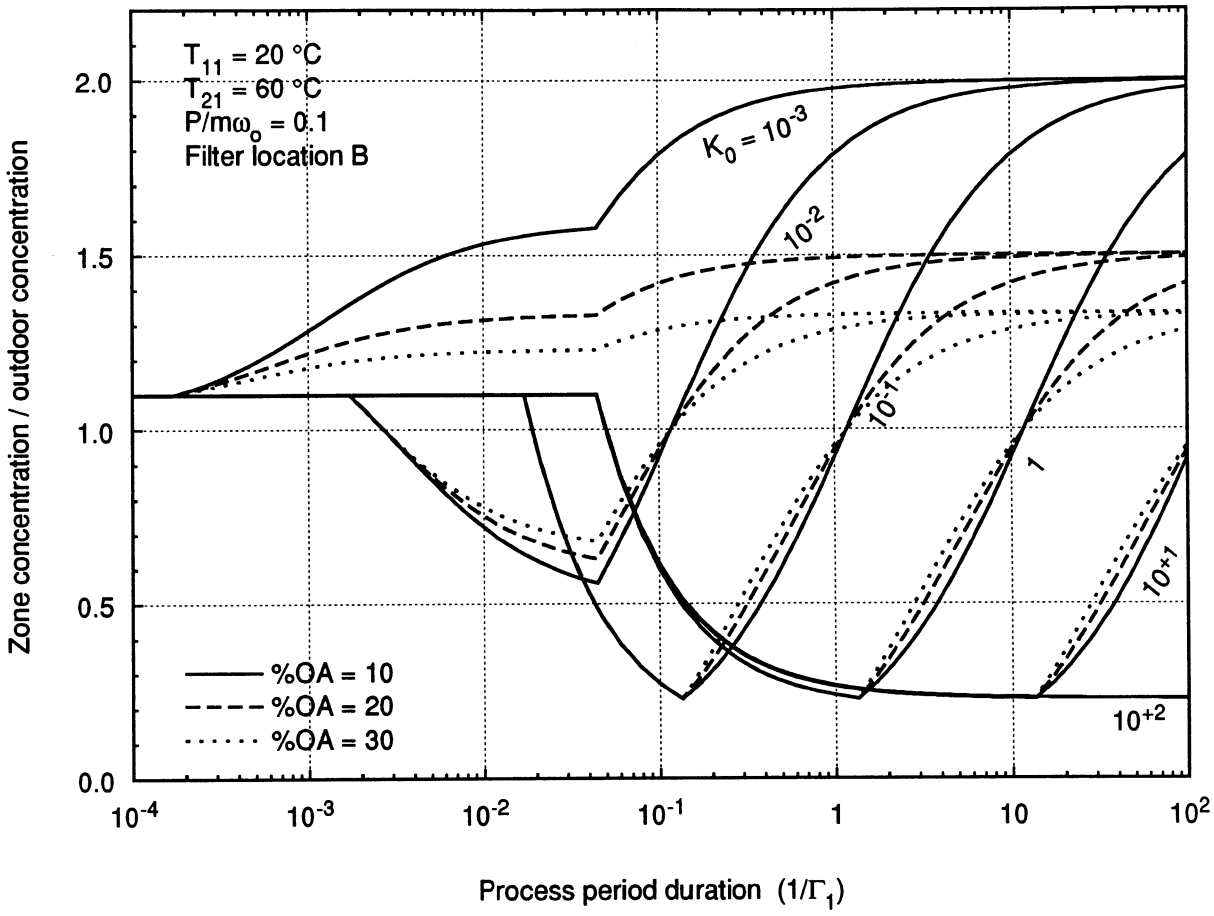

Figure 6.34 Zone concentration at different amounts of outdoor air.

6.4 Effect of finite transfer coefficients

The equilibrium (infinite transfer coefficient) solutions presented in this chapter represent an ideal case. As such, some behavior results which is non-intuitive, e.g., the infinite concentration pulse of zero width for the Case 2 regeneration side analysis. With finite transfer coefficients, the sharp edges of the waves become smeared. The infinite pulse becomes a finite, sinusoidal-type pulse. The region of zero concentration becomes a region of very low concentration.

If what the equilibrium solution represents is unrealistic, then why was it studied? The answer is that it provides insight into the behavior of the adsorption filter. The simpler solution makes it easier to examine the effect of different variables and parameters. In addition, since the finite transfer coefficient solution must be computer numerically, knowledge of the equilibrium solution can indicate potential problem areas which may arise in the numerical solution of the finite transfer coefficient equations.

A finite difference computer program, MOSHMX, for analyzing the steady-state performance of rotary regenerative desiccant wheels with finite transfer coefficients was developed by Maclaine-Cross [127]. It has been used by researchers studying desiccant dehumidifiers [1, 132, 159, 242]. Several modifications were made to MOSHMX so that it could be used for the analysis of rotary regenerative adsorption filters. These modifications, a brief description of the program, and some example runs are included in Appendix B. Problems with convergence and with the step size estimation were encountered when trying to use MOSHMX for Case 2 contaminants. More work is needed in order to apply MOSHMX successfully over the entire range of pollutants.

6.5 Filter sizing

Once the operating value of $1/\Gamma_1$ has been selected, a rough estimate of the wheel "size" can be determined. Because this estimate is based on the equilibrium solution, it represents a minimum wheel size. To actually design a filter, an analysis based on finite transfer coefficients would be required, and the actual wheel would be larger. This estimate based on the equilibrium solution is used merely to give a feel for the wheel size. Starting with the definition of $1/\Gamma_1$ in Equation 4.3.10, the quantities in the equation can be calculated as follows:

$$m_m = \frac{1}{2}\hat{\rho}_c \phi_1 r^2 \tag{6.5.1}$$

$$\theta_1 = \frac{\phi_1}{\left(\frac{2\pi}{60}\right)(\text{rpm})} \tag{6.5.2}$$

$$\dot{n}_{air} = \tilde{\rho}_{air} Q \tag{6.5.3}$$

Substituting into Equation 4.3.10, and solving for the required wheel rotation speed in rpm:

$$(\text{rpm}) = \frac{60\tilde{\rho}_{air} Q}{\pi \hat{\rho}_c \left(\frac{1}{\Gamma_1}\right)} \frac{1}{Lr^2} \tag{6.5.4}$$

The percentage of the wheel designated for processing can be found from the ratio of $1/\Gamma_1$ to $1/\Gamma_2$:

$$\frac{\phi_1}{\phi_2} = \frac{v_{air,2}\left(\frac{1}{\Gamma_1}\right)}{v_{air,1}\left(\frac{1}{\Gamma_2}\right)} \tag{6.5.5}$$

For a wheel 0.15 m (0.5 ft) thick, operating at rotation speed of one revolution per hour, and taking $\hat{\rho}_c = 480$ kg/m^3 (30 lbm/ft^3) [243] and $\tilde{\rho}_{air} = 0.0409$ kgmol/m^3 (0.00256 lbmol/ft^3), Figure 6.35 illustrates the required wheel radius for several values of $1/\Gamma_1$. $\hat{\rho}_c$ is the apparent density of a packed granular activated carbon bed.

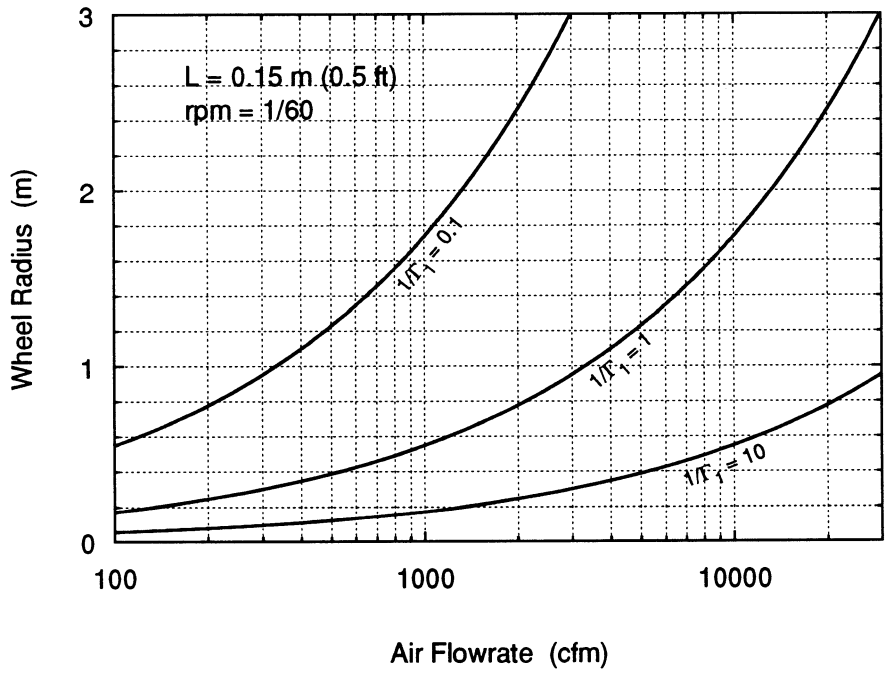

Figure 6.35 Example of wheel sizing given the dimensionless process period duration and the air flowrate.

6.6 Example calculation

Suppose that one wished to add a rotary regenerative carbon filter at location B of an existing system to lower the indoor concentration of a contaminant with $K_0 = 1$ kgmol/(kg·atm). The current indoor concentration of the contaminant is twice that of outdoors, the system operates at 10% outdoor air, and the total air flowrate is 3000 cfm (5100 m^3/hr). From Figure 6.21, the dimensionless pollutant generation rate is equal to 0.1. At these conditions, if the amount of outdoor air were increased to 100% the zone concentration would be reduced to 1.1 times the outdoor concentration.

Assuming the parameter values listed in Table 4.6, and an air temperature of 20°C entering the filter, the $K_0 = 1$ kgmol/(kg·atm) curve in Figure 6.22 shows the zone to outdoor concentration as a function of process period duration for a regeneration temperature of 60°C. Operating at $1/\Gamma_1 = 1$ will give near optimal performance for the specified contaminant. The zone concentration would be reduced to 0.238 times the outdoor concentration, which is between 1/5 and 1/4 of the zone concentration that could be achieved with no filter at 100% outdoor air. The $K_0 = 1$ kgmol/(kg·atm) curve in Figure 6.32 illustrates the effect of regeneration temperature. If the regeneration temperature were 40°C instead of 60°C, the zone concentration would increase to 0.324 times the outdoor concentration. For a 0.15 m (0.5 ft) thick wheel with a rotation speed of one revolution per hour, the required wheel radius, from Figure 6.35, is 0.954 m (3.13 ft). For comparison with the fixed bed filters, using the bulk density of carbon given in Section 6.5, and at a flowrate of 3000 cfm, the wheel consists of 150 lb carbon/1000 cfm. By rotating the wheel at a faster speed, a smaller wheel radius is required. If the filter had been placed at location A instead of B, the air flowrate through the filter would be only 2700 cfm (4590 m^3/hr), and the required wheel radius would be reduced to 0.902 m

(2.96 ft).

For a more complex example, consider the design of a filter to remove the five VOCs listed in Table 2.8. Assume that the HVAC system operates at 10% outdoor air and that all five contaminants are generated at the same rate, a rate such that the indoor concentration of each contaminant is equal to 3 times the outdoor concentration with no filter. Assume that the isotherm slopes are equal to the values given in Table 2.8. Values of the heat of adsorption for methane, acetylene, ethane, and acetone from various references are listed in Table 2.2. Average values of Δh_s for these four contaminants were plotted versus molecular weight, shown in Figure 6.36. The results of a least-squares linear curve fit are also shown in the figure. From this curve-fit, the heat of adsorption of acetaldehyde is estimated as 11 kcal/gmol. The isotherm slopes (K_0 values) and heats of adsorption for the five contaminants are summarized in Table 6.3.

Table 6.3 Five pollutants, their estimated isotherm slopes and heats of adsorption.

		Mol. Wt.	K_0 [kgmol/(kg·atm)]	Δh_s [kcal/gmol]
methane	CH_4	16.043	1.87×10^{-3}	4.8
acetylene	C_2H_2	26.038	2.39×10^{-2}	7.0
ethane	C_2H_6	30.070	9.06×10^{-2}	6.7
acetaldehyde	CH_3CHO	44.054	2.91	11
acetone	CH_3COCH_3	58.080	1.88×10^{1}	14

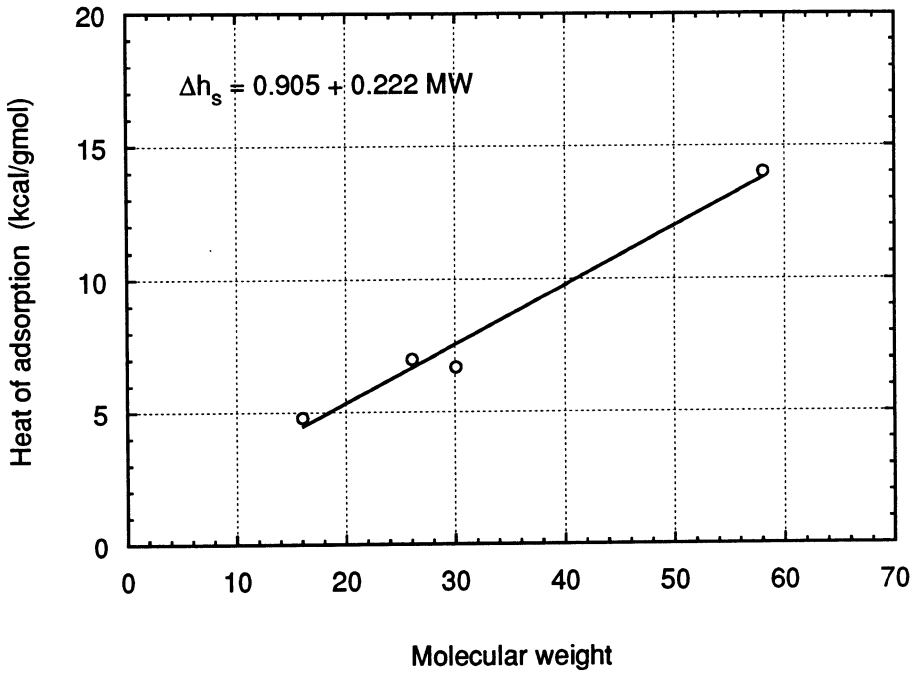

Figure 6.36 Heat of adsorption plotted versus molecular weight.

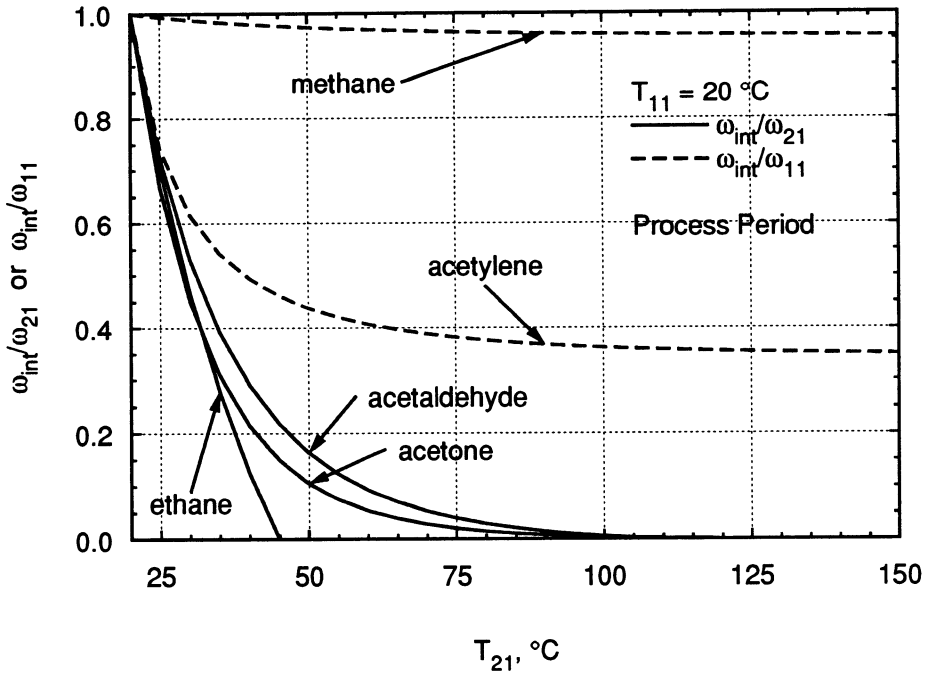

Figure 6.37 Intermediate concentration of the five contaminants versus regeneration temperature.

For a process temperature of 20°C, Figure 6.37 shows the intermediate concentration for the five contaminants as a function of regeneration temperature. Methane and acetylene are Case 3 contaminants, ethane is Case 1 below about 45°C and Case 2 above this temperature. Acetaldehyde and acetone are Case 1 contaminants. The most significant reductions in the intermediate temperature occur below about 60°C, and thus 60°C appears to be an appropriate regeneration temperature, not considering heat and mass transfer effects.

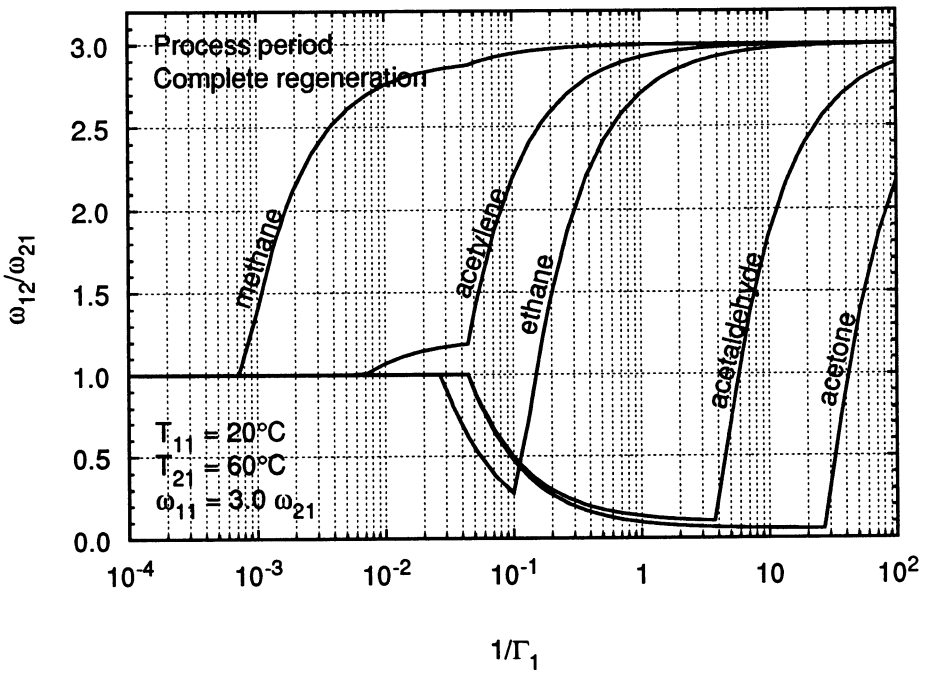

Figure 6.38 Process average outlet concentration for the five contaminants.

Figure 6.38 shows the process period average outlet concentration for the five pollutants at a regeneration temperature of 60°C. Figure 6.39 shows the zone concentration of the five pollutants at the specified conditions and a regeneration temperature of 60°C. To achieve any significant reduction in the concentration of methane, the wheel would have to be rotated quickly, i.e., at $1/\Gamma_1 \leq 10^{-2}$. To reduce the

concentrations of the other four contaminants, operating at $1/\Gamma_1 = 10^{-1}$ will reduce the zone concentrations for all four contaminants below the zone concentrations which could be obtained with 100% outdoor air and no filter. If the pollutants acetaldehyde and acetone were of particular concern, and it was not as important to reduce the concentration of the other three pollutants, then operation at $1/\Gamma_1 = 1$ would achieve near minimum possible zone concentrations, while still somewhat reducing the concentration of acetylene and ethane. Table 6.4 lists the five pollutants and the concentration reduction relative to that obtained with no filter at 10% outdoor air and 100% outdoor air.

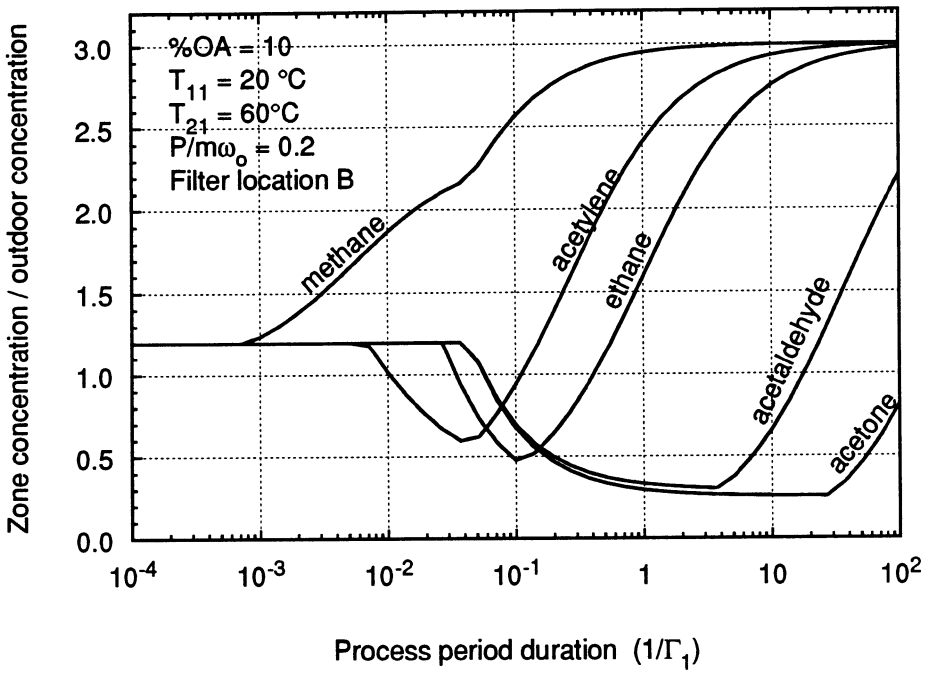

Figure 6.39 Zone concentration for the five contaminants.

All of the above calculations were based on the assumption of infinite heat and mass transfer coefficients, and as such only represent a "best possible" estimation of the filter performance. For a real system, where the transfer coefficients are finite, higher regeneration temperatures and a larger filter wheel would be required.

Table 6.4 Zone concentrations for the five pollutants at two different wheel rotation speeds.

	$1/\Gamma_1 = 10^{-1}$			$1/\Gamma_1 = 1$		
	$\frac{\omega_{z,\text{ filter, 10\% OA}}}{\omega_o}$	$\frac{\omega_{z,\text{ filter, 10\% OA}}}{\omega_{z,\text{ no filter, 10\% OA}}}$	$\frac{\omega_{z,\text{ filter, 10\% OA}}}{\omega_{z,\text{ no filter, 100\% OA}}}$	$\frac{\omega_{z,\text{ filter, 10\% OA}}}{\omega_o}$	$\frac{\omega_{z,\text{ filter, 10\% OA}}}{\omega_{z,\text{ no filter, 10\% OA}}}$	$\frac{\omega_{z,\text{ filter, 10\% OA}}}{\omega_{z,\text{ no filter, 100\% OA}}}$
methane	2.5630	0.85	2.14	2.9488	0.98	2.46
acetylene	0.9357	0.31	0.78	2.4065	0.80	2.01
ethane	0.4760	0.16	0.40	1.5919	0.53	1.33
acetaldehyde	0.6975	0.23	0.58	0.3338	0.11	0.28
acetone	0.6758	0.23	0.56	0.2964	0.10	0.25

Chapter 7

Conclusions and Recommendations

The task of designing an adsorption filter for indoor air quality control is, at present, sort of a "chicken-and-egg" problem. Much of the experimental data (e.g., adsorption isotherms, mass transfer coefficients, etc.) needed for design does not exist. Yet without first determining whether the concept is even feasible, there is no point in gathering the tremendous amount of experimental data necessary. The goal of this project, therefore, was to attempt to determine, without detailed information about the adsorption process, if the concept of a rotary regenerative carbon filter for indoor air quality control could be successful, and also to determine what adsorption characteristics are required for the design to be feasible.

A review of the indoor air quality literature revealed that at the present time, the causes and the exact nature of indoor air quality problems are not yet established. Pollutant identities and "safe" concentration levels are often unknown. Measured concentrations of specific contaminants vary, although typically they are in the low ppb range. Volatile organic compounds (VOCs) are a group of pollutants which are often removed from air by adsorption on activated carbon fixed-bed filters. The number of individual VOCs present in indoor air is often greater than 100, and varies from building to building.

Adsorption properties for the different contaminants (even known contaminants) are virtually non-existent in the low ppb range. This lack of data includes adsorption isotherms, heats of adsorption, the effect of multiple simultaneously adsorbing components, and the effect of water vapor on the adsorption. Research has been done at

higher concentrations, but the ability to extrapolate the results to the very low indoor air quality concentrations is questionable. In light of the lack of adsorption data and the uncertainties in the pollutant identities, the design was carried out by considering all contaminants as obeying a linear isotherm with temperature dependence governed by the Clausius-Clapeyron equation, and neglecting any interference effects. Both of these assumptions theoretically would be true at low enough concentrations. Examination of existing low concentration isotherm data suggested that the range of isotherm slopes for different VOCs on activated carbon varies widely, from $K_0=1x10^{-3}$ kgmol/(kg·atm) to $1x10^{2}$ kgmol/(kg·atm) and possibly larger.

A review of the commercial activated carbon air filter industry revealed that the filters, which are typically thin fixed-bed filters, are sized simply based on the pounds of carbon per cfm. Predictions or estimates of filter lifetime are not supplied by the manufacturers, and determination of the carbon filter's ability to remove different contaminants is based on a list which rates contaminants on a scale of 1 to 4. Calculations show that for many pollutants, the useful lifetime of the fixed-bed carbon filters used in HVAC systems is short. A study of other applications in which activated carbon has been used for removing pollutants from air revealed two trends: more carbon per cfm of air flow is used in other applications, and useful lifetimes were often short.

Some initial conclusions are as follows:

- Design of an adsorbent filter for indoor air quality control is difficult because the problem is not well-defined. The indoor air quality problem is not yet understood or quantified. Also, basic adsorption data is lacking in the low concentration range.

- Based on the literature review, activated carbon is the best adsorbent for removing VOCs.
- Thin fixed-bed activated carbon filters such as currently used in HVAC applications do not effectively remove VOCs.

Model equations were developed and attention was focused on solving the equilibrium (infinite transfer coefficient) equations. By making appropriate assumptions, the solution to the mass and energy equations in the low concentration region with a linear isotherm becomes algebraically simple. This low concentration linear isotherm solution consists of two or three discontinuities which propagate through the matrix. The effect of the low concentration assumption was shown to be negligible in the ppm range and below. The approach used to solve the equations helped to indicate areas of the solution in which somewhat unexpected behavior occurs.

The filter outlet concentration during the process period was shown to consist of at most three different concentrations: the regeneration inlet concentration, the process inlet concentration, and an intermediate concentration. For some contaminants, under the appropriate conditions, the intermediate value is equal to zero. Graphs illustrating the effect of different parameters and variables on the intermediate concentration, the process period average outlet concentration, and the pollutant zone concentration, assuming perfect mixing in the zone and a constant pollutant generation rate, were presented. Some specific conclusions are as follows:

- By making appropriate assumptions, the equilibrium solution of the model equations can be reduced to an algebraically simple form which facilitates the filter design.

- Based on the equilibrium solution and considering the entire system and the cost of heating the regeneration air stream, there will be an optimum regeneration temperature since the rate of concentration reduction decreases with increasing temperature. Higher temperatures, however, increase the rate of mass transfer, so that higher regeneration temperatures than indicated by the equilibrium solution would be advantageous.
- The specific heat ratio (c_m/c_{air}) should be minimized. Assuming that the specific heat of air is constant, it is necessary to minimize the specific heat of the matrix and any supports, etc. which affect the heat transfer.
- Two filter locations were examined, in the return air duct (filter location A) and in the supply air duct (filter location B). The filter in the supply air duct reduces the steady-state zone concentration more than the filter in the return air duct, but requires more air to be processed.
- By operating the wheel at slow enough rotation speeds ($1/\Gamma_1 \geq 1$), the increase in temperature through the filter is small and would not significantly affect the heating and cooling requirements for the air.
- Assuming that isotherm slope correlates at least approximately with molecular weight, for many of the indoor air VOCs the rotary regenerative carbon filter design looks promising. For example, the molecular weights of 25 VOCs identified by Grot et al. [6] in an indoor air quality study were between 50 and 200 kg/kgmol. The molecular weight of acetone is 58.08 and the estimated isotherm slope for acetone used in this study was $K_0=1.88\text{x}10^1$ kgmol/(kg·atm).

Thus many indoor air VOCs may have K_0 values greater than $1x10^1$, and in this range of K_0 values, the concentration reduction capacity of the rotary filter is excellent.

In the course of this project, many areas for future study have been identified. Basic experimental work on measuring and quantifying the adsorption properties and characteristics of VOCs in the low concentration range is necessary. Almost no experimental adsorption data of any type exist in the low ppb range. Isotherms as a function of temperature and interference effects from multiple simultaneous adsorbing species are two particular areas. Another issue is whether or not the carbon can be regenerated to its original capacity; experimental data taken by a co-worker [241] has indicated that acetone does not completely desorb, and that there is a continual decline in the adsorptive capacity of the carbon.

The effect of water vapor is a very important issue. Water vapor is always present in indoor air. Although the general rule-of-thumb is that water vapor does not affect VOC adsorption on activated carbon below 50% relative humidity, further investigation is necessary, particularly since both Werner [111] and Nelson et al. [112] have observed that the effect of water vapor is more pronounced at lower VOC concentrations.

Experimental work is needed to verify the modeling results. However, until the adsorption property data is known (e.g., isotherms), such experiments could only provide qualitative validation. Experimental testing of the lifetime of some commercial fixed-bed filters by monitoring the upstream and downstream concentrations would be interesting.

If interference effects are found to be significant, then models which take into account these effects must be considered and the impact on the filter design assessed. Another area of modeling which was not considered as part of this project is the transient

operation of the rotary regenerative carbon filter. The filter was always assumed to be operating at steady-state. Since pollutant levels are not constant, the transient operation is of interest. Brandemuehl [159] has studied the transient operation of desiccant wheels for air conditioning applications.

A non-equilibrium (finite transfer coefficient) model capable of handling the Case 2 intermediate concentration regions identified in the equilibrium analysis needs to be developed. Using the equilibrium and the non-equilibrium modeling results, it may be possible to develop ε-NTU type correlations.

From a design point of view, there are a large number of different configurations and operating conditions which can be explored. For example, what is the effect of multiple filter wheels in series, possibly rotated at different speeds or regenerated at different temperatures? What happens if the regeneration temperature is varied throughout the regeneration period?

As a step towards practical implementation and design, some sort of "VOC-activated carbon" meter which could provide a link between an actual sample of indoor air and the filter design, bypassing a detailed identification of all the contaminants, would be extremely useful. For example, in elution chromatography, a pulse of a mixture is introduced into a chromatograph. The time that it takes the different components of the mixture to move through the chromatograph is proportional to the isotherm slope. There is likely to be a way to take the output from a chromatographic analysis of an indoor air quality sample and then base the filter design on this output, without identifying and quantifying each individual component.

Appendix A

EQSOL2A.C

```
#include <stdio.h>
#include <stdlib.h>
#include <math.h>

/* Function declarations */

void output();


/* Global variable declarations */

double xh0p, xm0p[2], xhfp, xmfp[2], invgp, gammap, thfp, tmfp[2];
double xh0r, xm0r[2], xhfr, xmfr[2], invgr, gammar, thfr, tmfr[2];
double sigma, k[2], kalt[2], kp, kr, tp, tr, t0, dhs, r, p, k0, invs;
double xintp[2], tintp[2], xintr[2], tintr[2], tm0p[2], tm0r[2], th0p, th0r;
double tch0p, tcm0p[2], tchfp, tcmfp[2], tch0r, tcm0r[2], tchfr, tcmfr[2];
double tcintp[2], tcintr[2], invgtot, xb[4], tb[4], xintpm, tintpm;
int flagp[2], flagr[2], iter, j, i, nwave, iflag[2];

FILE *out;
FILE *frame;

main ()
{
  out = fopen("eqdat2a.dat", "w");
  frame = fopen("eqbox2a.dat", "w");

/* These are various quantities used throughout: */

  iflag[0] = 0; iflag[1] = 0;
  sigma = 1300./29163.;
  p = 1.;
  dhs = 41860000.;
  r = 8314.4;
  t0 = 25. + 273.15;
  k0 = 1.0e-01;

  tp = 10. + 273.15;
  tr = 20. + 273.15;
  kp = k0 * p * exp(dhs/r*(1/tp-1/t0));
  kr = k0 * p * exp(dhs/r*(1/tr-1/t0));

/* The regeneration temperature must be greater than or equal to the
   process temperature; if not, stop the program: */

  if (kr >= kp) {
     printf("\n Tr must be greater than Tp\n\n");
     exit(1);
     }
```

```
/* This determines the number of possible mass waves: */

  if ((kp <= sigma && kr <= sigma) || (kp >= sigma && kr >= sigma))
     nwave = 1;
  else
     nwave = 2;

/* Here are some more definitions: */

  invs = 1.0/sigma;
  invgp = kp * 3.0 / 4.0;
  invgr = sigma * 1.2;
  invgtot = invgp + invgr;

/* These are the initial conditions: */

  xh0p = 0.0; th0p = 0.0;
  for (i=0; i<nwave; i++) {
     xm0p[i] = 0.0; tm0p[i] = 0.0;
     }

  for (iter = 0; iter <= 100; iter++) {

/* This is the position of the heat wave at the end of the process
   period: */

     xhfp = (double)min( invs*invgp + xh0p, 1.0 );
     thfp = (double)min( sigma*(1.0-xh0p), invgp );

/* For the mass wave, determine which wavespeed is appropriate
   (depending on which side of the heat wave it is on): */

     if (nwave == 1) {
        if (xm0p[0] < xh0p) {
           k[0] = kp;
           kalt[0] = kr;
           }
        else if (xm0p[0] > xh0p) {
           k[0] = kr;
           kalt[0] = kp;
           }
        else {
           if (kr > sigma && kp > sigma) {
              k[0] = kp;
              kalt[0] = kr;
              }
           else if (kr < sigma && kp < sigma) {
              k[0] = kr;
              kalt[0] = kp;
              }
           else {
              printf("Error: there should be two mass waves\n");
              }
           }
        }
     else {
        if (xm0p[0] > xh0p) xm0p[0] = xh0p;
        if (xm0p[1] < xh0p) xm0p[1] = xh0p;
        k[0] = kp;
        kalt[0] = 0.0;
```

```
        k[1] = kr;
        kalt[1] = 0.0;
        }

/* Determine the point at which the mass and heat waves intersect: */
      for (i=0; i<nwave; i++) {
         xintp[i] = (k[i] * xm0p[i] - sigma * xh0p) / (k[i] - sigma);
         tintp[i] = (xm0p[i] - xh0p) / (invs - 1.0/k[i]);
         }
      if (nwave==2) {
         xintpm = (k[1]*xm0p[1] - k[0]*xm0p[0]) / (k[1] - k[0]);
         tintpm = (xm0p[1] - xm0p[0]) / (1.0/k[0] - 1.0/k[1]);
         if (xintpm > 0.0 && xintpm < 1.0 && tintpm > 0.0 && tintpm < invgp) {
            printf("\n Mass waves intersect - this is not OK\n\n");
            exit(1);
            }
         }

      for (i=0; i<nwave; i++) {

/* If the intersection point is within the process period, then compute
   the final position of the mass wave from the intersection point: */

         if (xintp[i] > 0.0 && xintp[i] < 1.0 && tintp[i] > 0.0 && tintp[i] < invgp) {
            if (nwave == 2) {
               printf("\n Should not have a p int pt !\n\n");
               exit(1);
               }
            flagp[i] = 1;
            xmfp[i] = (double)min( 1.0/kalt[i]*(invgp-tintp[i]) + xintp[i], 1.0 );
            tmfp[i] = (double)min( kalt[i]*(1.0-xintp[i]) + tintp[i], invgp );
            }

/* Otherwise, compute the final position of the mass wave based on the
   starting point */

         else {
            flagp[i] = 0;
            xmfp[i] = (double)min( 1.0/k[i] * invgp + xm0p[i], 1.0 );
            tmfp[i] = (double)min( k[i] * (1.0-xm0p[i]), invgp );
            }
         }

/*  ---------- Regeneration Period ---------- */

/* Now, set up for the regeneration period: */

      xh0r = xhfp; th0r = 0.0;
      for (i=0; i<nwave; i++) {
         xm0r[i] = xmfp[i];
         tm0r[i] = 0.0;
         }

/* This is the position of the heat wave at the end of the regen period: */

      xhfr = (double)max( -invs*invgr + xh0r, 0.0 );
      thfr = (double)min( -sigma*(0.0-xh0r), invgr );

/* For the mass wave, determine which wavespeed is appropriate
   (depending on which side of the heat wave it is on) */
```

```
      if (nwave == 1) {
         if (xm0r[0] < xh0r) {
            k[0] = kp;
            kalt[0] = kr;
            }
         else if (xm0r[0] > xh0r) {
            k[0] = kr;
            kalt[0] = kp;
            }
         else {
            if (kp > sigma && kr > sigma) {
               k[0] = kr;
               kalt[0] = kp;
               }
            else if (kp < sigma && kr < sigma) {
               k[0] = kp;
               kalt[0] = kr;
               }
            else {
               printf("Trouble with the number of waves\n");
               exit(1);
               }
            }
         }
      else {
         for (i=0; i<nwave; i++) {
            if (xm0r[i] < xh0r) {
               k[i] = kp;
               kalt[i] = sigma;
               }
            else if (xm0r[i] > xh0r) {
               k[i] = kr;
               kalt[i] = sigma;
               }
            else {
               k[i] = sigma;
               kalt[i] = sigma;
               iflag[i] = 1;
               }
            }
         }

/* Determine the point at which the mass and heat wave intersect: */

      for (i=0; i<nwave; i++) {
         if (iflag[i] == 1) {
            iflag[i] = 0;
            xintr[i] = -1.0;
            tintr[i] = -1.0;
            break;
            }
         xintr[i] = (-k[i]*xm0r[i] - (-sigma)*xh0r) / (-k[i] - (-sigma));
         tintr[i] = (xm0r[i] - xh0r) / (-invs - 1.0/(-k[i]));
         }

/* If the intersection point is within the regen period, then compute
   the final position of the mass wave from the intersection point: */
```

```
      for (i=0; i<nwave; i++) {
         if (xintr[i] > 0.0 && xintr[i] < 1.0 && tintr[i] > 0.0 && tintr[i] < invgr) {
            flagr[i] = 1;
            xmfr[i] = (double)max( -1.0/kalt[i]*(invgr-tintr[i]) + xintr[i], 0.0 );
            tmfr[i] = (double)min( -kalt[i]*(0.0-xintr[i]) + tintr[i], invgr );
            }

/* Otherwise, compute the final position of the mass wave based on the
   starting point: */

         else {
            flagr[i] = 0;
            xmfr[i] = (double)max( -1.0/k[i] *invgr + xm0r[i], 0.0 );
            tmfr[i] = (double)min( -k[i] * (0.0-xm0r[i]), invgr );
            }
         }

      output();

/* Check to see if more iterations are necessary: */

      if (nwave == 1) {
         if (fabs(xmfr[0]-xm0p[0]) < 1.0e-03 && fabs(xhfr-xh0p) < 1.0e-03)
            break;
         }
      else {
         if (fabs(xmfr[0]-xm0p[0]) < 1.0e-03 && fabs(xhfr-xh0p) < 1.0e-03
            && fabs(xmfr[1]-xm0p[1]) < 1.0e-03)
            break;
         }

      xm0p[0] = xmfr[0];
      xm0p[1] = xmfr[1];
      xh0p = xhfr;
   }

/* Output final results: */

   printf("\n");
   printf("1/gammap = %e\n", invgp);
   printf("1/gammar = %e\n", invgr);
   printf("kp = %e\n", kp);
   printf("kr = %e\n", kr);
   printf("sigma = %e\n\n", sigma);

   printf("heat in p start: %e %e\n", xh0p, th0p);
   printf("heat in p end:   %e %e\n", xhfp, thfp);
   printf("heat in r start: %e %e\n", xh0r, th0r);
   printf("heat in r end:   %e %e\n\n", xhfr, thfr);

   if (nwave == 1) {
      printf("mass in p start: %e %e\n", xm0p[0], tm0p[0]);
      printf("mass in p end:   %e %e\n", xmfp[0], tmfp[0]);
      printf("mass in r start: %e %e\n", xm0r[0], tm0r[0]);
      printf("mass in r end:   %e %e\n\n", xmfr[0], tmfr[0]);

      printf("p int: %e %e\n", xintp[0], tintp[0]);
      printf("r int: %e %e\n", xintr[0], tintr[0]);
      }
   else {
      printf("mass in p start: %e %e %e %e\n", xm0p[0], tm0p[0], xm0p[1], tm0p[1]);
```

```
      printf("mass in p end:   %e %e %e %e\n", xmfp[0], tmfp[0], xmfp[1], tmfp[1]);
      printf("mass in r start: %e %e %e %e\n", xm0r[0], tm0r[0], xm0r[1], tm0r[1]);
      printf("mass in r end:   %e %e %e %e\n\n", xmfr[0], tmfr[0], xmfr[1], tmfr[1]);

      printf("p int: %e %e %e %e\n", xintp[0], tintp[0], xintp[1], tintp[1]);
      printf("r int: %e %e %e %e\n\n", xintr[0], tintr[0], xintr[1], tintr[1]);
      }


/* Output wave positions for the last iteration: */

  iter = ++iter;
  output();

  fclose(out);
  fclose(frame);
}


/* Function output: prints output to a file */

void output()
{

/* Calculate cumulative times: */

  if (iter == 0) {
      tch0p = th0p; tchfp = thfp; tch0r = invgp; tchfr = tch0r + thfr;
      for (i=0; i<nwave; i++) {
         tcm0p[i] = tm0p[i]; tcmfp[i] = tmfp[i]; tcm0r[i] = invgp; tcmfr[i] = tcm0r[i] +
tmfr[i];
         tcintp[i] = tintp[i]; tcintr[i] = tch0r + tintr[i];
         }
      }
  else {
      tch0p = tch0p + invgtot;
      tchfp = tch0p + thfp;
      tch0r = tch0r + invgtot;
      tchfr = tch0r + thfr;

      for (i=0; i<nwave; i++) {
         tcm0p[i] = tcm0p[i] + invgtot;
         tcmfp[i] = tcm0p[i] + tmfp[i];
         tcm0r[i] = tcm0r[i] + invgtot;
         tcmfr[i] = tcm0r[i] + tmfr[i];
         tcintp[i] = tch0p + tintp[i];
         tcintr[i] = tch0r + tintr[i];
         }
      }

/* Output wave positions for this iteration: */

   if (nwave == 1) {
      fprintf(out, "%4d %13.5e %13.5e %13.5e %13.5e\n", iter, xh0p, tch0p, xm0p[0],
tcm0p[0]);
      if (flagp[0] == 1) fprintf(out, "%4d %13.5e %13.5e %13.5e %13.5e\n", iter, xintp[0],
tcintp[0], xintp[0], tcintp[0]);
      fprintf(out, "%4d %13.5e %13.5e %13.5e %13.5e\n", iter, xhfp, tchfp, xmfp[0],
tcmfp[0]);
      fprintf(out, "%4d %13.5e %13.5e %13.5e %13.5e\n", iter, xh0r, tch0r, xm0r[0],
tcm0r[0]);
      if (flagr[0] == 1) fprintf(out, "%4d %13.5e %13.5e %13.5e %13.5e\n", iter, xintr[0],
```

```
tcintr[0], xintr[0], tcintr[0]);
      fprintf(out, "%4d %13.5e %13.5e %13.5e %13.5e\n", iter, xhfr, tchfr, xmfr[0],
tcmfr[0]);
      }
   else {
      fprintf(out, "%4d %11.5e %11.5e %11.5e %11.5e %11.5e %11.5e\n", iter, xh0p, tch0p,
xm0p[0], tcm0p[0], xm0p[1], tcm0p[1]);
      fprintf(out, "%4d %11.5e %11.5e %11.5e %11.5e %11.5e %11.5e\n", iter, xhfp, tchfp,
xmfp[0], tcmfp[0], xmfp[1], tcmfp[1]);
      fprintf(out, "%4d %11.5e %11.5e %11.5e %11.5e %11.5e %11.5e\n", iter, xh0r, tch0r,
xm0r[0], tcm0r[0], xm0r[1], tcm0r[1]);
      if (flagr[0] == 1) fprintf(out, "%4d %11.5e %11.5e %11.5e %11.5e %11.5e %11.5e\n",
iter, xintr[0], tcintr[0], xintr[0], tcintr[0], xm0r[1], tcm0r[1]);
      if (flagr[1] == 1) fprintf(out, "%4d %11.5e %11.5e %11.5e %11.5e %11.5e %11.5e\n",
iter, xintr[1], tcintr[1], xmfr[0], tcmfr[0], xintr[1], tcintr[1]);
      fprintf(out, "%4d %11.5e %11.5e %11.5e %11.5e %11.5e %11.5e\n", iter, xhfr, tchfr,
xmfr[0], tcmfr[0], xmfr[1], tcmfr[1]);
      }

/* Output box for this iteration: */

   if (iter == 0) {
      fprintf(frame, "%13.5e %13.5e\n", 0.0, 0.0);
      xb[0] = 0.0; tb[0] = invgp;
      xb[1] = 1.0; tb[1] = invgp;
      xb[2] = 1.0; tb[2] = invgtot;
      xb[3] = 0.0; tb[3] = invgtot;
      }
   else {
      for (j=0; j<=3; j++)
         tb[j] = tb[j] + invgtot;
      }

   for (j=0; j<=3; j++)
      fprintf(frame, "%13.5e %13.5e\n", xb[j], tb[j]);

}
```

Appendix B

A computer program for estimating the steady-state performance of a rotary regenerative desiccant dehumidifier with finite heat and mass transfer coefficients was developed by Maclaine-Cross [127] in 1974. The program, called MOSHMX (Method of Solving Heat and Mass X(trans)fer), has been used and modified by various researchers, e.g., [1, 129, 132, 159, 242, 244]. In order to use the program to simulate a rotary regenerative activated carbon filter for removing trace VOCs from indoor air, several modifications were made to MOSHMX:

1. All variables and functions were converted to double precision.
2. Because MOSHMX had only been used to model desiccant dehumidifiers, the properties of water vapor were imbedded throughout the program. The numeric values were replaced by variables and inputs were added. The program consists of many subroutines, so that common blocks were added and modified, as were parameter lists.

The differential equations solved are identical to Equations 4.3.15 through 4.3.18, except for slightly different dimensionless space (ξ) and time (ζ) variables, i.e.

$$\frac{\partial W}{\partial \zeta} + \frac{\partial \omega}{\partial \xi} = 0 \tag{B.1}$$

$$\frac{\partial \omega}{\partial \xi} = \omega^* - \omega \tag{B.2}$$

$$\frac{\partial H}{\partial \zeta} + \frac{\partial h}{\partial \xi} = 0 \tag{B.3}$$

$$\frac{\partial h}{\partial \xi} = Le\ c_{air}(T - t) + h_i(\omega^* - \omega) \tag{B.4}$$

where

$$\xi = NTU_m x \tag{B.5}$$

$$\zeta = NTU_m \tau \tag{B.6}$$

and the Lewis number is introduced as

$$Le = \frac{NTU_t}{NTU_m} \tag{B.7}$$

The finite difference scheme is second-order accurate and the option exists of using Richardson extrapolation to zero grid size. For more detailed explanations and a derivation of the finite difference equations, see, for example, Maclaine-Cross [127], Klein [242], or Rau [244]. Working from Taylor series expansions of the differential equations, an expression for the fluid phase temperature and concentration at the next space node and the solid phase temperature and concentration at the next time node can be derived:

$$\begin{bmatrix} t_{j+1,k} \\ \omega_{j+1,k} \\ T_{j,k+1} \\ W_{j,k+1} \end{bmatrix} = \begin{bmatrix} t_{j-1,k} \\ \omega_{j-1,k} \\ T_{j,k-1} \\ W_{j,k-1} \end{bmatrix} + \begin{bmatrix} \frac{1}{\Delta\xi}+\frac{Le}{2} & 0 & -\frac{Le}{2} & 0 \\ 0 & \frac{1}{\Delta\xi} & 0 & \frac{1}{\Delta\zeta} \\ 0 & \frac{1}{\Delta\xi}+\frac{1}{2} & \frac{1}{2}\frac{(\partial W/\partial T)}{(\partial W/\partial \omega^*)} & \frac{-1}{2(\partial W/\partial \omega^*)} \\ \frac{1}{\Delta\xi}\left(\frac{\partial h}{\partial t}\right) & \frac{1}{\Delta\xi}\left(\frac{\partial h}{\partial \omega}\right) & \frac{1}{\Delta\zeta}\left(\frac{\partial H}{\partial T}\right) & \frac{1}{\Delta\zeta}\left(\frac{\partial H}{\partial W}\right) \end{bmatrix}^{-1} \begin{bmatrix} Le(T_{j,k-1}-t_{j-1,k}) \\ 0 \\ \omega^*_{j,k-1}-\omega_{j-1,k} \\ 0 \end{bmatrix} \qquad \text{(B.8)}$$

where j and k indicate the node number in the space and time direction respectively. The values of the temperature and concentration at the current node (j,k) are calculated as averages:

$$t_{j,k} = \frac{1}{2}(t_{j+1,k} + t_{j-1,k}) \tag{B.9}$$

$$\omega_{j,k} = \frac{1}{2}(\omega_{j+1,k} + \omega_{j-1,k}) \tag{B.10}$$

$$T_{j,k} = \frac{1}{2}(T_{j,k+1} + T_{j,k-1}) \tag{B.11}$$

$$W_{j,k} = \frac{1}{2}(W_{j,k+1} + W_{j,k-1}) \tag{B.12}$$

The coefficients of the 4 x 4 matrix in Equation B.8 depend on the temperatures and concentrations, and the equations are solved twice for each step. The first time the coefficients are calculated using the inlet quantities, and the second time the coefficients are evaluated at the temperatures and concentrations calculated from the first iteration. The calculations proceed through the process period, and the values at the end of the process period are used as the starting values for the regeneration period. A combination of two different iteration techniques is used to reach the steady-state values.

Three different step sizes are used in MOSHMX, one space step, $\Delta\xi$, and two time steps, $\Delta\zeta_1$ and $\Delta\zeta_2$, where $\Delta\zeta_1 < \Delta\zeta_2$. For the desiccant systems previously modeled, one of the waves (corresponding to the thermal wave in this work) was significantly faster than the other wave, so that a smaller time step ($\Delta\zeta_1$) was required to accurately model the initial portion of each period. The larger time step was used for the remainder of the

period. There are N_m space steps, N_{nf} small time steps, and N_{f2} large time steps. The number of steps is calculated automatically within MOSHMX, based on analysis by Maclaine-Cross [127], or alternatively, the number of steps can be input by the user.

In the past, MOSHMX has always been used to model desiccant dehumidifiers, which are in the Case 3 region. Although MOSHMX solves Case 1 and Case 3 contaminant problems for the rotary filter, problems were encountered with convergence and step size estimation when trying to run MOSHMX for Case 2 contaminants. As a result, no finite transfer coefficient solutions for the Case 2 region were obtained. Further modifications in order to accommodate the nature of the Case 2 solution are required, and these modifications represent an area of future work.

As an example of the output from MOSHMX, Figure B.1 illustrates the outlet concentration as a function of time for a Case 3 contaminant at different *NTU* values and Figure B.2 shows the corresponding outlet temperature. The equilibrium solution is indicated on the graphs by the line labeled $NTU = \infty$. The parameter values for this run were chosen so that both waves could be illustrated on the same plot (i.e., the waves are relatively close together). The smaller the value of the *NTU*, the more the waves are spread relative to the equilibrium solution. In the limit as *NTU* becomes large, the solution approaches the equilibrium solution.

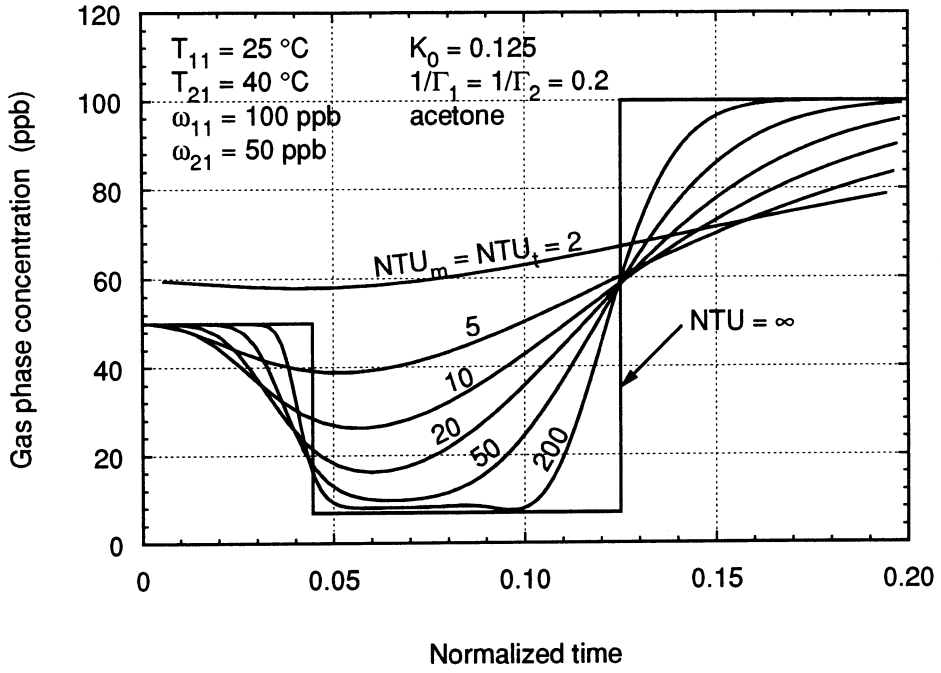

Figure B.1 Outlet concentration profile as a function of normalized time as computed by MOSHMX.

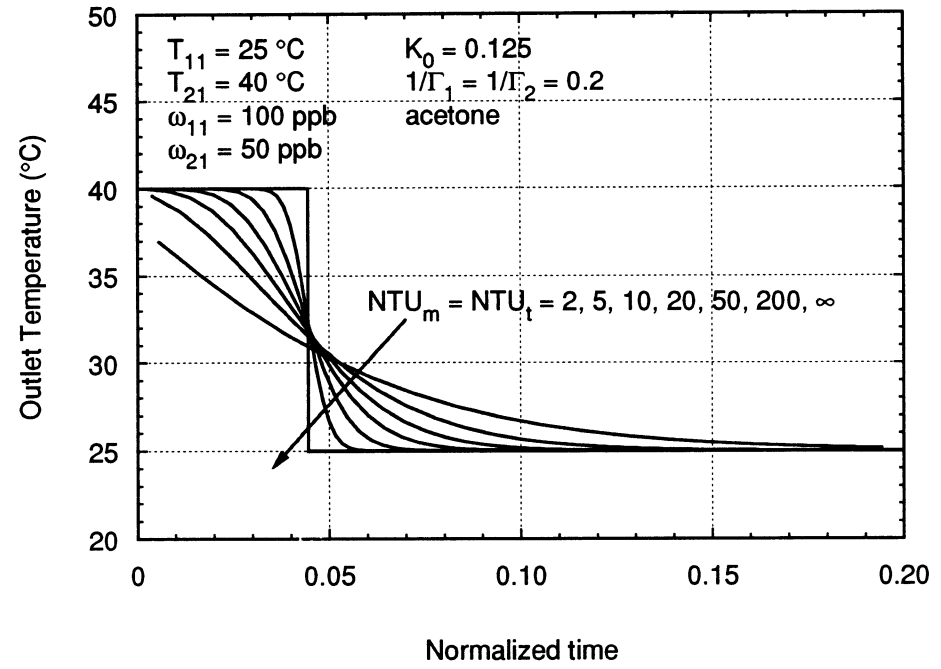

Figure B.2 Outlet temperature profile as a function of normalized time as computed by MOSHMX.

References

1. Jurinak, J. J. *Open cycle solid desiccant cooling -- component models and system simulations*, Ph.D. Thesis in Mechanical Engineering, University of Wisconsin-Madison, 1982.

2. Johansson, I. Determination of organic compounds in indoor air with potential reference to air quality, *Atmospheric Environment*, **12**, 1371-1377, 1978.

3. Miksch, R.R., Hollowell, C.D., and Schmidt, H.E. Trace organic chemical contaminants in office spaces, *Environment International*, **8**, 129-137, 1982.

4. Schields, H. C., and Weschler, C. J. Analysis of ambient concentrations of organic vapors with a passive sampler, *JAPCA*, **37**, 1039-1045, 1987.

5. Berglund, B., Berglund, U., Lindvall, T., Nicander-Bredberg, H. Olfactory and chemical characterization of indoor air. Towards a psychophysical model for air quality, *Environment International*, **8**, 327-332, 1982.

6. Grot, R. A., Hodgson, A. T., Daisey, J. M., and Persily, A. Indoor air quality evaluation of a new office building, *ASHRAE Journal*, 16-25, September, 1991.

7. Fanger, P. O. The new comfort equation for indoor air quality, *ASHRAE Journal*, October, 33-38, 1989.

8. Berglund, B., and Berglund, U., and Lindvall, T. Characterization of indoor air quality and "Sick Buildings," *ASHRAE Transactions*, AT-84-20, 1045-1055, 1984.

9. ASHRAE. 1989. *ASHRAE Standard 62-1989, Ventilation for Acceptable Indoor Air Quality*, Atlanta: American Society of Heating, Refrigerating, and Air-Conditioning Engineers, Inc.

10. Bayer, C. W., and Black, M. S. Capillary chromatographic analysis of volatile organic compounds in the indoor environment, *J. Chromatog. Sci.*, **25**, 60-64, 1987.

11. Molhave, L. Indoor air quality in relation to sensory irritation due to volatile organic compounds, *ASHRAE Transactions*, Part 1A, 306-316, 1986.

12. Berglund, B., Johansson, I., and Lindvall, T. — The influence of ventilation on indoor/outdoor air contaminants in an office building, *Environment International*, **8**, 395-399, 1982.

13. Berglund, B., Berglund, U., Lindvall, T. — Assessment of discomfort and irritation from the indoor air, *IAQ '86: Managing Indoor Air for Health and Energy Conservation*, ASHRAE, 138-149, 1986.

14. Noma, E., Berglund, B., Berglund, U., Johansson, I., and Baird, J.C. — Joint representation of physical locations and volatile organic compounds in indoor air from a healthy and a sick building, *Atmospheric Environment*, **22**(3), 451-460, 1988.

15. Chan, C.-C., Spengler, J. D., Ozkaynak, H., and Lefkopoulou, M. — Commuter exposures to VOCs in Boston, Massachusetts, *J. Air Waste Manage. Assoc.*, **41**(12), 1594-1600, 1991.

16. Oldaker, G. B., III, Taylor, W. D., and Parrish, K. B. — Investigations of indoor air quality at four large office buildings, *Proceedings of the First Annual IAQ Conference and Exposition*, Tampa, FL, National Coalition on Indoor Air Quality, 177-187, 1992.

17. Wang, T. C. — A study of bioeffluents in a college classroom, *ASHRAE Transactions*, Vol. 81, Part 1, 32-44, 1975.

18. Bayer, C. W., and Black, M. S. — IAQ evaluations of three office buildings, *ASHRAE Journal*, 48-53, July 1988.

19. Hisham, M. W. M., and Grosjean, D. — Air pollution in southern California museums: Indoor and outdoor levels of nitrogen dioxide, peroxyacetyl nitrate, nitric acid, and chlorinated hydrocarbons, *Environ. Sci. Technol.*, **25**(5), 857-862, 1991.

20. Fanger, P. O., Lauridsen, J., Bluyssen, P., and Clausen, G. — Air pollution sources in offices and assembly halls, quantified by the olf unit, *Energy and Buildings*, **12**, 7-19, 1988.

21. Smisek, M., and Cerny, S. — *Active carbon: Manufacture, properties and applications*, Elsevier Publishing Company, Amsterdam, 1970.

22. Lewis, W. K., Gilliland, E. R., Chertow, B., and Cadogan, W. P. — Adsorption equilibria: Hydrocarbon gas mixtures, *Ind. Eng. Chem.*, **42**(7), 1319-1326, 1950.

23. Treybal, R. E. — *Mass-Transfer Operations, 3rd Ed.*, McGraw-Hill, New York, 1980.

24. Ruthven, D. M. *Principles of adsorption and adsorption processes*, John Wiley and Sons, New York, NY. 1984.

25. Suzuki, M. *Adsorption Engineering*, Elsevier, New York, 1990.

26. Dubinin, M. M. Physical adsorption of gases and vapors in micropores, *Progress in Surface and Membrane Science*, Vol. 9, 1-70, 1975.

27. ASTM D2652-76: Standard definitions of terms relating to activated carbon.

28. Product literature from the Lewcott Corporation, Milbury, MA.

29. Calgon Carbon: The powerful attractions of activated carbon, *Pittsburgh High Technology*, July/August 1988.

30. ASTM D3467-88: Carbon tetrachloride activity of activated carbon.

31. Selection criteria for granular activated carbon (GAC), Tigg Corporation, Pittsburgh, PA, 1988.

32. Deitz, V. R. *Bibliography of Solid Adsorbents*, U.S. Cane Sugar Refiners and Bone Char Manufacturers, Washington, D.C., 1944.

33. Ponec, V., Knor, Z., and Cerny, S. *Adsorption on Solids*, CRC Press, Cleveland, Ohio, 1974.

34. Hill, T. L. Statistical mechanics of adsorption. V. Thermodynamics and heat of adsorption, *J. Chem. Physics*, **17**(6), 520-535, 1949.

35. Hill, T. L., Emmett, P. H., and Joyner, L. G. Calculation of thermodynamic functions of adsorbed molecules from adsorption isotherm measurements: nitrogen on graphon, *J. Am. Chem. Soc.*, **73**, 5102-5107 & 5933, 1951.

36. Myers, A.L., and Prausnitz, J.M. Thermodynamics of mixed-gas adsorption, *AIChE J.*, **11**(1), 121-127, 1965.

37. Hayhurst, D. T. Gas adsorption by some natural zeolites, *Chem. Eng. Commun.*, **4**, 729-735, 1980.

38. Hougen, O. A., and Watson, K. M. *Chemical Process Principles*, John Wiley and Sons, Inc., New York, 1947.

39. Schaefer, M. *Measurement of adsorption isotherms by means of gas chromatography*, M.S. Thesis in Chemical Engineering, University of Wisconsin-Madison, 1991.

40.	Deitz, V. R.	*Bibliography of Solid Adsorbents, 1943 to 1953. An Annotative Bibliographical Survey*, U.S. Dept. of Commerce, National Bureau of Standards, Washington, D.C., 1956.
41.	Chihara, K., Suzuki, M., and Kawazoe, K.	Adsorption rate on molecular sieving carbon by chromatography, *AIChE J.*, **24**(2), 237-246, 1978.
42.	Mason, J. P., and Cooke, C. E., Jr.	Adsorption of hydrocarbon gas mixtures at high pressure, *AIChE J.*, **12**(6), 1097-1103, 1966.
43.	Snyder, C. F., and Chao, K.-C.	Heat of adsorption of light hydrocarbons and their mixtures on activated carbon, *Ind. Eng. Chem. Fundam.*, **9**(3), 437-442, 1970.
44.	Czepirski, L., and Jagiello, J.	Virial-type thermal equation of gas-solid adsorption, *Chem. Eng. Sci.*, **44**(4), 797-801, 1989.
45.	Boucher, E. A., and Everett, D. H.	Determination of Henry's law constants, enthalpies and potential energies of adsorption, and surface areas by gas-solid chromatography: inert gases, nitrogen and methane on active carbon, *Trans. Faraday Soc.*, **67**, 2720-2725, 1971.
46.	Habgood, H. W., and Hanlan, J. F.	A gas chromatographic study of the adsorptive properties of a series of activated charcoals, *Can. J. Chem.*, **37**, 843-855, 1959.
47.	Robell, A. J., Arnold, C. R., Wheeler, A., Kersels, G. J., and Merrill, R. P.	Trace contaminant adsorption and sorbent regeneration, NASA CR-1582, N70-38501, Lockheed Missiles and Space Company, Palo Alto, CA, September, 1970.
48.	James, D. H., and Phillips, C. S. G.	The chromatography of gases and vapors. Part III. The determination of adsorption isotherms, *J. Chem. Soc.*, 1066-1070, 1954.
49.	Mantell, C.L.	*Adsorption*, 2nd Ed., McGraw-Hill, New York, 1951.
50.	Ruthven, D. M.	Sorption of oxygen, nitrogen, carbon monoxide, methane, and binary mixtures of these gases in 5A molecular sieve, *AIChE J.*, **22**(4), 753-759, 1976.
51.	Sing, K. S. W.	Reporting physisorption data for gas/solid systems, Rep. of the Physical Chemistry Division of the I.U.P.A.C., *Pure & Appl. Chem.*, **54**(11), 2201-2218, 1982.
52.	Hill, T. L.	Theory of physical adsorption, *Advances in Catalysis*, **4**, 211-258, 1952.

53.	Brunauer, S., Emmett, P. H., and Teller, E.	*J. Am. Chem. Soc.*, **60**, 309, 1938.
54.	Radke, C. J. and Prausnitz, J. M.	*Ind. Eng. Chem. Fundam.*, **11**(4), 445, 1972.
55.	Toth, J.	*Acta. Chim. Acad. Sci. Hung.*, **69**, 311, 1971.
56.	Chakravarti, D. N., and Dhar, N. D.	*Kolloid Z.*, **43**, 377, 1927.
57.	Young, D. M. and Crowell, A. D.	*Physical adsorption of gases*, Butterworths, Washington, 1962.
58.	Dubinin, M. M.	The potential theory of adsorption of gases and vapors for adsorbents with energetically nonuniform surfaces, *Chem. Rev.*, **60**, 235-241, 1960.
59.	Dubinin, M. M., and Kadlec, O.	Novel ideas in the theory of the physical adsorption of vapors on micropore adsorbents, *Carbon*, **25**(3), 321-324, 1987.
60.	Fairbridge, C., Ng, S. H., and Palmer, A. D.	Fractal analysis of gas adsorption on Syncrude coke, *Fuel*, **65**, 1759-1762, 1986.
61.	Avnir, D., Farin, D., and Pfeifer, P.	Chemistry in noninteger dimensions between two and three. II. Fractal surfaces of adsorbents, *J. Chem. Phys.*, **79**(7), 3566-3571, 1983.
62.	Avnir, D., Farin, D., and Pfeifer, P.	Molecular fractal surfaces, *Nature*, **308**, 261-263, 1984.
63.	Pfeifer, P., Avnir, D., and Farin, D.	Ideally irregular surfaces of dimension greater than two, in theory and practice, *Surface Science*, **126**, 569-572, 1983.
64.	Reid, R. C., Prausnitz, J. M., and Poling, B. E.	*The Properties of Gases and Liquids, 4th Ed.*, McGraw-Hill, New York, 1987.
65.	Grant, R. J., Manes, M., and Smith, S. B.	Adsorption of normal paraffins and sulfur compounds on activated carbon, *AIChE J.*, **8**(3), 403-406, 1962.
66.	Cook, W. H., and Basmadjian, D.	Correlation of adsorption equilibria of pure gases on activated carbon, *Canadian J. Chem. Eng.*, **42**, 146-151, August 1964.

67.	Grant, R. J., and Manes, M.	Correlation of some gas adsorption data extending to low pressures and supercritical temperatures, *I&EC Fundamentals*, **3**(3), 221-224, 1964.
68.	Lewis, W. K., Gilliland, E. R., Chertow, B., and Cadogan, W. P.	Adsorption equilibria: Pure gas isotherms, *Ind. Eng. Chem.*, **42**(7), 1326-1332, 1950.
69.	Sansone, E. B., and Jonas, L. A.	Prediction of activated carbon performance for carcinogenic vapors, *Am. Ind. Hyg. Assoc. J.*, **42**, 688-691, 1981.
70.	Sansone, E. B., Tewari, Y. B., and Jonas, L. A.	Prediction of removal of vapors from air by adsorption on activated carbon, *Environmental Science and Technology*, **13**(12), 1511-1513, 1979.
71.	Sansone, E. B., Jonas, L. A., and O'Brien, T. O.	Prediction of removal efficiency of activated carbons for vapors in air, *Carbon*, **19**(3), 231, 1981.
72.	Urano, K., Omori, S., and Yamamoto, E.	Prediction method for adsorption capacities of commercial activated carbons in removal of organic vapors, *Environ. Sci. Technol.*, **16**(1), 10-14, 1982.
73.	Stoeckli, H. F.	A generalization of the Dubinin-Radushkevich equation for the filling of heterogeneous micropore systems, *J. Colloid Int. Sci.*, **59**(1), 184-185, 1977.
74.	Richter, E., Schütz, W., and Myers, A. L.	Effect of adsorption equation on prediction of multicomponent adsorption equilibria by the ideal adsorbed solution theory, *Chem. Eng. Sci.*, **44**(8), 1609-1616, 1989.
75.	Kawazoe, K., Kawai, T., Eguchi, Y., and Itoga, K.	Correlation of adsorption equilibrium data of various gases and vapors on molecular-sieving carbon, *J. Chem. Eng. Japan*, **7**(3), 158-162, 1974.
76.	Costa, E., Sotelo, J. L., Calleja, G., and Marron, C.	Adsorption of binary and ternary hydrocarbon gas mixtures on activated carbon: experimental determination and theoretical prediction of the ternary equilibrium data, *AIChE J.*, **27**(1), 5-12, 1981.
77.	Okazaki, M., Tamon, H., and Toei, R.	Prediction of binary adsorption equilibria of solvent and water vapor on activated carbon, *J. Chem. Eng. Japan*, **11**(3), 209-215, 1978.

78.	Ustinov, E. A.	Equilibrium adsorption of mixtures by carbon adsorbents, *Russian Journal of Physical Chemistry*, **61**(8), 1095-1097, 1987; translated from *Zhurnal Fizicheskoi Khimii*, **61**, 2103-2107, 1987.
79.	Mehta, S. D., and Danner, R. P.	An improved potential theory method for predicting gas-mixture adsorption equilibria, *Ind. Eng. Chem. Fundam.*, **24**(3), 325-330, 1985.
80.	Forsythe, R. K., Jr.	*Adsorption and dispersion of selected organic gases flowing through activated carbon adsorber beds*, Ph.D. Thesis, Kent State University, 1988.
81.	Ramanathan, K., Debler, V. L., Kosusko, M., and Sparks, L. E.	Evaluation of control strategies for volatile organic compounds in indoor air, *Environmental Progress*, **7**(4), 230-235, 1988.
82.	Kyle, B. G., and Eckhoff, N. D.	Odor removal from air by adsorption on charcoal, EPA-650/2-74-084, PB-236-928, Kansas State University, 1974.
83.	Clapham, T. M., Junker, T. J., and Tobias, G. S.	Activated carbon-odorant removal from air quantified, *ASHRAE Transactions*, No. 2145, 75-86, 1970.
84.	Hines, A. L., Ghosh, T. K., Loyalka, S. K., and Warder, R. C., Jr.	Investigation of co-sorption of gases and vapors as a means to enhance indoor air quality. Phase I Report. Literature Review, University of Missouri-Rolla, GRI-90/0194, 1990.
85.	Ray, G. C., and Box, E. O., Jr.	Adsorption of gases on activated charcoal, *Ind. Eng. Chem.*, **42**(7), 1315-1318, 1950.
86.	Szepesy, I., and Illes, V.	Adsorption of gases and gas mixtures, I. Measurement of the adsorption isotherms of gases on active carbon up to pressures of 1000 torr, *Acta. Chim. Hung.*, **35**, 37-51, 1963.
87.	Szepesy, I., and Illes, V.	Adsorption of gases and gas mixtures, II. Measurement of the adsorption isotherms of gases on active carbon under pressures of 1 to 7 atm, *Acta. Chim. Hung.*, **35**, 53-60, 1963.
88.	Hansen, R. S., Murphy, J. A., and McGee, T. C.	Gas chromatographic measurement of gas-solid interaction potentials and solid surface areas, *Trans. Faraday Soc.*, **60**, 597-603, 1964.
89.	Costa, E., Calleja, G., Marrón, C., Jiménez, A., and Pau, J.	Equilibrium adsorption of methane, ethane, ethylene, and propylene and their mixtures on activated carbon, *J. Chem. Eng. Data*, **34**(2), 156-160, 1989.

90.	Astakhov, V. A., Lukin, V. D., and Masharova, L. P.	Adsorption equilibria on molecular-sieve carbons, *Russian J. Phys. Chem.*, 1641-1644, 1957; translated from *Zh. Fiz. Khimii*, **31**(8) 1733-1737, 1957.
91.	Gonzalez, A. J., and Holland, C. D.	Adsorption of equilibria of the light hydrocarbon gases on the activated carbon and silica gel, *AIChE Journal*, **17**(2), 470-475, 1971.
92.	Lewis, W. K., Gilliland, E. R., Chertow, B., and Milliken, W.	Vapor-adsorbate equilibrium. II. Acetylene-ethylene on activated carbon and on silica gel, *J. Am. Chem. Soc.*, **72**, 1157-1159, 1950.
93.	Suzuki, M., and Sakoda, A.	Gas adsorption on activated carbons with size distribution of micropores, *J. Chem. Eng. Japan*, **15**(4), 279-285, 1982.
94.	Lewis, W. K., Gilliland, E. R., Chertow, B., and Bareis, D.	Vapor-adsorbate equilibrium. III. The effect of temperature on the binary systems ethylene-propane, ethylene-propylene over silica gel, *J. Am. Chem. Soc.*, **72**, 1160-1163, 1950.
95.	Lewis, W. K., Gilliland, E. R., Chertow, B., and Hoffman, W. H.	Vapor-adsorbate equilibrium. I. Propane-propylene on activated carbon and on silica gel, *J. Am. Chem. Soc.*, **72**, 1153-1157, 1950.
96.	Dubinin, M. M.	Adsorption properties and microporous structures of carbonaceous adsorbents, *Carbon*, **25**(5), 593-598, 1987.
97.	Dubinin, M. M., and Polstyanov, E. F.	On the adsorption properties of carbon adsorbents communication 6. Investigation of the equilibrium adsorption of vapors within a broad range of temperatures on activated charcoals with various microporous structures, *Bulletin of the Academy of Sciences of the USSR: Division of Chemical Science*, **4**, 583-589, 1966; translated from *Izv. Akad. Nauk SSSR*, **4**, 610-620, 1966.
98.	Ripperger, S., and Germerdonk, R.	Binary adsorption equilibria of organic compounds and water on active carbon, *Ger. Chem. Eng.*, **6**, 249-255, 1983.
99.	Forsythe, R., Czayka, M., Madey, R., and Povlis, J.	The volume adsorption capacity of activated carbon for selected trace contaminants, *Carbon*, **16**, 27-29, 1978.
100.	Scamehorn, J. F.	Removal of vinyl chloride from gaseous streams by adsorption on activated carbon, *Ind. Eng. Chem. Process Des. Dev.*, **18**(2), 210-217, 1979.

101.	Masukawa, S., and Kobayashi, R.	Adsorption equilibrium of the system methane-ethane-silica gel at high pressures and ambient temperatures, *J. Chem. Eng. Data*, **13**(2), 197-199, 1968.
102.	Mikhail, R. SH., and Shebl, F. A.	Adsorption in relation to pore structures of silicas. I. Organic vapor adsorption on microporous silica gel, *J. Colloid. Int. Sci.*, **32**(3), 505-517, 1970.
103.	Pendleton, P., and Zettlemoyer, A. C.	A study of the mechanism of micropore filling. II. Pore filling of a microporous silica, *J. Colloid Int. Sci.*, **98**(2), 439-446, 1984.
104.	Salam, E. M. A., Chung, R., and Duffie, J. A.	Adsorption of methyl alcohol, acetone and diethylamine on silica gel, *Extrait du Bulletin de l'Institut du Desert d'Egypte*, **8**(2), 161-170, 1958.
105.	Lee, H., and Chi, C. W.	Carbon dioxide removal from air by sodium-x molecular sieve under nonisothermal conditions, *AIChE Symposium Series: Adsorption Technology*, **67**(117), 84-89, 1971.
106.	Dubinin, M. M., Zhukovskaya, E. G., and Murdmaa, K. O.	Investigation of the adsorption properties and secondary porous structure of adsorbents exhibiting molecular sieve action. Communication 12. Specific peculiarities of microporous adsorbents in the adsorption of vapors of various substances, *Akademia Nauk SSSR Bulletin*, 590-596, 1966; translated from *Izvestiya Akademii Nauk SSSR*, **4**, 620-627, 1966.
107.	Ainscough, A. N., and Dollimore, D.	Adsorption capacity of moelcular sieve type carbons, *Langmuir*, **3**(5), 708-713, 1987.
108.	Huang, J.-C., and Madey, R.	Application of potential theory to adsorption of binary mixtures on activated carbon, *Carbon*, **20**(2), 118-120, 1982.
109.	Nelson, G.O., and Correia, A.N.	Respirator cartridge efficiency studies: VIII. summary and conclusions, *Am. Ind. Hyg. Assoc. J.*, **37**, 514-525, 1976.
110.	Turk, A.	Source control by gas-solid adsorption and related processes, in *Air Pollution, 2nd. ed., Vol.III, Sources of Air Pollution and Their Control*, A.C. Stern, Ed., Academic Press, 497-519, 1968.
111.	Werner, M. D.	The effects of relative humidity on the vapor phase adsorption of trichloroethylene by activated carbon, *Am. Ind. Hyg. Assoc. J.*, **46**(10), 585-590, 1985.
112.	Nelson, G.O., Correia, A.N., and Harder, C.A.	Respirator cartridge efficiency studies: VII. effect of relative humidity and temperature, *Am. Ind. Hyg. Assoc. J.*, **37**, 280-288, 1976.

113. Keener, T. C., and Zhou, D. Prediction of activated carbon adsorption performance under high relative humidity conditions, *Envionmental Progress*, **9**(1), 40-46, 1990.

114. Godish, T. *Indoor air pollution control*, Lewis Publishers, Chelsea, MI, 1989.

115. Purecel and Side-Carb activated carbon air purifiers specifications guide, Bulletin 19-196, Cambridge Filter Corporation, Syracuse, NY.

116. IAQ^3 60, 90, 95 Brochure, International Air Filter, Inc., Elgin, IL.

117. Cambridge Side-Carb Air Filters, Bulletin 196E, Cambridge Filter Corporation, Syracuse, NY.

118. Personal communication with Cambridge Filter Corporation, Spring 1992.

119. Kasmark, J. W., Jr. Activated carbon: How does it work?, *Proceedings of the First Annual IAQ Conference and Exposition*, Tampa, FL, National Coalition on Indoor Air Quality, 119-123, 1992.

120. Guide for selection and use of Purecel and Side-Carb activated carbon filters, Bulletin 610C, Cambridge Filter Corporation, Syracuse, NY.

121. Munkelt, F.H. Air purification and deodorization by use of activated carbon, *Refrigerating Engineering Application Data - Section 42*, in *Refrigerating Engineering*, 1-8, September, 1948.

122. Mahajan, B. M. A method for measuring the effectiveness of gaseous contaminant removal filters, NISTIR 89-4119, August, 1989.

123. Kovach, J. L. *Gas-Phase Adsorption*, Section 3.1 in *Handbook of Separation Techniques for Chemical Engineers, 2nd Ed.*, P.A. Schweitzer, Editor, McGraw-Hill, 1988.

124. Hammerton, D. Performance of carbon-impregnated non-woven polyester filter media on gaseous, airborne contaminants, *Proceedings of the First Annual IAQ Conference and Exposition*, Tampa, FL, National Coalition on Indoor Air Quality, 91-97, 1992

125. Sparks, L. E. Air cleaners and indoor air quality, *ASHRAE Journal*, 45, July 1988.

126. Cooper, C. D., and Alley, F. C. *Air Pollution Control: A Design Approach*, PWS Publishers, Boston, 1986.

127. Maclaine-Cross, I. L. *A theory of combined heat and mass transfer in regenerators*, Ph.D. thesis, Monash University, Australia, 1974.

128.	Van den Bulck, E., Mitchell, J. W., and Klein, S. A.	Design theory for rotary heat and mass exchangers - I. Wave analysis of rotary heat and mass exchangers with infinite transfer coefficients, *Int. J. Heat Mass Transfer*, **28**(8), 1575-1586, 1985.
129.	Van den Bulck, E., Mitchell, J. W., and Klein, S. A.	Design theory for rotary heat and mass exchangers - II. Effectiveness - number-of-transfer units method for rotary heat and mass exchangers, *Int. J. Heat Mass Transfer*, **28**(8), 1587-1595, 1985.
130.	Van den Bulck, E.	*Analysis of Solid Desiccant Rotary Dehumidifiers*, M.S. Thesis in Mechanical Engineering, University of Wisconsin-Madison, 1983.
131.	Van den Bulck, E.	*Convective heat and mass transfer in compact regenerative heat exchangers*, Ph.D. Thesis in Mechanical Engineering, University of Wisconsin-Madison, 1987.
132.	Schultz, K. J.	*Rotary solid desiccant dehumidifiers. Analysis of models and experimental investigation*, Ph.D. Thesis in Mechanical Engineering, University of Wisconsin-Madison, 1987.
133.	Close, D. J., and Banks, P. J.	Coupled equilibrium heat and single adsorbate transfer in fluid flow through a porous medium - II. Predictions for a silica-gel air-drier using characteristic charts, *Chemical Engineering Science*, **27**, 1157-1169, 1972.
134.	Pesaran, A. A., and Bingham, C. E.	*Desiccant contamination research: report on the desiccant contamination test facility*, SERI/TP-254-3457, July 1991.
135.	Relwani, S. M., and Moschandreas, D. J.	Indoor pollutant control capabilites of a desiccant dehumidifier system, IIT Research Institute, GRI 86/0200, August 1986.
136.	Daisey, J. M., and Hodgson, A. T.	Initial efficiencies of air cleaners for the removal of nitrogen dioxide and volatile organic compounds, *Atmospheric Environment*, **23**(9), 1885-1892, 1989.
137.	Lamb, A. B., Wilson, R. E., and Chaney, N. K.	Gas mask adsorbents, *The Journal of Industrial and Engineering Chemistry*, **11**(5), 420-439, 1919.
138.	Fieldner, A. C., Teague, M. C., and Yoe, J. H.	Protection afforded by army gas masks against various industrial gases, *The Journal of Industrial and Engineering Chemistry*, **11**, 622-623, 1919.
139.	Nelson, G.O., and Harder, C.A.	Respirator cartridge efficiency studies: VI. effect of concentration, *Am. Ind. Hyg. Assoc. J.*, **37**, 205-216, 1976.

140.	Hall, T., Breysse, P., Corn, M., and Jonas, L. A.	Effects of adsorbed water vapor on the adsorption rate constant and the kinetic adsorption capacity of the Wheeler kinetic model, *Am. Ind. Hyg. Assoc. J.*, **49**(9), 461-465, 1988.
141.	Wood, G. O., and Moyer, E. S.	A review of the Wheeler equation and comparison of its applications to organic vapor respirator cartridge breakthrough data, *Am. Ind. Hyg. Assoc. J.*, **50**(8), 400-407, 1989.
142.	Yoon, Y. H., and Nelson, J. H.	Application of gas adsorption kinetics I. A theoretical model for respirator cartridge service life, *Am. Ind. Hyg. Assoc. J.*, **45**(8), 509-516, 1984.
143.	Yoon, Y. H., and Nelson, J. H.	Application of gas adsorption kinetics - II. A theoretical model for respirator cartridge service life and its practical implications, *Am. Ind. Hyg. Assoc. J.*, **45**(8), 517-524, 1984.
144.	Yoon, Y. H., and Nelson, J. H.	Effects of humidity and contaminant concentration on respirator cartridge breakthrough, *Am. Ind. Hyg. Assoc. J.*, **51**(4), 202-209, 1990.
145.	Grubner, O., and Burgess, W. A.	Calculation of adsorption breakthrough curves in air cleaning and sampling devices, *Environmental Science and Technology*, **15**(11), 1346-1351, 1981.
146.	Nelson, G.O., and Harder, C.A.	Respirator cartridge efficiency studies: V. Effect of solvent vapors, *Am. Ind. Hyg. Assoc. J.*, **35**, 391, 1974.
147.	Carhart, H. W., and Thompson, J. K.	Removal of contaminants from submarine atmospheres, in *Removal of Trace Contaminants from the Air*, V. R. Deitz, Ed., *ACS Symposium Series 17, American Chemical Society*, 1975.
148.	Eaton, H. G., Thompson, J. K., and Carhart, H. W.	Feasibility of the total hydrocarbon analyzer for evaluating the life of charcoal beds, Naval Research Laboratory, NRL Report 7712, AD-778659, April, 1974.
149.	Olcott, T. M.	Development of a sorber trace contaminant control system including pre- and post-sorbers for a catalytic oxidizer, NASA-CR-2027, N72-26079, Lockheed Missiles and Space Company, Sunnyvale, CA, 1972.
150.	Olcott, T. M., et. al.	Design, fabrication, and test of a trace contaminant control system, NASA-CR-147860, N76-31908, LMSC-D462467, Lockheed Missiles and Space Company, Sunnyvale, CA, 1975.

151.	McNulty, K. J., Goldsmith, R. L., Goldsmith, G. A., Hoover, P. R., Nwankwo, J., and Turk, A.	Evaluation of techniques for removal of spacecraft contaminants from activated carbon, NASA-CR-151968, N77-20159, The Walden Division of Abcor, Inc., March 1977.
152.	Bethea, R. M.	*Air Pollution Control Technology*, Van Nostrand Reinhold Company, New York, 1978.
153.	Nelson, T. P., Blacksmith, J. R., and Randall, J. L.	Full-scale carbon adsorption applications study, Radian Corp, Austin, TX, EPA/600/2-85/012, PB85-172906, February 1985.
154.	Larsen, E. S., and Pilat, M. J.	Moving bed adsorption system for control of VOCs from an aircraft painting facility, *J. Air Wast Manage. Assoc.*, **41**, 1199-1206, 1991.
155.	Larsen, E. S., and Pilat, M. J.	Design and testing of a moving bed VOC adsorption system, *Environmental Progress*, **10**(1), 75-82, 1991.
156.	Klobucar, J. M., and Pilat, M. J.	Continuous flow thermal desorption of VOC's from activated carbon, *Environmental Progress*, **11**(1), 11-17, 1992.
157.	Uota, M., and Smock, R. M.	Odor removal studies in refrigerated storage, *Refrigerating Engineering*, March, 256-259, 1948.
158.	Gerhardt, F.	Air purification in apple and pear storages, *Refrigerating Engineering*, February, p. 145, 1950.
159.	Brandemuehl, M. J.	*Analysis of heat and mass regenerators with time varying or spatially nonuniform inlet conditions*, Ph.D. Thesis in Mechanical Engineering, University of Wisconsin-Madison, 1982.
160.	Gidaspow, D., and Onischak, M.	Regenerative sorption of nitric oxide: a concept for environmental control and kinetics for ferrous sorbents, *Canadian Journal of Chemical Engineering*, **51**, 337-344, 1973.
161.	Kast, W., and Otten, W.	The breakthrough in fixed bed adsorbers: methods of calculation and the effects of process parameters, *International Chem. Eng.*, **29**(2), 197-211, 1989.
162.	Lapidus, L., and Amundson, N. R.	Mathematics of adsorption in beds. VI. The effect of longitudinal diffusion in ion exchange and chromatographic columns, *J. Phys. Chem.*, **56**, 984, 1952.
163.	DeVault, D.	The theory of chromatography, *J. Am. Chem. Soc.*, **65**, 532, 1943.

164.	Cooney, D. O., and Lightfoot, E. N.	Existence of asymptotic solutions to fixed-bed separations and exchange equations, *I&EC Fundamentals*, **4**(2), 233-236, 1965.
165.	Heerdt, E. D.	*Non-isothermal local equilibrium adsorption*, Ph.D. Thesis in Chemical Engineering, University of Minnesota, 1969.
166.	Glueckauf, E.	Theory of chromatography. Part 9. The "theoretical plate" concept in column separations, *Trans. Faraday Soc.*, **51**, 34-44, 1955.
167.	Rhee, H.-K.	*Studies on the theory of chromatography*, Ph.D. Thesis in Chemical Engineering, University of Minnesota, 1968.
168.	Robell, A. J., and Merrill, R. P.	Gaseous contaminant removal by adsorption: II. Adsorption dynamics in fixed beds, *Chem. Eng. Prog. Symp. Series*, **65**(96), 100-108, 1969.
169.	Tudge, A. P.	Studies in chromatographic transport. I. A simplified theory, *Canadian Journal of Physics*, **39**, 1600-1610, 1961.
170.	Tudge, A. P.	Studies in chromatographic transport. II. The effect of adsorption isotherm shape, *Can. J. Phys.*, **39**, 1611, 1961.
171.	Rhee, H.-K.	Equilibrium theory of multicomponent chromatography, in *Percolation Processes: Theory and Applications*, Sijthoff & Noordhoff International Publishers B.V., Alphen aan den Rijn, The Netherlands, 285-328, 1981.
172.	Rhee, H.-K., Aris, R., and Amundson, N.R.	On the theory of multicomponent chromatography, *Proc. Royal Soc.*, **A267**, 419, 1970.
173.	Glueckauf, E.	Theory of chromatography. VII. The general theory of two solutes following non-linear isotherms, *Disc. Faraday Soc.*, **7**, 12-25, 1949.
174.	Basmadjian, D., Ha, K. D., and Pan, C.-Y.	Nonisothermal desorption by gas purge of single solutes in fixed-bed adsorbers. I. Equilibrium theory, *Ind. Eng. Chem., Process Des. Dev.*, **14**(3), 328-340, 1975.
175.	Basmadjian, D., Ha, K. D., and Pan, C.-Y.	Nonisothermal desorption by gas purge of single solutes from fixed-bed adsorbers. II. Experimental verification of equilibrium theory, *Ind. Eng. Chem., Process Des. Dev.*, **14**(3), 340-347, 1975.
176.	Amundson, N. R., Aris, R., and Swanson, R.	On simple exchange waves in fixed beds, *Proc. Royal Soc.*, **A286**, 129, 1965.

177.	Pan, C.Y., and Basmadjian, D.	An analysis of adiabatic sorption of single solutes in fixed beds: pure thermal wave formation and its practical implications, *Chem. Eng. Sci.*, **25**, 1653-1664, 1970.
178.	Pan, C.Y., and Basmadjian, D.	An analysis of adiabatic sorption of single solutes in fixed beds: equilibrium theory, *Chem. Eng. Sci.*, **26**, 45-57, 1971.
179.	Cassie, A. B. D.	Propagation of temperature changes through textiles in humid atmospheres. Part II.-Theory of propagation of temperature change, *Trans. Faraday Soc.*, **36**, 453, 1940.
180.	Banks, P. J.	Coupled equilibrium heat and single adsorbate transfer in fluid flow through a porous medium - I. Characteristic potential and specific capacity ratios, *Chemical Engineering Science*, **27**, 1143-1153, 1972.
181.	Rhee, H.-K., Heerdt, E. D., and Amundson, N. R.	An analysis of an adiabatic adsorption column: Part II. Adiabatic adsorption of a single solute, *Chem. Eng. J.*, **1**, 279-290, 1970.
182.	Rhee, H.-K., and Amundson, N.R.	An analysis of an adiabatic adsorption column: Part 1. Theoretical development, *Chem. Eng. J.*, **1**, 241-254, 1970.
183.	Rhee, H.-K., and Amundson, N.R.	An analysis of an adiabatic adsorption column: Part IV. Adsorption in the high temperature range, *Chem. Eng. J.*, **3**, 121-135, 1972.
184.	Rhee, H.-K., Heerdt, E. D., and Amundson, N. R.	An analysis of an adiabatic adsorption column: Part III. Adiabatic adsorption of two solutes, *Chem. Eng. J.*, **3**, 22-34, 1972.
185.	Hougen, O. A., and Marshall, W. R., Jr.	Adsorption from a fluid stream flowing through a stationary granular bed, *Chem. Eng. Progress*, **43**(4), 197-208, 1947.
186.	Chen, T.-L., and Hsu, J. T.	Prediction of breakthrough curves by the application of Fast Fourier Transform, *AIChE Journal*, **33**(8), 1387-1390, 1987.
187.	Buso, A., Paratella, A., and Trotta, A.	The solution of the dynamic adsorption beds using the finite element method, *Comput. chem. Engng.*, **12**(2/3), 247-251, 1988.
188.	Chang, A. S. T., and Hwang, G.-W.	Simulation of breakthrough curves by a moving zone collocation method, *Computers chem. Engng.*, **13**(3), 281-290, 1989.
189.	Raghavan, N. S., and Ruthven, D. M.	Numerical simulation of a fixed-bed adsorption column by the method of orthogonal collocation, *AIChE J.*, **29**(6), 922-925, 1983.

190.	Ferrell, J. K., Rousseau, R. W., and Branscome, M. R.	The development and testing of a mathematical model for complex adsorption beds, *Ind. Eng. Chem., Process Des. Dev.*, **15**(1), 114-122, 1976.
191.	Amundson, N. R.	A note on the mathematics of adsorption in beds, *J. Phys. Coll. Chem.*, **52**, 1153, 1948. Currently this is the *J. Phys. Chem.*
192.	Kasten, P. R., Lapidus, L., and Amundson, N. R.	Mathematics of adsorption in beds. V. Effect of intraparticle diffusion in flow systems in fixed beds, *J. Phys. Chem.*, **56**, 683, 1952.
193.	Gariepy, R. L., and Zwiebel, I.	Adsorption of binary mixtures in fixed beds, *AIChE Symposium Series: Adsorption Technology*, **67**(117), 17-24, 1971.
194.	Ramachandran, P. A., and Dudukovic, M. P.	Solution by triple collocation for periodic operation of heat regenerators, *Computers & Chemical Engineering*, **8**(6), 377-388, 1984.
195.	Ramachandran, P. A., and Dudukovic, M. P.	A moving finite element method for transient problems with steep gradients, *Chemical Engineering Science*, **39**(7/8), 1321-1324, 1984.
196.	Carter, J. W.	Isothermal and adiabatic adsorption in fixed beds, *Trans. Instn. Chem. Engrs*, **46**, T213-T222, 1968.
197.	Phillips, J.B., Wright, N.A., and Burke, M.F.	Probabilistic approach to digital simulation of chromatographic processes, *Separation Science and Technology*, **16**(8), 861-884, 1981.
198.	Klinkenberg, A.	Heat transfer on cross-flow heat exhangers and packed beds. Evaluation of equations for penetration of heat or solutes, *Ind. Eng. Chem.*, **46**(11), 2285-2289, 1954.
199.	Acrivos, A.	Method of characteristics technique: Application to heat and mass transfer problems, *Ind. Eng. Chem.*, **48**(4), 703-710, 1956.
200.	Liapis, A. I., and Rippin, D. W. T.	A general model for the simulation of multi-component adsorption from a finite bath, *Chem. Eng. Sci.*, **32**, 619-627, 1977.
201.	Mees, P. A. J., Gerritsen, A. W., and Verheijen, P. J. T.	Fast calculation of breakthrough curves in nonisothermal fixed-bed adsorbers, *AIChE Journal*, **35**(8), 1380-1384, 1989.
202.	Fan, L. T.	Mathematical simulation of an adsorber for pollutant removal, Kansas State University, EPA-650/2-74-110, PB-239-331, October 1974.
203.	Cooney, D. O.	Numerical investigation of adiabatic fixed-bed adsorption, *Ind. Eng. Chem., Proc. Des. Dev.*, **13**(4), 368-373, 1974.

204.	Pan, C.Y., and Basmadjian, D.	Constant-pattern adiabatic fixed-bed adsorption, *Chem. Eng. Sci.*, **22**, 285-297, 1967.
205.	Yoshida, H., and Ruthven, D. M.	Dynamic behaviour of an adiabatic adsorption column - I. Analytic solution for irreversible adsorption, *Chem. Eng. Sci.*, **38**(6), 877-884, 1983.
206.	Mathiprakasm, B., and Lavan, Z.	Performance predictions for adiabatic desiccant dehumidifiers using linear solutions, *J. Sol. Energy Engng.*, **102**, 73-79, 1980.
207.	Raghavan, N. S., and Ruthven, D. M.	Dynamic behaviour of an adiabatic adsorption column - II. Numerical simulation and analysis of experimental data, *Chem. Eng. Sci.*, **39**(7/8), 1201-1212, 1984.
208.	Carter, J. W.	A numerical method for prediction of adiabatic adsorption in fixed beds, *Trans. Instn. Chem. Engrs*, **44**, T253-T259, 1966.
209.	Sircar, S., and Kumar, R.	Adsorption of a dilute adsorbate: Effects of small changes in the column temperature, *Ind. Eng. Chem. Process Des. Dev.*, **22**(2), 280-287, 1983.
210.	Jeffreson, C. P.	Prediction of breakthrough curves in packed beds: I. Applicability of single parameter models, *AIChE Journal*, **18**(2), 409-420, 1972.
211.	Chase. C. A., Gidaspow, D., and Peck, R. E.	Adiabatic adsorption in a regenerator, *Chem. Eng. Prog. Symp. Series*, **65**(96), 34-47, 1969.
212.	Meyer, O. A., and Weber, T. W.	Nonisothermal adsorption in fixed beds, *AIChE J.*, **13**(3), 457, 1967.
213.	Nagel, G., Kluge, G., and Flock, W.	Modelling of non-isothermal multi-component adsorption in adiabatic fixed beds - I. The numerical solution of the parallel diffusion model, *Chem. Eng. Sci.*, **42**(1), 143-153, 1987.
214.	Kluge, G., Flock, W., and Nagel, G.	Modelling of non-isothermal multi-component adsorption in adiabatic fixed beds - II. On the relative velocities of concentration and temperature fronts, *Chem. Eng. Sci.*, **42**(1), 155-162, 1987.
215.	Harwell, J. H., Liapis, A. I., Litchfield, R., and Hanson, D. T.	A non-equilibrium model for fixed-bed multi-component adiabatic adsorption, *Chem. Eng. Sci.*, **35**, 2287-2296, 1980.
216.	Wong, Y. W., and Niedzwiecki, J. L.	A simplified model for multicomponent fixed bed adsorption, *AIChE Symposium Series: Adsorption and Ion Exchange*, No. 219, Vol. 78, 120-127, 1982.

217.	Sircar, S., and Kumar, R.	Adiabatic adsorption of bulk binary gas mixtures: Analysis by constant pattern model, *Ind. Eng. Chem. Process Des. Dev.*, **22**, 271-280, 1983.
218.	Liapis, A. I., and Crosser, O. K.	Comparison of model predictions with non-isothermal sorption data for ethane-carbon dioxide mixtures in beds of 5A molecular sieves, *Chem. Eng. Sci.*, **37**(6), 958-961, 1982.
219.	Smoller, J.	*Shock Waves and Reaction-Diffusion Equations*, Springer-Verlag, New York, 1983.
220.	Coulson, C. A., and Jeffrey, A.	*Waves: A mathematical approach to the common types of wave motion*, Longman, New York, 1977.
221.	Chang, T., and Hsiao, L.	*The Riemann Problem and Interaction of Waves in Gas Dynamics*, Longman Scientific & Technical, Essex, England, 1989.
222.	Jeffrey, A.	*Quasilinear Hyperbolic Systems and Waves*, Pitman Publishing, London, 1976.
223.	Keyfitz, B. L.	Some elementary connections among nonstrictly hyperbolic conservation laws, in *Nonstrictly Hyperbolic Conservation Laws*, ed. B L. Keyfitz and H. C. Kranzer, *Contemporary Mathematics*, **60**, 67-78, 1985.
224.	Liu, T.-P.	The Riemann problem for general 2x2 conservation laws, *Trans. Amer. Math. Soc.*, **199**, 89-112, 1974.
225.	Keyfitz, B. L., and Kranzer, H. C.	A system of non-strictly hyperbolic conservation laws arising in elasticity theory, *Arch. Rat. Mech. Anal.*, **72**, 219-241, 1980.
226.	Schaeffer, D. G., and Shearer, M.	The classification of 2 x 2 systems of non-strictly hyperbolic conservation laws, with application to oil recovery, *Comm. of Pure and Applied Math.*, **XL**, 141-178, 1987.
227.	Keyfitz, B. L., and Kranzer, H. C., Editors	*Non-strictly Hyperbolic Conservation Laws, Contemporary Mathematics Volume 60.* American Mathematical Society: Providence, RI. 1985.
228.	Lindquist, W. B., Editor	*Current progress in hyperbolic systems: Riemann problems and computations, Contemporary Mathematics Volume 100.* American Mathematical Society: Providence, RI. 1988.

229.	Bohannon, B.	A system of conservation laws with a parabolic degeneracy, in *Current progress in hyperbolic systems: Riemann problems and computations*, ed. W. B. Lindquist, *Contemporary Mathematics*, **100**, 161-184, 1988.
230.	Isaacson, E., Marchesin, D., and Plohr, B.	Transitional shock waves, in *Current progress in hyperbolic systems: Riemann problems and computations*, ed. W. B. Lindquist, *Contemporary Mathematics*, **100**, 125-146, 1988.
231.	Shearer, M., Schaeffer, D. G., Marchesin, D., and Paes-Leme, P. L.	Solution of the Riemann problem for a prototype 2 x 2 system of non-strictly hyperbolic conservation laws, *Arch. Rat. Mech. Anal.*, **97**, 299-320, 1987.
232.	Barkve, T.	The Riemann problem for a nonstrictly hyperbolic system modeling nonisothermal, two-phase flow in a porous medium, *SIAM J. Appl. Math.*, **49**(3), 784-798, 1989.
233.	Keyfitz, B. L.	A survey of nonstrictly hyperbolic conservation laws, in *Nonlinear Hyperbolic Problems*, ed. A. Dold and B. Eckmann, *Lecture Notes in Mathematics*, 152-162, 1986.
234.	Johansen, T., and Winther, R.	The solution of the Riemann problem for a hyperbolic system of conservation laws modeling polymer flooding, *SIAM J. Math. Anal.*, **19**(3), 542-566, 1988.
235.	Baker, B., III, and Pigford, R. L.	Cycling zone adsorption: quantitative theory and experimental results, *Ind. Eng. Chem. Fundam.*, **10**(2), 283-292, 1971.
236.	Chen, H. T., and Hill, F. B.	Characteristics of batch, semicontinuous, and continuous equilibrium parametric pumps, *Separation Science*, **6**(3), 411-434, 1971.
237.	Wankat, P. C.	Continuous recuperative mode parametric pumping, *Chemical Engineering Science*, **33**, 723-733, 1978.
238.	Pigford, R. L., Baker, B., III, and Blum, D. E.	An equilibrium theory of the parametric pump, *I&EC Fundamentals*, **8**(1), 144-149, 1969.
239.	Lavie, R., and Reilly, M. J.	Limit cycles in fixed beds operated in alternating modes, *Chemical Engineering Science*, **27**, 1835-1843, 1972.
240.	Wankat, P. C.	The relationship between one-dimensional and two-dimensional separation processes, *AIChE J.*, **23**(6), 859-867, 1977.

241. Boor, R. M.S. Thesis in Mechanical Engineering, University of Wisconsin-Madison, to be completed in December 1992.

242. Klein, H. *Heat and mass transfer in regenerative enthalpy exchangers*, M.S. Thesis in Chemical Engineering, University of Wisconsin-Madison, 1988.

243. Type BPL granular carbon: Mesh sizes 4x6 and 4x8, Bulletin 27-118a, Calgon Carbon Corporation, Pittsburgh, PA.

244. Rau, J. J. *Thermodynamic characteristics of lithium chloride in rotary heat and mass exchangers*, M.S. Thesis in Chemical Engineering, University of Wisconsin-Madison, 1989.

Other references which were not cited:

Abbott, M. B. *An Introduction to the Method of Characteristics*, Thames and Hudson, London, 1966.

Alhamid, M. I. *Packed bed and rotary desiccant dehumidifier in air-conditioning systems*, Thesis, Katholieke Universiteit Leuven, 1990.

Aris, R., and Amundson, N. R. *Mathematical Methods in Chemical Engineering: Vol. 2. First-Order Partial Differential Equations with Applications*, Prentice-Hall, Inc., Englewood Cliffs, NJ, 1973.

Avnir, D., and Pfeifer, P. Fractal dimension in chemistry. An intensive characteristic of surface irregularity, *Nouveau Journal de Chemie*, **7**(2), 71-72, 1983.

Barnett, S. *Matrix Methods for Engineers and Scientists*, McGraw-Hill UK, Maidenhead, England, 1979.

Basmadjian, D., and Wright, D. W. Non-isothermal sorption of ethane-carbon dioxide mixtures in beds of 5A molecular sieves, *Chem. Eng. Sci.*, **36**, 937-940, 1981.

Bell, J. B., Trangenstein, J. A., and Shubin, G. R. Conservation laws of mixed type describing three-phase flow in porous media, *SIAM J. Appl. Math.*, **46**(6), 1000-1017, 1986.

Berkley, R. E., Varns, J. L., and Pleil, J. — Comparison of portable gas chromatographs and passivated canisters for field sampling airborne toxic organic vapors in the United States and the USSR, *Environ. Sci. Technol.*, **25**(8), 1439-1444, 1991.

Bevan, M. A. J., Proctor, C. J., Baker-Rogers, J., and Warren, N. D. — Exposure to carbon monoxide, respirable suspended particulates, and volatile organic compounds while commuting by bicycle, *Environ. Sci. Technol.*, **25**(4), 788-791, 1991.

Bhaskar, G. V., and Do, D. D. — A simple solution for nonisothermal adsorption in a single particle, *Chem. Eng. Sci.*, **44**(5), 1215-1219, 1989.

Blankenship, D. W. — *The thermodynamics of adsorption hysteresis in the system xenon on controlled-pore glass*, Ph.D. Thesis in Chemistry, Georgia Institute of Technology, July, 1982.

Bullock, C. E., and Threlkeld, J. L. — Dehumidification of moist air by adiabatic adsorption, *ASHRAE Transactions*, **72**, 301-313, 1966.

Burevski, D. — The application of the Dubinin-Astakhov equation to the characterization of microporous carbons, *Colloid & Polymer Sci.*, **260**, 623-627, 1982.

Carter, J. W. — Some aspects of the prediction of performance of a large air-dryer, *Trans. Instn. Chem. Engrs*, **46**, T222-T224, 1968.

Chan, C.-C., Ozkaynak, H., Spengler, J. D., and Sheldon, L. — Driver exposure to volatile organic compounds, CO, ozone, and NO_2 under different driving conditions, *Environ. Sci. Technol.*, **25**(5), 964-972, 1991.

Chen, H. T., Rak, J. L., Stokes, J. D., and Hill, F. B. — Separations via continuous parametric pumping, *AIChE J.*, **18**(2), 356-361, 1972.

Chessick, J. J., and Zettlemoyer, A. C. — Immersional heats and the nature of solid surfaces, in *Advances in Catalysis*, Volume XI, Academic Press, New York, 263-299, 1959.

Chou, G. F., and Prausnitz, J. M. — Adiabatic flash calculations for continuous or semicontinuous mixtures using an equation of state, *Fluid Phase Equilibria*, **30**, 75-82, 1986.

Close, D. J. — Characteristic potentials for coupled heat and mass transfer processes, *Int. J. Heat Mass Transfer*, **26**(7), 1098-1102, 1983.

Colome, S. D., Spengler, J. D., and McCarthy, S. — Comparisons of elements and inorganic compounds inside and outside of residences, *Environment International*, **8**, 197-212, 1982.

Cotterman, R. L., Bender, R., and Prausnitz, J. M. — Phase equilibria for mixtures containing very many components. Development and application of continuous thermodynamics for chemcial process design, *Ind. Eng. Chem. Process Des. Dev.*, **24**, 194-203, 1985.

Cotterman, R. L., and Prausnitz, J. M. — Flash calculations for continuous or semicontinuous mixtures using an equation of state, *Ind. Eng. Chem. Process Des. Dev.*, **24**, 434-443, 1985.

Du, P. C., and Mansoori, G. A. — Phase equilibrium computational algorithms of continuous mixtures, *Fluid Phase Equilibria*, **30**, 57-64, 1986.

Dubinin, M. M., and Lezin, Y. S. — Determination of the parameters of the microporous structure of adsorbents, *Bulletin of the Academy of Sciences of the USSR: Division of Chemical Sciences*, 899-902, 1968; translated from *Izvestiya Akademii Nauk SSSR*, **5**, 939-943, 1968.

Dubinin, M. M., Lezin, Y. S., Kadlec, O., and Zukai, A. — Application of computers in the calculation of the parameters of the microporous structure of adsorbents, *Russian Journal of Physical Chemistry*, **42**(4), 1968; translated from *Zh. Fiz. Khimii*, **42**, 969, 1968.

Engle, P. M., and Bauder, C. J. — Characteristics and application of high performance dry filters, *ASHRAE Journal*, May, 72-75, 1964.

Fanger, P. O. — Introduction of the olf and the decipol units to quantify air pollution perceived by humans indoors and outdoors, *Energy and Buildings*, **12**, 1-6, 1988.

Filippova, I. V., and Filippov, L. K. — Role of blurring factors in the theory of the adsorption dynamics of mixtures, *Russian J. Phys. Chem.*, **61**(8), 1117-1122, 1987, translated from *Zh. Fiz. Khimii*, **61**, 2145-2153, 1987.

Fisk, W. J., Spencer, R. K., Grimsrud, D. T., Offermann, F. J., Pedersen, B., and Sextro, R. — *Indoor Air Quality Control Techniques: Radon, Formaldehyde, Combustion Products*, Noyes Publications, Park Ridge, NJ, 1987.

Foo, S. C., Bergsman, K. H., and Wankat, P. C. — Multicomponent fractionation by direct, thermal mode cycling zone adsorption, *Ind. Eng. Chem. Fundam.*, **19**(1), 86-93, 1980.

Frazier, S. E.	Filter element, filter, and method for removing odors from indoor air, U.S. Patent #4604110, General Time Corporation, Aug. 5, 1986.
Friday, D. K., and LeVan, M. D.	Hot purge gas regeneration of adsorption beds with solute condensation: Experimental studies, *AIChE Journal*, **31**(8), 1322-1328, 1985.
Fripiat, J. J., Gatineau, L., and Van Damme, H.	Multilayer physical adsorption on fractal surfaces, *Langmuir*, **2**, 562-567, 1986.
Glessner, A. J., and Myers, A. L.	The sorption of gas mixtures in molecular sieves, *Chem. Eng. Prog. Symp. Series*, **65**(96), 73-79, 1969.
Goldstein, S., and Murray, J. D.	On the mathematics of exchange processes in fixed columns. III. The solution for general entry conditions, and a method of obtaining asymptotic expressions, *Proc. Roy. Soc. A*, **252**, 334-347, 1959
Goldstein, S., and Murray, J. D.	On the mathematics of exchange processes in fixed columns. IV. Limiting values, and correction terms, for the kinetic-theory solution with general entry conditions, *Proc. Roy. Soc. A*, **252**, 348-359, 1959
Gregory, R. A., and Sweed, N. H.	Equilibrium theory of cycling zone adsorption, *Ind. Eng. Chem. Fundam.*, **10**(2), 280-283, 1971.
Gregory, R. A., and Sweed, N. H.	Parametric pumping: behavior of open systems. Part II. Experiment and computation, *Chem. Eng. J.*, **4**, 139-148, 1972.
Grimsrud, D. T., and Teichman, K. Y.	The scientific basis of Standard 62-1989, *ASHRAE Journal*, October, 51-54, 1989.
Grubner, O.	Statistical moments theory of gas-solid chromatography: diffusion-controlled kinetics, *Advances in Chromatography*, **6**, 173-209, 1968.
Gutsche, B., and Kgaa, H.	Phase equilibria in oleochemical industry - application of continuous thermodynamics, *Fluid Phase Equilibria*, **30**, 65-73, 1986.
Harten, A., and Lax, P. D.	A random choice finite difference scheme for hyperbolic conservation laws, *SIAM J. Numer. Anal.*, **18**(2), 289-315, 1981.
Hasz, J. W., and Barrere, C. A., Jr.	Prediction of equilibrium adsorption capacity and heats of adsorption by the Polanyi potential theory, *Chem. Eng. Prog. Symp. Series*, **65**(96), 48-56, 1969.

Helfferich, F. G. — Multicomponent ion exchange in fixed beds: Generalized equilbrium theory for systems with constant separation factors, *Ind. Eng. Chem. Fund.*, **6**(3), 362-364, 1967.

Hellman, T. M., and Small, F. H. — Characterization of the odor properties of 101 petrochemicals using sensory methods, *Journal of the Air Pollution Control Association*, **24**(10), 979-982, 1974.

Hobson, J. P., and Armstrong, R. A. — A study of physical adsorption at very low pressures using ultrahigh vacuum techniques, *J. Phys. Chem.*, **67**, 2000-2008, 1963.

Holden, H., and Risebro, N. H. — Stochastic properties of the scalar Buckley-Leverett equation, *SIAM J. Appl. Math.*, **51**(5), 1472-1488, 1991.

Hsu, J. T., and Dranoff, J. S. — Numerical inversion of certain Laplace transforms by the direct application of Fast Fourier Transform (FFT) algorithm, *Comput. chem. Engng.*, **11**(2), 101-110, 1987.

Huang, J.-C., Forsythe, R., and Madey, R. — Gas-solid chromatography of methane-helium mixtures: Transmission of a step increase in the concentration of methane through an activated carbon adsorber bed at 25 C, *Sep. Sci. Tech.*, **16**(5), 475-486, 1981.

Hughes, P. J., Klein, S. A., and Close, D. J. — Packed bed thermal storage models for solar air heating and cooling systems, *ASME Journal of Heat Transfer*, **98**(2), 336, 1976.

Hwang, K. C. — A transient performance method for CO_2 removal with regenerable adsorbents, AIResearch Manufacturing Company, Los Angeles, CA, NASA CR-112098, October 1972.

Hyun, S. H., and Danner, R. P. — Determination of gas adsorption equilibria by the concentration-pulse technique, *AIChE Symposium Series: Adsorption and Ion Exchange*, No. 219, Vol. 78, 19-28, 1982.

Izotova, T. I., and Dubinin, M. M. — Micrporous structure of active carbons, *Russian Journal of Physical Chemistry*, **39**(11), 1492-1496, 1965.

Janssen, J. E. — Ventilation for acceptable indoor air quality, *ASHRAE Journal*, October, 40-48, 1989.

Jaroniec, M. — Thermodynamics of gas adsorption on heterogeneous microporous solids, *Langmuir*, **3**, 795-799, 1987.

Jedrzejak, A., and Jablonski, M. — Prediction of adsorption of organic component and water vapour mixture onto activated carbon, *Monatshefte für Chemie*, **119**, 187-194, 1988.

Jonas, L. A., Rehrmann, J. A., and Eskow, J. M.	Kinetics of trace gas adsorption from contaminated air, *ACS Symposium Series 17: Removal of Trace Contaminants from the Air*, V.R. Deitz, Ed., 110-121, 1975.
Jurinak, J. J., and Mitchell, J. W.	Recirculation of purged flow in an adiabatic counterflow rotary dehumidifier, *ASME Journal of Heat Transfer*, **106**, 369-375, 1984.
Jurinak, J. J., Mitchell, J. W., and Beckman, W. A.	Open-cycle desiccant air conditioning as an alternative to vapor compression cooling in residential applications, *ASME Journal of Solar Energy Engineering*, **106**, 252-260, 1984.
Kehat, E., and Heineman, M.	Desorption of normal paraffins from molecular sieve 5A, *Ind. Eng. Chem. Process Des. Dev.*, **9**(1), 72-78, 1970.
Keyfitz, B. L.	Change of type in three-phase flow: A simple analogue, *J. Diff. Eqns.*, **80**, 280-305, 1989.
Keyfitz, B. L.	Admissibility of conditions for shocks in conservation laws that change type, *SIAM J. Math. Anal.*, **22**(5), 1284-1292, 1991.
Keyfitz, B. L., and Kranzer, H. C.	The Riemann problem for some non-strictly hyperbolic systems of conservation laws, *Notices Amer. Math. Soc.*, **23**, A-127-128, 1976.
Keyfitz, B. L., and Kranzer, H. C.	Existence and uniqueness of entropy solutions to the Riemann problem for hyperbolic systems of two nonlinear conservation laws, *J. Diff. Eqns.*, **27**, 444-476, 1978.
Kinkead, D. A.	Pleated DPCC-based adsorbers: New technology for air purification, *ASHRAE Journal*, 35-40, November 1990.
Klein, G., Tondeur, D., and Vermeulen, T.	Multicomponent ion exchange in fixed beds: General properties of equilbrium systems, *Ind. Eng. Chem. Fund.*, **6**(3), 339-350, 1967.
Knaebel, K. S.	Multistage cycling zone adsorption for purification of binary mixtures, *AIChE Symposium Series: Adsorption and Ion Exchange*, **78** (219), 128-135, 1982.
Knaebel, K. S., and Pigford, R. L.	Equilibrium and dissipative effects in cycling zone adsorption, *Ind. Eng. Chem. Fundam.*, **22**(3), 336-346, 1983.
Kucera, E.	Contribution to the theory of chromatography. Linear non-equilibrium elution chromatography, *J. Chromatog.*, **19**, 237-248, 1965.
LaGrone, F. S.	Potential community exposure to toxic chemicals, *Environ. Sci. Technol.*, **25**(3), 366-368, 1991.

Langer, G., Roethe, A., Roethe, K.-P., and Gelbin, D. — Heat and mass transfer in packed beds - III. Axial mass dispersion, *Int. J. Heat Mass Transfer*, **21**, 751-759, 1978.

Lee, T. V., Huang, J.-C., Rothstein, D., and Madey, R. — Correlation of adsorption isotherms of hydrocarbon gases on activated carbon, *Carbon*, **22**(6), 493-495, 1984.

Leonardos, G., Kendall, D., and Barnard, N. — Odor threshold determinations of 53 odorant chemicals, *Journal of the Air Pollution Control Association*, **19**(2), 91-95, 1969.

Liu, T.-P., and Smoller, J. A. — On the vacuum state for the isentropic gas dynamics equations, *Adv. Appl. Math.*, **1**, 345-359, 1980.

Lopatkin, A. A. — Use of the Gibbs equation in deriving partial adsorption isotherms, *Russian J. Phys. Chem.*, **61**(7), 1011-1012, 1987, translated from *Zh. Fiz. Khimii*, **61**, 1940-1943, 1987.

Maclaine-Cross, I. L., and Banks, P. J. — Coupled heat and mass transfer in regenerators - Prediction using an analogy with heat transfer, *Int. J. Heat Mass Transfer*, **15**, 1225-1242, 1972.

Marsh, H., and Rand, B. — The chracterization of microporous carbons by means of the Dubinin-Radushkevich equation, *J. Colloid Interface Sci.*, **33**(1), 101-116, 1970.

Masamune, S., and Smith, J. M. — Adsorption rate studies - significance of pore diffusion, *AIChE J.*, **10**(2), 246-252, 1964.

Masters, K. J., and McEnaney, B. — Structural analysis of microporous carbons using the Dubinin-Radushkevich equation, *J. Colloid and Interface Sci.*, **95**(2), 340-345, 1983.

Masterton, W. L., Slowinski, E. J., and Stanitski, C. L. — *Chemical Principles*, 5th Ed., Saunders College Publishing, Philadelphia, PA, 1981.

Meir, D., and Lavie, R. — Continuous cyclic zone adsorption, *Chemical Engineering Science*, **29**, 1133-1138, 1974.

Michelsen, M. L. — An efficient general purpose method for the integration of stiff ordinary differential equations, *AIChE J.*, **22**(3), 594-597, 1976.

Natusch, D. F. S., Hudson, J. L., Solomon, R. L., Tanner, R., and Miguel, A. — Adsorption of odorous pollutants by active manganese dioxide, EPA-650/2-74-063, PB-234-458, University of Illinois at Urbana-Champaign, June, 1974.

Nero, A. V., Jr. — Controlling indoor air pollution, *Scientific American*, **258**(5), 42-48, 1988.

Nolan, J. T., McKeehan, T. W., and Danner, R. P. — Equilibrium adsorption of oxygen, nitrogen, carbon monoxide, and their binary mixtures on molecular sieve type 10X, *J. Chem. Eng. Data*, **26**, 112-115, 1981.

Novosel, D., Relwani, S. M., and Moschandreas, D. J. — Development of a desiccant based environmental control unit, *IAQ 87: Practical Control of Indoor Air Problems*, ASHRAE, 261-264, 1987.

Pesaran, A. A. — *Moisture transport in silica gel particle beds*, UCLA-ENG-8310, prepared for DOE/SERI under Grant No. DE-FG02-80CS84056, February 1983.

Petryaeva, G. S., Kel'tsev, N. V., and Timofeeva, E. A. — Adsorption of n-hexenes and n-hexane on synthetic zeolites, *Bulletin of the Academy of Sciences of the USSR: Division of Chemical Science*, **8**, 1787-1789, 1967, translated from *Izvestiya Akademii Nauk SSSR, Seriya Khimicheskaya*, **8**, 1860-1862, 1967.

Pfeifer, P., and Avnir, D. — Chemistry in noninteger dimensions between two and three. I. Fractal theory of heterogeneous surfaces, *J. Chem. Phys.*, **79**(7), 3558-3565, 1983.

Pigford, R. L., Baker, B., III, and Blum, D. E. — Cycling zone adsorption, a new separation process, *I&EC Fundamentals*, **8**(4), 848-851, 1969.

Reilley, C. N., Hildebrand, G. P., and Ashley, J. W., Jr. — Gas chromatographic response as a function of sample input profile, *Analytical Chemistry*, **34**(10), 1198-1213, 1962.

Rodrigues, A. E. — Modeling of percolation processes, in *Percolation Processes: Theory and Applications*, Sijthoff & Noordhoff International Publishers B.V., Alphen aan den Rijn, The Netherlands, 31-82, 1981.

Rodrigues, A. E., and Tondeur, D., Editors — *Percolation Processes: Theory and Applications*, Sijthoff & Noordhoff International Publishers B.V., Alphen aan den Rijn, The Netherlands, 1981, or *Proceedings of the NATO Advanced Study Institute on Percolation Processes: Theory and Applications*, Espinho, Portugal, July 17-29, 1978.

Ross, S., and Olivier, J. P. — *On Physical Adsorption*, Interscience Publishers, New York, 1964.

Roy, D., and Gidaspow, D. — A cross flow regenerator - a Green's matrix representation, *Chem. Engng. Sci.*, **27**, 779-793, 1972.

Ruthven, D. M., and Ching, C. B. — Counter-current and simulated counter-current adsorption separation processes, *Chem. Eng. Sci.*, **44**(5), 1011-1038, 1989.

Schumann, T. E. W. — Heat transfer: a liquid flowing through a porous prism, *J.F.I*, **208**(1245), 405-416, Sept. 1929.

Sheridan, J. C., and Mitchell, J. W. — A hybrid solar desiccant cooling system, *Solar Energy*, **34**, 187-193, 1985.

Snyder, C. F. — Experimental equilibrium adsorption capacity and calculated isosteric heat of adsorption for ethane-Columbia NXC 8x10 activated carbon, *Chem. Eng. Prog. Symp. Series*, **65**(96), 57-64, 1969.

Stalkup, F. I., and Kobayashi, R. — High-pressure phase-equilibrium studies by gas-liquid partition chromatography, *AIChE J.*, **9**(1), 121-128, 1963.

Stenzel, M. H., and Merz, W. J. — Use of carbon adsorption processes in groundwater treatment, *Environmental Progress*, **8**(4), 257-264, 1989.

Strikwerda, J. C. — *Finite Difference Schemes and Partial Differential Equations*, Wadsworth & Brooks/Cole, Belmont, CA, 1989.

Sweed, N. H., and Gregory, R. A. — Parametric pumping: modeling direct thermal separations of sodium chloride-water in open and closed systems, *AIChE J.*, **17**(1), 171-176, 1971.

Sweed, N. H., and Wilhelm, R. H. — Parametric pumping: separations via direct thermal mode, *I&EC Fundamentals*, **8**(2), 221-231, 1969.

Tondeur, D. — Theory of ion-exchange columns, *Chem. Eng. J.*, **1**, 337-345, 1970.

Tondeur, D., and Klein, G.	Multicomponent ion exchange in fixed beds: Constant-separation-factor equilibrium, *Ind. Eng. Chem. Fund.*, **6**(3), 351-361, 1967.
Turk, A., Mehlman, S., and Levine, E.	Comparative odor control performance of activated carbon and permanganated alumina, *Atmospheric Environment*, **7**, 1139-1148, 1973.
Tveito, A., and Winther, R.	Existence, uniqueness, and continuous dependence for a system of hyperbolic conservation laws modeling polymer flooding, *SIAM J. Math. Anal.*, **22**(4), 905-933, 1991.
Van Damme, H., and Fripiat, J. J.	A fractal analysis of adsorption processes by pillared swelling clays, *J. Chem. Phys.*, **82**(6), 2785-2789, 1985.
van Leersum, J. G.	*Heat and mass transfer in regenerators*, Ph.D. Thesis, Mechanical Engineering, Monash University, Clayton, Victoria, Australia, 1975.
Vermeulen, T., and Klein, G.	Recent background developments for adsorption column design, *AIChE Symposium Series: Adsorption Technology*, **67**(117), 65-74, 1971.
Villadsen, J. V., and Stewart, W. E.	Solution of boundary-value problems by orthogonal collocation, *Chem. Eng. Sci.*, **22**, 1483-1501, 1967.
Villermaux, J.	Theory of linear chromatography, in *Percolation Processes: Theory and Applications*, Sijthoff & Noordhoff International Publishers B.V., Alphen aan den Rijn, The Netherlands, 83-140, 1981.
Wakao, N.	Particle-to-fluid transfer coefficients and fluid diffusivities at low flow rate in packed beds, *Chem. Eng. Sci.*, **31**, 1115-1122, 1976.
Wakao, N., Tanaka, K., and Nagai, H.	Measurements of particle-to-gas mass transfer coefficients from chromatographic adsorption experiments, *Chemical Engineering Science*, **31**, 1109-1113, 1976.
Wakao, N., and Funazkri, T.	Effect of fluid dispersion coefficients on particle-to-fluid mass transfer coefficients in packed beds, *Chem. Eng. Sci.*, **33**, 1375-1384, 1978.
Walas, S. M.	*Phase Equilibria in Chemical Engineering*, Butterworth Publishers, Boston, 1985.
Walker, P. L., Jr., and Shelef, M.	Carbon dioxide sorption on carbon molecular sieves, *Carbon*, **5**, 7-11, 1967.

Wankat, P. C.	Multicomponent cycling zone separations, *Ind. Eng. Chem. Fundam.*, **14**(2), 96-102, 1975.
Wankat, P. C.	Cyclic separation processes, *Separation Science*, **9**(2), 85-116, 1974.
Wankat, P. C., Middleton, A. R., and Hudson, B. L.	Steady-state continuous, multicomponent separations in regenerated two-dimensional cascades, *Ind. Eng. Chem., Fundam.*, **15**(4), 309-317, 1976.
Weast, R. C., Ed.	*CRC Handbook of Chemistry and Physics, 1st Student Edition*, CRC Press, Boca Raton, 1988.
Weber, T. W., and Chakravorti, R. K.	Pore and solid diffusion models for fixed-bed adsorbers, *AIChE J.*, **20**(2), 228-238, 1974.
Wilhelm, R. H., Rice, A. W., Rolke, R. W., and Sweed, N. H.	Parametric pumping: a dynamic principle for separating fluid mixtures, *Ind. Eng. Chem. Fundam.*, **7**(3), 337-349, 1968.
Wood, G. O., and Ackley, M. W.	A testing protocol for organic vapor respirator canisters and cartridges, *Am. Ind. Hyg. Assoc. J.*, **50**(12), 651-654, 1989.
Zwiebel, I., Gariepy, R. L., and Schnitzer, J. J.	Fixed bed desorption behavior of gases with non-linear equilibria: Part I. Dilute, one component, isothermal systems, *AIChE Journal*, **18**(6), 1139-1147, 1972.

ASTM D2854-89: Apparent density of activated carbon.

ASTM D2862-82: Particle size distribution of granular activated carbon.

ASTM D3686-89: Sampling atmospheres to collect organic compound vapors (activated charcoal tube adsorption method).

ASTM D3687-89: Analysis of organic compound vapors collected by the activated charcoal tube adsorption method.

ASTM D4597-87: Sampling workplace atmospheres to collect organic gases or vapors with activated charcoal diffusional samplers.

ASTM D4598-87: Sampling workplace atmospheres to collect gases or vapors with liquid sorbent diffusional samplers.

A description of the Adsorption Predictice Technique (APT), Tigg Corporation, Pittsburgh, PA.

Modular adsorbers: Activated carbons, other sorbents, Bulletin NCE 117, Tigg Corporation, Pittsburgh, PA.